The University Of Sheffield.

Structural and functional studies of proteins expressed from the *gly1* locus of pathogenic *Neisseria*

By:

Jessica Tarrant

A thesis submitted in partial fulfilment of the requirements for the degree of Doctor of Philosophy

The University of Sheffield
Faculty of Medicine, Dentistry and Health
Department of Infection, Immunity and Cardiovascular Disease

May 2018

Summary

Neisseria meningitidis and *Neisseria gonorrhoeae* are closely related human-specific pathogens that colonise mucosal surfaces. *N. meningitidis* is the most common cause of bacterial meningitis and septicaemia in the UK, whilst *N. gonorrhoeae* causes sexually transmitted infections. In 2017 the latter was classified by the World Health Organization as a high priority organism for research and development of new treatments, as antibiotic resistance is rapidly spreading and several extensively drug resistant strains exist.

The work described here focuses on the *gly1* locus (gonolysin 1), which consists of two open reading frames (ORFs 1 and 2) first identified in *N. gonorrhoeae* and highly conserved in other pathogenic *Neisseria*. These genes are hypothesized to play a role in the battle between host and pathogen for the essential nutrient iron, an important factor in pathogenicity and the outcome of infection.

Previous studies have shown that Gly1ORF1 binds haemin and may be important for *N. meningitidis* survival using haemin or haemoglobin as an iron source. The structure of the wild type *N. meningitidis* Gly1ORF1 protein has been solved in this study. Further characterisation of haemin binding function has been achieved through multiple biophysical techniques. Analysis of knock-out mutants created in this study show that unlike in *N. meningitidis,* Gly1ORF1 is not essential for utilisation of haemin or haemoglobin as iron sources in *N. gonorrhoeae*. Preliminary investigations to identify alternative functions have been carried out and provide scope for future work to identify the role of this conserved protein.

The first reported study of *gly1ORF2,* which shares partial homology with the *E. coli* haem biosynthesis enzyme Uroporphyrinogen III synthase (UroS), is also presented here. Genetic complementation in *E. coli* has confirmed that it is the neisserial *hemD* homologue that encodes UroS. This is supported by the observation that *N. gonorrhoeae* null mutants require an exogenous haem source for survival. The protein has been purified and techniques including circular dichroism, bio-layer interferometry and bioinformatics have been employed to study its structure and interactions. Overall

the results of this study add to our understanding of haem/iron metabolism in *Neisseria* and provide scope for further study of this area that may contribute to development of new treatments or prophylactics.

Acknowledgements

I would first like to thank my supervisor Professor Jon Sayers for his support, advice and encouragement, especially during my final year. I also thank the Faculty of Medicine, Dentistry and Health for the faculty scholarship that enabled me to undertake this project. Many people have helped me through my doctoral research, from those who have provided technical support and taught me new skills to friends who have provided support and laughter in difficult times, I apologise if I don't have space to thank them all! I must thank past and present members of the Sayers group: Sarb for patiently answering my endless questions, Janine for fantastic technical support, Jason for being my crystallography guru and Roxanne for having fun in the lab and hiding dinosaur stickers everywhere! From the department of Molecular Biology and Biotechnology I would like to thank Professor Pat Baker for his great kindness in sharing his expertise in crystallography and Nate Adams and Peter Davis who gave up their time to assist me. I have had the privilege to meet some truly kind and inspiring friends during my time as a doctoral student in particular Emily, Lucy, Sayali, Andrea, Izzy. Without their friendship and support I wouldn't have made it this far. Outside of the lab I want to thank my lovely friends in Sheffield and my childhood friends ESJAC who have always believed in me and helped me to enjoy life away from the bench (occasionally!). Thank you to my wonderful family, in particular my parents for their unwavering support and who have inspired me in everything I do. And finally Alex, for his patience, love and encouragement. You have always been there for me even though this has been difficult for you too. Here's to a bright future.

Table of Contents

List of Figures

List of tables

List of Abbreviations

ACP	Adhesin complex protein
ALA	5-aminolevulininc acid
APS	Ammonium persulphate
ATP	Adenosine triphosphate
BHI	Brain heart infusion
bp	Base pair
BSA	Bovine serum albumin
CD	Circular dichroism
CPS	Capsular polysaccharide
CSF	Cerebrospinal fluid
CTD	C-terminal domain
CV	Column volume
DNA	Deoxyribonucleic acid
DPBG	Deuteroporphyrin IX 2,4 bis ethylene glycol
DPHCl	Deuteroporphyrin IX dihydrochloride
DTPA	Diethylenetriaminepentaacetic acid
DTT	Dithiothreitol
EDTA	Ethylenediaminetetraacetic acid
GCCDM	Gonococcal chemically defined media
GGI	Gonococcal genetic island
Hb	Haemoglobin

HMB	Hydroxymethylbilane
IMAC	Immobilised metal ion chromatography
IPTG	Isopropyl-β-D-thiogalactopyranoside
Kb	Kilobase
kDa	Kilo Dalton
Lbp	Lactoferrin binding protein
Lf	Lactoferrin
LOS	Lipooligosaccharide
LPS	Lipopolysaccharide
mRNA	Messenger RNA
NET	Neutrophil extracellular trap
NG	Neisseria gonorrhoeae
NM	Neisseria meningitidis
OD	Optical density
OM	Outer membrane
OMR	Outer membrane receptor
OMV	Outer membrane vesicle
ORF	Open reading frame
PBG	Porphobilinogen
PBP	Periplasmic binding protein
PBS	Phosphate buffered saline
PCR	Polymerase chain reaction
PMSF	Phenylmethylsulfonyl fluoride

RBS	Ribosomal binding site
RMSD	Root mean square deviation
RNA	Ribonucleic acid
ROS	Reactive oxygen species
SDS	Sodium dodecyl sulphate
SEC	Size exclusion chromatography
SEM	Standard error of the mean
sRNA	Small regulatory RNA
TBDT	TonB dependent transporter
Tbp	Transferrin binding protein
Tdf	TonB dependent function protein
TE	Tris-EDTA
TEMED	Tetramethylethylenediamine
Tf	Transferrin
tRNA	Transfer RNA
UV	Ultraviolet
WT	Wild type

Chapter 1. Introduction. Molecular pathogenesis of *Neisseria*

The genus *Neisseria* contains two species of importance to human disease: *Neisseria meningitidis* and *Neisseria gonorrhoeae.* These Gram-negative diplococci are obligate human pathogens, which predominantly colonise the mucosal surfaces of the upper respiratory tract (*N. meningitidis*) and urogenital tract (*N. gonorrhoeae*). A third, *Neisseria lactamica,* can cause invasive disease in extremely rare cases. These infections have occurred in immunocompromised patients such as those receiving chemotherapy or organ transplants (Everts et al., 2010; Schifman and Ryan, 1983; Zavascki et al., 2006).

N. meningitidis asymptomatically colonises the nasopharynx, with transient carriage rates in the general population of approximately 10%. The carriage rate is drastically increased in parts of the population including adolescents, military recruits and university students where it can reach close to 100% (Christensen et al., 2010). The overwhelming majority of colonisation events are harmless. However, occasionally the bacteria traverse the epithelium to cause invasive disease. This can take the form of septicaemia, haemorrhagic fever or meningitis (invasion of the blood-brain barrier and infection of the meninges). The onset of invasive disease is rapid and patients can die within 24 hours of symptoms appearing. Despite the availability of antibiotic treatments the worldwide mortality rate for invasive disease is still 8-14% and much higher in some developing countries. Up to 19% of survivors are left with life-changing disabilities including neurodevelopmental difficulties and amputations (Pace and Pollard, 2012).

N. meningitidis has been categorized into 13 serotypes based on the structure of the polysaccharide capsule and serogroups A, B, C, Y and W135 cause the majority of invasive infections. Serogroups B and C cause the most cases in Europe and North America, in 2016-2017 53% cases in the UK were serotype B (Public Health England, 2017). Serogroup A strains are mainly responsible for infections in the “meningitis belt” of sub-Saharan Africa, where seasonal epidemics can cause infection rates of over 1/1000 (Stephens, 2009). Effective conjugate vaccines against type A have recently been developed and their widespread use has successfully controlled outbreaks, leading to a significant decrease in cases (Mohammed et al., 2017). A

technique called multi-locus sequence typing (MLST), based on sequencing fragments of seven housekeeping genes, is now used to further classify *N. meningitidis* strains and identify hypervirulent lineages (Maiden et al., 1998). However, there is no core set of genes that distinguishes between strains more likely to be carriage or invasive (Stephens, 2009). The probability of invasive disease is also determined by host susceptibility, with risk factors including age, smoking status and co-infections contributing to colonization and infection rates (Kriz et al., 2000; Stanwell-Smith et al., 1994).

Unlike *N. meningitidis, N. gonorrhoeae* is not found as a commensal organism. It is most often a sexually transmitted infection (STI) that colonises the mucosal surfaces of the endocervix in females and the urethra in males. Gonorrhoea is the second most common STI in the UK, with 29,000 new cases reported in 2012 and the infection rate continues to rise year on year (Hughes and Field, 2015). The infection is generally uncomplicated and easily diagnosed in males but roughly half of female cases are asymptomatic (Hughes and Field, 2015). This can result in infections being left untreated and more serious complications developing such as salpingitis (inflammation of fallopian tubes) and pelvic inflammatory disease (infection of the upper reproductive system), sometimes resulting in ectopic pregnancies or sterility (Edwards and Butler, 2011).

The direct economic burden of gonococcal disease to the NHS and public sector is predicted to be around £34 million for the period of 2013-2020 (Lucas, 2013). In addition to this, antimicrobial resistance in *N. gonorrhoeae* is becoming an increasing problem and strains are rapidly evolving resistance to all known antibiotics. A recent outbreak in the UK saw 48 confirmed cases of gonorrhoea with high level azithromycin resistance, the current treatment of choice (Public Health England, 2016). Several outbreaks of strains with high levels of resistance to ceftriaxone, a “last resort” treatment, have occurred in Japan, China, continental Europe and Australia (Unemo, 2015). Extensively drug resistant strains have the potential to spread globally, raising the possibility of gonorrhoea becoming an untreatable infection. It is currently classified as a high priority organism by the World Health Organisation requiring development of new antimicrobial treatments (World Health Organization, 2017).

This review will present a brief overview of neisserial virulence factors and mechanisms of pathogenesis. Two main factors involved in neisserial pathogenesis are adhesion to host cell surfaces and evasion of the host immune responses. The methods that *Neisseria* employ to overcome "nutritional immunity" imposed by the host (limitation of nutrients available to pathogens) will be highlighted.

1.1 Adhesion

Adhesion is necessary for both *N. gonorrhoeae* and *N. meningitidis* to resist clearance by mucociliary action on epithelial cell surfaces, and during invasive meningococcal disease for attachment to endothelial cells and resistance of flow in the blood stream. Adhesins are major virulence factors and *Neisseria* encode multiple redundant systems. Their roles and importance can vary depending on the site of infection and the gender of the host (Edwards and Apicella, 2004).

1.1.1 Major Adhesins - Type IV pili and opacity associated proteins Opa and Opc

The major neisserial adhesin is the type IV pilus, which initiates contact with epithelial cells. Pili are long filamentous structures composed of pilE monomers arranged in a helical fashion, protruding from a base on the inner membrane through a pore in the outer membrane formed by pilQ (Collins et al., 2001; Drake and Koomey, 1995). They possess the ability to extend and retract, powered by ATPase PilT located in the inner membrane base plate, which facilitates "twitching motility" and is also essential for DNA transformation (Wolfgang et al., 1998a, 1998b). Pilus fibres are incredibly robust due to the strong interactions between PilE subunits, which can only be denatured by detergent treatment or temperatures over 60°C (Li et al., 2012). Recent high-resolution X-ray structural data for PilE, along with cryo-EM modelling of the whole pilus assembly, have shown that the N-terminal sections of PilE in the filament core are melted and unstructured and this can facilitate their flexibility and elasticity, helping the bacterium resist shear stresses (Kolappan et al., 2016). There are 23 proteins involved in type IV pilus assembly and biogenesis of which 15 are essential, a diagram of the pilus structure is shown in Figure 1.1.

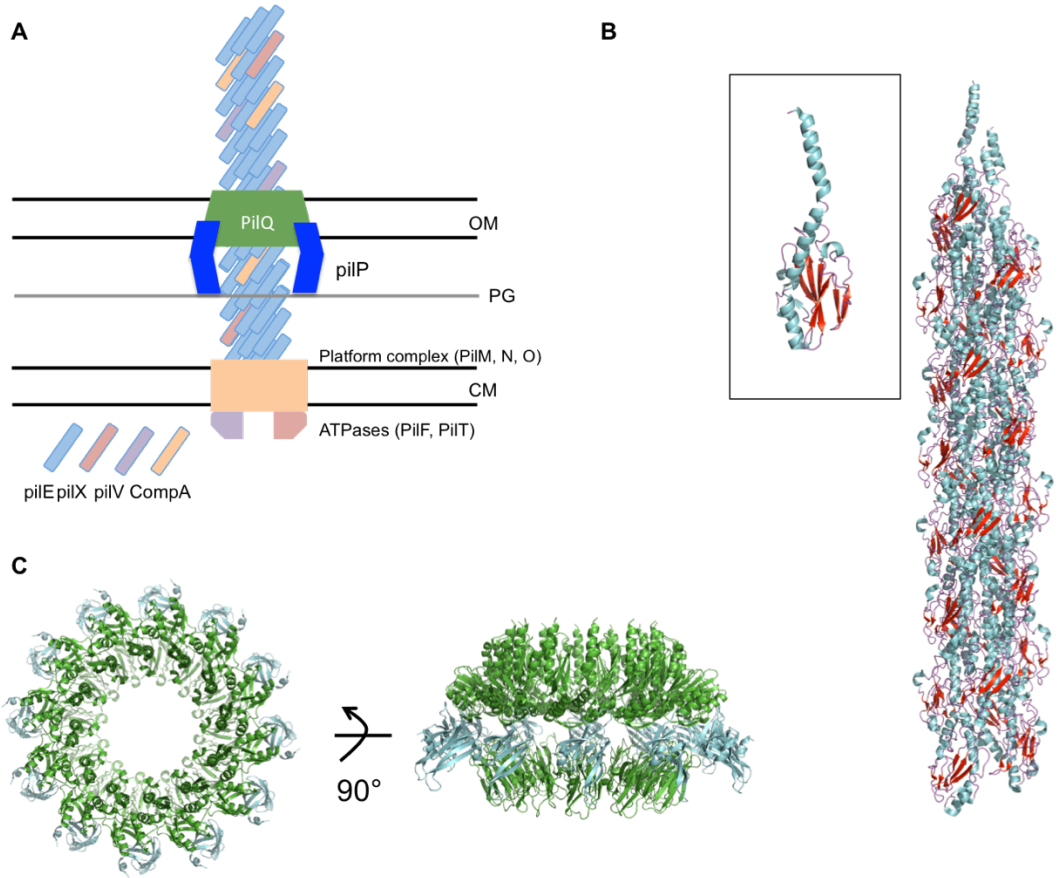

Figure 1.1 Type IV pilus assembly and structure of components
A) Schematic representation of the Type IV pilus assembly. The pilus fibre is assembled from PilE monomers and protrudes through a pore in the outer membrane (OM) formed by 12 PilQ monomers. The C-terminal domain of PilP interacts with the PilQ dodecamer. The fibre is anchored into the base plate machinery consisting of PilM, PilO and PilN in the cytoplasmic membrane (CM). The ATPase enzymes PilF and PilT generate energy for pilus extension and contraction. Minor pilins including PilX, PilV, PilC and CompA are associated with the pilin fibre and fulfil various functions such as regulating the number of pili and facilitating interaction with host receptors **B**) Cartoon model of the *N. meningitidis* Type IV pilus fibre assembled from X-ray crystallography and cryo-electron microscopy. The PilE monomers are arranged in a helical fashion, with the α-helical domains (cyan) clustered at the centre of the fibre and the β-sheet domain (red) facing outwards. Inset is crystal structure of the full-length PilE monomer from *N. gonorrhoea*. Created from PDB files 5KUA and 2HI2 using Pymol. **C**) Top and side view of the model of *N. meningitidis* pilQ assembly and interaction with C-terminal domain of PilP. A pore is formed of 12 PilQ monomers (green) and stabilised by interaction with the C-terminus of PilP (blue). Created using Pymol with PDB file 4AV2.

The outer membrane opacity proteins Opa and Opc are adhesins that are involved in the intimate adhesion stages following the initial type IV pili contact. Opa proteins are expressed by both *N. meningitidis* and *N. gonorrhoeae*, whereas Opc is only expressed by *N. meningitidis* (Zhu et al., 1999). There are up to 11 different *opa* genes in *N. gonorrhoeae,* and the surface-exposed Opa proteins exhibit high antigenic variability, often achieved through recombination of different *opa* genes in the same isolate (Bhat et al., 1991). An NMR solution structure of Opa_{60} (Figure 1.2) shows that the protein adopts an 8-stranded transmembrane β-barrel conformation with 4 extracellular loops (Fox et al., 2014). Loops 2 and 3 are hypervariable and exhibit high levels of sequence diversity but are dynamic over nanosecond time scales in the NMR structures and this could allow them to interact with host receptors despite sequence variation (Fox et al., 2014). Opc is encoded by a single gene in *N. meningitidis* and does not exhibit as much antigenic variation as Opa, however its level of expression differs through phase variation (Zhu et al., 1999). The crystal structure of Opc shows that it is a 10 stranded β-barrel with multiple highly flexible extracellular loops (Figure 1.2) (Luan et al., 2007; Prince et al., 2002).

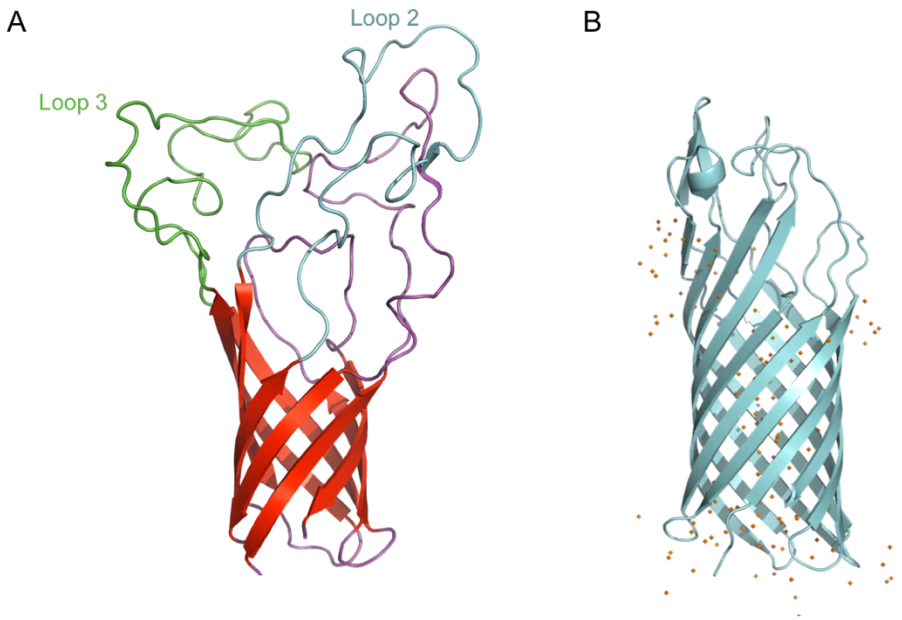

Figure 1.2 Structural models of *N. gonorrhoeae* Opa_{60} and *N. meningitidis* Opc adhesins
A) Cartoon depiction of *N. gonorrhoeae* Opa_{60} NMR solution structure. The 8 stranded β-barrel (red) is completely embedded into the outer membrane and the 4 flexible loops protrude into the extracellular space. Loops 2 (cyan) and 3 (green) are hypervariable and dynamic. **B)** Cartoon depiction of *N. meningitidis* Opc(A) crystal structure. The 10 stranded β-barrel (cyan) traverses the outer membrane. Water molecules in the structure are shown as orange dots. Figures created from PDB files 2MAF and 1K24.

1.1.2 *Neisseria meningitidis* adhesion mechanisms

The type IV pili has been identified as the most important adhesin for initial contact with epithelial cells and PilC, a phase-variable pilin that is thought to be located at the tip of the pilus fibre, plays an essential role in this interaction (Rudel et al., 1995; Virji et al., 1993). The main epithelial cell surface receptor that interacts with the pilus was thought to be CD46, a complement regulatory receptor expressed on all cell types apart from erythrocytes (Källström et al., 1997). However, this has been thrown into doubt as CD46 was not found to be essential for adherence in later studies and it is still unclear what the host receptor is (Kirchner and Meyer, 2005; Kirchner et al., 2005). Following initial adhesion pilus retraction powered by the ATPase PilT brings the bacteria closer to the epithelial cell surface allowing for more intimate adhesion (Pujol et al., 1999).

In order for intimate adhesion to occur between the host cell surface and meningococcal outer membrane receptors, the expression of pili and the capsule are

downregulated. This is thought to occur through the action of the CrgA regulatory protein (Deghmane et al., 2002), although these findings have not been replicated elsewhere (Morelle et al., 2003). The major outer membrane proteins involved in intimate adhesion are the Opa and Opc proteins. Most types of Opa bind to members of the carcinoembryonic antigen cell adhesion molecule (CEACAM) receptor family, and some have specificity for heparan sulphate proteoglycan (HSPG) and integrins (Chen et al., 1995). Opc binds HSPG and integrins through vitronectin and fibronectin in the extracellular matrix (Virji et al., 1995).

During invasive meningococcal disease the type IV pili are involved in adhesion to human brain and peripheral endothelial cells. The CD147 receptor has been identified as the primary target for pili-mediated binding and the pilin subunits PilE (major pilus fibre pilin) and PilV are essential for this interaction (Bernard et al., 2014). Initial (localized) adhesion of a few meningococci is followed by the formation of microcolonies on the endothelial surface and this is mediated by the pilin subunits PilX and PilV (Brissac et al., 2012; Hélaine et al., 2005). These periplasmic minor pilins control the number of pili that the bacterium express, and this regulates aggregation and host cell interaction (Imhaus and Duménil, 2014).

A second host cell receptor, the β2-adrenoceptor (β2AR), is recruited to the site of microcolonies (Coureuil et al., 2010). This is a G-protein coupled receptor, and pilin interactions stimulate β-arrestin mediated signalling pathways that lead to accumulation of cholesterol, ezrin-radixin-moesin (ERM) proteins, and several transmembrane receptors to form a “cortical plaque” beneath the microcolonies (Coureuil et al., 2014). These signalling events trigger actin cytoskeleton rearrangements and the formation of microvilli-like protrusions from the membrane that protect the meningococcal colonies from shear stress in the vasculature (Coureuil et al., 2010; Mikaty et al., 2009). The formation of cortical plaques recruits the polarity complex, which is usually present at the intercellular junctions between endothelial cells and promotes the formation of tight junctions (Coureuil et al., 2009). This leads to break down of the tight junctions, which can cause leakage of the vasculature in addition to opening up a potential paracellular route through which the bacteria may migrate to cross the blood-brain barrier. Disseminated neisserial infections have been

shown to stimulate the upregulation of CEACAM receptors on endothelial cells, and Opa interactions with this receptor could be involved in adherence to these surfaces (Muenzner et al., 2000, 2001).

1.1.3 Neisseria gonorrhoea adhesion mechanisms

N. gonorrhoeae adhesion mechanisms differ depending on the site of infection and the sex of the host. For infection of the male urethra the pilus binds to the I-domain of $\alpha_1\beta_1$ or $\alpha_2\beta_1$ integrins (Edwards and Apicella, 2005). This binding event triggers interaction with asialoglycoprotein (ASGP-R), a receptor that also recognises the surface lipooligosaccharides (LOS). ASGP-R stimulation leads to the formation of actin pedestals underneath the adherent bacteria followed by endocytosis and internalisation of the gonococci (Harvey et al., 2001). The significance of Opa proteins in gonococcal adherence is unclear, as primary urethral epithelial cell cultures do not express the CEACAM receptors (Edwards and Apicella, 2004).

Infection of the female lower reproductive tract does not require expression of Opa proteins or the presence of CEACAM receptors (Edwards et al., 2002; Swanson et al., 2001). Pili play a major role in the initial interaction, the ability of pili-deficient *N. gonorrhoeae* FA1090 mutants to adhere to and invade human endocervical cells was almost completely inhibited compared to wild type (Edwards et al., 2002). Gentamycin resistance assays demonstrated that complement receptor 3 (CR3) was essential for gonococcal invasion of human endo- and ectocervical cells (Edwards et al., 2001). CR3 recognises the C3b complement components that bind to the gonococcal porin proteins and LOS and this allows for intimate adhesion of the bacteria following initial pili recognition. Signalling through CR3 activates Rho GTPases and triggers actin cytoskeleton rearrangement to produce membrane protrusions or “ruffles”. These structures promote adherence and also facilitate internalisation of the bacteria by macropinocytosis (Edwards et al., 2000). Immortalised epithelial cell lines do not express CR3, and in these cell types Opa and LOS appear to mediate interactions with these cells, but the significance of this *in vivo* is unclear (Minor et al., 2000).

1.2 Evasion of host immune mechanisms

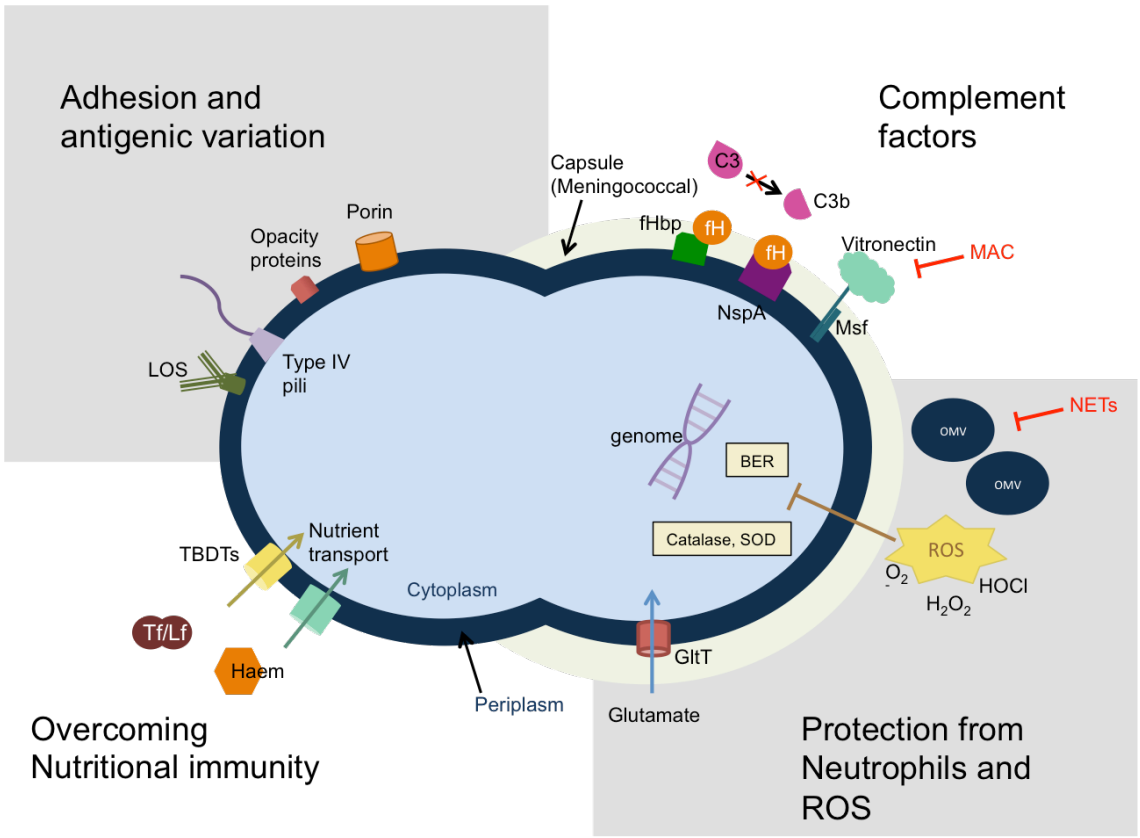

Figure 1.3 Overview of neisserial virulence factors and methods of evading host immune system

A summary of the major virulence factors and mechanisms of immune evasion in *N. meningitidis* and *N. gonorrhoeae* discussed in this review. **Adhesion and antigenic variation:** Surface structures including Type IV pili, LOS, Porins and Opacity proteins are involved in initiating and maintaining interactions with host cells. They are involved in invasion of the epithelium and endothelium in *N. meningitidis* invasive disease. Antigenic variation of these structures contributes to evasion of adaptive immunity along with molecular mimicry by the meningococcal capsule. **Complement factors:** The meningococcal capsule prevents C3b deposition on the bacterial surface and can promote negative complement regulator factor H binding to C3b. NspA and fHpb also bind factor H and inhibit C3b formation. Msf binds vitronectin that inhibits the action of the membrane attack complex (MAC). **Protection from Neutrophils and ROS:** *N. meningitidis* releases outer membrane vesicles (OMVs) that bind to neutrophil extracellular traps (NETs) preferentially over whole bacteria. Import of glutamate by GltT maintains intracellular redox potential. Neisseria express detoxifying enzymes catalase and superoxide dismutase (SOD) that combat protein damage by reactive oxygen species (ROS). Base excision repair (BER) repairs DNA damage from ROS. **Overcoming nutritional immunity:** TonB dependent transporters (TBDTs) bind and import essential nutrients to overcome the host nutrient limitation strategies "nutritional immunity". Neisseria use transferrin (Tf) and lactoferrin (Lf) and free haem or haem from haemoglobin as sources of iron (Figure based on Lo et al., 2009 and Quillin and Seifert, 2018, copyright permissions granted).

1.2.1 Complement system

The complement system is a network of soluble plasma proteins and membrane bound receptors that constitute a major part of the innate immune system. It is involved in pathogen recognition and clearance and integrates with other immune pathways. The result of complement activation is the deposition of the component C3b onto the bacterial surface. This opsonisation can target the membrane attack complex (MAC), which creates lytic pores in the cell membrane, and also recruit and modulate other components of the innate and adaptive immune systems. The complement pathway can be activated in three different ways, the classical pathway (through antibody recognition of pathogens), the lectin pathway (through mannose-binding-lectin interaction with bacterial polysaccharides) and the alternative pathway (spontaneous hydrolysis of C3 into C3b). Complement activity is tightly controlled and regulated by a host of soluble factors in order to prevent damage to human cells and tissues. These include the negative regulators such as factor H, which can both prevent the formation of C3b and help to cleave and inactivate it, and vitronectin a negative regulator of the terminal complement pathway that can prevent formation of the MAC (Murphy, 2011).

Complement is perhaps the most important host defence against invasive meningococcal disease evidenced by the fact that inherited or acquired complement deficiencies, particularly in the terminal complement pathway (C5-C9), drastically increase susceptibility (Figueroa and Densen, 1991). The rate of systemic meningococcal infection in the general population is 0.0072%, but in individuals with late complement or properdin deficiencies it is between 46 and 57% and they are often recurring (Figueroa and Densen, 1991). Although complement components are mainly circulated in the serum, epithelial cells do express complement receptors and secrete some complement components in order to protect mucosal surfaces, and therefore *N. gonorrhoeae* also comes into contact with this immune defence (Edwards et al., 2002; Hill et al., 1993). Genome wide screens in *N. meningitidis* identified that most genes conferring resistance to complement-mediated killing were involved in biogenesis of the polysaccharide capsule or lipopolysaccharides (LPS) (Geoffroy et al., 2003).

1.2.2 Capsule

Capsular polysaccharides expressed by *N. meningitidis* are a major virulence factor and determinant of invasive disease. Un-encapsulated strains or mutants unable to synthesise capsule components are more sensitive to complement-mediated killing *in vitro*, whereas strains that upregulate capsule biosynthesis are very resistant (Gordon, 1989; Uria et al., 2008). *N. gonorrhoeae* does not possess the biosynthetic genes to express the capsule. Of the 13 capsule polysaccharide (CPS) types (the basis of the serotypes), four of those that are associated with invasive meningococcal disease share the common feature of containing sialic acid (Gordon, 1989). Sialic acid is expressed on host endothelial cells and plays a role in protecting the host from complement activity by enhancing the ability of the negative regulator factor H binding to C3b, preventing C3b deposition at the host cell surface.

Serogroup B and C sialic acid capsule expressing strains have been shown to downregulate the alternative complement pathway responses (Gordon, 1989; Ram et al., 1998a). This is thought to occur through enhancement of factor H binding to C3b, preventing C3b deposition on the bacterial cell surface in a similar way to the protection of host cells (Ram et al., 1998a). CPS from W135 and Y serogroups actually enhance alternative pathway activation serving as targets for C3 deposition, but these strains cannot be killed by the alternative pathway alone (Ram et al., 2011). In addition, all major disease-causing serogroup capsules have been shown to inhibit the classical pathway by interfering with C1q binding to antibodies at the bacterial surface – the first step in the classical pathway (Agarwal et al., 2014). A common mechanism to all capsule serotypes is blocking the insertion of membrane attack complex (MAC) in the terminal stages of the complement cascade (Ram et al., 1999). The different capsule structures interact with the complement system in diverse ways that are not fully understood, but all result in evasion of complement-mediated killing.

Capsule expression is differentially regulated throughout colonisation and invasive disease. It is hypothesised that expression of the capsule inhibits adhesion to epithelial cells because it blocks access to the host cell receptors for adhesins essential for intimate interactions such as porins, Opa and LOS (Deghmane et al., 2002). Capsule expression is regulated by phase variation of biosynthesis genes, structural

modifications and differential transcription of transport proteins and the methods used differ between serogroups (Tzeng et al., 2016). Genes coding for capsule biosynthesis were also identified as being regulated in a temperature dependent manner by the presence of RNA "thermosensors" in their 5' untranslated region (Loh et al., 2013). This suggests that increases in temperature such as during inflammation could trigger a more invasive phenotype (encapsulated). Strains can undergo "capsule switching", where horizontal transfer occurs between the capsule loci of two co-colonizing strains facilitated by the natural competence of *Neisseria* (Swartley et al., 1997). Capsule switching has been observed during epidemic outbreaks and can provide an escape from immunity provided by capsular based vaccines (Tsang, 2007).

1.2.3 Lipopolysaccharide

Lipopolysaccharides (LPS) are surface exposed components of Gram-negative outer membranes and play an important role in interactions with the immune system. LPS consists of an inner core of heptose molecules bound to the membrane-anchored lipid A through 2-keto-3-deoxy-D-manno-2-octulosonic acids, and an outer core of variable polysaccharides. Neisserial LPS lacks the long side chain "O-antigen" that is expressed by other Gram-negative species, and is therefore often called lipooligosaccharide (LOS) (Jennings et al., 1999). Both *N. meningitidis* and *N. gonorrhoea* can add sialic acid to some LOS immunotypes, imparting similar protective properties to the *N. meningitidis* groups B, C, W and Y capsule.

Sialylation of LOS is important for *N. gonorrhoeae* evasion of complement-mediated killing, and has been shown to modulate both the classical and alternative pathways. Sialylated LOS can block binding of antibodies against porin by masking the porin epitopes and it also enhances binding of the classical and alternative pathway inhibitor factor H to porin B (Elkins et al., 1992; Madico et al., 2007). Some studies have shown that *N. gonorrhoeae* mutants that are unable to sialylate LOS have reduced virulence *in vivo* in mouse models (Wu and Jerse, 2006). The importance of *N. meningitidis* LOS for complement evasion and virulence is less well defined, as *in vitro* experiments show that sialylated LOS does not enhance factor H binding to the surface (Madico et al., 2007). *N. meningitidis* strains deficient in the lacto-N-neotetraose (LNT) epitope where sialic acid would normally be added have been isolated from human disease

cases, and mutants unable to sialylate LOS could still cause invasive disease in infant rats (Mackinnon et al., 1993; Vu et al., 2012). Together these findings suggest that the capsule may be the more important for complement evasion in meningococci, but this function can be fulfilled by sialylated LOS in the un-encapsulated gonococci.

1.2.4 Binding complement regulatory proteins

In addition to capsule and LOS, *Neisseria* express a number of surface structures that can interact with the soluble complement regulatory factors. *N. gonorrhoeae* trimeric porin Por1A binds to factor H through extracellular loops and has been shown to provide serum resistance to otherwise sensitive (non-sialylated) strains, whereas meningococcal porins do not significantly bind factor H (Madico et al., 2007; Ram et al., 1998b). *N. meningitidis* express two other outer membrane protein shown to bind factor H, NspA and factor H binding protein (fHbp) (Lewis et al., 2010; Madico et al., 2006). FHbp is a major antigen that forms part of both the Bexsero® and Trumenba® (bivalent fHbp) vaccines against serogroup B meningococci (Gandhi and Balmer, 2016; Gorringe and Pajon, 2012). Although *N. gonorrhoeae* encode a potential fHbp homologue with over 90% identity, this protein is not expressed at the cell surface and does not bind factor H (Jongerius et al., 2013).

N. meningitidis can also inhibit the terminal stages of the complement pathway and the formation of the membrane attack complex (MAC). The Opc protein and an adhesin called meningococcal surface fibril (Msf) can both bind to vitronectin, a negative regulator that protects cells from lysis by the MAC (Griffiths et al., 2011).

1.2.5 Interactions with neutrophils/ protection from ROS

One of the major characteristics of neisserial disease is strong stimulation of the innate immune response and an influx of neutrophils to the urogenital tract or the CSF (Stephens, 2009). This response accounts for much of the damage to host tissues during the disease and produces symptoms such as the neutrophil-rich discharge seen in most gonococcal infections. Neutrophils are the most abundant white blood cell in the human body and are often called the “first responders” to infection. They possess intracellular granules that contain antimicrobial peptides, reactive oxygen species (ROS), and degradation enzymes such as lysozyme (Burg and Pillinger, 2001).

Neutrophils can kill bacteria extracellularly by the release of granule components or production of neutrophil extracellular traps (NETs) – secreted DNA coated with antimicrobial peptides (Brinkmann et al., 2004). Alternatively they can internalise bacteria by phagocytosis, where the bacteria are taken up into phagosomes that fuse with the granules to form phagolysosomes, and degraded. *Neisseria* species can resist these methods of killing by neutrophils, *in vitro* up to 70% of bacteria incubated with neutrophils remain viable and up to 40% of phagocytosed bacteria survived inside phagosomes (Criss et al., 2009).

Neisseria can both survive and repress neutrophil extracellular antimicrobial activities. They express catalase and superoxide dismutase proteins that detoxify ROS and contribute to virulence in mouse models (Johnson et al., 1993; Soler-García and Jerse, 2004; Wilks et al., 1998). *N. meningitidis* encodes a GltT transporter that imports L-glutamate and converts it to glutathionie to maintain cytoplasmic redox potential and resist ROS damage (Talà et al., 2011). Other proteins have been implicated in protection from oxidative stress by DNA microarray techniques and include an iron-regulated operon NMB1436-38 (Grifantini et al., 2004). The porin proteins may supress ROS production, as the purified proteins inhibit fusion of the neutrophil granules with phagosomes (Lappann et al., 2013). However, *N. meningitidis* PorAB^{-} mutants could still inhibit oxidative bursts, indicating that there are redundant mechanisms for inhibition (Peak et al., 2016). *N. gonorrhoeae* modulates the neutrophil response by triggering downregulation of ROS production and switch to more NET activity (Gunderson and Seifert, 2015). *Neisseria* escape NET killing in multiple ways, for example *N. meningitidis* releases outer-membrane vesicles (OMVs) that bind preferentially to NETs over whole bacteria, and is also protected from antimicrobial peptides by lipid A modifications (Lappann et al., 2013). One function of NETs is to sequester essential nutrients from bacteria, imposing “nutritional immunity”. Both *N. meningitidis* and *N. gonorrhoeae* require the expression of zinc uptake receptors to survive exposure to NETs where the host protein calprotectin sequesters zinc (Jean et al., 2016; Lappann et al., 2016).

Neutrophil phagocytosis of *Neisseria* can occur through opsonisation of the bacteria by C3b, or by interaction of Opa proteins and CEACAM receptors (Criss and Seifert, 2012;

Martin et al., 2016). Once inside phagocytes *Neisseria* can delay phagolysosome maturation and survive and replicate inside the cells in processes that may involve porin proteins (Mosleh et al., 1998). They also resist the actions of degradative enzymes and antimicrobial peptides in the phagolysosome through modification of cell wall and cell surface structures. *O*-acetylation of peptidoglycan by peptidoglycan *O*-acyltransferase (PacA) helps *Neisseria* resist the actions of lysozyme, and addition of a phosphoethanolamine moiety to LOS by lipopolysaccharide transporter periplasmic protein (LptA) protects from antimicrobial peptides and complement (Dillard and Hackett, 2005; Lewis et al., 2009). Intracellular *N. gonorrhoeae* has been observed to modulate host gene expression, downregulating iron-binding proteins and increasing the intracellular pool of free iron creating a nutrient rich niche inside phagocytes (Zughaier et al., 2014).

Neisseria have been observed to form microcolonies on the surface of neutrophils and enter the cells in a non-phagocytic manner, allowing them to survive in intracellular compartments separate from the phagolysosome (Söderholm et al., 2011). The formation of colonies on the neutrophil may also facilitate spread of the bacteria, as these colonised neutrophils were able to cross epithelial cell layers *in vivo* (Söderholm et al., 2011). Overall the recruitment of neutrophils may actually be beneficial to *Neisseria* for several reasons: their inflammatory responses can damage surrounding tissues releasing nutrients, they can provide a protective niche for replication inside phagosomes or other intracellular compartments, and can facilitate access of the bacteria to new tissues.

1.2.6 Evasion of adaptive immunity

Both *N. meningitidis* and *N. gonorrhoeae* are adept at subverting the adaptive immune response. This is mostly due to the high frequency of antigenic variability displayed in Opa proteins, LOS and type IV pili. Opa proteins can be encoded by up to 4 different genes in *N. meningitidis* and 11 genes in *N. gonorrhoeae* at different locations in the genome (Bhat et al., 1991). Recombination between the Opa genes in an isolate generates antigenic diversity in the hypervariable surface exposed loops (Bilek et al., 2009). Opa and LOS expression is subject to phase variation where transcription is randomly switched on and off depending on changes in DNA repeat numbers during

replication (Stern et al., 1986). The major pilin subunit *pilE* displays antigenic diversity through recombination with the silent pilin *pilS* (Hagblom et al., 1985; Perry et al., 1987). Some neisserial outer membrane proteins can also stimulate the production of blocking antibodies, which bind to antigens but do not stimulate complement mediated killing (Rice and Kasper, 1982; Rice et al., 1986; Semchenko et al., 2016) . This has implications for the selection of vaccine targets, as some antigens may stimulate antibody production but not elicit any immune responses (complement mediated or adaptive).

Immunoglobulin A1 (IgA1) is the most abundant antibody present on mucosal surfaces where it binds to and agglutinates potentially pathogenic microbes, allowing them to be more effectively removed by ciliary action (Woof and Kerr, 2006). *Neisseria* encode an IgA1 protease (IgAP) that cleaves the hinge region of the IgA1 heavy chain at a proline rich site (Plaut et al., 1975; Vitovski and Sayers, 2007). This cleavage hinders the agglutination process and can also produce a blocking effect, where the cleaved antigen binding region (Fab) can still bind to neisserial surfaces, potentially masking them from other immunoglobulins (Mansa and Kilian, 1986). IgAP could also play a role in other stages of the immune response. LAMP-1 (lysosome associated protein 1) is susceptible to IgAP cleavage, and its degradation may inhibit lysosome maturation and promote neisserial survival inside epithelial cells and leukocytes (Hauck and Meyer, 1997; Lin et al., 1997). IgaP has also been shown to cleave the tumour necrosis factor-α (TNFα) receptor TNF-RII on the surface of monocyte cell line cells, leading to decreased TNFα induced apoptosis (Beck and Meyer, 2000). These varied functions suggest that IgAP may be an important virulence factor, and there is a correlation between IgAP expression levels and virulence in *N. meningitidis* as invasive isolates have higher levels of IgAP activity than carriage isolates (Hopper et al., 2000). However, studies using human male volunteers and *in vitro* models have produced conflicting results regarding IgAP significance for pathogenesis depending on the model system used (Cooper et al., 1984; Hauck and Meyer, 1997; Johannsen et al., 1999; Lin et al., 1997; Parsons et al., 2004).

N. meningitidis carriage or infection elicits specific anti-meningococcal antibody production, and the presence of these antibodies is relatively widespread in the

general population (Trotter et al., 2007, 2012). In addition, carriage of the closely related non-pathogenic species *N. lactamica* can protect against *N. meningitidis* colonisation and infection, both through the stimulation of cross-reactive antibodies and a microbial competition effect (Deasy et al., 2015; Evans et al., 2011). Polysaccharide capsule-based vaccines against *N. meningitidis* serogroups A, C, Y and W have been used for a many years and provide protection from single serogroups. Polysaccharide conjugate vaccines that provide wider serogroup protection and longer lasting immunity are also available (Gasparini and Panatto, 2011). Serogroup B meningococcal disease has proved much more difficult to develop vaccines against, primarily due to the molecular mimicry of its capsule polysaccharide, which is identical to glycan moieties on the human host neural cell adhesion molecule (NCAM-1) (Stephens, 2009). Two vaccines have been developed that are effective at killing serogroup B strains in serum bactericidal assays- Bexsero® (4CMenB), which contains outer membrane proteins and OMVs, and the bivalent factor H binding protein (fHBp) vaccine (Trumenba®) (Gandhi and Balmer, 2016; Gorringe and Pajon, 2012). Immunization programs have been initiated in the UK and elsewhere, and initial studies show high levels of effectiveness (Feavers and Maiden, 2017; Parikh et al., 2016). However, invasive strains that do not express these antigens have been described and their long-term effectiveness is yet to be determined (Harrison et al., 2006; Lucidarme et al., 2011).

N. gonorrhoeae infections do not always induce the development of protective immune memory and repeated infections are relatively common. A study of active-duty Army personnel in the United States found that of individuals with a first gonorrhoea infection, 13.7% of men and 14.4% of women had a repeat infection (Bautista et al., 2017). A 2009 meta-analysis of studies conducted worldwide and in various populations identified similar rates of reinfection where the median rate of reinfection for women was 11.7% (Hosenfeld et al., 2009). This is partly due to the immunosuppressive environment of the genital tract, particularly the endocervix, which is rich in the cytokine TGFβ that downregulates T cell responses (Edwards and Butler, 2011). *N. gonorrhoeae* can also induce the upregulation of TGFβ production in

mouse models and inhibit T cell and B cell activity through Opa-CEACAM interactions manipulating the host response towards the innate immune system (Liu et al., 2011).

Major hurdles in the development of a vaccine for *N. gonorrhoeae* are the incomplete understanding of pathogenesis and absence of good model systems. The transcriptome of *N. gonorrhoeae* samples isolated from infected females differed significantly from that of bacteria grown *in vitro* (McClure et al., 2015). This demonstrates that unlike the case with *N. meningitidis, in vitro* serum bactericidal assays may not be sufficient to identify effective vaccines for *N. gonorrhoeae.* The best model system is human male challenge, but this can only represent the early stages of disease and the findings may not translate into female infections (Edwards et al., 2016). The involvement of different adhesins during colonisation of male and female hosts may mean that different antigens are available as targets. In addition, the stage of female reproductive cycle at the time of infection has been shown to affect the severity and outcome of the disease in mouse models, due to differing antibody responses and nutrient availability (Islam et al., 2015).

1.3 Resisting "nutritional immunity" through haem / iron acquisition

Iron is an essential nutrient for nearly all living organisms and the most common redox-active metal found in biological systems (Andreini et al., 2008). Iron-containing proteins participate in a wide variety of cellular processes, including DNA replication, transcription, and central metabolism. Iron levels and location are strictly regulated in the human body, as reactive oxygen species produced by the conversion of ferrous (Fe^{2+}) to ferric (Fe^{3+}) iron can cause damage to DNA, lipids and other proteins. This tight control over iron availability also plays a role in combatting infections by limiting access to this essential nutrient for pathogens in a process termed nutritional immunity.

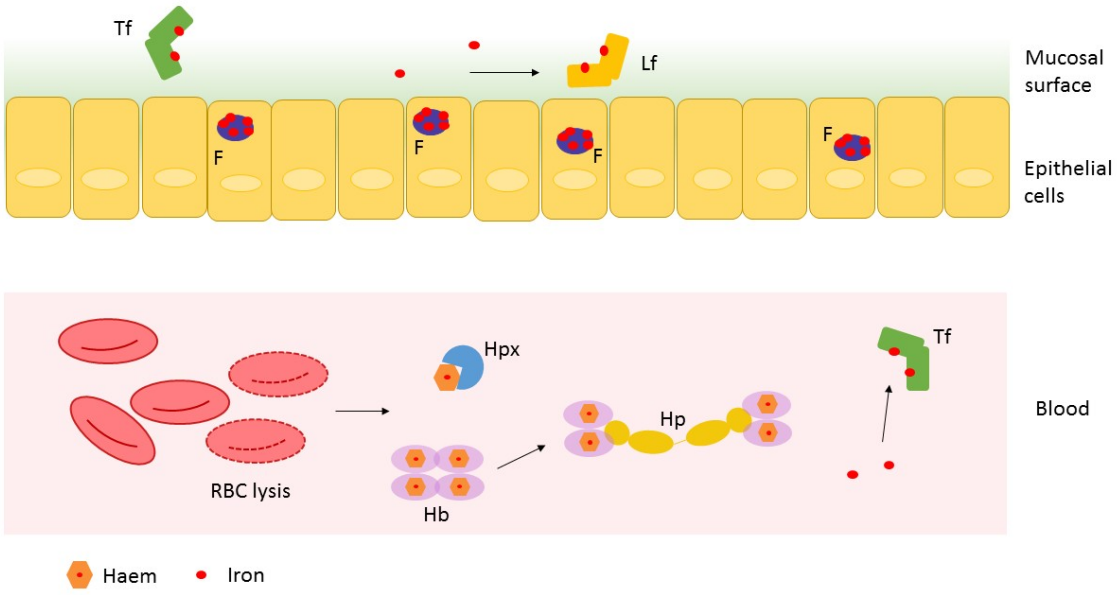

Figure 1.4 Iron limitation strategies in the human host
Fe^{3+} is stored intracellularly in the ferritin complex (F). At mucosal surfaces lactoferrin (Lf) and sometimes transferrin (Tf) sequester free iron. In the blood stream transferrin acts as an intercellular iron transporter and free iron scavenger. A large proportion of iron in the human body is in ferrous (Fe^{2+}) form in complex with haem, bound by haemoglobin (Hb) in erythrocytes (RBC). If Hb is released upon RBC lysis it is bound as a dimer by haptoglobin (Hp). Free haem is bound by haemopexin (Hpx). Figure based on Hood and Skaar with permission (Hood and Skaar, 2012).

Most iron in the human host is bound to the intracellular storage protein ferritin, or in complex with the tetrapyrrole haem (Pogoutse and Moraes, 2017). The majority of haem is present as a co-factor for the erythrocyte oxygen carrier protein haemoglobin. Free haem is also tightly controlled due to its own toxic nature and is bound by the protein haemopexin in the serum (Dyer et al., 1987). Haemoglobin released upon erythrocyte lysis is bound as a dimer by haptoglobin (Kristiansen et al., 2001). An overview of haem and iron limitation strategies at epithelial surfaces and in the blood stream can be seen in Figure 1.4.

Transferrin is found in the serum and its main function is to deliver iron to cells in a receptor mediated process. It can also be found in mucosal membranes, particularly during inflammation (Agarwal et al., 2005). It serves an additional function by binding free iron in the blood to protect the host from toxicity, and establishing a low-iron environment that is inhospitable for bacterial pathogens. Lactoferrin is closely related in sequence and structure to transferrin (Wally and Buchanan, 2007). It is found in secretions such as milk where it primarily functions as an iron scavenger and is not known to function in iron transport or delivery. Lactoferrin is also found in polymorphonuclear leukocyte granules and plays a role in mucosal immune responses by limiting local free iron concentrations (Ganz and Nemeth, 2015). Human transferrin and lactoferrin share around 60% sequence identity and their structures consist of two homologous domains termed the N-lobe and C-lobe which each bind one iron atom (Wally and Buchanan, 2007).

Restricting levels of inorganic iron and haem in body fluids and at surfaces plays a dual role in protecting the host, as in addition to preventing ROS damage to host tissues it combats infections by imposing nutritional immunity on pathogens and limiting their access to essential nutrients. As obligate human pathogens, *Neisseria* species have evolved various methods of scavenging iron and haem to overcome this immunity and establish infections.

1.3.1 Iron uptake systems in Neisseria - TonB dependent transporters

The outer membrane receptors involved in iron and haem acquisition belong to the TonB dependent transporter (TBDT) family. TBDTs are involved in the transport of

many essential nutrients in Gram-negative organisms, but the majority of those characterised are specific for iron complexes (Noinaj et al., 2010).

TBDT structures are highly similar despite their differing specificities, examples of the *Serratia marcescens* HasR haemophore receptor and *E. coli* FecA ferric citrate receptor are shown in Figure 1.5 (Krieg et al., 2009; Yue et al., 2003). The receptor consists of two domains, a transmembrane β-barrel of 22 antiparallel strands, and an N-terminal domain made up of a β-sheet and α-helices which folds inside the β-barrel to form a 'plug' (Cobessi et al., 2010; Krieg et al., 2009). The outer membrane loops vary between different types of TBDTs and give them their specificity. The N-terminal domain also contains the TonB box, a semi-conserved sequence usually around 9 amino acids long that interacts with the periplasmic TonB/ExbBD complex that provides energy for the translocation of substrates.

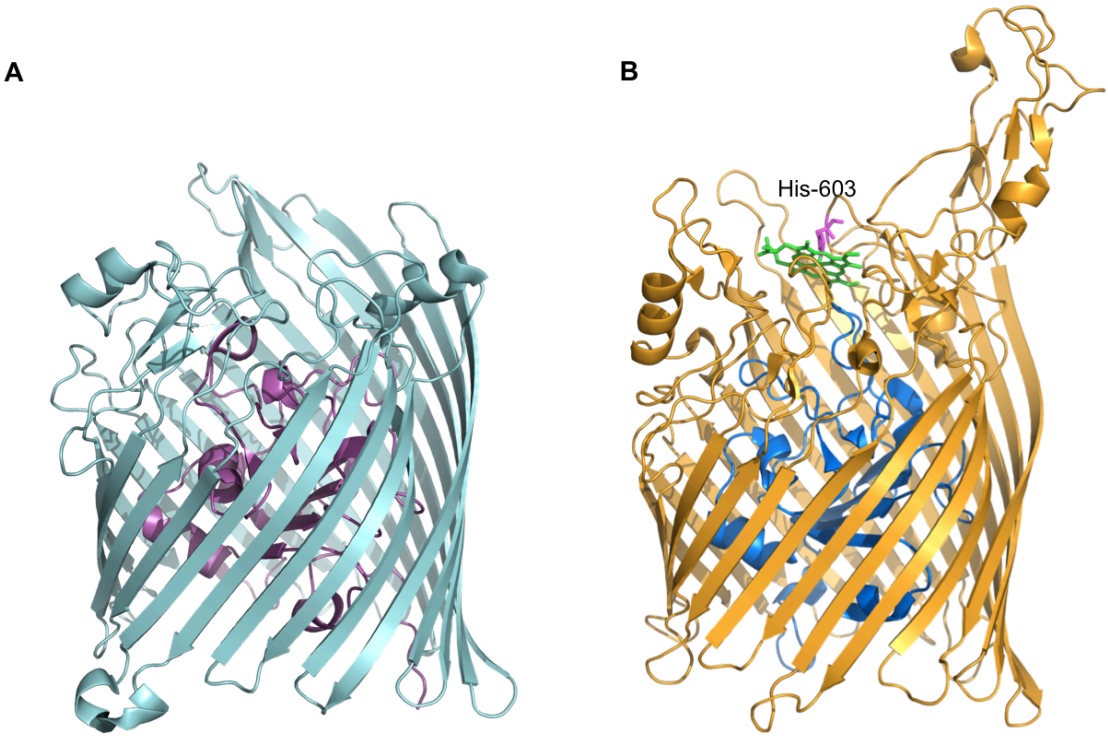

Figure 1.5 Examples of TonB dependent receptor structures
Cartoon representations of the crystal structures of two bacterial outer membrane receptors that share the classical TonB dependent receptor structure with 22 stranded β-barrel, a "plug domain and 11 extracellular loops. **A)** *E. coli* ferric citrate transporter FecA. The barrel domain is coloured cyan and the N-terminal plug magenta **B)** *Serratia marcescens* HasR haemophore receptor with haem (green sticks) bound to histidine 603 highlighted in pink. Figure created in Pymol using PDB files 1PO0 and 3CSL.

1.3.2 Transferrin and Lactoferrin receptors - TbpAB and LbpAB

The human glycoproteins lactoferrin and transferrin can both be used as an iron source by *Neisseria* species with very high efficiency (McKenna et al., 1988; Schryvers and Gonzalez, 1990). Iron is internalised in an energy dependent process and the human proteins do not enter the bacterial cell (McKenna et al., 1988). Transferrin is a readily available iron source for pathogens due to its extracellular location and transferrin receptors have been identified in many Gram-negative human and animal pathogens (Cornelissen, 2003; Otto et al., 1992).

Neisseria acquire transferrin and lactoferrin via "two-component systems" consisting of an outer membrane TonB dependent transporter protein and an associated surface lipoprotein. The transferrin receptor system contains outer-membrane protein TbpA and a surface-located lipoprotein TbpB, which is encoded adjacently upstream in the genome. TbpA is essential for transferrin utilization as mutants lacking this gene cannot survive when transferrin is the only iron source (Cornelissen et al., 1992). TbpB is not essential for transferrin utilization, but mutants lacking this gene only had around 50% efficiency of internalising iron from transferrin compared to wild type *in vitro* (Anderson et al., 1994).

N. meningitidis TbpA is a member of the TBDT family and in addition to the classical structural features it contains a long extracellular loop (loop3 – coloured orange in Figure 1.6) with a helix that inserts into the iron binding site of the C-lobe of human transferrin (Noinaj et al., 2012). This helix contains a conserved lysine reside which is thought to change the charges of residues within the binding site, causing the cleft to open and release the iron (Noinaj et al., 2012). The mechanism by which iron travels through the pore is unclear, but a conserved motif on the plug domain (Glu-Ile-Tyr-Glu, EIYE) is essential for transferrin utilisation and may bind directly to iron (Banerjee et al., 2012; Noto and Cornelissen, 2008).

The surface lipoprotein TbpB has a bi-lobed structure that is anchored into the membrane by a flexible N-terminal extension (Calmettes et al., 2012). The lobes each consist of an 8-stranded β-barrel and a β-"handle" subdomain (Figure 1.6 B). The structure of TbpB in complex with human transferrin shows that they interact extensively through residues in the TbpB N-lobe 'cap' region and the C-lobe of

transferrin (Calmettes et al., 2012). TbpB has greater affinity for holo-transferrin, and stabilizes this form through specific residues in the crystal structure, so could act to create a reservoir of iron-loaded transferrin near to the cell surface (Calmettes et al., 2012; Retzer et al., 1998). The mechanism of transfer between TbpB and TbpA is still very unclear. The anchor domain of TbpB is required for interaction with TbpA (Yang et al., 2011), and binding of holo-transferrin causes conformational changes that bring it into closer contact with TbpA (Noinaj et al., 2012). A stable ternary complex of TbpAB and transferrin can be isolated by size exclusion chromatography and has been visualised by negative staining electron microscopy (Noinaj et al., 2012), but there is disagreement about whether the receptor proteins can interact in the absence of transferrin.

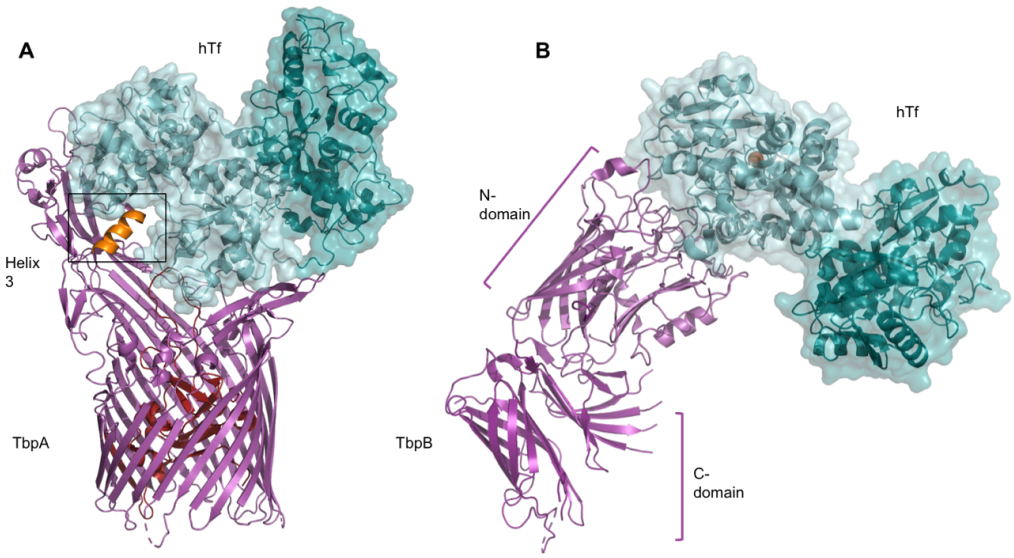

Figure 1.6 *N. meningitidis* transferrin receptor structures in complex with human transferrin.

A) Crystal structure of outer membrane receptor TbpA in complex with human transferrin represented in cartoon style. TbpA shares the classic family TBDT structure, with a 22 stranded β-barrel (pink) and N-terminal plug domain (dark red). TbpA binds the C-lobe of human transferrin (cyan) and the loop 3 helix (orange, highlighted in black box) inserts into the transferrin iron binding site opening the cleft and releasing the iron. **B)** Crystal structure of the bi-lobed TbpB protein. The N-domain interacts with the C-lobe of human transferrin (cyan). Iron is shown as brown sphere in Tf C-lobe binding site. Figure created with Pymol from PDB files 3V8X and 3VE1 (Calmettes et al., 2012; Noinaj et al., 2012)

The neisserial TbpAB receptors have binding specificity only for human transferrin protein (Schryvers and Gonzalez, 1990). Early studies showed mice injected with human transferrin suffered very high mortality rates when infected with *N. meningitidis* whereas normally the infection is rapidly cleared, indicating that iron acquisition from human transferrin is a prerequisite for colonization and pathogenesis (Schryvers and Gonzalez, 1989). Humanized mice expressing human transferrin have since been developed and used as a model for infection (Zarantonelli et al., 2007). However, findings from other models contradict this such as a mouse vaginal challenge where mutant TbpAB *N. gonorrhoeae* could successfully cause infection (Jerse et al., 2002).

The lactoferrin receptor LbpAB is an analogous system to TbpAB, with a TBDT LbpA and a surface lipoprotein LbpB. A homology model of LbpA has been produced based on TbpA and it shares the EIYE plug motif and the extracellular helix loop domain, indicating that release of iron from lactoferrin is achieved in the same way as from transferrin (Noinaj et al., 2013). LbpB is a bi-lobed lipoprotein and the structure of the N-lobe shows that it is very similar to TbpB, with an 8-stranded β-barrel and the β-"handle" subdomain, and that it interacts with holo-lactoferrin specifically through the N-lobe in a similar manner to TbpB and holo-transferrin (Brooks et al., 2014).

The lactoferrin receptor proteins may play a role in protection from host defences. In contrast to TbpB, LbpB is not always anchored into the membrane as it can be cleaved by NalP membrane protease (Roussel-Jazédé et al., 2010). This raises questions as to whether iron acquisition from lactoferrin is its primary function. LbpB contains unique loops rich in anionic residues that are absent from TbpB. These residues were demonstrated to be important in protection from antimicrobial peptides including lactoferricin, a proteolytic product of lactoferrin (Morgenthau et al., 2012). Recent evidence suggests that LbpB is able to bind lactoferrin at secondary sites on the LpbB C-lobe, and the lipoprotein could be selectively released by NalP cleavage at sites of inflammation as a protective measure to sequester excess lactoferrin (Ostan et al., 2017).

1.3.3 Haem transporters - HpuAB and HmbR

Neisseria encode two receptor systems capable of scavenging haem from human haemoproteins, HmbR and HpuAB. These systems allow *Neisseria* to utilize free haem, haemoglobin and haemoglobin-haptoglobin, but not haem bound to haemopexin or albumin (Dyer et al., 1987). Like the transferrin and lactoferrin receptor systems, HpuAB is a two-component system consisting of a surface exposed lipoprotein HpuA and a transmembrane TBDT receptor HpuB. Both components of this system are required for haem acquisition from haemoglobin (Hb) and haemoglobin-haptoglobin (Lewis et al., 1998). In contrast to previous studies, it has recently been demonstrated that the lipoprotein HpuA can bind directly to human haemoglobin (Rohde and Dyer, 2004; Wong et al., 2015). The structure of *Kingella denitrificans* (a closely related member of the *Neisseriaceae* family) HpuA has been solved in both its apo form and in complex with human haemoglobin (Wong et al., 2015). HpuA is a single-lobed protein that shares similar structure to the C-lobe of TbpB. A distinguishing feature is two long loops that have hydrophobic residues protruding from their distal ends. One monomer of HpuA interacts directly with a dimer of Hb, and the hydrophobic loops are important for this binding (Wong et al., 2015). These loops are subject to strong immune selection and as such there are no conserved haem binding motifs, but Hb binding is retained by the presence of hydrophobic residues (Harrison et al., 2013; Wong et al., 2015). According to the crystal structure of the complex, one of the haem groups in the Hb dimer would be held proximal to the membrane, possibly close to the HpuB pore to allow for easier binding. More detailed structure-function studies need to be carried out to understand how HpuA and B interact and work together to enable haem extraction and transport into the periplasm.

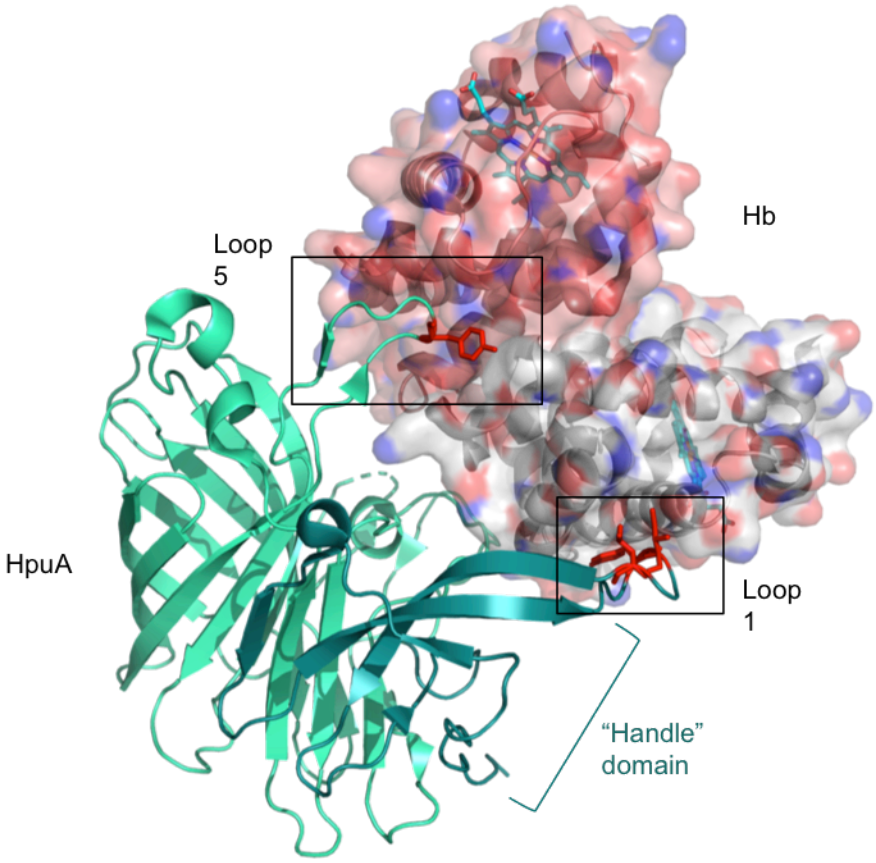

Figure 1.7 Crystal structure of *Kingella denitrificans* HpuA in complex with human haemoglobin Cartoon representation of the crystal structure of HpuA in complex with a dimer of haemoglobin (Hb). The "handle" domain of HpuA is shown in darker blue and the "barrel" domain in lighter green. The two long hydrophobic loops, loop 1 and 5, are highlighted in black boxes and the residues that interact with Hb are depicted as red sticks (Y60, I61, L64, Y272). Hb is bound so that one monomer containing a haem motif (blue sticks) is held proximal to the outer cell membrane, potentially to increase possibility of binding and uptake through HpuB. Figure created in Pymol using PDB file 5EE4.

N. meningitidis express a second TBDT haemoglobin receptor HmbR but this gene is degenerate in *N. gonorrhoeae* due to the presence of a premature stop codon (Jordan et al., 2005; Stojiljkovic et al., 1995). HmbR is thought to be a single-component receptor, as it is not co-transcribed with an upstream lipoprotein. Although no crystal structure is available for HmbR, topology modelling suggest that HmbR shares the common structural features of TBDTs, and several studies have identified important residues for haem binding and utilization that can help to build a picture of the mechanism (Evans et al., 2010; Mokry et al., 2014; Perkins-Balding et al., 2003).

Comparison of haem receptor sequences from many Gram-negative bacteria show that in addition to the TonB-box, two motifs FRAP and NPNL are highly conserved. An invariant histidine residue is also located between the two and both HpuB and HmbR share these features. The FRAP (Phe-Arg-Ala-Pro) and NPNL (Asn-Pro-Asn-Leu) motifs are likely to be important for haem extraction from haemoglobin, as HmbR mutants lacking them were able to bind Hb but not internalise the haem, whereas internalisation of free haem was not affected (Perkins-Balding et al., 2003). In addition to this, an intact N-terminal plug domain is essential for haem utilization, unlike haemoglobin receptors from other species (Perkins-Balding et al., 2003). The conserved histidine residue was not found to be essential for haem utilization in HmbR, and instead spectroscopic evidence suggests that Fe^{3+} in haem is co-ordinated by tyrosine ligands (Mokry et al., 2014).

No studies have been carried out to identify the important functional regions of HpuB, but as it shares 28% homology with HmbR including the FRAP and NPNL motifs it may extract and transport haem in a similar way. However, as HpuB can only utilize haem with the help of the lipoprotein HpuA there may be differences in binding sites and affinities that merit further investigation (Lewis et al., 1998).

The haem receptors appear to be especially important for *N. meningitidis* pathogenesis. Epidemiological studies indicate that at least one haem receptor is expressed in all disease isolates, and that HmbR is more likely to be present in disease isolates than carriage isolates (Harrison et al., 2009, 2013). *N. meningitidis* mutants lacking a functional HmbR were attenuated in an infant rat model (Stojiljkovic et al., 1995). However, a study using an *ex vivo* human whole blood model found no difference in the proliferation of *hmbR* mutant or wild type bacteria because they were growing in a transferrin dependent manner (Bidmos et al., 2015). This difference could be explained by the specificity of neisserial transferrin receptors for human transferrin, which would have prevented transferrin dependent growth in the rat model (Schryvers and Gonzalez, 1990).

1.3.4 (Liu et al., 2006)Other/Uncharacterised iron or haem specific TBDTs

Several putative TBDTs have been identified in neisserial genomes and named TonB-dependent-function (Tdf) proteins (Turner et al., 2001). TdfF is a 78 kDa TBDT, encoded downstream from a putative periplasmic iron transporter *fetB2*. This locus is only present in pathogenic strains of *Neisseria* (Turner et al., 2001). TdfF may be involved in intracellular iron acquisition, as *N. gonorrhoeae* mutants lacking TdfF were defective for intracellular survival, but could be rescued by the addition of excess iron (Hagen and Cornelissen, 2006). Expression of TdfF has only has been detected during growth in cell culture medium with serum and it is not thought to be directly iron regulated (Cornelissen and Hollander, 2011).

TdfG is a 136 kDa iron-repressed outer-membrane protein with homology to haemoglobin transporters (Jackson et al., 2010; Turner et al., 2001). This receptor is encoded by all gonococcal genomes but has not been annotated in any of the sequenced *N. meningitidis* genomes (Turner et al., 2001). *N. gonorrhoeae* TdfG knock out mutants retained the ability to use haem as a sole iron source, but as *Neisseria* are thought to have redundant haem utilization systems, further studies investigating different growth conditions are needed to identify the particular importance of TdfG.

TdfH is another large TBDT with features typical of haem transporters, however mutants with inactivated TdfH retained ability to utilize haem (Turner et al., 2001). Recent evidence suggests that it is instead involved in acquisition of zinc from the neutrophil produced zinc sequestering protein calprotectin (Jean et al., 2016). Another neisserial zinc receptor ZnuD was also implicated as a potential haem receptor, as it shares the FRAP/NPNL motifs specific to haem receptors and it is regulated by both zinc and iron availability (Turner et al., 2001). ZnuD expressed in a haem auxotroph strain of *E. coli* could support growth in the presence of haem and the protein could be captured on haemin agarose beads from membrane preparations (Kumar et al., 2012). However, the structural data does not support a role in haem utilization, as modelling shows that the potential binding site is too narrow to accommodate haem (Calmettes et al., 2015).

1.3.5 Siderophores

Siderophores are secreted small molecule iron chelators produced by a range of bacteria that can scavenge iron from the extracellular environment. They have high affinities for iron (III), allowing them to compete with transferrin and lactoferrin for free iron in the host (Boukhalfa and Crumbliss, 2002). Siderophore structures are diverse, but most co-ordinate iron in either a hydroxycarboxylate, catecholate, or hydroxamate dependent manner (Boukhalfa and Crumbliss, 2002). Although *Neisseria* do not produce their own siderophores they can utilize iron from the *E. coli* siderophore ferric-enterobactin through the TBDT receptor FetA (Carson et al., 1999). Other xenosiderophores have also been identified as substrates for FetA such as salmochelin and dihydroxybenzoylserin (DHBS) (Hollander et al., 2011). This method of hijacking siderophores from different species could be evolutionarily advantageous in the mucosal environment where there are many other co-colonising species, as *Neisseria* do not have to expend energy on producing their own siderophores (Barber and Elde, 2015).

1.3.6 Haemophores

Haemophores are secreted proteins that fulfil a similar role to siderophores but have a high affinity for haem and can acquire it from host haem proteins. The first haemophore identified was HasA from *S. marcescens,* which is expressed and secreted under iron limiting conditions (Letoffe et al., 1994). Haemophores have now been identified in many pathogenic Gram-negative species, and are functionally similar to either HasA or the *H. influenzae* HxuA haemophores (Gao et al., 2010; Ochsner et al., 2000; Rossi et al., 2001). No haemophore-mediated systems for haem uptake have been identified in *Neisseria* species to date.

HasA delivers haem to a TBDT haem transporter HasR (Ghigo et al., 1997) (Figure 1.8). HasR alone can support growth with haem or haemoglobin in a reconstituted *E. coli* system, but has a low efficiency of haem uptake and predicted low affinity for haem (Ghigo et al., 1997). The presence of HasA greatly assists haem acquisition from haemoglobin, and allows growth of the bacteria at lower concentrations (Ghigo et al., 1997). HasA type haemophores have been identified in *Pseudomonas aeruginosa, Yersinia pestis* and *Porphyromonas gingivalis,* and a receptor similar to HasR has been

identified in *Vibrio cholerae* (Gao et al., 2010; Mey and Payne, 2001; Ochsner et al., 2000; Rossi et al., 2001).

The structures of HasA both with bound haem (apo-HasA) and without (holo-HasA) show that the residues His32 and Tyr75 are directly involved in haem binding (Arnoux et al., 1999; Wolff, 2002) (Figure 1.8). Upon haem binding, loop 32 that contains the His32 axial ligand undergoes a significant conformational change and moves 30Å closer to the loop containing Tyr75, binding haem in a 'tweezer like' manner (Wolff, 2002). These two residues are exactly conserved in the HasA homologues in *Y. pestis* and *P. aeruginosa* (Ochsner et al., 2000; Rossi et al., 2001). HasA has also been observed to undergo domain swapping to form a stable complex with haem that cannot bind to HasR (Czjzek et al., 2007). This could function to store haem for later use or limit availability for competing bacteria.

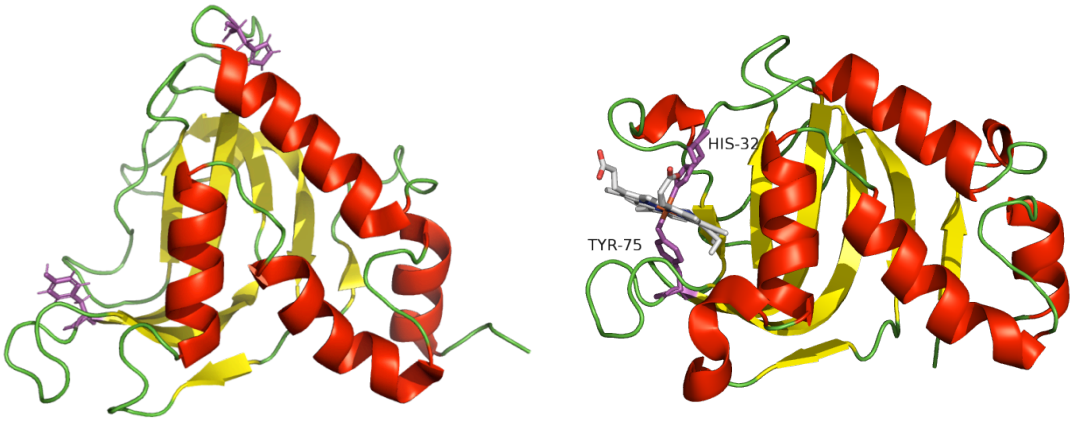

Figure 1.8 Crystal structure of *Serratia marcescens* apo-HasA (left) and NMR solution structure of holo-HasA (right). Upon haem binding loop 32, which contains histidine 32, undergoes a large conformational change to bring it closer to tyrosine 75. Secondary structure elements are colour coordinated, red α-helices, yellow β-strands and green loops. Axial ligand residues tyrosine 75 and histidine 32 are highlighted in magenta. The haem is represented as sticks and coloured according to elements grey (C) red(O) and orange (Fe). Pictures created using Pymol with PDB files 1B2V and 1YBJ.

The second class of haemophore found in Gram-negative bacteria is the HxuA-type. These are found only in the *Pasteurellaceae* genus, which includes the haem auxotrophic pathogen *H. influenzae* (Cope et al., 1994). Unlike HasA, HxuA does not

bind haem directly but instead binds to the host high affinity haem scavenging protein haemopexin, causing it to release free haem which can then be transported by the OM receptor HxuC (Cope et al., 1995, 1998). This effectively broadens the range of haem sources available to the pathogen. HxuA is expressed as part of a three-component system from the HxuCBA gene cluster. HxuC is the TonB dependent haem outer membrane receptor and HxuB is another β-barrel OM protein that is probably involved in HxuA secretion (Cope et al., 1995; Morton et al., 2007). The mechanism of action for the HxuCBA system is still relatively unclear. HxuA inactivates haemopexin so that haem is released into the local environment, but it is not known whether HxuA interacts with HxuC directly or how HxuA dissociates from haemopexin (Cope et al., 1998; Morton et al., 2007).

1.3.7 TonB energy coupling

Iron and haem import through TBDTs is an active process requiring energy harvested from the inner membrane of Gram-negative bacteria. This is achieved by coupling to the TonB protein complex that spans the periplasm and consists of three proteins, TonB, ExbB and ExbD (Higgs et al., 2002; Pawelek et al., 2006)(Higgs et al., 2002; Pawelek et al., 2006). ExbB and ExbD are located together in the inner membrane and contact the N-terminal transmembrane helix of TonB, while the globular C terminal domain of TonB directly contacts the TonB box of the outer-membrane receptors (Pawelek et al., 2006; Pawelek et al., 2006). Structural evidence shows that the TonB complex consists of a pentamer of ExbB, a dimer of ExbD and at least one TonB monomer (Celia et al., 2016). In this model one monomer of ExbD fits inside of the transmembrane pore created by the ExbB pentamer, the other ExbD sits next to this in the inner membrane and the two ExbD monomers dimerize through their periplasmic domain. TonB interacts with ExbD through the periplasmic domain to form a functional energy transducing complex (Celia et al., 2016). Energy is produced by movement of protons through the ExbB pore from the periplasm to the cytoplasm, possibly facilitated by movement of ExbD within the pore in a rotational or “piston-like” motion (Celia et al., 2016). The interaction of TonB with ExbD allows transduction of energy to the outer membrane transporter through conformational changes in TonB (Ollis et al., 2012).

The structure of the TonB C-terminal domain (CTD) in complex with the *E. coli* ferrichrome outer-membrane receptor FhuA shows that an inter-protein β-sheet is formed between the TonB box consensus sequence of FhuA (^{8}TITVTA^{13}) and the CTD β-sheet of TonB (Pawelek et al., 2006; Pawelek et al., 2006). This indicates that protein-protein interactions are important in energy transduction to the outer membrane receptor. Substrate binding to outer membrane receptors can initiate conformational changes and modulate TonB-OMR interactions. The structure of *Shigella dysenteriae* haem receptor ShuA indicates that the TonB box is hidden until haem binding causes a conformational change to allow interaction with TonB and energy harvesting (Cobessi et al., 2010). Kinetic studies showed similar substrate modulation of TonB interactions in *Serratia marcescens* HasR (Lefèvre et al., 2008). Modelling studies suggest that upon interaction with the TonB box, TonB can exert a downward force, partially unfolding the plug domain of the TBTD and allowing passage of the substrate through the pore and into the periplasm (Chimento et al., 2005; Gumbart et al., 2007).

Specific TonB homologs that participate in haem/iron acquisition have been identified. The *S. marcescens* HasR receptor has a dedicated energy transducing complex called HasB, and the structure of its periplasmic domain reveals a unique fold and a slightly different recognition sequence on HasR than the conventional TonB box (de Amorim et al., 2013; Paquelin et al., 2001). The fold shares more structural similarity with the TolA protein in Gram-negative bacteria than TonB (de Amorim et al., 2013), and this suggests that there could be more specific TonB homologues that have not yet been identified in bacterial genomes due to divergent sequence or structural features.

Crystallographic studies have produced conflicting solutions for TonB complex and receptor structures, especially regarding conformation of the TonB box and interacting regions where it is shown in a variety of conformations from disordered to ordered (Noinaj et al., 2010). This reflects the idea that this is a dynamic interaction involving different energy states that cannot be accurately captured by crystallographic methods (Ghosh and Postle, 2005). As the TonB box is an essential part of the TBDTs it is important to understand its conformation and dynamics during substrate transport. To meet this aim, (Ferguson et al., 2002; Pawelek et al., 2006; Yue et al., 2003) novel methods should be developed to allow structures to be verified and mechanisms and

binding kinetics to be studied accurately. A novel approach to studying TonB dependent receptors was demonstrated in a 2014 study where FhuA was incorporated into nanodiscs, a membrane mimetic in a detergent free system (Mills et al., 2014). Kinetic data from this experiment suggested that FhuA had significantly weaker affinity for TonB than in detergents, and that the structure of the TonB box could be affected by detergents (Mills et al., 2014).

1.3.8 TonB independent transport

Some studies have found that neisserial mutants lacking *tonB/ExbBD* can still utilize haem or siderophores as iron sources, pointing to the existence of TonB-independent mechanisms for their uptake (Desai et al., 2000; Stojiljkovic and Srinivasan, 1997; Strange et al., 2011). The type IV secretion system (T4SS) encoded by some strains of *N. gonorrhoeae* on the gonococcal genetic island (GGI) has been implicated in iron uptake, as it supports iron-dependent intracellular survival of TonB mutants (Zola et al., 2010). The mechanism by which this occurs is unclear but it is not dependent on the secretion of DNA - one of the main functions of the T4SS (Zola et al., 2010). It is possible that iron could be entering through the T4SS pore, similar to the way that the type IV pili component PilQ allows some passive transport of iron across the outer membrane (Chen et al., 2004). Alternatively the type IV SS could secrete another factor that liberates free iron intracellularly, or allow the bacteria to occupy a particular iron rich niche that is not accessible otherwise (Ramsey et al., 2011).

Neisseria may encode redundant TonB like systems, similar to the HasB complex from *S. marcescens* that specifically interacts with haem uptake receptors (Paquelin et al., 2001). There is a putative TonB homologue encoded on the GGI called *yfd,* however this was not found to be essential for intracellular survival in the absence of TonB (Hamilton et al., 2005; Zola et al., 2010).

1.3.9 Periplasmic transport

After iron or haem complexes have been transported through the outer membrane they are ferried across the periplasmic space and inner membrane by ABC (ATP binding cassette) transport systems. These are ATP dependent systems that consist of a periplasmic binding protein (PBP), a transmembrane permease and a lipoprotein that binds ATP (Wilks and Burkhard, 2007).

Ferric iron extracted from lactoferrin or transferrin is transferred from the outer membrane receptors to the periplasmic binding protein FbpA, part of the FbpABC transport system (Chen et al., 1993). FbpA has been shown to bind directly to TbpA during transfer of the ferric iron (Siburt et al., 2009). After iron binding FbpA loses affinity for TbpA and is released into the periplasm and associates with the transmembrane permease FbpB, which transports iron into the cytoplasm using energy derived from hydrolysis of ATP by FbpC.

Transport of haem through the periplasm and into the cytoplasm is FbpABC independent in *Neisseria* (Khun et al., 1998). Haem specific periplasmic binding proteins have been identified in many Gram-negative bacteria and several crystal structures have been solved. They share a conserved fold with other class III PBPs, with an N- and C-domain connected by a single helix and a substrate binding cleft between the two domains (Ho et al., 2007; Mattle et al., 2010; Naoe et al., 2017). Other than a conserved tyrosine that coordinates haem in all of the structures, the haem binding pocket varies considerably between homologues. The *Yersinia pestis* (HmuT), *Burkholderia cenocepacia* (BhuT) and *Roseflexus sp.* RS-1 (RhuT) haem PBPs crystallised with two haem molecules bound in the substrate binding cleft, whereas *S. dysenteriae* ShuT and *P. aeruginosa* PhuT only bound one haem (Ho et al., 2007; Mattle et al., 2010; Naoe et al., 2017).

There are several uncharacterised putative ABC transporter systems annotated in the neisserial genomes but functional characterisation will have to be carried out to identify the haem specific system due to low sequence homology between species. The periplasmic binding protein specific for the siderophore ferric enterobactin is FetB, encoded adjacently downstream of the receptor FetA (Biegel Carson et al., 1999). A putative *fetB* paralogue is encoded upstream from TdfF and annotated as *fetB2,* this may also be involved in iron or haem transport across the periplasm (Turner et al., 2001).

1.3.10 Downstream treatment of haem

Upon entering the cytoplasm haem must be quickly processed due to its potential toxicity. Cytoplasmic haem binding proteins exist in some bacteria, such as *Shigella* ShuS and *P. aeruginosa* PhuS, that are likely to bind haem in a non-toxic form allowing

transfer to haem degradation or haem-containing proteins (Lansky et al., 2006; Wyckoff et al., 2005)(Lansky et al., 2006; Wyckoff et al., 2005). No cytoplasmic haem binding homologues have been identified in *Neisseria* species but they do encode a homologue to the mammalian haem oxygenase enzyme (*hemO*). Pathogenic *Neisseria* mutants lacking *hemO* could not grow with haem as the sole iron source (Zhu et al., 2000a). The neisserial haem oxygenase shares around 20% homology with the human enzyme and they have a similar overall fold with a conserved histidine ligand that binds haem (Schuller et al., 2001). Haem oxygenase liberates iron by cleaving the haem pyrrole ring to generate the linear tetrapyrrole biliverdin, carbon monoxide and free iron. Free iron is sequestered by the intracellular storage protein bacterioferritin or incorporated into bacterial enzymes.

Neisseria can incorporate intact exogenous haem into its own haemoproteins, as haem biosynthetic mutants are able to survive when haem or haemoglobin is supplied in the growth media, but the mechanism by which this occurs is still unknown (Turner et al., 1998). The question of whether haem is imported by bacterial pathogens mainly for use as an iron source or for direct for incorporation into bacterial haem proteins has not been the subject of many studies. Radiolabelling experiments in *Bacillus subtilis* and *Staphylococcus aureus* showed that exogenous haem is incorporated into cytochromes and found associated with the cytoplasmic membrane (Schiött et al., 1997; Skaar et al., 2004).

1.3.11 Regulation of haem/iron uptake systems

To minimize cytotoxic damage and conserve energy, most pathogens implement strict control over expression of iron and haem acquisition systems during infection. Several studies have identified genes that are regulated in response to iron in both *N. meningitidis* and *N. gonorrhoeae* (Ducey et al., 2005; Grifantini et al., 2003; Jackson et al., 2010; Yu et al., 2016). Exact numbers of genes regulated by iron varies according to identification methods, but 233 genes have been identified in *N. meningitidis* (Grifantini et al., 2003) and between 158 and 300 in *N. gonorrhoeae* (Jackson et al., 2010; Yu et al., 2016).

Many iron-regulated genes are controlled by the ferric uptake regulator (Fur). Genes under this control have a conserved Fur box sequence in their promoters, which is the

nATwATnATwAT (n = any base, w = A or T) repeat sequence in *Neisseria* species, similar to those in other bacteria (Grifantini et al., 2003). The Fur protein has been well established as an iron responsive transcriptional repressor. When Fur is complexed with Fe in plentiful iron conditions, it forms a homodimer that binds to the DNA Fur box and prevents RNA-polymerase (RNAP) binding and transcription. However, in poor iron conditions most Fur molecules will not be in complex with iron and return to monomeric from that cannot bind to the Fur box, shifting the equilibrium in favour of polymerase binding and transcription (Figure 1.9) (reviewed in Troxell and Hassan, 2013).

Genome wide expression studies have shown that some genes are upregulated in response to iron replete conditions in a Fur dependent manner (Ducey et al., 2005; Grifantini et al., 2003; Jackson et al., 2010; Yu et al., 2016). The majority of these genes encode proteins involved in respiration and energy metabolism and this is consistent with an increase in growth rate in iron replete conditions (Jackson et al., 2010). Fur has been shown to induce gene expression in a variety of ways, indirectly through the regulation of small regulatory RNA (sRNA) expression, directly by blocking binding of another repressor, or binding to regulatory DNA sequences that promote RNA polymerase association (Yu and Genco, 2012). A pool of iron-responsive sRNAs has been identified in *N. gonorrhoeae*, some of which are regulated by the Fur-repressible sRNA NrrF (Jackson et al., 2017). Together these findings show that the number of Fur regulated proteins is much larger than can be identified from the presence of Fur-box promoters as many are regulated indirectly and subject to fine tuning at the post-transcriptional level.

In *N. meningitidis* the MisR/S two-component regulatory system has been shown to regulate *HmbR, hemO* and *TdfH* expression independently of Fur (Tzeng et al., 2008; Zhao et al., 2010). In *N. gonorrhoeae TbpA* and *TbpB* were also found to be under control of MisR/S, which can both activate and repress transcription of these genes (Kandler et al., 2016). Two component systems function by sensing environmental stimuli and transducing the signal into the cell, allowing bacteria to adapt to different niches. MisR is an inner membrane phosphokinase protein and MisS is a cytoplasmic transcriptional regulator. Only four two-component systems have been identified in

Neisseria, fewer than generally found in proteobacteria (Kandler et al., 2016). The environmental stimuli for MisR/S are unknown, it has been implicated in Mg^{2+} sensing, but could respond to multiple signals to compensate for the fewer two-component systems found in *Neisseria* species (Newcombe et al., 2005). The MisR/S system is required for infection of lower genital tract mouse model and controls a wide variety of genes (Gangaiah et al., 2017).

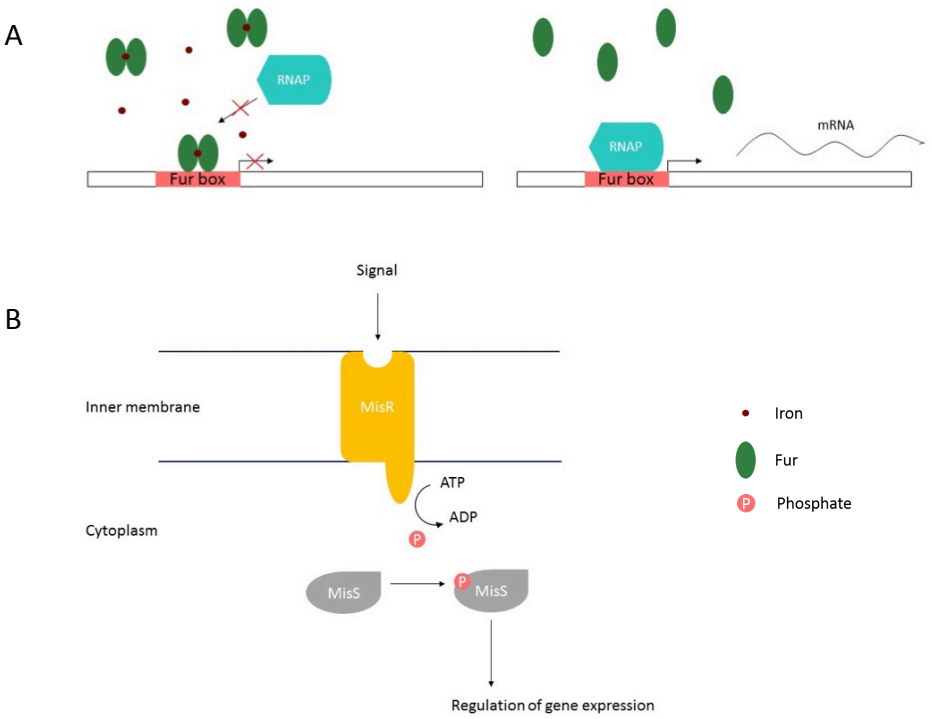

Figure 1.9 Regulation of gene expression by Fur repression and the MisR/S two component system.
A) Under iron replete conditions, iron enables the dimerization of Fur. The dimer associates with the Fur box sequence preventing RNA polymerase (RNAP) association with promoter sequences and transcription. At lower iron concentrations, Fur is found in monomeric form that does not bind to the Fur box, allowing access for RNAP and transcription. Figure based on (Troxell and Hassan, 2013) **B)** The MisR/S two-component regulatory system regulates several haem/iron uptake systems independently of Fur. An as yet unidentified signal is transduced through the inner membrane by activity of MisR, a transmembrane phosphokinase that phosphorylates the transcriptional regulator MisS via hydrolysis of ATP.

There may be other uncharacterised mechanisms for controlling haem/iron utilization system expression. For example, *N. meningitidis* mutants lacking the Sel-1 like repeat protein NMB0419 displayed decreased expression of several proteins including HmbR, TbpAB, LbpAB, FetA and TonB/ExbBD, and were consequently deficient in using

haemoglobin or transferrin as a sole iron source (Li et al., 2017). This protein is predicted to have a periplasmic or extracellular location so it is not directly a transcriptional regulator, but it could play a role in sensing environmental conditions and possibly interact with a two-component regulatory system to counteract the Fur repression system.

In addition to the above mechanisms where gene expression is regulated by environmental stimuli, *Neisseria* modify expression of many genes by phase variation. Genes subject to phase variation contain either poly(G) or poly(C) repeats in their promoter regions or open reading frames that are subject to slipped-strand mispairing during DNA replication. This can cause frame-shift mutations that cause the protein to be constitutively expressed "ON" or not "OFF". Populations of colonising strains contain bacteria with genes in the phase ON and OFF and this can allow them to quickly adapt to changing environmental niches. In *Neisseria meningitidis hmbR* and *hpuA* and *fetA* are regulated by phase variation (Carson et al., 2000; Lewis et al., 1999). The *fetA* gene contains a poly(C) region in the promoter region and expression can be switched between a high and low expression level (Carson et al., 2000). Poly(G) tracts are located within the *hpuA* and *hmbR* open reading frames and control expression in an ON/OFF manner.

1.4 Haem biosynthesis in Neisseria

In addition to being a potential iron source, haem is an essential compound that is required as a prosthetic group for proteins. The majority of haem-containing proteins are involved in oxidative metabolism or sensing and synthesis of other gases including carbon monoxide and nitric oxide (Gilles-Gonzalez and Gonzalez, 2005). Many Gram-negative human pathogens synthesise haem to fulfil their requirements via a multi stage pathway, which is shown in Figure 1.10. The final stage of the pathway requires the insertion of iron into the porphyrin ring by an enzyme called ferrochelatase. The iron must be acquired from the host and this links iron availability and expression of receptor systems to haem biosynthesis. All the enzymes involved in the classical porphyrin biosynthesis pathway are annotated in the published *N. meningitidis* and *N. gonorrhoeae* genomes (listed in table 1.1) but none of the gene products have been studied biochemically.

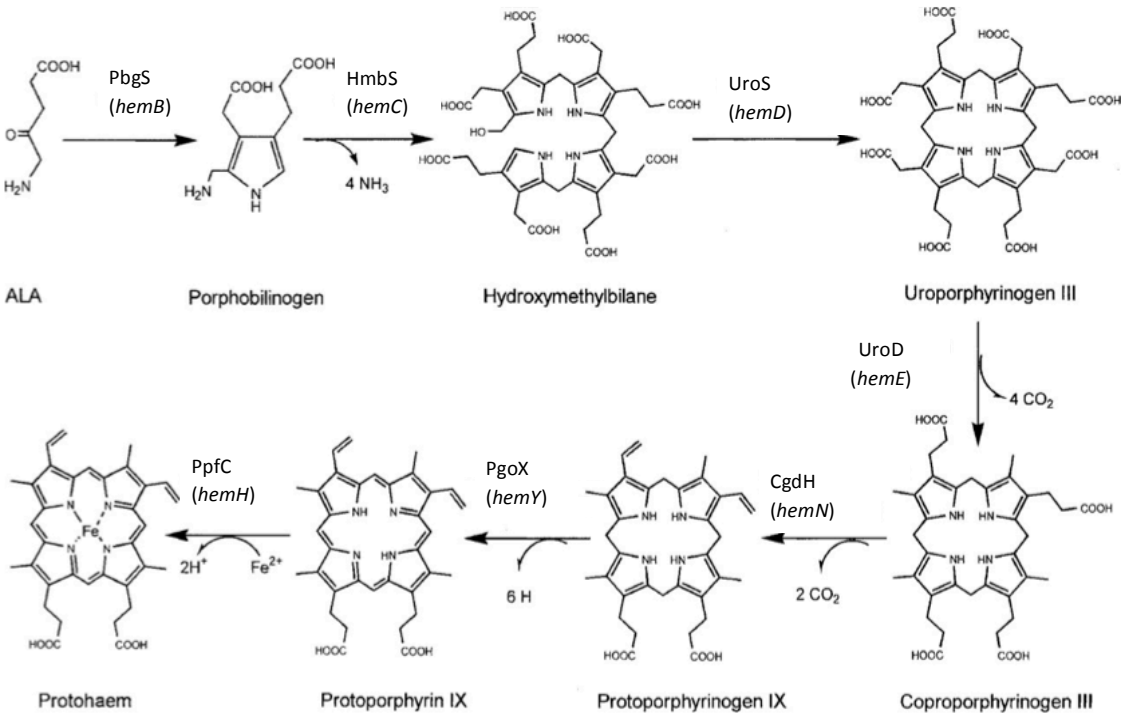

Figure 1.10 Overview of the Classical haem biosynthesis pathway from 5-aminolevulininc acid (ALA) to protohaem. The core tetrapyrrole biosynthesis pathway shared by all organisms known to carry out biosynthesis consists of the enzymes PbgS, HmbS and Uros that produce the first cyclic intermediate uroporphyrinogen III. The biochemical stages following this in the "Classical" pathway are conserved between Gram-negative bacteria and eukaryotes but the enzymes catalysing the reactions differ between organisms. The abbreviated protein names are shown and the genes annotated in *Neisseria* are provided in brackets. See table 1.1 for full enzyme names. Reproduced from Panek and O'Brien, copyright permission granted (Panek and O'Brian, 2002).

Table 1.1 classical porphyrin biosynthesis pathway enzymes, abbreviations and gene names

Enzyme name	Abbreviation	Gene
Glutamyl-tRNA reductase	GtrR	*hemA*
Glutamate-1-semialdehyde-2,1-aminomutase	GsaM	*hemL*
Porphobilinogen synthase	PbgS	*hemB*
Hydroxymethylbilane synthase	HmbS	*hemC*
Uroporphyrinogen III synthase	UroS	*hemD*
Uroporphyrinogen decarboxylase	UroD	*hemE*
Coproporphyrinogen dehydrogenase	CgdH	*hemN*
Protoporphryinogen oxidase	PgoX	*hemY*
Protoporphryinogen ferrochelatase	PpfC	*hemH*

1.4.1 Bacterial porphyrin biosynthesis

The first committed tetrapyrrole biosynthesis pathway intermediate is 5-aminolevulininc acid (ALA). *Neisseria* species, like most bacteria, synthesise ALA from glutamyl-tRNA in a two-step processes named the C_5 pathway. The two enzymes, glutamyl-tRNA reductase (GtrR) and glutamate-1-semialdehyde-2,1-aminomutase (GsaM), catalyse the release of glutamate-1-semialdehyde (GSA) from glutamyl-tRNA and subsequent conversion to ALA (Jahn et al., 1992). GtrR is a dimeric enzyme with an unusual asymmetric V-shape and biochemical and structural evidence show that GtrR and GsaM form a complex (Lüer et al., 2005; Moser et al., 2001; Nogaj and Beale, 2005; Zhao et al., 2014). GsaM is a more compact globular dimer, which sits in the middle of the V-shaped GtrR so that their active sites are within close proximity, allowing channelling of the unstable GSA intermediate (Ge et al., 2010).

Following this, ALA enters the "core" tetrapyrrole pathway, which consists of three enzymes that are conserved across all tetrapyrrole producing species - porphobilinogen synthase (PbgS), hydroxymethylbilane synthase (HmbS) and uroporphyrinogen III synthase (UroS). These enzymes catalyse the conversion of ALA to uroporphyrinogen III, the first cyclic intermediate in the tetrapyrrole pathway.

PbgS has two ALA binding sites and catalyses the condensation of two ALA molecules to form the monopyrrole porphobilinogen (PBG). It is found as a homo-octamer and requires metal for activity, but the specific ions needed and their binding sites differ between organisms (Jaffe, 2000). Animal and yeast PbgS homologues bind zinc in their active site but this is not the case for prokaryotes, which are either magnesium or potassium dependent (Jaffe, 2000; Petrovieh et al., 1996). Examination of the *N. meningitidis* MC58 *hemB* sequence (NP_273584.1) shows that it contains an aspartate rich metal binding site in the active site, along with an allosteric magnesium binding site. Biochemical characterisation will be required to determine the metal specificity of the neisserial PbgS active site.

The next enzyme in the pathway HmbS forms the linear tetrapyrrole hydroxymethylbilane from four monomers of PBG. This enzyme is also known as porphobilinogen deaminase, as it deaminates PBG and releases ammonia during catalysis. The structure of *E. coli* HmbS was the first to be solved and has three

domains with a dipyrromethane co-factor covalently attached to a conserved cysteine residue in domain three, forming the active site in the cleft between the domains (Louie et al., 1996; Louie GV, Brownlie PD, Lambert R, Cooper JB, Blundell TL, Wood SP, Warren MJ, Woodcock SC, 1992). Structures of the human, *Arabidopsis* and several Gram-negative bacteria have been solved and all share very similar overall fold and active site conformation (Azim et al., 2014; Moynie et al., 2013; Roberts et al., 2013; Song et al., 2009). The co-factor forms a covalent bond with the PBG substrate during the elongation of the pyrrole chain and enzyme-intermediate complexes can be isolated with between 1 and 4 PBG substrates attached (Jordan et al., 1988). Radiolabelling showed that the PBG monomers are attached in a sequential fashion. The dipyrromethane co-factor is assembled from two monomers of the substrate PBG, and the HmbS apo-enzyme can generate its own co-factor (Shoolingin-Jordan et al., 1996).

The final conserved enzyme in the core tetrapyrrole pathway is uroporphyrinogen III synthase (UroS), which joins the first and fourth pyrrole ring of HMB to generate the cyclic intermediate uroporphyrinogen III (uro'gen III). In this reaction the D-ring of HMB (the fourth PBG monomer added) is flipped so that the acetate and propionate side chains are in the opposite position compared to the other three rings (Jordan, 1991). HMB can cyclize non-enzymatically without flipping the D-ring to form the metabolically inactive uroporphyrinogen I isomer, therefore UroS has a very high turnover rate to ensure that the majority of HMB is funnelled into uroporphyrinogen III (Tsai et al., 1987).

UroS homologues have been identified in the genome sequences of almost all organisms that carry out tetrapyrrole biosynthesis, however they share relatively low sequence homology. For example, the *E. coli* and *Bacillus subtilis hemD* genes share only 25% identity (Panek and O'Brian, 2002). Site directed mutagenesis studies have failed to identify any residues essential for activity in all homologues. A tyrosine residue (Y166) was found to abolish enzyme activity in *Synechococcus elongatus* but only reduced activity to 50% in the human enzyme (Mathews et al., 2001; Roessner et al., 2002).

Crystal structures of the human and two bacterial UroS homologues have been solved and they share remarkable structural homology despite low sequence conservation (Mathews et al., 2001; Peng et al., 2011; Schubert et al., 2008). They show that the protein is composed of two domains connected by a double stranded β linker, with a large active site cleft positioned between the two. Comparisons of the crystal structures show that the linker is flexible and may adopt different conformations during catalysis, as the structure of *Thermus thermophilus* UroS in complex with the product shows a more condensed conformation (Schubert et al., 2008). This structure also shows that most hydrogen bonding of the tetrapyrrole product is with main chain NH groups, and only three active site residue side chains form hydrogen bonds with the A ring of the substrate (Lys141, His165, and Gln194) but none are totally conserved (Schubert et al., 2008). The enzyme-product structure suggests a mechanism where the A and B ring of the substrate are held rigidly in place by hydrogen bonds between their acetate, propionate and carboxylate groups and enzyme main chain and side chains, leaving the C and D rings with more flexibility to allow for the conformational changes during inversion of D ring.

Further information about UroS function can be gained from the study of naturally occurring polymorphisms in the human population. Defects in human UroS function cause the rare autosomal recessive disease congenital erythropoietic porphyria. A variety of mutations can be responsible for this but one, C73R, accounts for around 40% of cases (Frank et al., 1998). Biochemical characterisation showed that this mutation along with several other common disease-causing variants did not reduce enzyme activity *in vivo* but instead disrupt residues that form part of an α-helix that is key for stability (Fortian et al., 2009).

Together the structural and biochemical characterisation of UroS homologues suggest that instead of the enzyme possessing any specific catalytic residues its overall structure provides a favourable environment for the formation of the uro'gen III isomer over the uro'gen I isomer. The structural fold seems to be the most important requirement for activity, and this is retained between the homologues despite considerable variation in primary sequence.

For haem synthesis the product of UroS (uro'gen III) undergoes several side group modifications to become protoporphyrin IX, to which ferrous iron (Fe^{2+}) is added by ferrochelatase (*hemH*) to form protohaem (Panek and O'Brian, 2002). The pathway from uro'gen III to protohaem is conserved between eukaryotes and Gram-negative bacteria and termed the "classical" pathway (Figure 1.10). Until recently the classical pathway was thought to be conserved in all organisms, however whole genome studies have challenged this and it is now known that archaea and Gram-positive prokaryotes possess alternative pathways that contain sirohaem and coproporphyrin precursors respectively which branch off after the three core stages of the conversion of ALA to uroporphyrinogen III (Bali et al., 2011; Kühner et al., 2014; Lobo et al., 2015).

Even though the classical pathway intermediates are conserved, the enzymes and mechanisms that carry out each stage can differ between organisms depending on whether they carry out the reactions in an oxygen dependent or independent manner (Dailey et al., 2017). Genes encoding the enzymes uroporphyrinogen decarboxylase (*hemE*), coproporphyrinogen dehydrogenase (*hemN*), protoporphyrinogen oxidase (*hemY*) and protoporphyrinogen ferrochelatase (*hemH*) have been annotated in all the sequenced neisserial genomes.

1.4.2 Regulation of haem biosynthesis

Due to the toxic nature of haem and its precursors such as protoporphyrin IX, it is expected that haem biosynthesis is tightly controlled in all organisms. It would be reasonable to hypothesise that as iron is a limiting nutrient and essential for completing the haem biosynthesis pathway, that this pathway may be regulated in response to iron availability. This has only been observed in some *alphaproteobacteria* where the iron response regulator (irr) represses transcription of many haem biosynthesis genes in low iron conditions. In high iron conditions, irr binds to ferrochelatase, where it is either degraded or inactivated by the presence of haem (Hamza et al., 1998).

Unlike haem acquisition systems, the haem biosynthesis pathway does not seem to be under the control of the iron-responsive Fur repressor in *Neisseria* as no Fur-box sequences were identified upstream of these genes (Grifantini et al., 2003). No changes in the transcription or expression of haem biosynthesis genes in response to

iron availability have been detected in *Neisseria* species (Basler et al., 2006; Ducey et al., 2005; Grifantini et al., 2003; Jackson et al., 2010).

In many organisms the key pathway step that is regulated is the biosynthesis of ALA by GtrR and GsaM. Overexpression of GtrR in *E. coli* results in ALA and porphyrin accumulation and addition of haem to cell extracts decreases the activity of the enzyme (Chen et al., 1996; Javor and Febre, 1992). Haem availability also regulates *Salmonella enterica* GtrR activity, where the enzyme is destabilised by allosteric haem binding and subsequent proteolytic degradation (Wang et al., 1999). Recent data produced from affinity purification and mass spectrometry experiments studying the human haem biosynthesis pathway suggests the existence of a mitochondrial "metabolon" which could help to regulate synthesis and tie it to iron availability (Medlock et al., 2015). This complex may consist of the final two enzymes of the pathway protoporphyrin oxidase and ferrochelatase and the first enzyme aminolevulinic acid synthase-2, along with iron transport proteins and other iron metabolism proteins (Medlock et al., 2015). This lends further support to the idea that ALA synthesis is a rate-limiting step that could be regulated in response to haem synthesis by ferrochelatase. A further advantage of this complex also includes protection from the reactive species porphyrins and free iron, as imported iron can be immediately incorporated into haem. Complex formation between the haem biosynthesis enzymes in prokaryotes has not been studied, except for the interaction of GsaM and GtrR in the C_5 pathway, but they may exist and serve a regulatory function or facilitate channelling of reactive intermediates.

The mechanisms employed to regulate haem biosynthesis in prokaryotes are diverse and findings in one species cannot be broadly applied. It will require focused genetic and biochemical studies to elucidate the mechanisms used by *Neisseria* species.

1.4.3 Haem biosynthesis and pathogenesis

The contribution of haem synthesis to the pathogenesis of *Neisseria* is essentially unstudied. There is limited *in vitro* evidence suggesting that haem biosynthesis is important for neisserial intracellular survival. Turner *et al*. showed that *N. gonorrhoeae* Δ*hemA* and Δ*hemH* mutants had reduced intracellular survival but grew normally in liquid culture supplemented with either haem or haemoglobin, as they had functional

haem uptake systems (Turner et al., 1998). This suggests that *Neisseria* are unable to obtain haem from within epithelial cells, perhaps due to the specificity of the OM receptors for haemoglobin, which is not a major haemoprotein in epithelial cells.

In *Staphylococcus aureus,* mutants lacking *hemA* or *hemB* display a small colony variant phenotype and this has been shown to inhibit colonisation of certain tissues including the heart and liver in murine models (Von Eiff et al., 1997; Hammer et al., 2013). Additionally, genome wide *in vivo* studies have identified haem biosynthesis genes as being important for fitness and pathogenesis in a number of species (Palace et al., 2014; Skurnik et al., 2013; Wang et al., 2014). These experiments highlight the differing requirements for haem biosynthesis according to specific niche or stage of infection, for example *hemY* mutants in *P. aeruginosa* were defective at colonising the gastrointestinal tract but the gene is not essential in other niches (Skurnik et al., 2013).

Overall these studies suggest that haem biosynthesis is important for the fitness of pathogens, but that its significance may vary according to the specific niche or stage of infection. There may be some niches where haem requirements can be satisfied fully by acquisition of host haem and others where the pathogen must rely on biosynthesis.

Many aspects of neisserial haem uptake and biosynthesis are still not understood such as, how exogenous haem is transported from the periplasm, whether there are any more uncharacterised haem uptake systems, whether all the annotated haem biosynthesis genes are functional and how haem biosynthesis is regulated. Proteins involved in iron and haem acquisition are potentially interesting candidates for vaccine targets due to their surface exposed location and importance for survival. However, a more complete understanding of their expression and regulation is required to advance this field of study.

1.5 The *gly1* locus

The *gly1* (gonolysin 1) locus was identified in a screen for *N. gonorrhoeae* toxins and named due to the haemolytic ability of *E. coli* expressing the genes when grown on blood agar plates (Arvidson et al., 1999). This was mapped to two open reading frames, a 420 bp gene (*ORF1*) and 741 bp gene (*ORF2*) that begins 38 nucleotides downstream of the *ORF1* stop codon. Lack of any clear promoter sequences upstream

of *ORF2* suggests that the genes may be co-transcribed. Subsequent work in our group using high-stringency southern blotting has shown that *ORF1* is highly conserved in several *N. gonorrhoeae*, *N. meningitidis* and *N. lactamica* strains (Meadows, 2005).

The ORF1 gene encodes a 140 amino acid protein with an N-terminal signal sequence that is predicted to target the protein to the periplasm. Expression of the ORF1 protein product was detected in the outer membrane fractions of *N. gonorrhoeae* at low levels (Arvidson et al., 1999). The *gly1* locus was determined to be non-essential *in vivo* for growth in liquid and solid culture (Arvidson et al., 1999). Surprisingly, *N. gonorrhoeae* mutants lacking this locus displayed increased toxicity towards the epithelial layer in human fallopian tube cultures (Arvidson et al., 1999). Some studies have identified *gly1ORF1* as being upregulated on contact with epithelial cells, due to the presence of the Contact Regulatory Element of *Neisseria* (CREN aka Rep2) upstream in the promoter region (Deghmane et al., 2003; Morelle et al., 2003). Despite this, expression of Gly1ORF1 is not essential for meningococcal or gonococcal adhesion or invasion of epithelial cells *in vivo* (Deghmane et al., 2003; Morelle et al., 2003; Sathyamurthy, 2011).

ORF1 does not share any homology with any genes outside of the *Neisseriaceae* and *Kingella* genera and no function has been assigned to any homologues in the databases. Genome database searches using the PSI-BLAST algorithm have identified potential distantly related homologues in a range of Gram-negative species. This putative protein family is characterised the presence of a periplasmic targeting signal sequence, a disulphide bond between residues at the N and C- termini, and predominantly β-sheet predicted secondary structure (McMellon, 2016). The ORF2 gene product shares some homology with *E. coli hemD* protein product Uroporphyrinogen III synthase (UroS), sharing 28% identity over 75% of the sequence (e value = 3e-13, residues 8-199). In *Neisseria* genomes these two open reading frames are positioned directly upstream of three other putative haem biosynthesis genes *hemX, hemY* and *hemE*. These factors led to speculation that the locus could be involved in haem utilization or metabolism. As Gly1ORF1 is potentially secreted or outer membrane associated, it was assayed for haem binding ability and was shown to

be able to bind to both haemin- and haemoglobin- agarose beads in pull down assays (Sathyamurthy, 2011; Wierzbicka, 2014).

A *Δgly1ORF1* mutant was created in *N. meningitidis* MC58 by insertion of an erythromycin resistance cassette into the ORF1 gene (Sathyamurthy, 2011). Growth experiments in minimal media suggested that unlike the wild type this mutant could not grow when haem or haemoglobin were the only available iron sources. There was no detectable growth defect in the mutant in rich media or when iron was supplied in the form of ferric nitrate.

A yeast two-hybrid screen using human cDNA identified erythrocyte band protein 4.2 (EPB4.2), a major component of the erythrocyte cytoskeleton, as a potential interacting partner of Gly1ORF1 in the host (Meadows, 2005). Fluorescently labelled Gly1ORF1 interacted with a mouse cell line expressing human EPB4.2 whereas it did not adhere to the mock transfected cells (Sathyamurthy, 2011). This interaction has not been confirmed using purified EPB4.2, possibly due to misfolding of the recombinant protein produced from an *E. coli* expression system (Wierzbicka, 2014).

As a surface exposed antigen, Gly1ORF1 has also been investigated as a potential vaccine candidate. Serum bactericidal assays have demonstrated that *N. meningitidis* MC58 was significantly more sensitive to complement-mediated killing upon addition of anti-Gly1 antibodies (Sathyamurthy, 2011; Wierzbicka, 2014). The *N. gonorrhoeae* homologue was recently identified in an *in silico* hierarchical screen for potential universal vaccine candidates for gonococcal disease due to the fact that it is highly conserved (Jain et al., 2016).

1.6 Project aims

Complete characterisation of the *gly1* locus and its potential role in haem homeostasis and resisting nutritional immunity is important, considering the threat of multidrug resistance gonorrhoea and the urgent need for novel treatments and prophylactics.

This work set out to explore the following hypotheses:

- Gly1ORF1 is a haem binding protein involved in scavenging host haem to combat nutritional immunity

- The gene *gly1ORF2* encodes the neisserial Uroporphyrinogen III synthase enzyme

The aims of the project were to:

- Optimize methods to enable biophysical characterisation of Gly1ORF1/ haem interactions and improve structural data
- Express and purify the *gly1ORF2* gene product and carry out structural, biochemical, biophysical and functional characterisation
- Investigate the function of each gene in the *gly1* locus *in vivo* in *N. gonorrhoeae* through the creation of single and double knock out mutants and analysis of resulting growth phenotypes.

Chapter 2. Materials and Methods

2.1. Bacterial strains and culturing conditions

2.1.1 *Escherichia coli*

Table 2.1. *E. coli* strains used in this study

Strain	Genotype	Source
K-12 M72	*ac*(am) *trp*(am) *rpsL* λ *c*I857 Δ*H*1 *bio*252	O'Connor and Timmis, 1987
BL21 Star™ (DE3)	F⁻ *omp*T *hsd*S_B (r_B^-, m_B^-) *gal dcm rne*131 (DE3)	Invitrogen
SASZ31	F⁻ *hisG1 xyl-7 hemD31 metE46 mobA2 ΔargH1 rplL9 thiE1*	Chartrand et al., 1979
XL1-Blue	*recA1 endA1 gyrA96 thi-1 hsdR17 supE44 relA1 lac* [F′ *proAB lacIq ZΔM15* Tn*10* (Tet^r)].	Stratagene

E. coli strains were grown in LB broth: 10 g/L tryptone (Oxoid) 5 g/L yeast extract (Oxoid) 5 g/L NaCl or for expression, 4YT: 32 g/L tryptone 5 g/L yeast extract 5 g/L NaCl. Agar plates were made using the above recipes with the addition of 15 g/L agar (Oxoid). For plasmid selection ampicillin was added to a final concentration of 100 µg/ml.

Strain SASZ31 was shipped from the Coli Genetic Stock Centre, Yale on a sterile filter paper disc. It was aseptically placed onto a brain heart infusion (BHI), 0.5% yeast extract and 0.2% glucose (all Sigma) agar plate. A drop of LB media was used to rehydrate the disk and a sterile loop was used to streak out liquid and obtain single colonies.

2.1.2 *Neisseria gonorrhoeae*

N. gonorrhoeae strain MS11 was grown on Columbia agar plus chocolate horse blood plates either purchased from Scientific Laboratory Supplies or made using 39 g/L Columbia agar base (Merck), autoclaved and cooled to 55°C, supplemented with 5% horse blood, heated to 80°C to lyse blood cells. For some transformations and

experiments GCB plates were used made to the following recipe: Proteose peptone No. 3 (BD Biosciences, NJ, USA) 15.1 g/L, Corn Starch 1.01 g/L, K_2HPO_4 4.03 g/L, KH_2PO_4 1.01 g/L, NaCl 5.03 g/L, agar 11.32 g/L, 1% Vitox (Oxoid). Kanamycin was used for selection of transformants at 80 µg/ml.

Liquid culture for *N. gonorrhoeae* transformation was GCBL media (Proteose peptone No. 315 mg/ml, K_2HPO_4 4 mg/ml, KH_2PO_4 1 mg/ml, NaCl 5mg/ml) and rich media for growth was BHI broth, 0.5% yeast extract, 0.042% sodium hydrogen carbonate.

Chemically defined media for *N. gonorrhoeae* (GC CDM)

Stock solutions:

Solution 1: Sodium chloride 58.45 g, potassium sulphate 10 g, magnesium chloride 2.18 g, ammonium chloride 2.2 g, EDTA 0.03 g in 250 ml H_2O

Solution 2: Potassium phosphate (dibasic) 17.42 g, potassium phosphate (monobasic) 13.61 g in a final volume of 100 ml H_2O

Solution 3: L-aspartic acid 1.0 g, L-glutamic acid 2.6 g, L-arginine HCl 0.3 g, glycine 0.05 g, L-serine 0.1 g, L-leucine 0.18 g, L-isoleucine 0.06 g, L-valine 0.12 g, L-tyrosine 0.14 g, L-cysteine 0.11 g, L-cystine (dissolved in 1 M HCl) 0.08 g, L-alanine 0.2 g, L-lysine 0.1 g, L-proline 0.1 g, L-tryptophan 0.16 g, L-threonine 0.1 g, L-phenylalanine 0.05 g, L-asparagine.H_2O 0.05 g, L-glutamine 0.1 g, L-histidine 0.05 g, L-methionine 0.03 g, glutathione (reduced form) 0.1 g in a final volume of 500 ml H_2O

Solution 4: Thiamine HCl 0.02 g, calcium pantothenate 0.019 g, thiamine pyrophosphate chloride (cocarboxylase) 0.0048 g in 100 ml with H_2O

Solution 5: Biotin 0.015 g in 50 ml 50% ethanol

Solution 6: Calcium chloride dihydrate 0.37 g, iron (III) nitrate nonahydryate 0.04 g in 10 ml H_2O

Hypoxanthine solution: Hypoxanthine 0.25 g, 0.1 M NaOH aqueous 50 ml

Phenol red solution: 1 mg in 100 ml H_2O

All filter sterilised and stored at room temperature except solution 3 stored at 4°C.

Make up of final media per 100 ml: 2.5 ml Solution 1, 2 ml Solution 2, 25 ml Solution 3, 1 ml Solution 4, 1 ml Solution 5, 0.1 ml Solution 6 (substitute with alternative iron sources as necessary), 1 ml hypoxanthine solution, 1 ml phenol red solution, 10 mM

glucose, 2 mM lactate, 10 mM sodium hydrogen carbonate. Adjust to pH 7.0 with 1 M sodium hydroxide.

2.2. Electrophoretic methods

2.2.1 SDS-Polyacrylamide gel electrophoresis

A 10% resolving gel was prepared using 4.5 ml deionised water (dH_2O), 3.3 ml 30% (w/v) acrylamide, 2 ml 500 mM Tris Bicine pH 8.3, 100 µl 10% (w/v) sodium dodecyl sulfate (SDS), 50 µl ammonium persulphate (100 mg ml-1) and 16 µl N,N,N',N'-tetramethylethylenediamine (TEMED). The stacking gel was made up of 1.5 ml 250 mM TrisHCl (pH 6.9), 1 ml deionised water, 0.5 ml 30% (w/v) acrylamide, 30 µl 10% (w/v) SDS, 20 µl ammonium persulphate and 10 µl TEMED. Once the resolving gel was set the stacking gel was poured on top and a comb inserted to form the sample wells. The loading buffer used in all SDS-PAGE experiments unless stated otherwise consisted of 2 ml 10% (w/v) SDS, 2 ml glycerol, 5 ml 250 mM Tris pH 6.9, 1 ml water and 0.05% bromophenol blue. Dithiothreitol (DTT) crystals were added to fresh aliquots before adding to sample for reducing SDS-PAGE. To visualise protein separation gels were stained with Coomassie blue solution (0.2% Coomassie Brilliant Blue R solution, 40% methanol, 10% acetic acid).

2.2.2 Agarose gel electrophoresis

Plasmid DNA was separated using 1% (w/v) agarose gels. Agarose powder was dissolved in TAE buffer (40 mM Tris, 20 mM acetic acid, 1 mM EDTA) by boiling then allowed to cool slightly before adding ethidium bromide to a final concentration of 0.5 µg/ml. The solution was poured into a plate, a comb inserted to form the sample wells and allowed to set. For electrophoresis the gel was inserted into a tank and covered with 1x TAE and samples run at 4 V cm^{-1}. Samples were visualised using a UV trans-illuminator.

2.2.3 Western blot

Gly1ORF1 protein was detected by western blotting. Protein samples were separated by SDS PAGE (section 2.2.1) then the gel was washed in transfer buffer (2.9 g Tris, 1 g glycine, 100 ml methanol, volume adjusted to 500 ml with dH_20) for 15 minutes. The proteins were transferred onto nitrocellulose membrane in a semi-dry transfer cell (Biorad) at 10 V for 60 minutes. After transfer the membrane was soaked in blocking

buffer (PBS-Tween with 5% (w/v) skimmed milk powder) for one hour at room temperature or overnight at 4°C. The membrane was washed in PBS-T for 30 minutes at room temperature then probed with the primary antibody in PBS-T 1% (v/v) skimmed milk powder for 1 hour at room temperature. Excess antibody was removed by washing with PBS-T for 30 minutes before probing with the secondary antibody conjugated to HRP in PBS-T 1% (v/v) milk powder for 1 hour. The membrane was again washed in PBS-T for 30 minutes the proteins were detecting using Pierce ECL Western Blotting substrate (Thermo Scientific) and visualised using a BioRad ChemiDoc XRS+ imaging system.

2.3 Cloning

For cloning genes for recombinant protein overexpression in *E. coli* specific primers were designed with restriction enzyme sites at the 5' ends. Several additional bases were added to the 5' end to ensure efficient restriction enzyme activity.

Table 2.2 Name, sequence and description of DNA primers used in this study

Name	Description	Sequence 5'-3'	Restriction enzyme Site
NM_HemD_RBS_F	*N. meningitidis* (NM) HemD forward, optimized RBS	AATGAATTCAAGAGGAGAAAACATATGGAAACAGCGAAACCCGTCATGCT	EcoR1
NM_HemD_R	NM HemD reverse, double stop codon	AAAAAAGCTTATTATTAATTTGAGGTTCCGGGAAAGACCAT	HindIII
NM_Dbl_F	forward for Gly1ORF1 and ORF2 NM	AATAAAGAATTCCGCCCTATGTGTTGCCCTAA	EcoR1
NM_NTORF1_F	NM ORF1 forward	TTTCGAATTCTAAGGAAATACGATGAA	EcoR1
NM_NTORF1_R	NM Non-tagged ORF1 reverse, double stop	AAAAAGCTTATTATTAGGAAAAATCGTCATCGTTG	HindIII
NM_HemC_F	NM HemC forward	AAATAGAATTCAACGCATTGAACATGAACCCGA	EcoR1
NM_HemC_R	NM HemC reverse, double stop	CCCAAGCTTATTATTAATTTTCCGTATTCAATACTGCTCCA	HindIII
NM_2_CHIS	NM C terminal(6x)His tag ORF2	AAAAAGCTTTTAATGGTGATGGTGATGGTGGCTCCCATTTGAGGTTCCGGGAAAGAC	HindIII

NM_2_NHIS	NM N-terminal(6x)His tag ORF2	AAATGAATTCCACCATCATCACCACCATGG CTGCATGGAAACAGCGAAACCCGTC	EcoR1
NM_ HemC_CHIS	NM C-terminal(6x)His tag HemC	AAAAAGCTTTTAATGGTGATGGTGATGGT GGCTCCCATTTTCCGTATTCAATACTG	HindIII
OEP_NG_Gly1F1	*N. gonorrhoeae* (NG) to clone DNA fragments to create mutants	GGACGTAAACCCAAAGGCG	N/A
OEP_NG_Gly1KanR1	NG as above	AAGCTGTCAAACATGAGAACCAAGGAGA ATTGAACTTCTATGTATTTGTTGTTGTCCG	N/A
OEP_NG_Gly1KanF2	NG mutant creation	GAATTGTTTTAGTACCTAGCCAAGGTGTG CCCGTGACTCATACGGAAAGC	N/A
OEP_NG_Gly1R2	NG mutant creation	GCAAGGCATTCATCAGAAAATCCC	N/A
OEP_NG_HemDF1	NG mutant creation	GTTTCAACCATTAAGGAAAT	N/A
OEP_NG_HemDKanR1	NG mutant creation	AAGCTGTCAAACATGAGAACCAAGGAGA ATGCTGTTTCCATCGCCTTATC	N/A
OEP_NG_HemDKanF2	NG mutant creation	GAATTGTTTTAGTACCTAGCCAAGGTGTG CGGAACAGTCTGCCCGAAGG	N/A
OEP_NG_HemDR2	NG	GGAATGTGTACTTCTGTTTCG	N/A
KanF	Amplifying Kan^R cassette forward	ATTCTCCTTGGTTCTCATGTTTGACAGCTT AT	N/A
KanR	Amplifying Kan^R cassette reverse	GCACACCTTGGCTAGGTACTAAAACAATT CAT	N/A
Q5SDM_Gly1_stop_F	Deletion of *gly1ORF1* start codon in puc18 forward primer	TAATTCCTTTCTGCCGTATTG	N/A
Q5SDM_Gly1_stop_R	Deletion of *gly1ORF1* start codon in puc18 reverse primer	TTACGTATTTCCTTAATGGTTG	N/A
NGGly1Fwd	NG *gly1ORF1* forward cloning/PCR screening	GGAATTCCTCAACACACAGGACGACACA	EcoRI
NGGly1Rvs	NG *gly1ORF1* reverse cloning/PCR screening	CCCAAGCTTGGGCGCTGTTTCCATCGCCTT AT	HindIII
NGHemDFwd	NG *gly1ORF2* forward cloning/PCR screening	GGAATTCCGCGGATAAGGCGATGGAAAC	EcoRI

NGHemDRvs	NG *gly1ORF1* reverse cloning/PCR screening	CCCAAGCTTGGGTGATGCCTGTATCTCGC GTA	HindIII
NGHemInt	NG Internal sequencing primer for gly1 locus	GTCAGTCCGGCCGCCGTTGA	N/A
NGglyInt	NG Internal sequencing primer for gly1 locus	GACAGGTGGCAAGGCATGGGCA	N/A

2.3.1 PCR amplification from genomic DNA

Genes of interest were amplified from *N. meningitidis* MC58 genomic DNA using primers shown above and KAPA hot start PCR readymix (Roche). PCR cycles were optimized for the T_m of the primers and the length of the target sequence. PCR products were analysed by agarose gel electrophoresis and bands of the correct size were excised and purified using a Monarch® DNA Gel Extraction Kit (New England Biolabs) or directly from the PCR mix using a Monarch® PCR/DNA Clean Up Kit (New England Biolabs) if only one band of the correct size was present on the gel.

2.3.2 Preparation of plasmid DNA

Plasmids used for protein overexpression in this study are pJONEX4 (containing a phage Lambda leftward promoter, λP_L) (Sayers and Eckstein, 1991), and pET21a (+) (containing a T7 promoter) (Novagen®). The cloning vector pUC18 was used for genetic complementation experiments in *E. coli* (Norrander et al., 1983). *E. coli* storage strains containing plasmids were streaked onto selective LB agar and a single colony was used to inoculate 3-5ml of LB/ampicillin and incubated overnight at an appropriate temperature. Plasmid purification was carried out using a Monarch® Plasmid Miniprep Kit (New England Biolabs) following the manufacturer's instructions.

2.3.3 Site directed mutagenesis Q5

Site directed mutagenesis was carried out using NEB Q5 site directed mutagenesis kit (New England Biolabs) following the manufacturer's instructions. Primers were designed using the NEB Base changer tool (https://nebasechanger.neb.com/) that replaced a 12 bp section at the start of Gly1ORF1 with a double stop codon. This included the start codon of the gene and a second ATG codon 10 bp downstream to

ensure that there would be no gene expression. Primers used for mutagenesis were Q5SDM_Gly1_stop_F and Q5SDM_Gly1_stop_R (see table 2.2) and PCR cycle times were used as suggested by the Base Changer tool.

2.3.4 Restriction digests

Restriction enzymes (NEB and Promega) were used to create complimentary ends on plasmid and insert DNA. Typically, 100 ng DNA and 1 unit enzyme were incubated for at least one hour at optimum temperature in 20 µl reaction volume. Restriction digests were analysed by agarose gel electrophoresis and the cut products were excised from the gel and purified using Monarch® DNA Gel Extraction Kit.

2.3.5 Ligation

Plasmid and insert DNA with complimentary sticky ends were mixed in 1:1, 1:3 and 3:1 molar ratios. Ligation reactions were carried out using T4 DNA ligase (Promega). The ligation mixture was placed in a beaker of ice overnight on the bench top so that the ice melted. This allows the optimum temperatures for annealing and ligation to be achieved successively. The enzyme was heat inactivated at 65°C for 20 minutes.

2.3.6 Preparation of chemically competent *E. coli* cells

The required strain of *E. coli* was streaked onto an agar plate and incubated overnight at the appropriate temperature. A single colony was picked to inoculate a 3 ml LB culture and grown overnight at the appropriate temperature. Overnight cultures were used to seed at 1:100 dilution in fresh LB as required and cultures were grown until A_{600nm} was approximately 0.4. The cells were harvested by centrifugation 1811 x *g* for 20 minutes at 4°C and the supernatant was discarded. Cells were resuspended in 30 ml ice cold sterile 0.1 M $CaCl_2$ then harvested again at 1811 x *g* for 20 minutes at 4°C and the supernatant discarded. The cells were resuspended by gently pipetting in 5 ml ice cold sterile 0.1 M $CaCl_2$ to make a smooth suspension then topped up with 35 ml 0.1 M $CaCl_2$. The suspension was left on ice for 60 minutes the harvested by centrifugation at 1811 x *g* for 20 minutes at 4°C. The supernatant was poured off and the cells were completely resuspended in 6 ml ice cold 15% glycerol/ 85 mM $CaCl_2$ by gentle pipetting. Cells were aliquoted into pre-chilled tubes and stored at -80°C.

2.3.7 Transformation

Either 1 ng of purified plasmid DNA or 5 µl ligation reaction was added to 100 µl competent *E. coli* cells in ice-cold tubes and gently mixed then incubated on ice for 60 minutes. The cells were then subjected to heat shock at 42°C for 30 seconds. Following addition of 400 µl LB media the cells were incubated at 37°C for 10 minutes then pelleted by centrifugation at 12225 x *g* for 5 minutes. The supernatant was removed and the cells were resuspended in the remaining 50 µl then plated onto LB agar plates with appropriate antibiotics. When transforming M72 cells with the pJONEX4 plasmid, the heat shock and 37°C incubation steps were omitted and the cells were incubated at ~ 22 -30°C.

2.4 Methods for creating and analysing *N. gonorrhoeae* mutants

Linear DNA constructs of around 2500bp were created by overlap extension PCR from 3 smaller PCR products. The constructs contained the kanamycin resistance cassette flanked by two regions of NG genomic DNA sequence >500 bp long. The >500 bp sequences were homologous to the genomic regions flanking the area to be replaced with the kanamycin resistance cassette. These regions contained at least one copy of the *Neisseria* DNA uptake sequence (DUS) atGCCGTCTGAA which is required for successful natural transformation of *Neisseria* (Goodman and Scocca, 1988).

2.4.1 Amplification of genomic DNA from NG

The PCR steps were carried out using KAPA HiFi Hotstart polymerase with cycle steps and concentrations of template DNA and primers optimized for each individual reaction. The kanamycin resistance cassette was amplified from a storage plasmid using the primers *KanF* and *KanR* (See table 2.2).

2.4.2 Overlap extension PCR

The two PCR products containing the flanking genomic sequences and the PCR product containing the kanamycin cassette were mixed in a 1:1:1 ratio along with the KAPA hot start PCR readymix. The primers were added to a final concentration of 5 pmol (from 100 pmol stock). PCR cycles were optimised for each reaction to generate sufficient product. The constructs were purified using a Monarch® DNA Gel Extraction Kit and quantified using a NanoDrop 1000 spectrophotometer.

After purification and sequencing, the constructs were inserted into the pCR^{TM}4Blunt-TOPO© vector using the Zero Blunt® TOPO© PCR Cloning Kit for Sequencing following the manufacturer's instructions and used to transform Top10 competent cells.

2.4.3 Transformation of NG

N. gonorrhoeae strain MS11 grown for 48 hours on GC agar plates supplemented with 1% Vitox (Oxoid) were re-suspended in 250 µl pre-warmed GCBL to an absorbance A_{600}= 0.2. The ~2500 bp PCR products (500 ng in a maximum volume of 20 µl TE buffer) were added to the cell suspension and incubated at 37°C, 5% CO_2 for 4 hours in a loose lid Bijou container. A control transformation of TE buffer alone was carried out simultaneously. The cells were plated onto GC agar (1% Vitox) supplemented with 80 µg/ml kanamycin, or chocolate agar supplemented with 80 µg/ml kanamycin for the Δ*hemD* and double mutants, and incubated at 37°C in 5% CO_2 for 24 – 48 hours.

Transformants were picked and resuspended in 30 µl TE buffer and boiled at 95°C for 15 minutes. 2.5 µl of this was used as template for PCR screening using the primers, NGGly1Fwd, NGGly1Rvs NGHemDFwd and NGHemDRvs (see table 2.2). PCR products were subsequently sequenced using the same primers to confirm that the kanamycin cassette insertions were successful. Mutants with the correct sequence were re-streaked onto selective media and then used to make glycerol stocks which were stored at -80°C.

2.4.4 Preparation of iron sources for use in growth assays

Haemin solution was purchased from Jena Bioscience as 0.25% (w/v) porcine haemin in 50% triethanolamine and was used at 7 µM final concentration. A 125 µM stock of human haemoglobin (Sigma) was prepared by dissolving in H_2O and was used at a 5 µM final concentration. A 12.5 µM stock of human holo-transferrin (Sigma) was prepared by dissolving in 1x PBS and used at 2.5 µM final concentration. All solutions were sterilised by passing through a 0.2 µm filter before use.

2.4.5 *N. gonorrhoeae* growth assays

To assess growth phenotypes of the mutants in liquid media, MS11 strains were streaked from freezer stocks onto GCB plates (1% Vitox) or chocolate agar plates and grown for 18-24 hours at 37°C in 5% (v/v) CO_2. Colonies were scraped from plates and

suspended in PBS then pelleted by centrifugation at 2000 x *g* for 2 minutes, then resuspended in appropriate media (GCCDM plus supplements or BHI plus supplements). This suspension was used to inoculate fresh media with the appropriate supplements to an optical density of A_{540} = 0.1. Cultures were grown at 37°C with constant shaking, and growth was monitored by absorbance at 540 nm at 2 hour time points.

Specific growth rates (μ) were calculated from absorbance (A) measurements in the logarithmic growth phase using the following equation where t = time in hours:

$$\mu = \frac{lnA_2 - lnA_1}{t_2 - t_1}$$

2.4.6 Iron disk assay

The MS11 strains were streaked from freezer stocks onto GCB plates (1% Vitox) and grown overnight at 37°C in 5% (v/v) CO_2. Colonies were scraped from plates and suspended in GCCDM without an iron source and diluted to optical density of A_{540} = 0.1 and 100 µl was spread onto GCB plates (1% Vitox) supplemented with 50 µM deferoxamine mesylate (Sigma, from a 50 mM stock prepared in sterile H_20). Sterile filter paper disks (6 mm diameter) were soaked with 10 µl haemin (7 µM) or haemoglobin (10 mg/ml) solution or sterile PBS and placed on top of the agar plates. The plates were incubated face up at 37°C in 5% (v/v) CO_2 for 24 hours.

2.4.7 Hydrophobic agent sensitivity plate assays

Colonies grown overnight on GCB plates were suspended in warm GCBL media and diluted to A_{540}=0.1. This solution was spread onto GCB (1% Vitox) plate and allowed to dry. Filter paper disks soaked in 10 µl haemin (7 µM), erythromycin (1.25 µg), Triton X-100 (1% v/v in H_20) solutions and control disks soaked in 1 x PBS were placed on top of the plates and the plates were incubated face up at 37°C in 5% (v/v) CO_2 for 24 hours. Plates were photographed and the diameter of the zone of inhibition was measured using ImageJ software.

2.4.8 Lysozyme sensitivity assay

Sensitivity of live *N. gonorrhoeae* wild type and Δ*gly1* was assessed using the method of Humbert *et al.* (2017) with modifications. Strains grown overnight on GCB (1% Vitox)

plates were resuspended in GCBL (1% Vitox, 0.042% sodium bicarbonate) then diluted in the same media 1:100 and grown for 2 hours at 37°C with shaking. The cultures were then diluted into GCBL (1% Vitox, 0.042% sodium bicarbonate) to OD_{540}= 0.2 with or without 10 µg/ ml recombinant human lysozyme (Sigma) and grown for 7 hours at 37°C with shaking. Cultures were serially diluted and plated onto GCB (1% Vitox) plates and incubated at 37°C in 5% (v/v) CO_2 for 18-24 hours. Colonies on the plates were counted and the fold change in colony forming units (CFU) between the cultures with human lysozyme (N) and without human lysozyme (N_0) using the equation N_0/N for each strain.

2.5. Recombinant protein overexpression in *E. coli*

2.5.1. Small scale expression using heat inducible system

A single colony from a freshly streaked plate of M72 *E. coli* cells containing pJONEX4 plasmid and gene insert was used to inoculate 3 ml LB media with 0.1 mg/ml ampicillin and the culture was incubated with shaking at 30°C overnight. 100 µl of overnight culture was transferred into 5 ml of LB with 0.1 mg/ml ampicillin and grown until A_{600nm} was approximately 0.4. Expression was induced by adding 5 ml of LB media pre-heated to 55°C and then incubating at 42°C for 1 hour. After induction the culture was incubated for 2 hours at 30°C. Cells were harvested and protein in the cells and supernatant was analysed by SDS-PAGE.

2.5.2. Large scale production using heat inducible system

Fresh LB media (5 mL) with 0.1 mg/ml carbenicillin was inoculated with 100 µl of overnight *E. coli* M72 culture and grown at 28°C throughout the day. This was then used to seed 500 ml of LB media with 0.1 mg/ml carbenicillin, incubated at 28°C overnight and then added to a fermenter containing 3 L of autoclaved 4YT media, 0.1 mg/ml carbenicillin and 500 µl Antifoam (Sigma). The culture was incubated at 30°C with stirring at 400 rpm until A_{600nm} reached approximately 2.0 then the temperature was increased to 42°C for 1.5 hours. The temperature was then lowered to 25°C for overnight incubation. Samples of cell lysate and supernatant taken before and after induction were analysed by SDS-PAGE to confirm protein expression. Cells were harvested by centrifugation at 9000 x *g* for 30 minutes at 20°C. For Gly1 production

the supernatant was transferred to sterile bottles and kept at room temperature due to the cold sensitive nature of the protein. Cell pellets were stored at -80°C.

2.5.3. Small scale expression using IPTG inducible system

A single colony of freshly transformed *E. coli* Bl21 Star (DE3) cells with vector and insert of choice was used to inoculate 3 ml of LB media with 0.1mg/ml ampicillin and 0.3% glucose and incubated overnight at 30°C. Overnight cultures were used to inoculate 5 ml LB media (1:50 dilution) with 0.1 mg/ml ampicillin and 0.1% (w/v) glucose, incubated at 30°C until optical density A_{600nm}= 1 then expression was induced by adding 0.1 mM IPTG. Time courses of expression were carried out by taking samples after 1 hour, 3 hour and overnight incubation and analysing cell pellet and supernatant by SDS-PAGE.

2.5.4 Protein expression using the autoinduction method

Proteins were expressed from plasmids under control of the T7 promoter following the method developed by Studier (Studier, 2005). BL21 Star (DE3) cultures with vector and insert of choice were grown overnight at 37°C in 50 ml non-inducing media (MDG) in the presence of appropriate antibiotics. MDG contained 1 ml 50xM (1.25 M Na_2HPO_4, 1.25 M KH_2PO_4, 2.5 M NH_4Cl, 0.25 M Na_2SO_3), 0.5 ml 1.88 M sodium aspartate, 0.7 ml 2 M glucose, 0.01 ml 1 M $MgSO_4$, 0.1 ml “1000 x” trace metals (Teknova). This culture was used to inoculate 1 L of the inducing media ZYM-5052 made up of 10 g N-Z-Amine AS, 5 g yeast extract, 20 ml 50xM, 2 ml 1 M $MgSO_4$, 0.2 ml “1000 x” trace metals and 20 ml 50x “5052” (0.5% glycerol, 0.05% glucose, 0.2% lactose). The 1 L flask cultures were grown at 37°C with vigorous shaking for 12 hours then at room temperature for up to 24 hours. Aliquots of culture were taken at regular time points and analysed for protein expression in comparison to the inoculum by SDS-PAGE. Cells were harvested by centrifugation at 9000 x *g* for 30 minutes at 20°C. The supernatant was transferred to sterile bottles and kept at room temperature due to the cold sensitive nature of the protein. Cell pellets were stored at -80°C.

2.6. Purification methods

2.6.1. Nickel chelate purification of Chis-Gly1ORf1 from culture supernatant

Supernatants containing secreted His-tagged Gly1ORF1 were filtered using Whatman filter paper to remove any large particles. Before loading on to the nickel chelate column $NiCl_2$ and imidazole were added to the supernatant at final concentrations of 1.5 mM 20 mM respectively to prevent stripping of the column due to non-specific interactions. Nickel chelate beads were loaded onto a column and washed with 2 column volumes (CV) of deionized H_20 and then equilibrated with 5 CVs of buffer containing 20 mM $Na_2PO^-_4$, 500 mM NaCl, 5% glycerol pH 8. Supernatant was passed through the column, then the column was washed with 5 CVs of equilibration buffer. Protein was eluted in a two-step imidazole wash, 3 CVs of 100 mM and 3 CVs of 500 mM imidazole, 1 CV fractions were collected during elution.

2.6.2 Preparation of cell lysates

Cell pellets were resuspended in 5 ml/g of lysis buffer (25 mM Tris pH 8, 200 mM NaCl, 5 mM EDTA) and lysozyme (Sigma) was added to a final concentration of 0.2 mg/ml and stirred at room temperature for 1 hour. PMSF (Sigma) from a stock solution made up in 100% ethanol was added to make a final concentration of 10 µg/ml followed by sodium deoxycholate (Sigma) to a final concentration of 500 µg/ml and the mixture was placed on ice for at least 1 hour until it became viscous. This was then sonicated on ice for 60 seconds in 10 second bursts at and insoluble material was removed by centrifugation at 40000 x *g* for 30 minutes at 4°C.

2.6.3 Ammonium sulphate fractionation

To find the optimum concentration of ammonium sulphate to precipitate the protein of interest from cell lysates solid ammonium sulphate was added to a 1 ml sample of lysate to make a 50% saturated solution. This was incubated on ice for 5 minutes then precipitated proteins were isolated by centrifugation at 12225 x *g* for 2 minutes. The supernatant was removed to a fresh tube and more solid ammonium sulphate was added to make a 75% solution and incubated and centrifuged as above. This was repeated once more to make an almost 100% solution. The precipitated protein pellets were then dissolved in 25 µl H_2O and analysed by SDS-PAGE. A concentration of

ammonium sulphate that precipitated the majority of the protein of interest but left some contaminating proteins soluble was chosen to scale up for the whole cell lysate. Solid ammonium sulphate was added gradually and the lysate was incubated on a roller overnight at 4°C. Proteins were harvested by centrifugation at 40000 x *g* for 30 minutes and resuspended in appropriate buffer for the following purification step. The resuspended proteins were then dialysed (see section 2.6.7) against an excess of buffer to remove any remaining ammonium sulphate.

2.6.4 Ion exchange chromatography

Anion exchange chromatography was carried out using 1 ml or 5 ml pre-packed Q columns (GE life Healthcare). Columns were equilibrated and loaded in a Q buffer of 25 mM Tris-HCl, 1 mM EDTA, 1 mM DTT, 5% glycerol at pH optimized for each protein. Proteins were eluted from the column using salt gradients produced using Q buffer with 1M NaCl. Cation exchange chromatography was carried out with pre-packed 1 ml or 5 ml SP columns (GE Healthcare). For purification using a pH between 5 and 6 the column was equilibrated and loaded with 50 mM sodium acetate buffer containing 1 mM EDTA, 1 mM DTT, and 5% glycerol. Between pH 6 – 7, a 20mM sodium phosphate or 50 mM MES buffer with 1 mM EDTA, 1 mM DTT, and 5% glycerol was used. Proteins were eluted using a salt gradient produced with the above buffers and addition of 1 M NaCl.

2.6.5 Size exclusion chromatography

Size exclusion chromatography was carried out as a final purification step using a Superdex 200 column (GE Healthcare). The column was equilibrated with 5 column volumes of buffer and 0.5 ml of protein at a maximum concentration of 10 mg/ml was injected onto the column. Fractions of 0.5 ml were collected and those corresponding to UV measurement peaks were analysed by SDS PAGE.

2.6.6 Determination of protein concentration

Concentrations of purified proteins were determined by A_{280} using a spectrophotometer and the theoretical absorbance of a 1 mg/ml solution as determined by ExPASy ProtParam (Gasteiger et al., 2005). This was 1.48 for Gly1ORF1, 0.86 for Gly1ORF2 (UroS/*hemD*) and 0.52 for HmbS (*hemC*).

2.6.7 Concentration, dialysis and storage of proteins

Dialysis tubing (Spectra/Por 1 6-8 kDa cut off, Spectrum labs) was prepared by soaking in distilled H_2O for 30 minutes to remove glycerin. The protein solution was added to the tubing and secured with clips. The dialysis bag was incubated in a large excess of buffer with gentle stirring for at least 16 hours. Proteins were concentrated using

Vivaspin® centrifugal concentrators (Sartorius Stedim Biotech) with an appropriate cut off membrane. For storage, gly1ORF1 was dialysed into 25 mM NaOAc, 50 mM NaCl pH4 and Gly1ORF2 and HmbS were stored in 20 mM Tris, 100 mM NaCl pH 8.2. Purified protein was either flash frozen at -80°C, mixed with 50% glycerol and stored at -20°C or stored at 4°C for shorter periods.

2.6.8 Acetone precipitation of proteins

Proteins were concentrated for SDS PAGE analysis using acetone precipitation. One volume of protein-containing solution was mixed with 3 volumes of ice-cold acetone and incubated on ice for 30 minutes. The solution was centrifuged for 10 minutes at 12225 x *g*, the supernatant removed and the pellet left to air dry. The pellet was then solubilised in a minimal volume of 10% SDS and analysed by SDS-PAGE.

2.6.9 Pre-crystallisation test (PCT^{TM})

A pre-crystallisation test was carried out on the purified proteins to determine the optimum concentrations to use in initial 96-well plate crystallisation trials. The test was carried out following the protocol from Hampton Research (Watson and O'Callaghan, 2005) but not with the commercial reagents. A 1 µl aliquot of protein was placed onto a siliconised glass cover slip and 1 µl of reagent was added without mixing. This was placed over a 1 ml reservoir of reagent in a 24 well plate and sealed and after 30 minutes results were viewed with a microscope. Reagents, results and recommendations are shown below.

- Reagent A1 - 0.1 M TRIS hydrochloride pH 8.5, 2.0 M ammonium sulphate
- Reagent B1 - 0.1 M TRIS hydrochloride pH 8.5, 1.0 M ammonium sulphate
- Reagent A2 - 0.1 M TRIS hydrochloride pH 8.5, 0.2 M magnesium chloride hexahydrate, 30% w/v polyethylene glycol 4,000

- Reagent B2 - 0.1 M TRIS hydrochloride pH 8.5, 0.2 M magnesium chloride hexahydrate, 15% w/v polyethylene glycol 4,000

Table 2.3 Summary of potential results and recommendations from the Pre-Crystallisation Test

PCT Reagent A1/B1 Results	PCT Reagent A2/B2 Results	Recommended Action
Heavy Amorphous Precipitate	Heavy Amorphous Precipitate	Dilute sample 1:1, repeat test
Clear	Clear	Concentrate sample to half the original volume, repeat test
Light granular precipitate	Clear	Perform Screen
Clear	Light granular precipitate	Perform Screen
Heavy Amorphous Precipitate	Light granular precipitate	Perform Screen
Heavy Amorphous Precipitate	Clear	Perform PCT with B1 & B2 / perform diagnostic testing
Clear	Heavy Amorphous Precipitate	Perform PCT with B1 & B2 / perform diagnostic testing

2.6.10 Protein crystallography

Crystallisation trials were carried out using Molecular Dimensions 96 well plate screens (PACT, JCSG+, pH Clear, Morpheus). The trials were set up using the sitting drop method in a 1:1 ratio of protein with a Mosquito® Crystal robot (TTP Labtech). Trials were carried out for all purified proteins at between 5 and 20 mg/ml. Plates were incubated at either 17°C or 8°C and visually checked at regular intervals for the presence of crystals. Crystals were looped by Jason Wilson, placed into cryopreservation solutions corresponding to the conditions they formed in and stored in liquid nitrogen. X-ray diffraction data was collected by Jason Wilson at Diamond Light Source.

For co-crystallisation trials with haemin, C-HisGly1 was diluted to 1 mg/ml in a 1 ml volume of 25 mM sodium acetate, 50 mM NaCl pH 5. Haemin solution (Jena bioscience) was added slowly until it was present at a 10 times molar excess. The mixture was incubated at room temperature for one hour, then concentrated to one tenth of the original volume using a Vivaspin concentrator with a 10 kDa molecular weight cut off. The concentrated solution was then filtered through a 2 µm filter (Millipore) to remove protein or haemin aggregates. Due to the strong absorbance spectra of haemin, the protein concentration could not be determined by A_{280} measurement. Dilutions of the sample were analysed by SDS-PAGE and compared to a sample of Gly1 of known concentration and the protein concentration in the co-crystallisation sample was determined to be approximately 3 mg/ml. Crystallisation trials using the PACT, JSCG+ and Morpheus 96-well format screens were carried out with a 1:1 ratio of buffer to protein with the sitting drop method.

2.6.11 Circular dichroism spectroscopy

Circular dichroism (CD) spectroscopy was carried out using a JASCO J810 spectropolarimeter in the Staniforth laboratory, Department of Molecular Biology and Biotechnology, University of Sheffield. Measurements were taken using protein at 5 µM concentration in 20 mM Tris, 50 mM NaCl pH 8.2. The settings are outlined in table 2.4 below.

Baseline measurements of the buffer were subtracted from the protein measurements and the ellipticity θ was converted to the molar residue ellipticity $[\theta]_{MRW}$ using the equation:

$$[\theta]_{MRW} = \frac{\theta x 100 x Mr}{cxdxN_A}$$

Where Mr is the mass of the protein in kDa, c is the protein concentration in mg/ml, d is the cell length and N_A is the number of amino acids. This unit is expressed in mdeg $cm^2 M^{-1}$.

Table 2.4 CD spectroscopy settings for secondary structure analysis

Condition	Setting
Sensitivity	100mdeg
Start	250 nm
End	190 nm
Data pitch	1 nm
Scanning	Continuous
Speed	50 nm/min
Response	4 seconds
Band width	1 nm
Accumulations	5
Cell length	0.1 cm
Temperature	25°C

2.7 Protein-protein interactions

2.7.1 Biolayer interferometry of protein-protein interactions

Biolayer interferometry was carried out using the BLItz system (ForteBio). His-tagged proteins were loaded onto a Ni-NTA biosensor and experiments were carried out using 30 second baseline measurements and 120 second loading, association and dissociation times. Non-tagged versions of the potential interacting partner proteins were used for association. Control measurements were carried out where no protein was loaded onto the biosensors to ensure that the interacting partner proteins did not bind to the biosensor non-specifically.

2.7.2 Glutaraldehyde crosslinking

Proteins were mixed at a final concentration of 1.5 mg/ml in 0.5 ml PBS and glutaraldehyde was added to make a 0.025% (v/v) final concentration, after serial dilution from a 25% stock solution (AppliChem). The mixture was incubated a room temperature for 1 hour then the reaction was quenched by the addition of Tris pH 8 to a 50 mM final concentration and incubated for a further 10 minutes. A 10 µl aliquot of the reaction mixture was mixed with 1:1 with SDS-PAGE loading dye and analysed by SDS-PAGE.

2.7.3 Microscale thermophoresis (MST)

C-his Gly1ORF1 was labelled using the Monolith NT^{TM} His-Tag Labelling Kit RED-tris-NTA (NanoTemper Technologies GmbH) following the manufacturer's instructions. C-his Gly1ORF1 was buffer exchanged into PBS 0.05% Tween-20 (PBS-T) using a Vivaspin 4 Turbo (MW cut off 5 kDa) centrifugal concentrator and diluted to make a 200 nM solution. The protein was mixed with the dye solution in a 2:1 ratio and incubated at room temperature for 30 minutes. The labelling mixture was then centrifuged for 10 minutes at 12225 x *g* and transferred to a sterile eppendorf tube ready for use.

To confirm the efficiency of the labelling reaction a binding affinity experiment was carried out with the dye solution and the C-his Gly1ORF1 protein. A 4 µM solution of C-his Gly1ORF1 was prepared in PBS-T and 20 µl was added to 10 µl of PBS-T in a PCR tube (tube 1) and mixed well. A 10 µl aliquot was then removed from tube 1 and serially diluted 1:1 to make 16 dilutions. An equal volume of dye solution (50 nM) was added to each tube and mixed thoroughly then incubated at room temperature for 30

minutes. The samples were loaded into Monolith NT.115 standard treated glass capillaries and measured using a Monolith NT.115 instrument (both NanoTemper Technologies GmbH) at room temperature (~19°C) with excitation power 80% MST setting medium and data analysed using the MO.Control software (NanoTemper Technologies GmbH) to determine a K_d for the labelling reaction.

Human lysozyme solution was prepared for MST experiments by dissolving lyophilized human lysozyme (Sigma) in 0.5 ml PBS-T to a concentration of 10 mg/ml and then purifying by size exclusion chromatography (see section 2.6.5) in PBS-T buffer to remove contaminants or degradation products. The fractions containing purified lysozyme were pooled and the protein concentration was determined to be 20 µM. The lysozyme solution was serially diluted in PBS-T 1:1 to make 16 dilutions in 10 µl volumes as above. To each dilution 10 µl of labelled C-his Gly1ORF1 (100 nM) was added and mixed thoroughly to make a final concentration of Gly1ORF1 in each sample of 50 nM. The samples were loaded into standard treated glass capillaries and measured with a Monolith NT.115 instrument at 40% LED/excitation and 40% MST power (medium setting).

2.8 Methods for studying haem interactions and biosynthesis

2.8.1 Haemin-agarose pull down assay

A 25 µl aliquot of haemin-agarose beads (Sigma) was washed three times in 1 x PBS pH 8.0 to remove the storage buffer. Purified Gly1ORF1 protein (90 µg) in 0.5 ml PBS was added to the beads along with bovine serum albumin (BSA, 100 µg) as a negative control, and incubated at room temperature on a roller for 30 minutes. The beads were then sedimented by centrifugation at 268 x *g* for 2 minutes and the supernatant containing unbound proteins removed. The beads were washed for 15 minutes with PBS and 0.5 M NaCl then sedimented again by centrifugation. Two more brief washes in PBS were performed and the sedimented beads were resuspended in 30 µl SDS loading dye and boiled for 5 minutes and analysed by SDS-PAGE along with samples from the wash steps.

2.8.2 Haemin binding to whole cells

The expression of HmbR and non-tagged Gly1ORF1 was induced in Bl21Star(DE3) cells carrying the relevant gene in the pET21a (+) plasmid by small-scale autoinduction as described in section 2.5.4. Bl21Star(DE3) cells carrying an empty pET21a (+) plasmid were subjected to the same treatment as a negative control. Cells were harvested after 24 hours growth by centrifugation at 9000 x *g* and expression of the proteins was confirmed by analysing a small sample by SDS-PAGE. The remaining cultures were washed with 1 x PBS then diluted in 1 x PBS to an absorbance of A_{600}=0.1 in a 1 ml volume with the addition of 40 µM haemin. The cells were incubated at room temperature for 60 minutes then harvested by centrifugation at 12225 x *g* for 5 minutes. The supernatants were removed and the cells suspended in 1 ml PBS without haemin and 5 µl was spotted onto nitrocellulose membrane. The membrane was left to dry and then soaked in 10 ml Pierce ECL Western Blotting substrate. The presence of haemin was detected by visualising the membrane using a BioRad ChemiDoc XRS+ imaging system, as haemin possesses intrinsic peroxidase activity. The results were analysed semi-quantitatively using ImageJ software.

2.8.3 UV-visible absorbance assays

C-his Gly1ORF1 was buffer exchanged into 1 x PBS pH 7.4 to remove storage glycerol and raise the pH using a Vivaspin Turbo 15 (5 kDa membrane cut off). Haemin was prepared by diluting soluble 0.25% (w/v) porcine haemin (Jena Bioscience) in PBS to make a 2 x concentrated solution. Haem analogues deuteroporphyrin IX 2,4 bis ethylene glycol (DPBG) and deuteroporphyrin IX dihydrochloride (DPHCl) (both Santa Cruz Biotechnology) were dissolved in DMSO then diluted in PBS to make 2 x concentrated solutions of around 6 µM. Gly1ORF1 and the haemin or analogues were mixed 1:1 and incubated for 5 minutes at room temperature. The reaction mixture was then centrifuged at 12225 x *g* for 2 minutes and the UV-visible absorbance spectra were measured from 220 to 800 nm in 3 nm intervals using a Nanodrop 1000 spectrophotometer. For assays involving a constant concentration of haemin or analogues and increasing protein, the haemin and analogues were used at around 3 µM final concentration. In the difference spectra assay involving increasing amounts of haemin the Gly1ORF1 concentration in the reaction was 10 µM and haemin

concentrations were 2.5, 5, 7.5, 10, 12.5, 15 and 20 µM. To calculate the difference spectra the spectrum of a particular concentration of haemin was subtracted from the spectrum with that concentration incubated with Gly1ORF1.

2.8.4 Hydroxymethybilane synthase (HmbS) assay

Specific activity for purified HmbS samples was determined following the method of Jordan *et al.* (1988) with some modifications. Porphobilinogen (50 nM, Sigma) in 20 mM Tris-HCl, 100 mM NaCl pH 8.2 was pre-warmed to 37°C. HmbS protein in the same buffer was added to a make a final volume of 220 µl and the reaction mixture was incubated at 37°C for 5 minutes. The reaction was quenched by the addition of 30 µl 6 M HCl and exposed to UV light for 30 minutes to convert the porphyrinogen products to porphyrins. Samples were then centrifuged for 10 minutes at 12225 x *g* and 0.1 ml aliquots of supernatant were made up to 1 ml in 1 M HCl. Absorbance was measured at 405.5 nm against a blank in which the reaction was quenched at time zero. The amount of porphyrins produced was calculated using ε=518000 M^{-1}. One unit is defined as the amount of HmbS required to synthesise 1.0 nmol of porphyrinogen I in 1 minute. The assay was carried out using 11.25 µg/ml of freshly purified non-tagged HmbS in each reaction.

Chapter 3. Structural and Biochemical Characterisation of Gly1ORF1

3.1 Introduction

There are few published studies that attempt functional characterisation of Gly1ORF1, but those that do test the hypothesis that the protein is involved in adhesion to, or invasion of host cells (Arvidson et al., 1999; Deghmane et al., 2003; Morelle et al., 2003). This is due to the presence of the CREN (Contact Regulatory Element of *Neisseria* a.k.a. REP2) element upstream of the locus and the fact that the protein is potentially surface located. These studies found that although Gly1ORF1 expression was upregulated upon contact with host cells, there was no difference in the ability of *Δgly1ORF1* mutants to adhere to or invade host cells (Arvidson et al., 1999; Deghmane et al., 2003; Morelle et al., 2003).

The *gly1* locus is located directly upstream of several genes that are predicted by sequence homology to be involved in porphyrin biosynthesis, as can be seen in Figure 3.1. The gene originally annotated *gly1ORF2* shares partial homology (28% identity over 75% of the sequence) with *E. coli hemD* (uroporphyrinogen III synthase) (Arvidson et al., 1999). This is followed by *hemX* (uroporphyrin-III C-methyltransferase), which is involved in the sirohaem and cobalamin synthesis pathways that branch from uroporphyrinogen III. The genes *hemY* (Protoporphyrinogen oxidase) and *hemE* (Uroporphyrinogen decarboxylase) are members of the classical haem biosynthesis pathway. This genomic location led our group to investigate the hypothesis that the *gly1* locus encodes proteins involved in haem uptake or homeostasis.

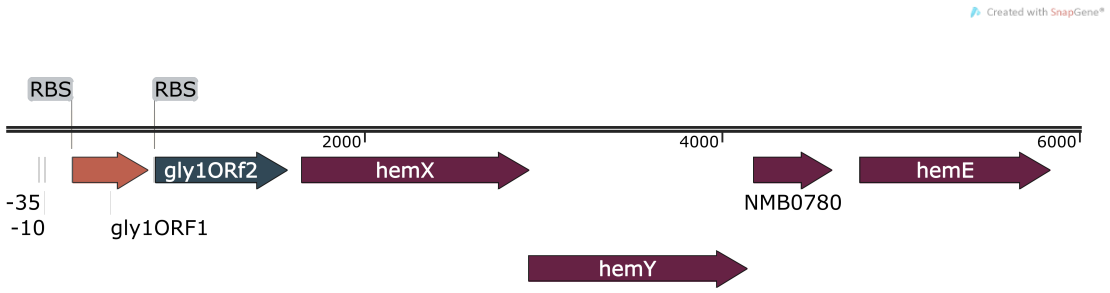

Figure 3.1 Genomic location of *gly1* locus
Representation of section of genome from *N. meningitidis* MC58 (accession no. NP_273818.1), showing the location of the *gly1* locus. The *gly1* locus consists of *gly1ORF1* (NMB0776) and *gly1ORF2* (NMB0777) annotated as a *hemD* homologue from sequence similarity. Genes encoding porphyrin biosynthesis enzymes in the region are *hemX* (NMB0778), *hemY* (NMB0779) and *hemE* (NMB0781). NMB0780 is an uncharacterised gene encoding a putative protein with predicted cytoplasmic location. The ribosome binding sites (RBS) and predicted promoter sequences (-10 and -35) are shown for the *gly1* locus. Base pairs indicated by the measurement scale. Created using SnapGene® software (from GSL Biotech; available at snapgene.com).

In order to determine whether Gly1ORF1 interacted with haem *in vivo,* the gene was cloned from *N. meningitis* MC58 and the protein product purified by affinity purification facilitated by the addition of a C-terminal 6xHis tag (Meadows, 2005). The CHisGly1ORF1 was enriched on haemin agarose beads in pull down assays, and showed evidence of the formation of dimers and larger multimers after incubation with haemin in solution (Sathyamurthy, 2011; Wierzbicka, 2014). Unfortunately, these interactions were not quantified kinetically as experiments to determine these data were beset with issues of both protein and haemin precipitation (Sathyamurthy, 2011; Wierzbicka, 2014).

Structural characterisation of Gly1ORF1 has been another area of study in our group, and we have aimed to identify potentially related proteins that share structural features, hoping to gain clues to function. The structure of the wild type *N. gonorrhoeae* Gly1ORF1 protein and *N. meningitidis* K12A mutant have been solved by x-ray crystallography and possess a novel fold termed the “beta-diablo fold.” This consists of two anti-parallel β-sheets layered against each other in a convex structure (Arvidson, unpublished; Wierzbicka, 2014). Although no well-conserved sequence homologues exist, knowledge of the structure has allowed potential homologues to be

identified in other species. These are characterised by similar length (135-140 aa), presence of N-terminal signal peptide (19-24 aa), presence of a disulphide (Cys-Cys) bond linking the first and last β-strand, and significant predicted β-strand content. Two motifs,"FSC" (located at 25-29 aa) and "YEYS" (located at 45-55 aa), were also used to classify putative homologues (McMellon, 2016). Related proteins were found in a wide range of Gram-negative species, many of which are human or animal pathogens, including *Haemophilus ducreyi*, *Salmonella enterica* and *Actinobacillus pleuropneumoniae* (see Figure 3.2). It is hypothesised that they could form a protein family that share similar functions. Evidence of their structural similarity was provided when the structure of the *Mannheimia haemolytica* Gly1ORF1 paralogue was solved by x-ray crystallography (McMellon, 2016). The two proteins shared remarkable structural homology, with similar placement of β-strands and disulphide bond, despite only sharing 16.4% sequence identity.

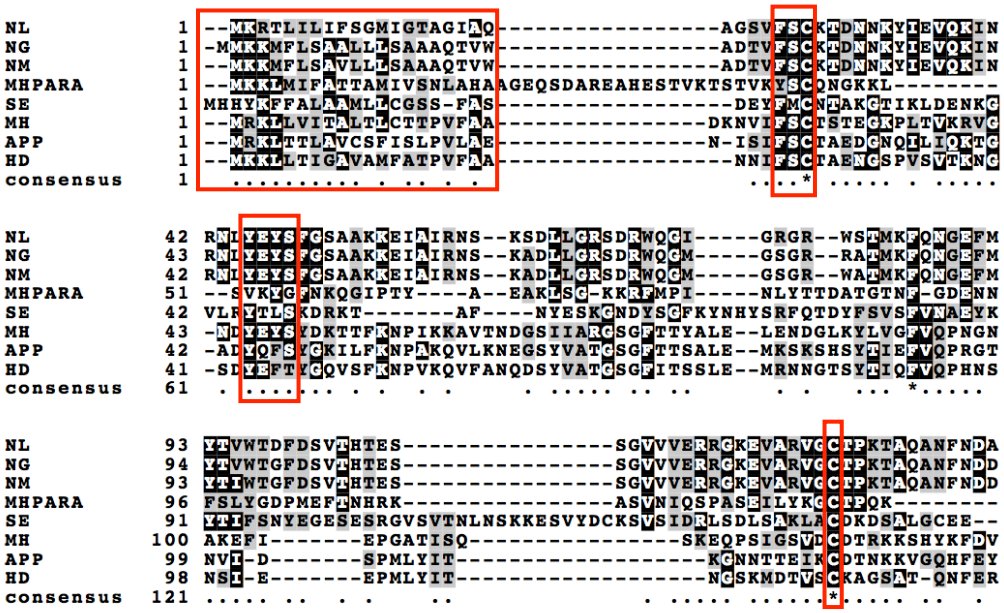

Figure 3.2 Multiple sequence alignment of putative Gly1ORF1 homologues identified in previous studies.
Alignment showing sequence similarities used to identify putative Gly1ORF1 homologues. The periplasmic targeting N-terminal signal sequence, the "FSC" and "YEYS" motifs and the cysteine that is predicted to form part of the disulphide bridge close to the C-terminus are highlighted in red boxes. Species name, acronym used in alignment and accession numbers are as follows: *N. lactamica* (NL) WP_003710927.1, *N. gonorrhoeae* (NG) ACF29206.1, *N. meningitidis* (NM) NP_273818.1, *M. haemolytica* (MH) EDN74135.1, *Mannheimia haemolytica* paralogue (MHPARA) AGK03253.1, *S. enterica* (SE) WP_000546623.1, *A. pleuropneumoniae* (APP) WP_005607867.1, *Haemophilus ducreyi* (HD) WP_005653509.1. Alignment created using Clustal Omega and Boxshade servers. Asterisks in the consensus line indicate residues conserved between all sequences and dots were there is some conservation between sequences. Black shaded residues are conserved in over 50% of sequences and grey shading indicates similar types of residues (polar/non-polar etc.)

An issue identified in the study of Gly1ORF1 homologues was that the histidine tags on the proteins could sometimes contribute to haemin binding ability in haemin agarose pull-down assays (McMellon, 2016). This was highlighted by the fact that the experimental control his-tagged human growth hormone bound to the haemin beads, a protein that does not bind haem in its full length, native form (Spolaore et al., 2005). Histidine is a known haem ligand in haemoproteins such as myoglobin and has been identified at binding sites in several haem uptake proteins (Bracken et al., 1999; Létoffé et al., 2005). Removing the histidine tag by enterokinase treatment abolished or greatly reduced the ability of some putative Gly1ORF1 family members to bind

haemin in the pull-down assays, casting uncertainty on the idea that these proteins share the function of haem binding *in vivo* (McMellon, 2016).

Previous attempts to express Gly1ORF1 protein without a histidine tag to levels that would facilitate purification have been largely unsuccessful. Good expression levels were achieved when the signal peptide was removed during cloning. However, the protein was insoluble and re-solubilisation was inefficient (Wierzbicka, 2014).

The aim at the outset of this chapter was to develop an efficient protocol for the purification of high yields of soluble non-tagged Gly1ORF1 protein. This was with a view to gather more accurate kinetic data on the potential interaction with haem and to carry out structural characterisation of the native protein. As part of this study the his-tagged wild type Gly1ORF1 protein has also been purified and used to gain additional insight into the structure and function of these proteins.

3.2 Results

3.2.1 Creating non-tagged *glyORF1* expression vectors

The native *gly1ORF1* gene was cloned into the expression vector pET21a(+), a plasmid that contains an ampicillin resistance gene where expression is driven from the strong T7 promoter. The *gly1ORF1* gene was amplified from *N. meningitidis* MC58 genomic DNA using primers NM_NTORF1_F and NM_NTORF1_R (see table 2.2 in Materials and Methods) to generate a 455 bp fragment with an EcoRI restriction site at the 5' end and a HindIII restriction site at the 3' end. This was purified by gel extraction, digested with the restriction enzymes and then ligated into the 5443 bp pET21a(+) plasmid that had been linearized with the same enzymes. The resulting plasmid was then transformed into XL1Blue *E. coli* cells. Purified plasmids from transformants were analysed for the presence of the correct insert using restriction digestion with EcoRI and HindIII and through PCR amplification using T7 forward and terminator primers. The red boxes in Figure 3.3 highlight the restriction band and PCR amplified fragment corresponding to non-tagged Gly1ORF1 which migrates just above the 0.4 kDa marker. The sequence and orientation of the insert in these plasmids was confirmed by sequencing with the T7 forward and terminator primers. The correctly sequenced plasmids were then transformed into fresh competent Xl1Blue cells for storage.

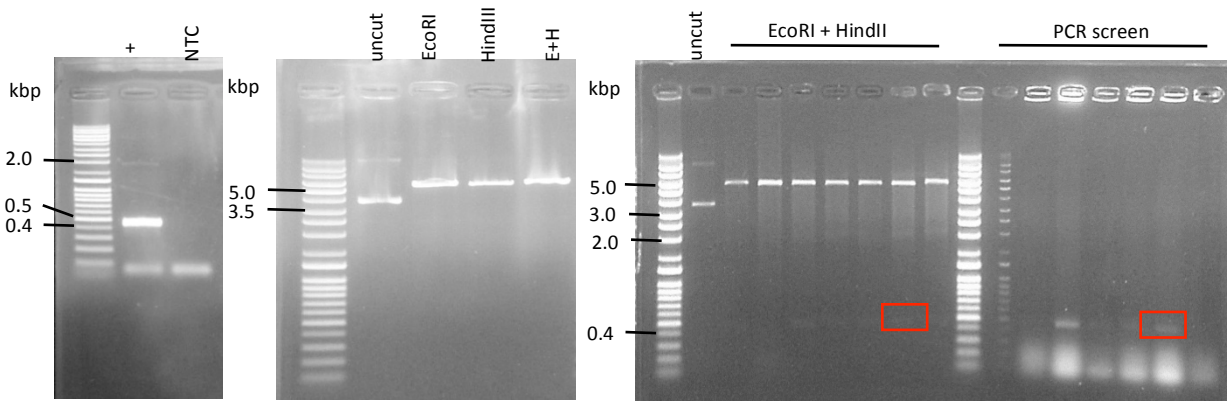

Figure 3.3 Cloning non-tagged *gly1ORF1* from *N. meningitidis* MC58 into pET21a
A) *gly1ORF1* amplified by PCR from genomic DNA (+) and (NTC) no template control reaction containing the cloning primers but no genomic DNA. **B)** Double restriction digest of pET21a with EcoRI and HindIII, lanes (E) and (H) are single digestions and (EH) shows the double digested plasmid which was used for ligation with the digested *gly1ORF1* insert. **C)** The ligated construct was transformed into XL1Blue *E.coli* cells and clones were screened by restriction digest with EcoRI and HindIII, and PCR using the T7 forward and T7 terminator primers followed by sequencing to confirm the correct orientation and sequence.

3.2.2 Small-scale expression studies of Gly1ORF1

The pET21*gly1ORF1* plasmid was transformed into Bl21(DE3) Star™ cells for expression by auto-induction following the method of Studier *et al.* (2008) (see Materials and Methods section 2.5.4). Faint bands corresponding to native Gly1ORF1 running slightly below the 15 kDa marker were observed in the supernatant at later time points of 26-30 hours of growth as shown in Figure 3.4.A. This protein was confirmed as Gly1ORF1 by western blot using anti-Gly1ORF1 polyclonal antibody. The amount of Gly1ORF1 in the cells was gradually depleted between 24 and 30 hours and there was a corresponding increase in the supernatant. This could suggest that Gly1ORF1 was secreted in a controlled manner, but the mechanism for this is still unknown.

In parallel to this, the genomic region containing both *gly1ORF1* and *ORF2* was cloned into the pJONEX4 vector in an attempt to co-express the proteins in M72 cells (by Lawrence Key). Expression of Gly1ORF1 from this construct was successful, with a band of around 13 kDa visible in the culture supernatants along with many other proteins presumably from cell or periplasm lysis (Figure 3.4.B). No expression of ORF2 was detectable in the cell pellets through coomassie staining. Western blot analysis

showed that Gly1ORF1 in the supernatant fraction migrated slightly faster in the SDS-PAGE gel than in the cellular fraction. This suggested that N terminal signal sequence was correctly processed before secretion resulting in a slightly lower molecular weight protein. This was confirmed by mass spectrometry analysis of the purified protein sample which identified only one peptide species with a molecular mass of 13.36 kDa, the predicted molecular mass of the mature protein computed using ExPASy protparam – see Appendix 1 (Gasteiger et al., 2005). The pJONEX4 construct was chosen as an efficient over producer of native Gly1ORF1 and used for large-scale production of the protein.

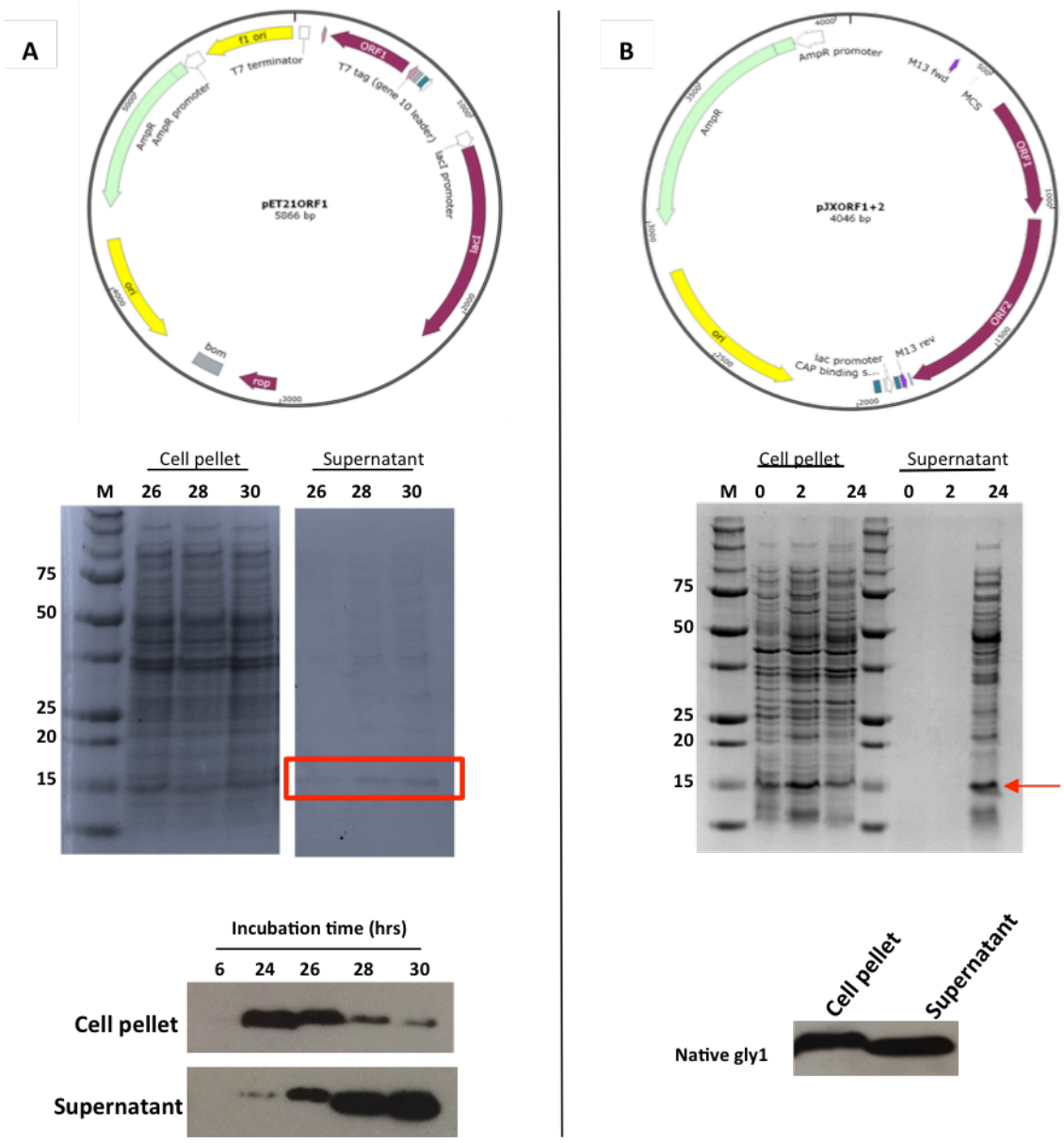

Figure 3.4 Expression of native Gly1ORF1 protein from pET21aORF1 (A) and pJONEX4-ORF1ORF2 (B) constructs

A) SDS PAGE gel showing expression of native Gly1ORF1 from the pET21a construct containing only ORF1 using auto-induction media. This occurred over time from 24 to 30 hours. Secretion of native Gly1ORF1 into the supernatant is shown inside the red box. Below, western blot using polyclonal anti-Gly1ORF1 antibodies shows protein produced being depleted from the pellet and secreted into the supernatant over time. **B)** SDS PAGE gels showing expression of native Gly1ORF1 from the pJONEX4 construct containing both ORF1 and ORF2. Samples taken at 0, 2 and 24 hours after induction. Western blot of the pellet and supernatant with anti-Gly1ORF1 antibodies shows that Gly1ORF1 in the supernatant migrates faster on the SDS PAGE gel, suggesting that the N-terminal signal sequence has been correctly processed and cleaved before secretion. This was confirmed by mass spectrometry analysis. Plasmid maps of pET21ORF1 and pJxORF1+2 created using SnapGene® software (from GSL Biotech; available at snapgene.com).

3.2.3 Large scale expression of native Gly1ORF1 from pJONEX4 construct and development of purification protocol

Native Gly1ORF1 (ntGly1ORF1) was expressed in large-scale culture by induction for 3 hours at 42°C followed by overnight growth at 28°C. Similar to the small-scale expression studies, the protein was clearly visible in the cellular and supernatant fractions after overnight growth. The culture supernatant was filtered to remove large particles and an analytical ammonium sulphate fractionation was carried out on a small sample as described in Materials and Methods section 2.6.3. The majority of the Gly1ORF1 protein precipitated at around 50% saturation, with many other proteins still staying soluble until 75% saturation (Figure 3.5 A). Proteins were precipitated from the large-scale expression supernatant at 50% ammonium sulphate saturation then dialysed against sodium acetate buffer and applied to a cation exchange column (SP Hi-Trap) and eluted over a NaCl gradient. The amount of protein recovered from ammonium sulphate precipitation was very low, as can be seen from the faint bands on the coomassie stained gels. Fractions that contained ntGly1ORF1 (4 and 5) were pooled and applied to a Hi-Trap Blue HP column as an affinity purification step. This column contains the aromatic dye compound Cibacron Blue F3G-A covalently attached to the matrix and is commonly used to purify albumin, a haem binding protein (Subramanian and Ross, 1984). Gly1ORF1 bound very strongly to the blue Sepharose medium, and was eluted at up to 1 M NaCl. Several washes at 1 M NaCl removed additional protein at the top end of the gradient but some Gly1ORF1 protein was only eluted using a 2 M NaCl wash. A total of approximately 1.3 mg ntGly1ORF1 was purified from 250 ml of supernatant using this method.

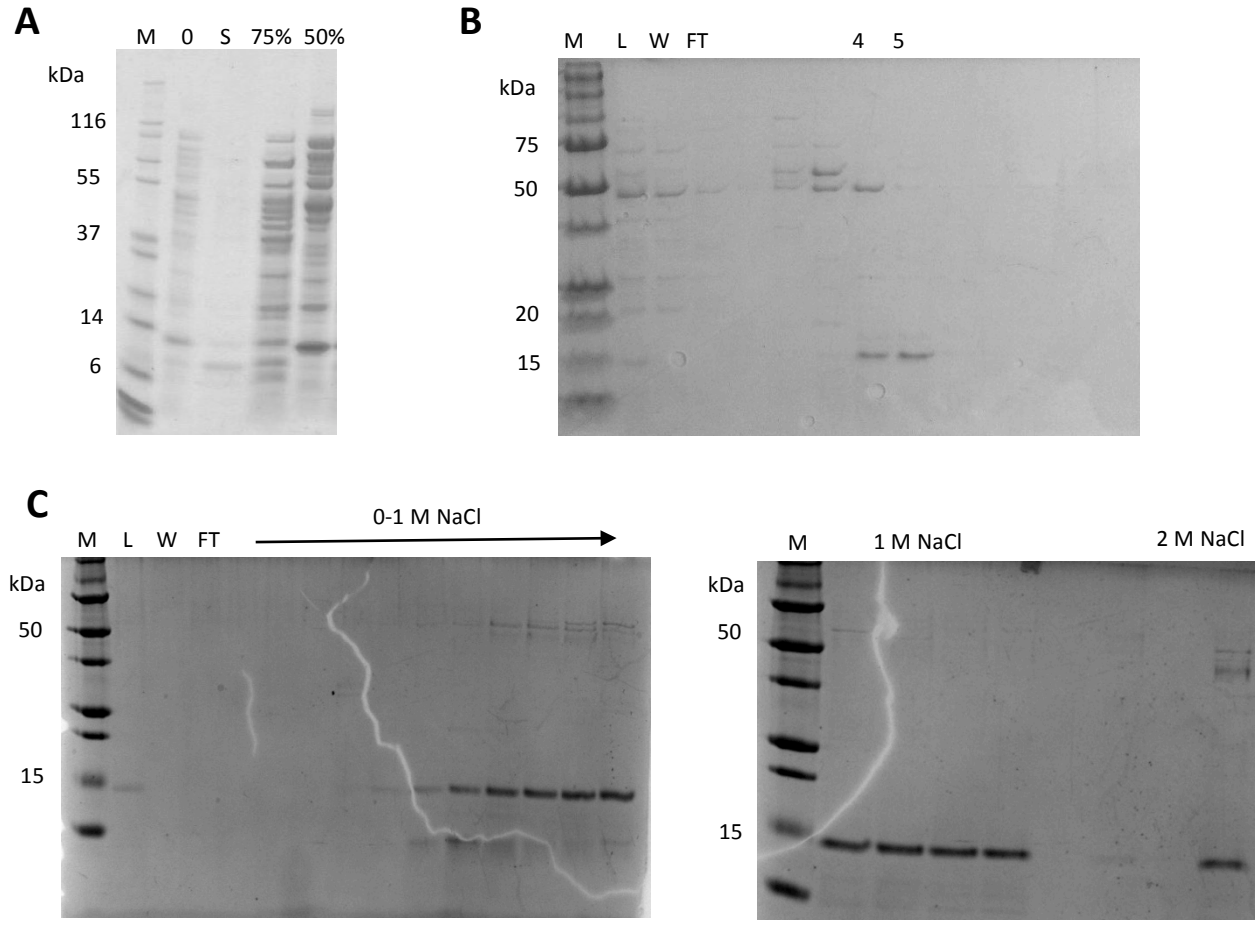

Figure 3.5 Purification of ntGly1ORF1 by cation exchange and affinity chromatography
A) Analytical ammonium sulphate precipitation using a small sample of supernatant (0) is the original sample, (S) is saturated with ammonium sulphate, and 75% and 50% saturated samples are shown after. Majority of ntGly1ORF1 precipitated at 50% saturation. **B)** Cation exchange purification of proteins precipitated from the supernatant. NtGly1ORF1 was eluted in fractions 4 and 5. **C)** Affinity purification using Blue Sepharose, ntGly1ORF1 was eluted over a gradient 0-1M NaCl. NtGly1ORF1 showed strong binding to this media and some protein only eluted at 2 M NaCl.

The low yields achieved in the purification scheme above were partly due to significant protein loss during the ammonium precipitation and dialysis stages. An alternative purification protocol was attempted that omitted this stage. Instead, the supernatant was diluted 1:1 with water to lower the ionic strength and then adjusted to pH 5.4 using acetic acid. This was applied to a high capacity cation exchange column (SP-Toyopearl) and eluted over a 0-1M NaCl gradient. As is shown in Figure 3.6 a large proportion of Gly1ORF1 did not bind to the column and can be seen in the flowthrough

(FT). Some Gly1ORF1 did bind to the column and was eluted over the first quarter of the NaCl gradient. The flowthrough fraction was diluted and passed through the column again, but each time the majority of Gly1ORF1 did not bind to the column. The fractions eluted from the cation exchange column that contained Gly1ORF1 were concentrated and applied to a superdex200 column for size exclusion chromatography. Gly1ORF1 was eluted in single peak and fractions containing the protein were pooled and concentrated to 0.5 mg/ml. The yield from this purification strategy was very low, with only 200 µg of protein purified from 150 ml of supernatant. It was not possible to concentrate the purified Gly1ORF1 produced from either method to more than 0.5 mg/ml using Vivaspin concentrators in the low pH buffer.

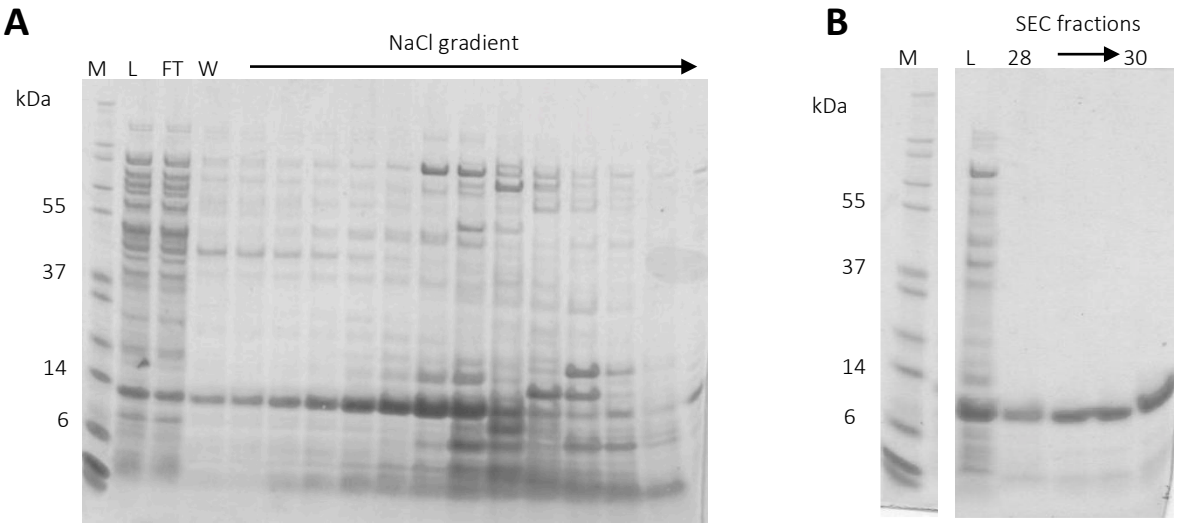

Figure 3.6 Purification of ntGly1ORF1 by cation exchange and size exclusion chromatography
A) Diluted and pH adjusted supernatant applied to high capacity cation exchange column. (L) load, (FT) flow through (W) low salt wash. The proteins were eluted over 0-1 M NaCl gradient. **B)** The purest fractions from the previous stage were pooled, concentrated and applied to a superdex200 column for size exclusion chromatography (SEC). (L) is the column load and Gly1ORF1 was eluted in fractions 28-30.

3.2.4 Haemin-agarose pull down of native Gly1ORF1

The ability of the non-tagged version of Gly1ORF1 to bind to haemin was assessed using the haemin-agarose pull-down method described in Materials and Methods 2.8.1. The proteins were incubated with haemin-agarose beads, and the amount of protein bound to the beads was analysed by SDS-PAGE after several washes in PBS. The stabilising protein bovine serum albumin (BSA) was used in excess to show that the beads were being sufficiently washed to remove any non-specifically interacting proteins. The gels were analysed semi-quantitatively by calculating density of the protein bands corresponding to Gly1ORF1 as a percentage of the lane total in both the "load" and "bound" lanes. As shown in Figure 3.7 both the C-histidine tagged and non-tagged version of the protein were significantly enriched on the haemin-agarose beads. The enrichment factor for the C-his protein was approximately 7, whereas for the non-tagged version it was 4. This suggests that the tag could increase the affinity of the protein for haemin, but the native protein still has significant affinity for haemin.

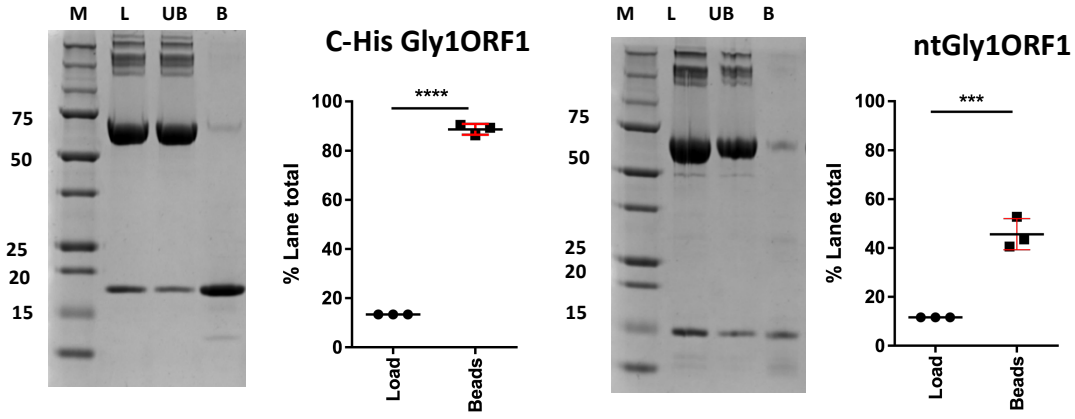

Figure 3.7 Comparison of Histidine tagged and non-tagged Gly1ORF1 binding to haemin agarose beads

SDS PAGE gels show **M)** KDa Marker **L)** Load of BSA at around 60 kDa and the lower molecular weight band of Gly1ORF1 **UB)** Unbound protein after incubation with the beads and **B)** proteins bound to the beads. Bar charts show the amount of Gly1ORF1 protein as a percentage of the total protein in the load and bead lanes quantified using ImageJ software and analysed using an independent t-test. Red error bars represent standard deviation. Both tagged and untagged protein were significantly enriched on the beads (****$p \leq 0.0001$, ***indicates $p \leq 0.001$).

3.2.5 Haem binding of *E. coli* cells expressing native Gly1ORF1

The ability of Gly1ORF1 to bind haemin at the bacterial cell surface was investigated using Bl21Star(DE3) *E. coli* expressing Gly1ORF1 from the pET21a plasmid. Protein expression was induced by autoinduction and after overnight growth cells were pelleted by centrifugation and resuspended to an optical density of A_{600} = 0.1 in PBS with the addition of 40 µM haemin. Cells expressing the *N. meningitidis* haemoglobin receptor (HmbR) were used as a positive control for haem binding and those containing only the empty pET21a vector were used as a negative control. After 60 minutes incubation at room temperature, the cells were pelleted by centrifugation, washed in PBS then 5 µl was spotted onto nitrocellulose membrane and the presence of haemin was detected using ECL reagent due to the intrinsic peroxidase activity haemin possesses.

The dot blots were semi-quantitatively analysed using Image J software to compare densitometry of the spots as a percentage of the "lane" total. Each lane consisted of one replicate of the negative and positive controls and an experimental sample. Cells expressing Gly1ORF1 bound significantly more haemin from solution than those containing the empty expression vector. Cells expressing HmbR could bind significantly more than both the Gly1ORF1 expressing cells and the negative controls. Figure 3.8 shows that the haem binding can be visually confirmed by inspecting the cell pellet after washing and centrifugation steps.

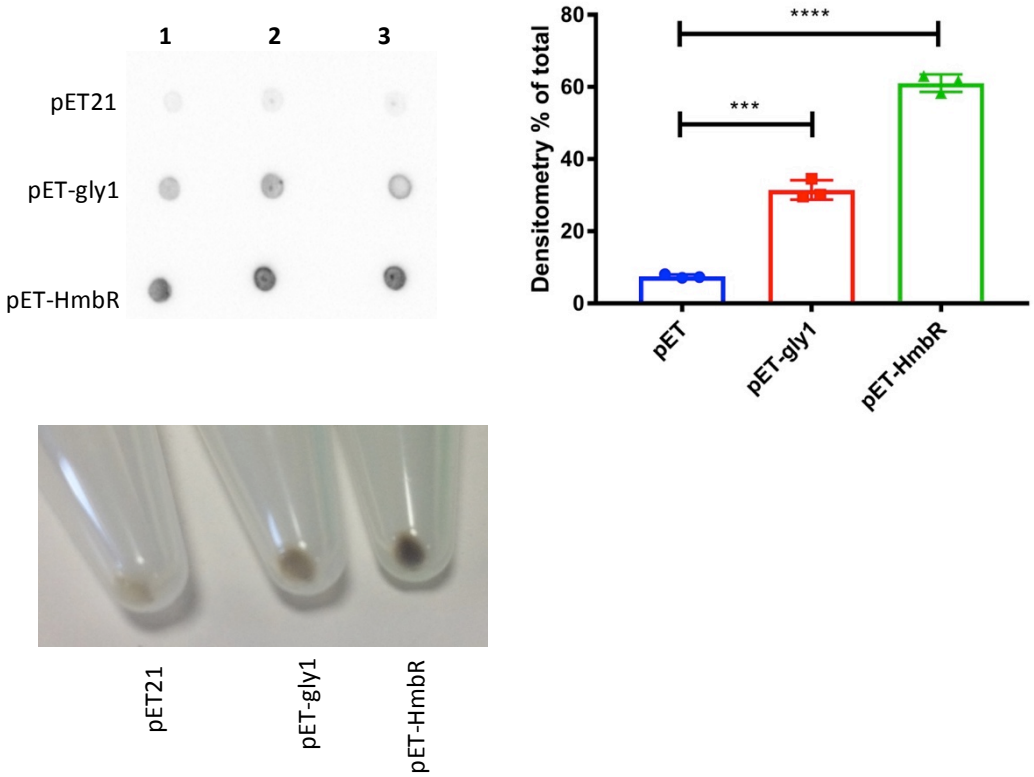

Figure 3.8 Haemin binding ability of *E. coli* expressing Gly1ORF1
Dot blot showing amount of haemin bound to *E. coli* cells expressing Gly1ORF1 and the haemoglobin receptor HmbR. Cells containing the empty expression vector pET21 were used as a negative control. Blots analysed by densitometry using ImageJ and expressed as percentage of lane total. Photograph shows after incubation with haemin cell pellets expressing Gly1ORF1 are darker than controls and HmbR cells are darker still, indicating more haemin bound. Densitometry analysed using unpaired t-tests *** p≤0.001, **** p≤0.0001.

3.2.6 Purification of C-His Gly1ORF1

The purification of high yields of native Gly1ORF1 protein was unsuccessful, but the assays described above show that the native Gly1ORF1 does have some innate haem binding ability. Therefore, C-terminal 6xhis-tagged Gly1ORF1 was produced using a pJONEX construct created by Meadows to carry out further assays (Meadows, 2005). C-His Gly1ORF1 was produced by large-scale heat inducible expression (see Materials and Methods 2.5.2) in M72 *E. coli* cells. A readily visible band corresponding to CHis-Gly1ORF1 that migrated slightly faster than the 20 kDa marker was detected via SDS-PAGE in the cell pellet after overnight incubation. Another band of the same size was present in the culture supernatant and was confirmed as Gly1ORF1 by western blot using a polyclonal rabbit anti-Gly1ORF1 antibody. CHis-Gly1ORF1 was purified from the filtered culture supernatant using a nickel chelate column. The supernatant was

supplemented with 20 mM imidazole and 200 mM NaCl to minimize non-specific binding to the column and 1.5 mM $NiSO_4$ was added to prevent stripping of the nickel column by other components of the culture supernatant as had been observed previously (Wierzbicka, 2014). CHis-Gly1ORF1 was eluted from the column by step increases of imidazole concentration and pure fractions were dialysed into 50 mM sodium acetate, 50 mM NaCl pH 4.

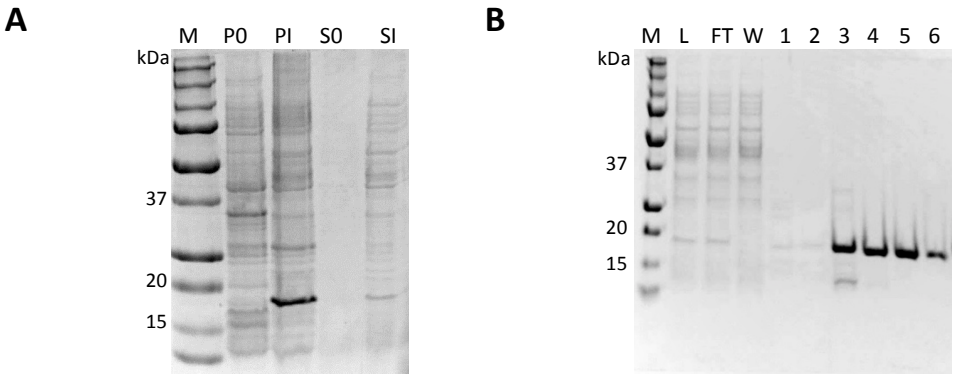

Figure 3.9 expression and purification of C-his Gly1ORF1 from pJONEX4 expression system
A) Expression of Gly1ORF1 in fermenter culture. Sample of the cells taken before induction (P0) and after overnight growth (PI) and of the culture supernatant (S0, SI). A band corresponding to C-his Gly1ORF1 around 17 kDa is present in the overnight samples of cell pellet and supernatant. **B)** C-his Gly1ORF1 purified from the culture supernatant by IMAC. Lanes show load (L), flow-through (FT), wash (W) and two elution steps of 100 mM (1,2) and 500 mM (3-6) Imidazole. Fraction 4 and 5 were pooled and concentrated for crystallography (36 ml at 0.311 mg/ml = 11.19 mg).

3.2.7 UV-visible spectra of C-hisGly1ORF1 interaction with haemin and haemin analogues

Changes in the UV-visible absorbance spectra of haemin can be indicative of a protein interaction. Haemin alone in a neutral pH solution exhibits a Soret band with a peak absorbance around 385 nm. Haem binding proteins have been shown to induce bathochromic (increasing peak wavelength), hypsochromic (decreasing peak wavelength) and hyperchromic (increase in the molar absorptivity) shifts in the haemin UV-visible spectrum (Karnaukhova et al., 2014; Qi et al., 1999; Sachla et al., 2014; Zhu et al., 2000b).

The UV-visible spectrum of haemin was analysed for changes caused by the presence of increasing amounts of Gly1ORF1. The spectra for the haem analogues deuteroporphyrin IX dihydrochloride (DPHCl) and deuteroporphyrin IX 2,4 bis ethylene glycol (DPBG) were also analysed for potential interactions. The structure of these compounds is shown in Figure 3.10, they are porphyrin based but do not contain a central metal iron.

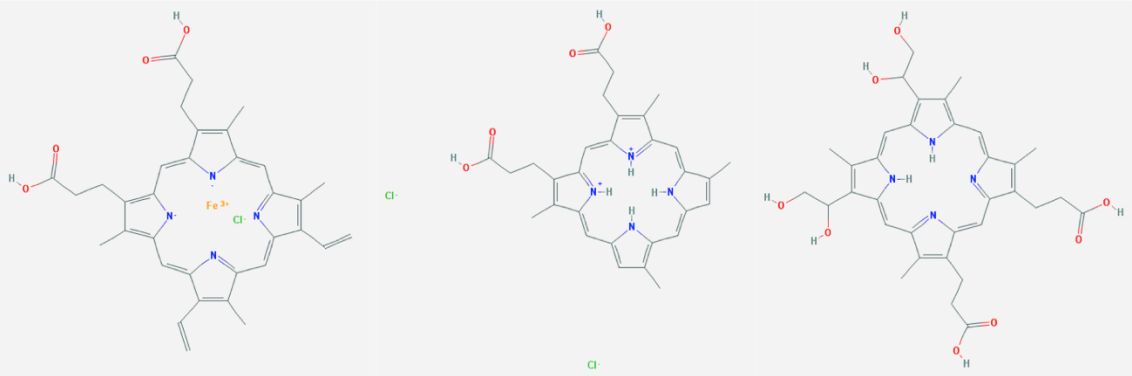

Figure 3.10 Structure of haemin and haem analogues used in this study
The 2D structures of haemin - left, deuteroporphyrin IX dihydrochloride (DPHCl)- middle and deuteroporphyrin IX 2,4 bis ethylene glycol (DPBG)- right. Both DPHCl and DPBG do not have a central coordinated metal ion and differ from haemin by their side chains. From PubChem (*https://pubchem.ncbi.nlm.nih.gov*)

In the bottom right panel of Figure 3.11 the change in absorbance at the peak of the spectra (calculated by subtracting the haemin/analogue alone value from the value when incubated with Gly1ORF1) is plotted against the concentration of Gly1ORF1 in the experiment. This shows that Gly1ORF1 caused a concentration dependent hyperchromic shift in the haemin spectra around the Soret peak– an increase in molar absorptivity at 388 nm. This was not caused by a precipitation effect because the absorbance was not increased across the spectrum. Increasing Gly1ORF1 concentration incubated with the haem analogues did not cause any concentration dependent changes in the spectra.

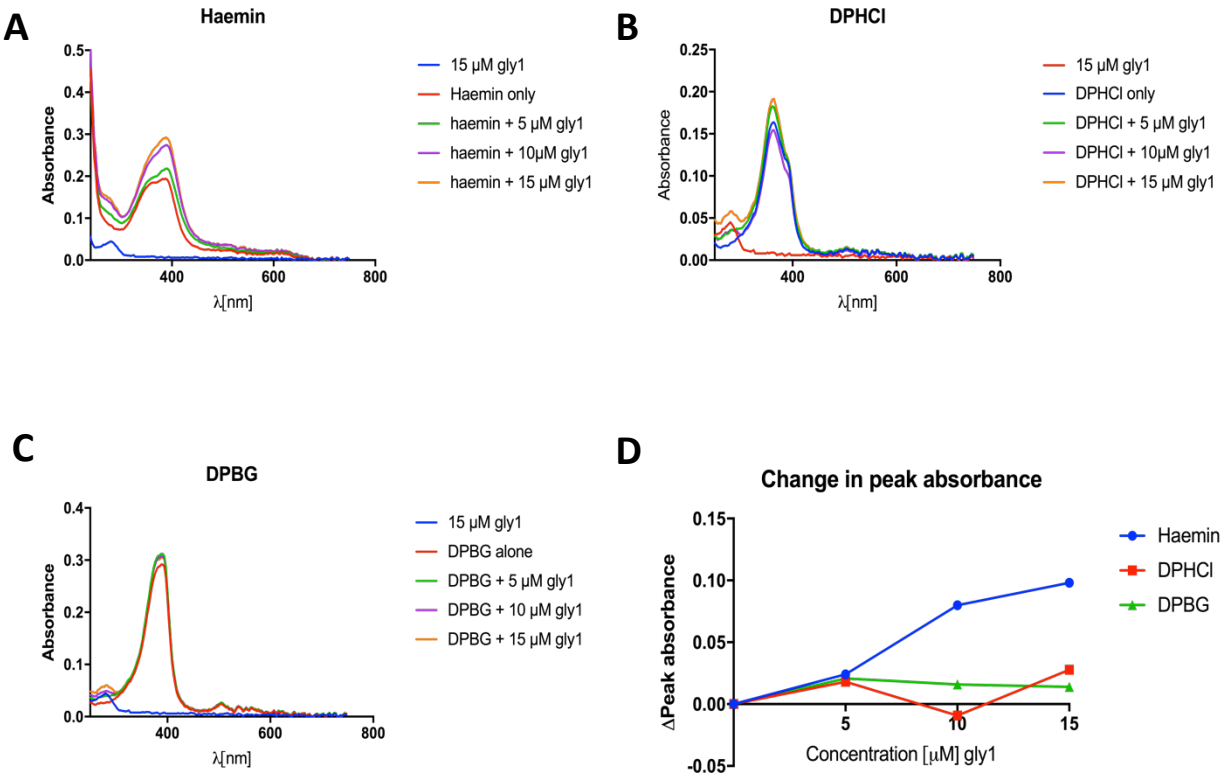

Figure 3.11 The effect of increasing Gly1ORF1 concentration on haemin and haem analogue UV-visible spectra
A) Haemin **B)** deuteroporphyrin IX dihydrochloride (DPHCl) and **C)** deuteroporphyrin IX 2,4 bis ethylene glycol (DPBG) at concentrations of between 3.6 and 3.8 µM were incubated with increasing concentrations of Gly1ORF1 and absorbance measured over wavelengths of 250-800nm (n=3). **D)** The increase in molar absorptivity (hyperchromic shift) at the peak wavelength was plotted against concentration of Gly1ORF1, the peak absorbance of haemin showed a Gly1ORF1 concentration dependent increase.

To further analyse the interaction of Gly1ORF1 with haemin the protein was used at a constant concentration of 10 µM and incubated with increasing amounts of haemin. The differences in the spectra of the concentrations of haemin alone (H) and the spectra of haemin incubated with Gly1ORF1 (GH) were calculated with the equation GH-H for each wavelength measurement. The difference spectra for each haemin concentration was plotted as shown in the top left panel of Figure 3.12 This shows that at the lowest haemin concentration (2.5 µM) the absorbance is increased across most of the spectrum, peaking at around 388 nm (bottom left panel Figure 3.12). With increasing concentrations of haemin the peak absorbance is not changed across the spectra but instead shows a change in the shape of the curve, and a bathochromic shift

in the region between 400 and 500 nm, with the peak difference at 418 nm. The change in absorbance at 418nm (ΔA_{418}) is shown in the top right panel of Figure 3.12.

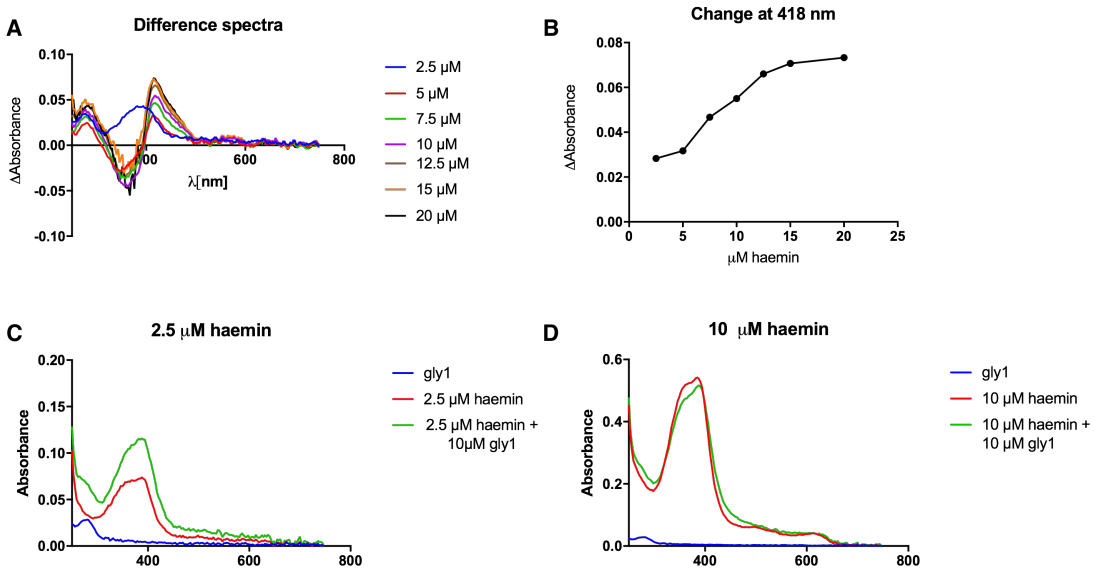

Figure 3.12 Difference spectra of Gly1ORF1 incubated with increasing haemin concentrations **A)** Difference spectra calculated by subtracting spectrum observed with concentration of haemin shown from spectrum of the same concentration of haemin incubated with 10 μM Gly1ORF1. **B)** Hyperchromic shift in the difference spectra at 418 nm plotted against haemin concentration. **C)** Examples of the spectra 2.5 μM and **D)** 10 μM haemin concentration spectra without (red) and with (green) addition of Gly1ORF1. At the lower concentration where Gly1ORF1 is in excess, there is a significant change in the spectra around the peak of 385 nm, at 10 μM with the addition of Gly1ORF1 there is a change in the shape of the peak, and an increase in absorbance around 418 nm.

3.2.8 Microscale thermophoresis of Gly1ORF1 interactions with haemin

The interaction of C-HisGly1ORF1 with haemin was studied using microscale thermophoresis. In this technique, fluorescently labelled protein is incubated with a potential ligand inside a glass capillary. A laser-generated temperature gradient is established in the capillary causing the movement (thermophoresis) of fluorescently labelled protein to change depending on several factors including its size and charge. The thermophoresis of the labelled protein incubated with increasing concentrations of ligand can be monitored by fluorescence and used to determine a K_d for the interaction.

Gly1ORF1 was exchanged into 1 x PBS 0.05% Tween-20 pH 7.4 buffer and fluorescently labelled using the Monolith NT^{TM} His-Tag Labelling Kit RED-tris-NTA (NanoTemper

Technologies GmbH) as described in Materials and Methods section 2.7.3. The protein concentration was constant at 50 nM in all experimental samples, and was incubated with decreasing concentrations of haemin (in 1 x PBS 0.05% Tween-20 pH 7.4) from 200 µM to 6.1 nM. Standard treated capillaries were used as they were determined to be optimal in the capillary test. The capillary scans show that there was no adsorption to the capillaries or ligand induced fluorescence changes. The highest four dilutions of haemin 200-50 µM were found to cause aggregation, so these had to be excluded from the measurements. Analysis of the measurements collected using the MO.Control software (NanoTemper Technologies GmbH) determined a dissociation constant (K_d) of 5.55 µM for the interaction between Gly1ORF1 and haemin. Attempts to replicate this experiment on subsequent days were unsuccessful due to significant issues with protein aggregation and adsorption. This was most likely due to the fact that the protein was stored in the pH 7.4 PBS-T buffer over several days and this pH is not optimal for solubility of Gly1ORF1, which is more stable in lower pH conditions.

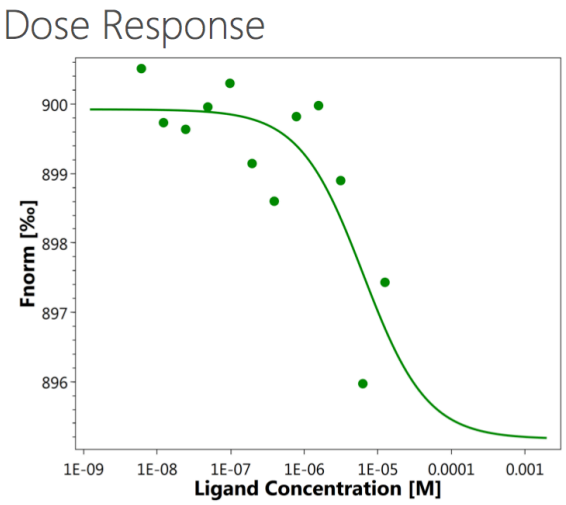

Figure 3.13 Microscale thermophoresis of Gly1ORF1 – haemin interactions
Dose response curve of Gly1ORF1 (50 nM) interaction with haemin (ligand) concentrations from 200 µM to 6.1 nM. The four highest haemin concentrations were excluded from the analysis because of protein aggregation. The line represents curve fitting using the equation for K_d determination.

3.2.9 Structural properties of C-HisGly1ORF1

3.2.9.1 Crystallisation trials – apo Gly1ORF1

Crystallisation trials were performed using the WT *N. meningitidis* Gly1ORF1 protein to generate crystals that could be used for x-ray diffraction and structure solution. Trials were carried out in 96-well plate format using the sitting drop method in a 1:1 ratio of protein to condition. The commercial screens PACT, JCSG+ (Molecular dimensions) and pH Clear (Qiagen) were used for initial screening. Crystals formed overnight in many conditions in the PACT and JCSG+ screens. The crystals were of similar morphology in all conditions as shown by the photographs in Figure 3.12, which shows the conditions that crystals were used for data collection. These were: PACT G12 (2 M sodium malonate, 0.1M Bis Tris propane pH 7.5, 20% PEG 3350), JCSG +F4 (0.1 M HEPES 20% v/v Jeffamine® M-600), JCSG+ G6 (0.2 M sodium malonate, 20% PEG 3350), JCSG+ B12 (0.2 M Tri-potassium citrate pH 8.3, 20% w/v PEG 3350) and JCSG+ D2 (0.2 M Magnesium chloride, 0.1 M Sodium HEPES pH 7.5, 30% v/v PEG 400).

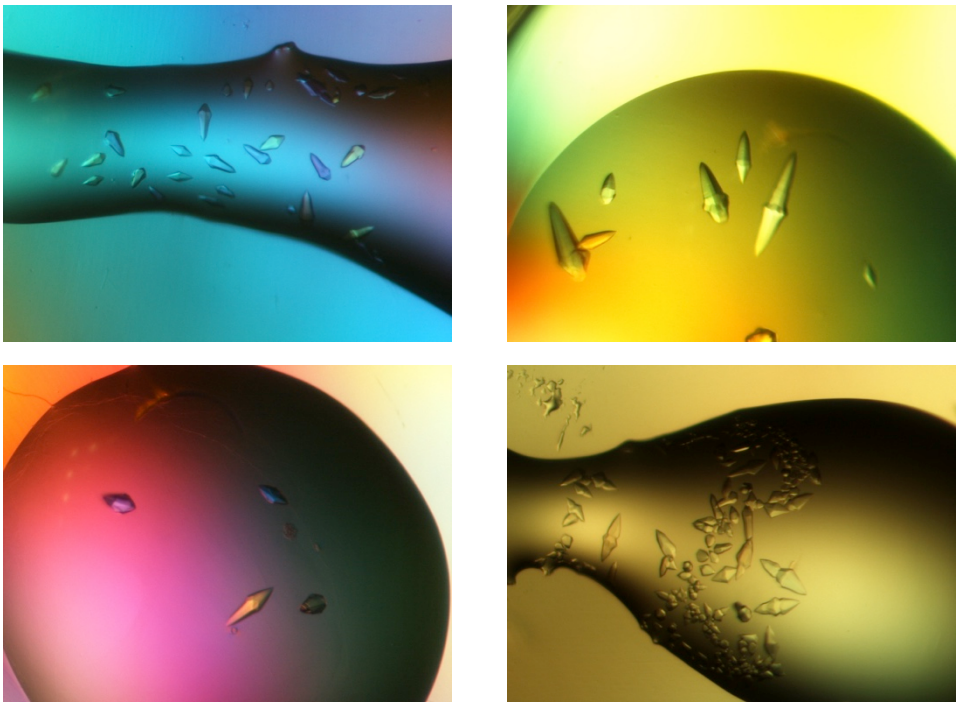

Figure 3.14 Crystals of C-HisGly1ORF1 used for x-ray diffraction data collection
C-HisGly1ORF1 crystals formed under many conditions in screens at 8 mg/ml, all with the same morphology. Crystals from the above conditions were harvested for data collection. Clockwise from top left: PACT G12 (2 M sodium malonate, 0.1M Bis Tris propane pH 7.5, 20% PEG 3350), JCSG +F4 (0.1 M HEPES 20% v/v Jeffamine® M-600), JCSG+ G6 (0.2 M sodium malonate, 20% PEG 3350), JCSG+ B12 (0.2 M Tri-potassium citrate pH 8.3, 20% w/v PEG 3350).

3.2.9.2 C-HisGly1ORF1 co-crystallisation with haemin

Co-crystallisation trials with C-HisGly1ORF1 and haemin were carried out as described in Materials and Methods section 2.6.10. Briefly, C-HisGly1ORF1 was diluted to 1 mg/ml in a 1 ml volume and soluble haemin solution was added until it was present at a 10 times molar excess. The protein and haemin solution was incubated for an hour then concentrated and filtered through a 0.2 µm filter. Protein concentration was estimated to be approximately 3 mg/ml by SDS-PAGE analysis.

Co-crystallisation trials were carried out in 96 well plate format using the sitting drop method in a 1:1 ratio of protein to condition. The commercial screens PACT, JCSG+, Morpheus (Molecular dimensions) were used. After four days crystals had grown in Morpheus G2 and G3 conditions that had similar morphology to the crystals formed in the absence of haemin. These drops also contained a red-coloured precipitate that was most probably formed from the haemin binding to imidazole, which was present at 0.1

M in both of these buffer conditions. Crystals with a different morphology were also found in JCSG+ D10 (0.2 M calcium acetate, 0.1 M Sodium cacodylate pH 6.5, 40% (v/v) PEG 300) and Morpheus G2.

3.2.9.3 Crystallographic data collection and processing

X-ray diffraction data was collected by Jason Wilson (University of Sheffield) at Diamond Light Source. The apo-Gly1ORF1 crystals all diffracted to between 2 and 2.5 Å resolution, space group P 6_3. The crystal from the haemin co-crystallisation screen condition Morpheus G3 diffracted to 2.28 Å in space group P 6_3. The crystals from JCSG+ D10 and Morpheus G2 that had a different morphology did not diffract. It was not possible to test whether these crystals were formed of protein or buffer components because only 2 were formed. The diffraction statistics for JCSG+ B12 apo-Gly1ORF1 crystals are shown in table 3.1.

Table 3.1 Apo-Gly1ORF1 JCSG+ B12 data collection processing statistics

Data collection	Native
Wavelength (Å)	0.9282
Resolution range (Å)	29.71-2.53 (2.60-2.53)*
Space group	$P6_3$
Unit cell (a,b,c) (Å) (α,β,γ) (°)	99.76, 99.76, 81.85 90, 90, 120
Total reflections	171533 (12208)
Unique reflections	15525 (1111)
Multiplicity	11.0 (11.0)
Completeness (%)	99.7 (97.4)
Mean I/σ	21.7 (2.8)
Wilson B factor (Å^2)	37.7152

*Figures in parenthesis refer to outer shell

Matthews cell content analysis was carried out in CCP4 and in the cases of both the apo-Gly1 and haemin co-crystallisation crystal predicted that 3 molecules per asymmetric unit should be expected. The calculation for the JCSG+ B12 crystal is shown in table 3.2. The most likely coefficient (V_M) is 2.56 $Å^3$/Da and solvent content of 51.95% with a probability of 0.73 (scale of 0 to 1.00).

Table 3.2 Matthews cell content analysis Apo-Gly1ORF1 JCSG+ B12

Number in asymmetric unit	Matthews coefficient ($Å^3$/Da)	% Solvent	Probability
1	7.67	83.98	0.00
2	3.84	67.97	0.05
3	**2.56**	**51.95**	**0.73**
4	1.92	35.93	0.21
5	1.53	19.92	0.00
6	1.28	3.90	0.00

3.2.9.4 Structure of wild type N. meningitidis Gly1ORF1 solved using molecular replacement

The diffraction data from JCSG+ B12 Gly1ORF1 crystals at 2.2 Å was chosen to solve the structure. The co-ordinates for *Neisseria meningitidis* K12A mutant Gly1ORF1 (provided by Jason Wilson) were used for molecular replacement using PhaserMR (McCoy et al., 2007). The co-ordinates of Gly1ORF1K12A chain B were isolated and saved to a separate file which was used as the model as this was the most complete chain in the structure. The sequence identity was set to 80% and the program was set to search for 3 molecules of the model in the asymmetric unit as was suggested by the Matthew's coefficient calculation. Molecular replacement using these settings was not successful, a single solution could not be found and the program ran for too long so the job was terminated. The number in the asymmetric unit search was changed to 2 molecules, as this had been the number in the original K12A structure solution. Using this setting a single solution was found with a translation function Z-score equivalent

(TFZ) of 60.2 and log likelihood gain (LLG) 3745, indicating a correct solution. This solution was then processed through 10 cycles of restrained refinement using refmac5 (Murshudov et al., 2011), which decreased the R factor from 0.34 to 0.25 and the R_{free} from 0.35 to 0.28.

3.2.9.5 Structure building, refinement and validation of model

The structure of JCSG+ B12 Gly1ORF1 was rebuilt in Coot (Emsley et al., 2010). Residues were removed where there was no electron density and built in where new density was present in the difference electron density map. Side chains were removed or added where possible, including the lysine side chain at position 12 in both chains. In between each phase of rebuilding refinement was carried out in refmac5. New electron density allowed the residues 52-55 in JCSG+ B12 chain B to be built showing the loop that has been absent from all previous structures. In the final model 224 out of a possible 236 residues were built (94.92%). The R factors were 0.224 R_{work} and 0.265 R_{free}, detailed refinement statistics are shown in table 3.3.

Table 3.3 Refinement statistics for apo-Gly1ORF1 JCSG+ B12

Rfactor	0.224
R_{free}	0.265
Protein residues	224
Ligands	8 atoms– 2x ethylene glycol
Water	63 atoms
RMSD (bonds) (Å)	0.0150
RMSD (angles) (°)	1.7113

When the electron density map could no longer be interpreted validation was carried out using MolProbity (Chen et al., 2010), and the results are shown in table 3.4 The model contained 97.22% favoured Ramachandran angles and no Ramachandran outliers. Of 175 residues where the side chains were built, 163 (93.14%) rotamers are

favoured and none are poor. The overall MolProbity score (combination of the clashscore, rotamer and Ramachandran evaluations) was very good for structures of this resolution, in the 100th percentile compared to 10098 structures with resolution 2.22Å ± 0.25Å.

Table 3.4 MolProbity structure validation table

All-Atom Contacts	Clashscore, all atoms:	0.6	100th percentile* (N=454, 2.22Å ± 0.25Å)
	Clashscore is the number of serious steric overlaps (> 0.4 Å) per 1000 atoms.		
Protein Geometry	Poor rotamers	0 (0.00%)	Goal: <0.3%
	Favored rotamers	163 (93.14%)	Goal: >98%
	Ramachandran outliers	0 (0.00%)	Goal: <0.05%
	Ramachandran favored	210 (97.22%)	Goal: >98%
	MolProbity score^ 0.84	100th percentile* (N=10098, 2.22Å ± 0.25Å)	
	Cβ deviations >0.25Å	0 (0.00%)	Goal: 0
	Bad bonds:	0/ 1747 (0.00%)	Goal: 0%
	Bad angles:	1 / 2358 (0.04%)	Goal: <0.1%
Peptide Omegas	Cis Prolines:	0 / 2 (0.00%)	Expected: ≤1 per chain, or ≤5%

*The 100th percentile is the best among structures of a similar resolution, the 0th is the worst.
^ The MolProbity score combines clashscore, Ramachandran and rotamer evaluations into a single score, normalised to be on the same scale as X-ray resolution.

3.2.9.6 Gly1ORF1 Structural analysis

The final model of Gly1ORF1 contained two monomers and 224 residues out of a possible 236. The C-terminal histidine tag was not visible on either chain and the signal sequence was also absent. The absence of the signal sequence suggests that it was recognised and processed by *E. coli,* as has been observed previously (Arvidson et al., 1999). The overall structure is very similar to the previously solved neisserial Gly1ORF1 proteins. It mainly consists of two anti-parallel β-sheets, the first made up of four β-strands and the second of five strands. They are connected by a short α-helix between residues 42 and 48. There is very little structural difference between the two monomers in the asymmetric unit, they align with an average RMSD (root mean square deviation) over 88 residues of 0.2 Å. Chain A was built from residue Asp1 to Ser118, however of the two monomers chain B is more complete, with the peptide

backbone of all residues between Thr2 and Ser118 built. The residues 52-58 and 81-83 could not be built in chain A. These residues form the loops between β-strands 5-6 and 7-8 respectively (labelled on Figure 3.14).

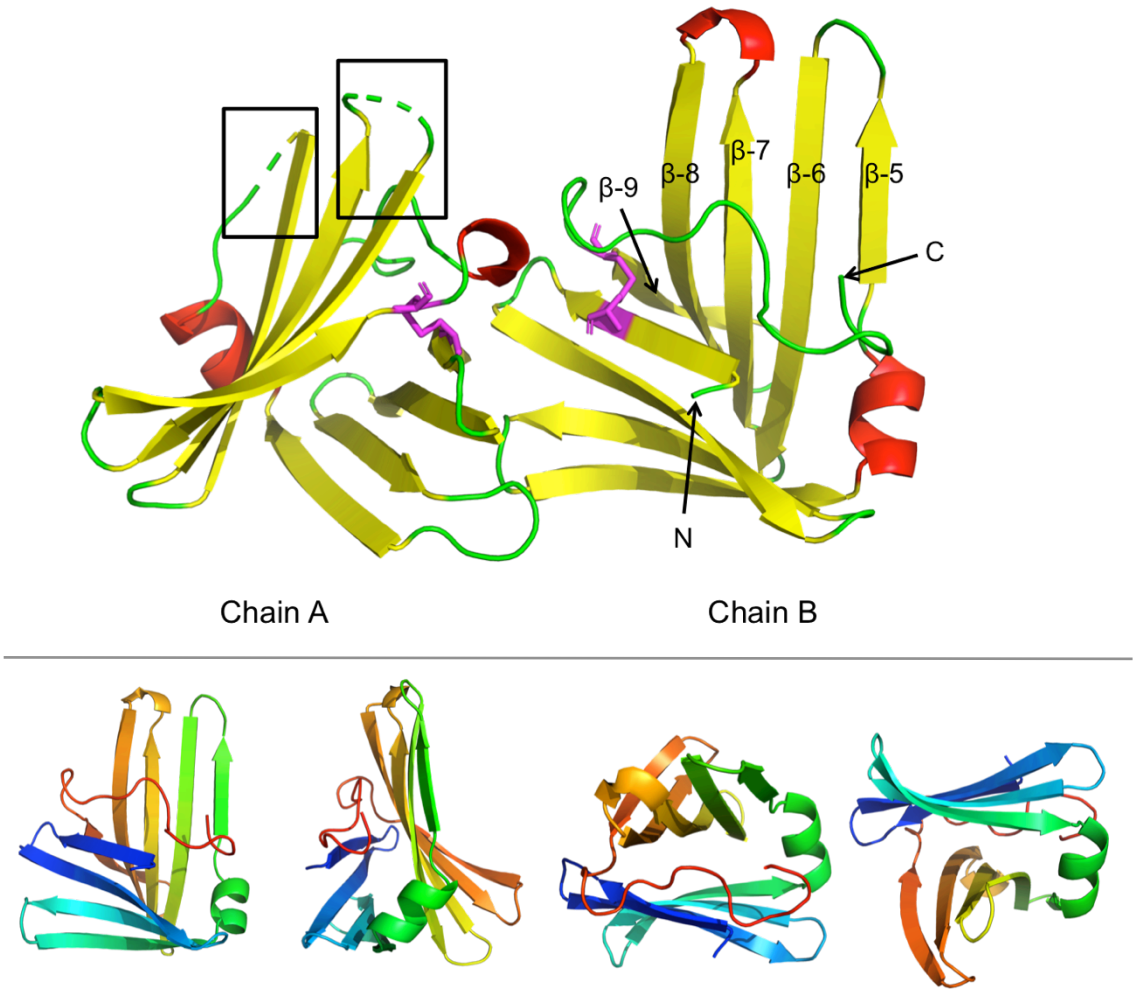

Figure 3.15 Structure of wild type *N. meningitidis* Gly1ORF1 solved by X-ray crystallography
Cartoon representation of the structure of Gly1ORF1 as it appears in the crystal cell. There are two chains in the asymmetric unit, chains A and B. Chains are coloured by secondary structure, β-strands yellow, α-helices red and loops green. The N and C termini of chain B are indicated with arrows. Chain B is more complete, with all the residues between 2 and 118 built. The two sections that could not be built in chain A are indicated in black boxes these are the loops between β-strands 5-6 and 7-8 as indicated on chain B. The disulphide bond between the cysteines on β-strands 1 and 9 are shown as magenta sticks. Views of four sides of chain B are shown below coloured from blue at the N-terminus to red at the C-terminus. Figure created in Pymol.

3.2.9.7 Gly1ORF1 biological assembly and interactions

Previous studies have shown evidence that Gly1ORF1 can form dimers and larger multimers, especially in the presence of haemin (Sathyamurthy, 2011; Wierzbicka, 2014). The Gly1ORF1 structure was analysed using the PISA server to determine whether any of the interactions in the crystal structure could be a biologically relevant dimeric form. Analysis revealed a potential assembly of two Gly1ORF1 monomers that fell in to a "grey area", where the program could not determine whether it would be stable in solution. Overall the assembly has a negative delta free energy of association (ΔG^{int} = -8.79 kJ mol^{-1}) but the delta free energy of dissociation is also negative (ΔG^{diss}= -6.69 kJ mol^{-1}) indicating that it may not be thermodynamically stable in solution. The buried surface area for this assembly is 11.8% (1380 Å buried out of 11710 Å total). One protein-protein interface was identified with a $\Delta^{i}G$ P-value less than 0.5 (0.165). This value suggests that the interface is more hydrophobic than would be expected for the protein surface and is likely to be a specific interaction instead of an artefact of crystal packing. The interface consists of 12 residues from chain B (10.3% of total residues) and 17 from chain A (15.9% of total residues). Figure 3.16 shows the proposed dimer and the black box inset of the protein-protein interface. Two residues from chain A (Glu35 and Tyr72) form hydrogen bonds with three residues from chain B (Val81, Gly56 and Arg59). Glu35 from chain A is particularly important for this interface as it forms three hydrogen bonds, two with B-Arg59 and one with B-Gly56. PISA analysis also shows that a salt bridge formed between A-Glu35 and B-Arg59 in this model. Previous structural studies of Gly1ORF1 have not carried out this kind of bioinformatic analysis to identify the likely biological dimer and protein-protein interface (Sathyamurthy, 2011; Wierzbicka, 2014). Instead they used the two Gly1ORF1 monomers as they appeared in the crystal cell in their attempts to identify potential haem binding pockets and residues. The analysis here shows that the dimer that was previously predicted is not likely to be stable in solution and therefore that residues predicted to be in the binding site are more likely distributed across the assembly surface.

Hydrogen bonds			
	Structure B	Distance (Å)	Structure A
1	Gly56 [N]	2.96	Glu35 [O]
2	Arg59 [NE]	3.22	Glu35 [OE1]
3	Arg59 [NH_2]	3.39	Glu35 [OE1]
4	Val81 [O]	2.68	Tyr72 [OH]

Salt Bridges			
	Structure B	Distance (Å)	Structure A
1	Arg59 [NE]	3.22	Glu35 [OE1]
2	Arg59 [NE]	3.70	Glu35 [OE2]
3	Arg59 [NH_2]	3.39	Glu35 [OE1]
4	Arg59 [NH_2]	3.57	Glu35 [OE2]

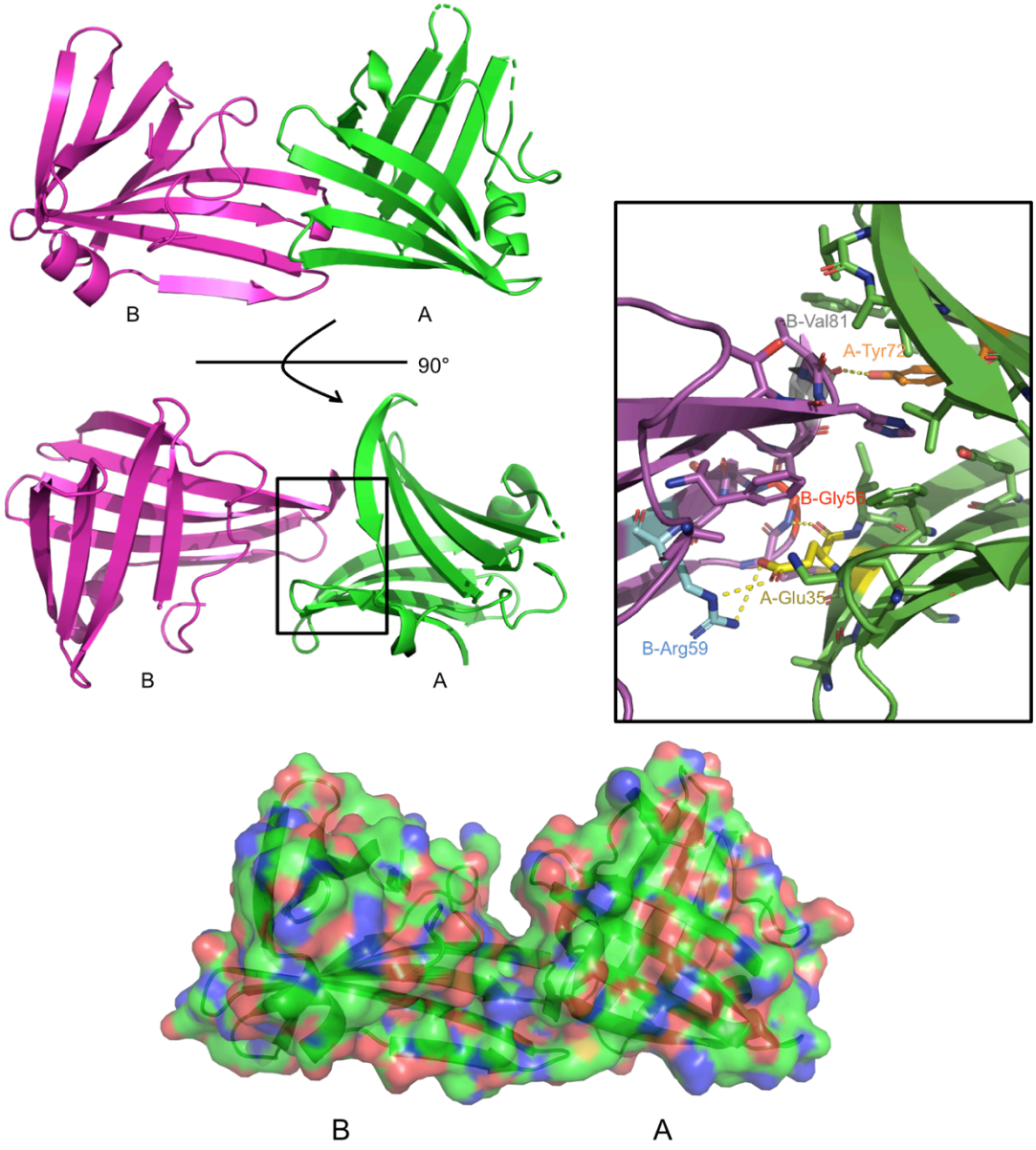

Figure 3.16 Gly1ORF1 dimeric assembly and interfacing residues predicted by PISA analysis
The two tables show the hydrogen bonds and salt bridges formed between monomers A and B. Specific atoms are shown in square brackets and the distance of the bonds in Å. A cartoon style side and top view of the assembly is shown below the tables. Chain B is coloured magenta and chain A green. The black box contains an enlarged view of the protein-protein interface. Interfacing residues are shown as sticks and those participating in hydrogen bonding are coloured differently. The four inter-chain hydrogen bonds are shown as yellow dotted lines. The bottom panel shows the solvent accessible protein surface. The surface is set to transparent to show the cartoon protein backbone inside. Surface colours are green for carbon, blue for nitrogen, and red for oxygen.

3.2.9.8 Structure of Gly1ORF1 from haemin co-crystallisation trial

To solve the structure of the protein using the crystal from the haemin co-crystallisation screen (Morpheus G3), the co-ordinates of chain B from the wild type Gly1ORF1 structure solved in this project (JCSG+ B12) were used for molecular replacement with PhaserMR. The program was set to search for two molecules of the model in the asymmetric unit and a single solution was produced with a TFZ score of 57.1 and LLG 3648. The Rfactor and R_{free} following molecular replacement were 0.3299 and 0.3446 respectively. The solution underwent 10 cycles of restrained refinement using Refmac5 that gave an R factor of 0.2392 and R_{free} 0.2784.The solution was viewed in Coot and the difference map density peaks analysed to determine whether the structure contained haemin. There were no areas of new density present that would indicate the presence of haemin.

3.3 Discussion

3.3.1 Expression and purification of non-tagged Gly1ORF1

Although it is possible to express and purify large quantities of C-hisGly1ORF1, purification of the native protein has so far proved difficult. Previous attempts to express the protein using the pJONEX4 and pET21a expression systems have resulted in very low levels of protein expression that did not allow for easy purification (Wierzbicka, 2014). Significant levels of expression were achieved when the signal peptide (residues 1-21) was removed, however, the protein was misfolded and insoluble (Wierzbicka, 2014). In this project an efficient *E. coli* over producing strain has been identified which appears to produce high levels of soluble native Gly1ORF1, much of which is secreted into the culture supernatant. This heat inducible construct contains both the *gly1ORF1* and *gly1ORF2* genes. Presence of the histidine tag on the C-terminus of ORF1 also allowed for high levels of expression so it may be due to stabilising the C-terminus.

Despite promising levels of protein expression apparent through SDS-PAGE analysis, yields of purified protein achieved from the protocols attempted here were very low. There are several stages in the protocols where a significant proportion of protein was lost. Initially proteins were precipitated from the supernatant using ammonium sulphate at 50% saturation in order to decrease the volume of the sample and

establish the correct buffer conditions for ion exchange chromatography. The yield of total protein from ammonium sulphate precipitation was low, and resulted in a low final yield at the end of the purification strategy.

NtGly1ORF1 bound very strongly to the blue-Sepharose media that was used as an affinity purification step and much of the protein was not eluted until NaCl concentration reached 1 or 2 molar. This could be investigated as a first step in the purification protocol, as it would be relatively specific and could potentially be used directly on the filtered supernatant without the need for dilution or pH adjustment.

The ammonium sulphate precipitation was omitted from the second purification protocol and the supernatant was diluted, pH adjusted and applied directly to a cation exchange column. The majority of Gly1ORF1 did not bind to this column and was eluted in the flowthrough. This was observed multiple times, as the flowthrough was diluted and passed through the column again each time only a small proportion of the protein would bind. A small amount did bind and was successfully purified using a subsequent size exclusion chromatography step. The yield from this purification protocol was also very low. This was partly due to problems encountered when concentrating the protein using Vivaspin concentrators before and after size exclusion chromatography. The protein concentration would often decrease dramatically during these steps, possibly getting stuck in the filter or precipitating even at this low pH that was optimal for the C-HisGly1ORF1 protein.

The small yields of native Gly1ORF1 protein produced here coupled with the problems concentrating the protein prevented any structural studies in this project. Protein concentrations optimal for crystal formation are typically in the range of 3-10 mg/ml, but it was not possible to achieve ntGly1ORF1 protein concentration of over 0.5 mg/ml in the pH 5.4 acetate buffer. In contrast the C-his Gly1ORF1 was soluble to over 15 mg/ml in this buffer. The pJONEX4 construct containing both *Gly1ORF1ORF1* and *ORF2* can produce significant levels of ntGly1ORF1 expression, similar to the expression levels of the C-his tag construct. It should be possible to purify large amounts of the native protein if the correct protocol is developed.

3.3.2 Haemin binding

The ability of C-his Gly1ORF1 to bind haemin has been demonstrated through haemin-agarose pull down experiments, haemin absorbance spectra, Microscale thermophoresis, and haemin peroxidase activity assays (McMellon, 2016; Sathyamurthy, 2011; Wierzbicka, 2014). It is thought that Gly1ORF1 binds to haem as a dimer, as spectroscopy and crosslinking experiments show the protein binding haemin in a 2:1 ratio (Sathyamurthy, 2011; Wierzbicka, 2014).

The C-His tagged protein has a tendency to precipitate in the presence of haemin, which has made it impossible to gather any meaningful biophysical data on this interaction. In addition, the removal of the His tag from some Gly1ORF1 homologues by enterokinase treatment abolished their haemin binding ability in pull down assays (McMellon, 2016). Histidine has affinity for haemin and is found as a haem ligand in many haem-binding proteins (Bracken et al., 1999; Létoffé et al., 2005). This raised concerns that the haem binding observed was not an intrinsic function of the protein and that it could have been a non-specific interaction enhanced by the presence of the histidine tag. It is possible that the enterokinase treatment could have denatured the proteins and destroyed genuine haem binding sites. It was therefore desirable to produce a non-tagged version of the protein that does not have to be subjected to any tag removal treatment.

To test whether the his-tag was contributing to *N. meningitidis* Gly1ORF1 haemin binding, a native (non-tagged) version of *N. meningitidis* Gly1ORF1 was produced and purified in this project. The low yields prevented extensive investigation of haemin binding functions, but pull-downs could be performed and show that the absence of the tag still allowed significant enrichment of Gly1ORF1 on the haemin-agarose beads. This suggests that the protein itself can bind haemin. Unfortunately, too little ntGly1ORF1 was purified to carry out any of the other haem binding assays for comparison, but they should be attempted once the ntGly1ORF1 purification protocol has been optimized. The ability of ntGly1ORF1 to bind to haemin was demonstrated in a bacterial cell model. *E. coli* cells expressing native Gly1ORF1 showed increased binding of haemin from solution when compared to cells possessing an empty expression vector. The *N. meningitidis* haemoglobin receptor HmbR was used as a

positive control for this assay and both HmbR and Gly1ORF1 significantly increased haemin binding. This indicates that Gly1ORF1 can bind haemin at the bacterial cell surface.

The results of the UV-visible spectra of haemin incubated with C-HisGly1ORF1 also indicate that Gly1ORF1 interacts with haemin, causing a change in the spectral properties of the compound. The hyperchromic and bathochromic shifts in the haemin spectra caused by Gly1ORF1 interaction were not observed in the haemin analogue (DPHCL and DPBG) spectra. This may indicate that Gly1ORF1 does not interact with them, either because they do not contain iron or because their additional side chains prevented interactions. In order to test whether the interaction between Gly1ORF1 and haemin is iron dependent these experiments could be repeated using protoporphyrins co-ordinating alternative transition metal ions such as cobalt, zinc, nickel or copper. These have been used to study haemophores such as *P. gingivalis* HmuY and have aided in the determination of haemin binding sites and axial ligands (Wójtowicz et al., 2013). Alternatively, there may have been an interaction that caused spectral shifts too subtle to detect with these methods. These analogues do not have coordinated metal ions and changes to the spin of metal ions normally causes the most visible shifts in spectra.

The MST analysis of the Gly1ORF1-haemin interaction suggested a K_d of 5.55 µM. Although the results could not be successfully replicated in this project, this can act as a comparison with previous analysis of Gly1ORF1 mutant interaction with haemin. Gly1ORF1 mutants G47R, M63A and Y72F all had haemin affinities up to 10 times stronger than this (K_d values 1.16, 1.07, 0.577 µM respectively)(Wierzbicka, 2014). However, it is not clear whether these changes to haemin indicate that these residues are specifically involved in haemin binding. M63A and Y72F side chains face inwards from β-sheets 5 and 7 (strands labelled in Figure 3.15) so are unlikely to be accessible for ligand binding.

The results in this study in addition to previous work support the hypothesis that Gly1ORF1 interacts with haem. However, without robust biophysical data on the interaction that would allow identification of the binding site it is not possible to

conclude whether any interactions between Gly1ORF1 and haem are specific or physiologically relevant.

3.3.3 Crystallography and structural analysis of WT *N. meningitidis* Gly1ORF1

Crystals of *N. meningitidis* WT Gly1ORF1 formed readily after optimisation, with most appearing overnight. The crystals grown in these trials were all morphologically similar, and similar to previous Gly1ORF1 crystals from *N. gonorrhoeae, N. meningitidis* Gly1ORF1 mutants and the Gly1ORF1 paralogue from *M. haemolytica* (Arvidson et al., 2003; McMellon, 2016; Wierzbicka, 2014). All of the Gly1ORF1 family proteins characterised structurally have crystallised in space group $P6_3$ and diffracted to similar resolutions (between 2.1 and 2.5 Å). The model built in this project has improved on previous Gly1ORF1 structures as it includes a complete protein backbone from residues 2 to 118. The two loops in chain B that connect β-strands 5-6 and 7-8 could be built as there was electron density present here that was not visible in the K12A map.

The validation carried out using MolProbity indicates that the model is generally very good compared to other structures at similar resolutions. However, the side chains of 49 out of the total built 224 residues (21.88%) could not be built due to poor electron density. Missing side chains can cause problems in interpretation of a crystal structure, particularly when looking at surface charges and identifying potential ligand binding pockets through bioinformatics. To further improve the Gly1ORF1 structure optimizations such as micro-seeding could be carried out to attempt to generate an alternative crystal form that may diffract to a higher resolution.

The solvent content of the crystals was predicted to be 67.97%, which is higher than usual for protein crystals. Matthews observed that majority of protein crystals have solvent content between 27 and 65 % with the average being 43% (Matthews, 1968). More recent analysis of proteins deposited in the protein data bank has revised this average to 51% with a mean V_M of 2.68 $Å^3$/Da but this varies according to crystal system or cell type (Chruszcz et al., 2008). For tetragonal crystal systems (including space group P 6_3) mean solvent content is 56% and mean Matthew's coefficient 3.04 $Å^3$/Da (Chruszcz et al., 2008). Crystals with lower solvent content tend to produce higher resolution diffraction data (Kantardjieff and Rupp, 2003). Dehydration of

protein crystals to lower the solvent content has improved diffraction of some crystals dramatically (Heras et al., 2003; Krauss et al., 2012; Kuo et al., 2003). This can be achieved through several methods, mostly involving equilibrating crystals in buffer with higher concentration of precipitants (Heras and Martin, 2005; Huang and Szebenyi, 2016). This may be a worthwhile optimization to attempt to improve the resolution of the Gly1ORF1 structure.

3.3.4 Biological assembly

The ability of Gly1ORF1 to form dimers has been observed using multiple techniques including dynamic light scattering, size exclusion chromatography, chemical crosslinking and non-reducing SDS-PAGE (Arvidson et al., 2003; Sathyamurthy, 2011; Wierzbicka, 2014). However, previous structural studies of Gly1ORF1 did not carry out any bioinformatic analysis of potential protein assemblies or dimer interfaces (Sathyamurthy, 2011; Wierzbicka, 2014). Instead they used the two monomers as they appeared in the crystal cell asymmetric unit to identify potential haemin binding pockets and created mutations in these areas in attempts to identify key residues for haemin binding. None of these mutations significantly affected solubility, oligomerisation or haemin binding ability of Gly1ORF1 (Sathyamurthy, 2011; Wierzbicka, 2014). Analysis in this study using the PISA server shows that the interface identified in previous studies is not likely to be stable in solution and instead has identified another assembly that may be the biologically relevant dimeric form. The PISA analysis could not definitely conclude whether the assembly identified in the WT Gly1ORF1 crystal would be stable in solution as the predicted affinity constants fell in to a “grey zone”. *In vitro* experiments would need to be carried out to verify whether this assembly is genuine. This could include creating mutations in the interfacing residues, especially Glu35 and Arg59 which form multiple hydrogen bonds and salt bridges between the two chains, and analysing dimer formation through the experimental methods mentioned above.

It would also be interesting to learn whether mutations disrupting this dimer interface affect the solubility of Gly1ORF1 and its behaviour in solution. The native form of the protein produced in this project was difficult to handle, as it often precipitated during concentration. The *N. meningitidis* Gly1ORF1 K12A mutant studied previously in our

group exhibited increased solubility compared to the wild type protein at higher protein concentrations (Wierzbicka, 2014). Comparison of the two crystal structures shows they do not differ significantly in structure, the two align with an RMSD of 0.26 Å. The lysine residue at position 12 on chain A forms part of the interface identified by PISA. If this is a biologically relevant interface, then the mutation of lysine to alanine could decrease the affinity between monomers and contribute to the different behaviour observed in solution.

It may be the case that the dimeric form of Gly1ORF1 is not present in these crystals and the conditions used in these experiments favour crystallisation of the monomeric form. Further optimizations could be carried out to ascertain whether alternative multimers could be crystallised. Some analysis suggests that temperature is an important factor in determining the crystal form when different crystal forms are competing (Fusco and Charbonneau, 2014). In addition, Gly1ORF1 has been observed to form dimers and larger multimers particularly in the presence of haemin (McMellon, 2016; Sathyamurthy, 2011; Wierzbicka, 2014), and this or an alternative small molecule ligand may be required to stabilise Gly1ORF1 dimer interactions.

3.3.5 Haemin binding structural analysis

Although diffracting protein crystals were successfully grown in the Gly1ORF1-haemin co-crystallisation trials, when the structures were solved by molecular replacement there was no additional electron density in the difference maps to indicate that haemin was present in the structures. This could be due to low occupancy of the ligand in the potential Gly1ORF1 binding sites. The affinity of WTGly1ORF1 and haemin is not known, but the MST results suggest a K_d in the micromolar range. Protocols for co-crystallisation generally suggest a ligand concentration of between 3 and 10 times the K_d of the interaction (Hoeppner et al., 2013; Müller, 2017). The haemin concentration in the co-crystallisation was 0.5 mM which is 100 times higher than the predicted K_d, so if there is a genuine interaction this concentration should be sufficient for co-crystallisation. An alternative method for generating protein-ligand crystals is soaking pre-formed protein crystals with ligand solution. This was attempted by previous members of our group but did not produce diffracting crystals (McMellon, 2016; Wierzbicka, 2014). This method is again hampered by the requirement for high

concentrations of ligand. Soaking can also produce misleading results due to crystal packing artefacts. Crystal packing can occlude ligand binding sites, or protein interfaces can be created in the lattice that would not be present in solution.

Harvesting and cryopreserving co-crystallised protein and ligand ready for diffraction can be particularly difficult. The ligand must be present at a sufficient concentration in the cryoprotectant and ligand is often lost from the crystal in these stages (Müller, 2017). Recent advances in crystallisation technology developed for screening chemical libraries for drug development could make this easier. These include plates pre-coated in ligand that protein crystals can form around and *in situ* ("in plate") diffraction to minimise handling of crystals (Gelin et al., 2015).

Some crystals were generated in the co-crystallisation trial that had a different morphology to the other Gly1ORF1 crystals but unfortunately they did not diffract. As there were only two crystals formed it was not possible to test whether they were protein or salt crystals as most methods for determining this, such as crushing the crystals or staining for protein, render the crystals unusable for diffraction. Further optimization around these conditions (JCSG+ D10 and Morpheus G2) could be carried out to improve the quality of these crystals for diffraction and to generate more to verify whether they contain protein.

It is difficult to predict haem binding sites from structural information alone, as there are a wide variety of haem binding mechanisms and binding motifs in structural databases. Proteins involved in haem uptake generally bind strongly to haem through an axial ligand which coordinates the central iron atom. This is most commonly histidine but can be lysine, tyrosine, cysteine or methionine. For example, the TBDTs HasR and ShuA coordinate haem through a conserved histidine residue, and the HasA haemophore used both a histidine and tyrosine residue to coordinate the iron atom (Deniau et al., 2003; Smith et al., 2015). If the correct biological dimer can be identified in crystallisation optimization, *in silico* techniques could be used to model binding sites and docking of haem into the protein. This would overcome the challenges of co-crystallisation and models could be experimentally confirmed through site directed mutagenesis studies. Techniques such as CD spectroscopy and NMR chemical shift mapping that have been essential for determining the haem ligands in many haem

uptake proteins including HasA, HasR and HmuY could be employed to confirm *in silico* models (Létoffé et al., 2001; Smith et al., 2015; Wójtowicz et al., 2013).

Chapter 4 – Characterising Gly1ORF2

4.1 Introduction

In *N. meningitidis* MC58 *gly1ORF2* is a 741 bp gene that begins 38 nucleotides downstream of the *ORF1* stop codon. A ribosome binding site is present upstream of the start codon but there are no obvious -10 or -35 promoter sequences, suggesting that the genes could be co-transcribed. In preliminary characterisation of the locus, both genes were studied together, the genes were both deleted via transposon insertion in *N. gonorrhoeae* and also cloned into *E. coli* for recombinant expression (Arvidson et al., 1999). No ORF2 polypeptide was detectable from *E. coli* expression in that study so no functional characterisation could be carried out. The *gly1ORF1* gene and protein from *N. meningitidis* MC58 has since been studied individually in several projects including this, and further clues to its biological function and structural features have been discovered (Meadows, 2005; Sathyamurthy, 2011; Wierzbicka, 2014). The Gly1ORF2 protein has not yet been studied independently and there is no reported experimental data to explain its function as of March 2018.

The *ORF2* gene product has some homology to *E. coli hemD* protein product Uroporphyrinogen III synthase (UroS), sharing 28% identity over 75% of the sequence (expect value = 3e-13, residues 8-199). Uroporphyrinogen III synthase is part of the conserved core of the tetrapyrrole biosynthesis pathway, which is present in almost all known organisms (Dailey et al., 2017). UroS is expressed at relatively low levels in the cell compared to other porphyrin biosynthesis enzymes but has a significantly higher turnover rate of substrate (Tsai et al., 1987). It is also much more thermo-labile than surrounding enzymes in the pathway, which has in the past caused difficulties in the isolation and characterisation of UroS homologues (Tsai et al., 1987). The reaction carried out by UroS and its proposed mechanism is shown in Figure 4.1, where the linear tetrapyrrole hydroxymethylbilane (HMB) is converted to uroporphyrinogen III (Uro'gen III), the first cyclic intermediate of the porphyrin pathway, through inversion of the D ring. In the absence of UroS HMB can circularise non-enzymatically without rearrangement of the D ring to form the uroporphyrinogen I isomer (Uro'gen I), which is metabolically inactive.

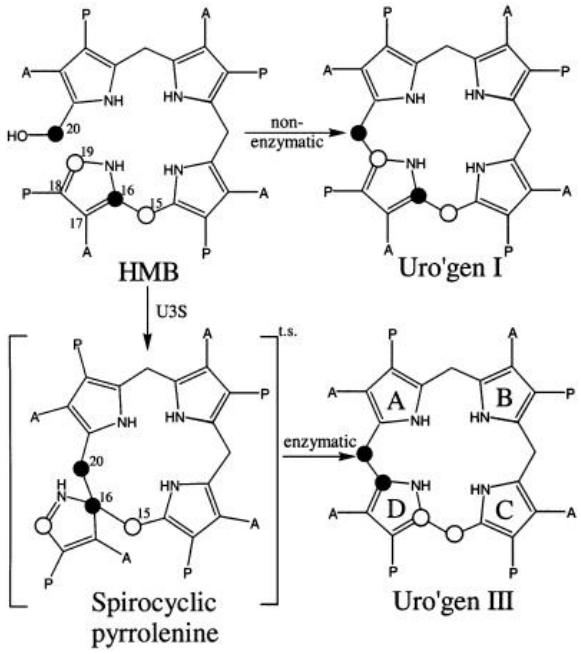

Figure 4.1 Reaction catalysed by Uroporphyrinogen III synthase (UroS)
UroS (U3S in this Figure) catalyses the conversion of hydroxymethylbilane (HMB) to Uroporphyrinogen III (Uro'gen III) through a proposed spirocyclic intermediate. The D ring is inverted to form an asymmetric product. HMB is non-enzymatically converted to Uroporphyrinogen I. Side chains shown as A (acetate) and P (propionate). Figure reproduced from Mathews *et al.* (2001) with permission.

Whole genome studies have identified *hemD* homologues in almost all prokaryotes that carry out haem biosynthesis (Panek and O'Brian, 2002), and the failure to identify *hemD* genes in some organisms is probably due to great divergence at the DNA sequence level. There is little conservation in protein sequence, the best characterised *hemD* genes from *E. coli* and *Bacillus subtilis* only share 25% identity. A structure-based sequence alignment of the human, *Thermus thermophilus, Arabidopsis thaliana* and *Synechococcus elongatus* enzymes identified only seven invariant residues (Schubert et al., 2008). In addition to this, only a few putative bacterial *hemD* genes have been confirmed experimentally to produce functional Uroporphyrinogen III synthase (Jordan and Warren, 1987; Peng et al., 2011; Roessner et al., 2002; Schubert et al., 2008; Stamford et al., 1995; Vannini et al., 2011).

Despite low sequence similarity those UroS homologues that have been purified and studied using X-ray crystallography share remarkably similar overall folds and structural features (Mathews et al., 2001; Peng et al., 2011; Schubert et al., 2008).

They contain two domains each consisting of an antiparallel β-sheet surrounded by α-helices, with two β-strand connectors between the domains. No conserved essential catalytic residues have been definitely identified and although an enzyme-product structure has been solved little is understood about the mechanism by which the enzymes carry out this complex reaction (Schubert et al., 2008).

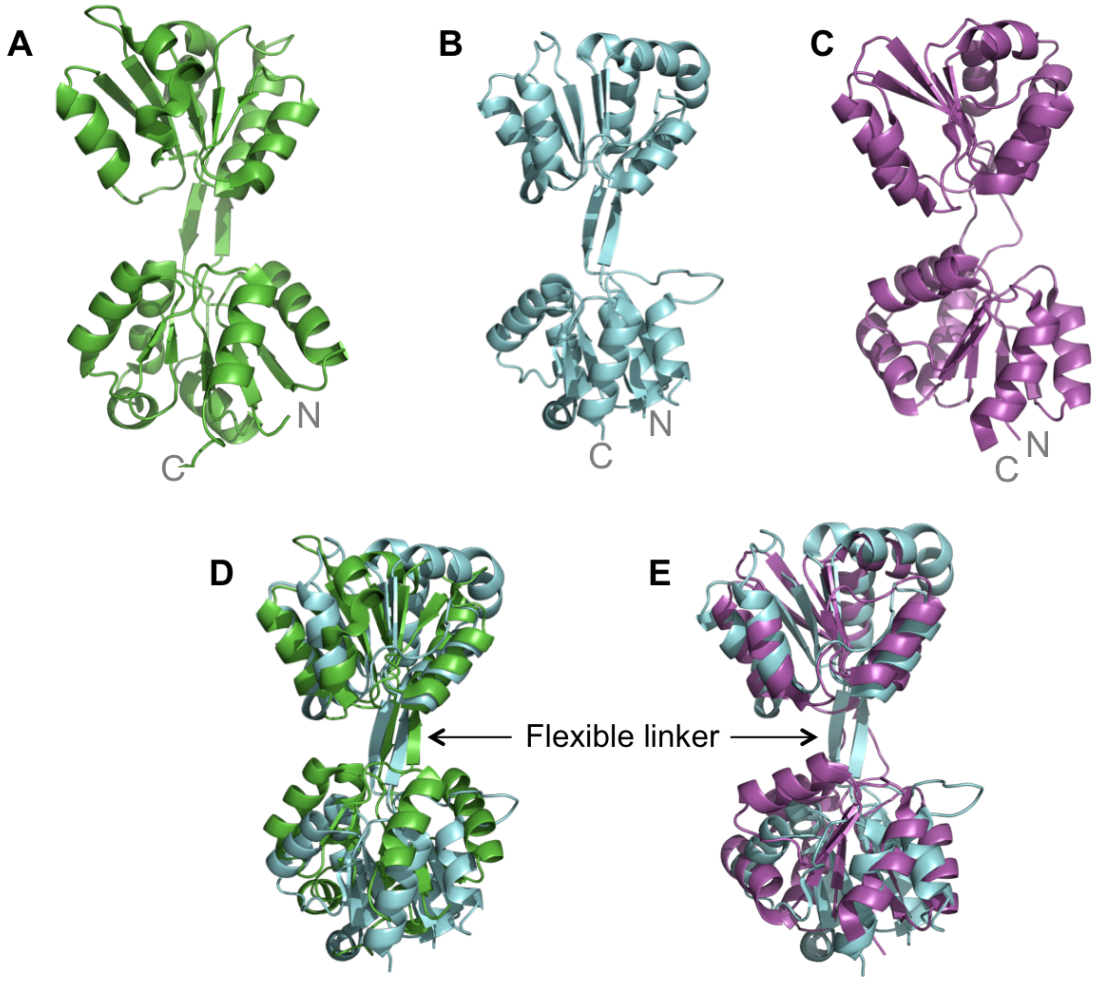

Figure 4.2 Structures of prokaryotic and eukaryotic UroS proteins
Cartoon representations the crystal structures of **A)** *Pseudomonas syringae* pv. tomato DC3000 **B)** Human and **C)** *Thermus thermophilus* UroS proteins. The N and C terminal residues are labelled in grey. **D)** Alignment of *P. syringae* (green) and human (blue) UroS, **E)** Alignment of *T. thermophilus* (pink) and human (blue) Uros. The flexible linker between the two domains forms two β-strands in the *P. syringae* and human proteins but has less ordered structure in *T. thermophilus* UroS. Figure created from PDB files 3RE1, 3D8N and 1JR2.

The aim of this chapter was to determine whether *gly1ORF2* encodes a functional uroporphyrinogen III synthase (UroS) protein. Here the cloning of the gene from *N.*

meningitidis MC58 into *E. coli* is described followed by expression and purification of the protein product. Physical characterisation of the protein has been carried out, along with preliminary experiments and optimizations in an effort to solve a crystal structure. *E. coli* genetic complementation experiments were performed to investigate *gly1ORF2* function. In addition, the preceding enzyme in the porphyrin biosynthesis pathway hydroxymethylbilane synthase (HmbS), encoded by the *hemC* gene, has also been cloned from MC58 and the protein product purified and characterised.

4.2. Results

4.2.1 Cloning gly1ORF2 from *N. meningitidis* MC58

In order to create an optimized expression construct, *gly1ORF2* was amplified from *N. meningitidis* MC58 genomic DNA using three sets of primer pairs to amplify three different products (primers used shown in Figure 4.3). Construct 1 contained the native *gly1ORF2* (Figure 4.3 panels A and B), construct 2 added an N-terminal 6xHis tag sequence to the gene and construct 3 a C-terminal 6xHis tag sequence (Figure 4.3 panels C and D). The sizes of the PCR products were 801 bp, 810 bp and 820 bp respectively. The native and C-His tagged sequence contained an optimized ribosome binding site and all ORFs were terminated with double stop codons. Each product was ligated into pJONEX4 via complementary sticky ends generated by EcoRI and HindIII restriction enzymes (Figure 4.3 panel C). Plasmids were transformed in M72 *E. coli* and correct clones were identified by PCR screening using the cloning primers or restriction digest of the purified plasmid using the enzymes used for cloning (EcoRI and HindIII), followed by DNA sequencing. The correct constructs were transformed into M72 cells for expression.

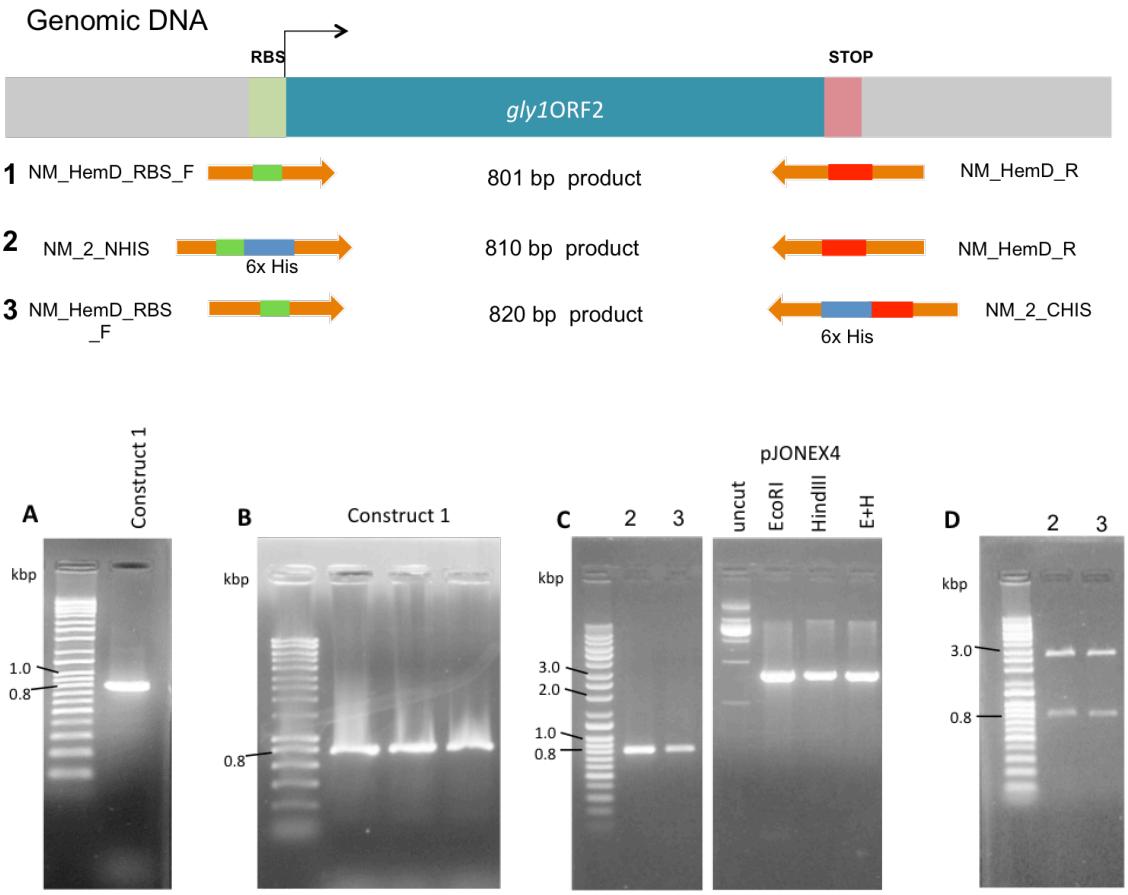

Figure 4.3 Creation of *N. meningitidis gly1ORF2* 6xHis tag and non-tagged expression constructs

Diagram shows the primer pairs used to create the *gly1ORF2* constructs, 1: native ORF2, 2: N-his tag ORF2, 3: C-his tag ORF2. Optimized ribosome binding sites on primers shown as green boxes, optimized stop codon shown as red boxes. 6xHis tag blue box. Agarose gels: **A)** PCR amplification of non-tagged *gly1ORF2* from *N. meningitidis* MC58 (construct 1). **B)** Non-tagged ORF2 Ligation products were used to transform *E. coli* M72 and positive colonies were screened by PCR with M13 forward and reverse primers. Three positive clones were sent for sequencing, and clone 2 was chosen as correct sequence. **C)** PCR amplification of N-his tag *gly1ORF2* (2) and C-terminal 6xHis tag *gly1ORF2* (3). Second half of gel shows double restriction digest of pJONEX4 uncut, single EcoRI digestion, single HindIII digestion and double digest (EH) (intervening lanes removed for clarity) which was used for ligation with digested gene inserts. **D)** Restriction digest screening with EcoRI and HindIII of His tagged constructs (2 & 3) show correct band sizes for insert and plasmid.

4.2.2 Recombinant production of Gly1ORF2 in *E. coli*

Small-scale expression, by heat induction, was carried out as described in Materials & Methods. The non-tagged ORF2 construct produced a readily detectable band just above the 25 kDa marker, which corresponds to the predicted molecular weight of this protein of 27.85 kDa. This protein band accounts for approximately 20% of protein content in the overnight samples as estimated from densitometry analysis (Figure 4.4,

panel A). Expression of N6His-ORF2 was less obvious. A small-scale nickel-agarose pull down was carried out using a crude cell lysate to identify whether the His tagged protein had been produced. Crude cell lysate was prepared by boiling the cell pellet in PBS with 3% SDS and removing insoluble material by centrifugation. Non-tagged ORF2 sample was used as a negative control, as the overexpressed protein did not bind to the beads, and 6xhis-HmbS was a positive control (Figure 4.4 B).

There were no significant protein bands associated with the beads in the N6His-ORF2 sample. This suggested that either the protein was not expressed, or was in the insoluble cellular fraction. For this reason, the non-tagged ORF2 construct was chosen to produce the protein on a larger scale for purification. Large-scale expression of ORF2 was carried out in a 5 L fermenter using 4YT media as described in Methods section 2.5.2.

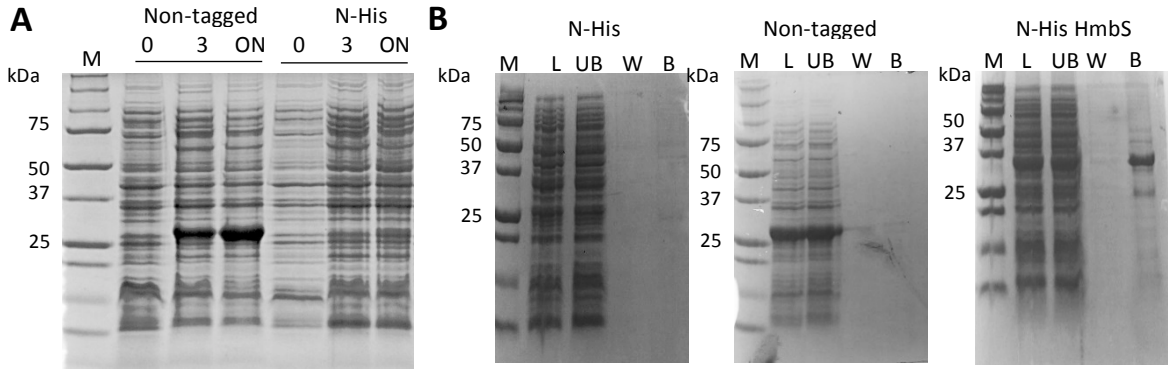

Figure 4.4 Gly1ORF2 small-scale expression studies
A) Small scale expression of non-tagged and N-His tagged ORF2 from pJONEX4 in M72 cells. Whole cell lysates before induction (0), after 3 hours at 42°C (3) and after overnight growth at 30°C (ON). A protein band corresponding to non-tagged ORF2 is clearly visible above the 25 kDa marker. No obvious over-expression is present in the N-his tagged cultures. **B)** Small scale pull-down experiments using Ni-NTA resin were used to detect his-tagged protein expression. No protein binding to the beads was detected from the N-his tagged cell lysate Non-tagged ORF2 was used as a negative control and his tagged HmbS lysates were used as a positive control for binding. L = load, UB = unbound protein, W= wash from beads in 500 mM imidazole, B= protein bound to beads.

4.2.3 Purification of Gly1ORF2 by ion exchange chromatography

After cell lysis (Materials and Methods 2.6.2) the ORF2 protein was found to be in the soluble fraction from the large-scale expression. Proteins were precipitated from the lysate using ammonium sulphate, dialysed against Q buffer pH 7.5, loaded onto an anion exchange column (Q Hi-Trap GE) and eluted over an NaCl gradient (Figure 4.5 B). Fractions containing the most ORF2 protein were pooled, buffer exchanged into MES buffer pH 6.5 and further purified by cation exchange (SP Hi-Trap, GE. Figure 4.5 C). Fractions containing the purest protein at high concentration were dialysed into 20 mM Tris 100 mM NaCl pH 8.2 then concentrated to 0.5 ml to a maximum of 10 mg/ml and loaded onto Superdex 200 column for size exclusion chromatography (Figure 4.5 D). This achieved a protein purity of over 95% according densitometry analysis of SDS-PAGE gels. The purified protein was stored as described in Materials and Methods section 2.6.7. Purified Gly1ORF2 was concentrated to 10 mg/ml for crystallisation trials.

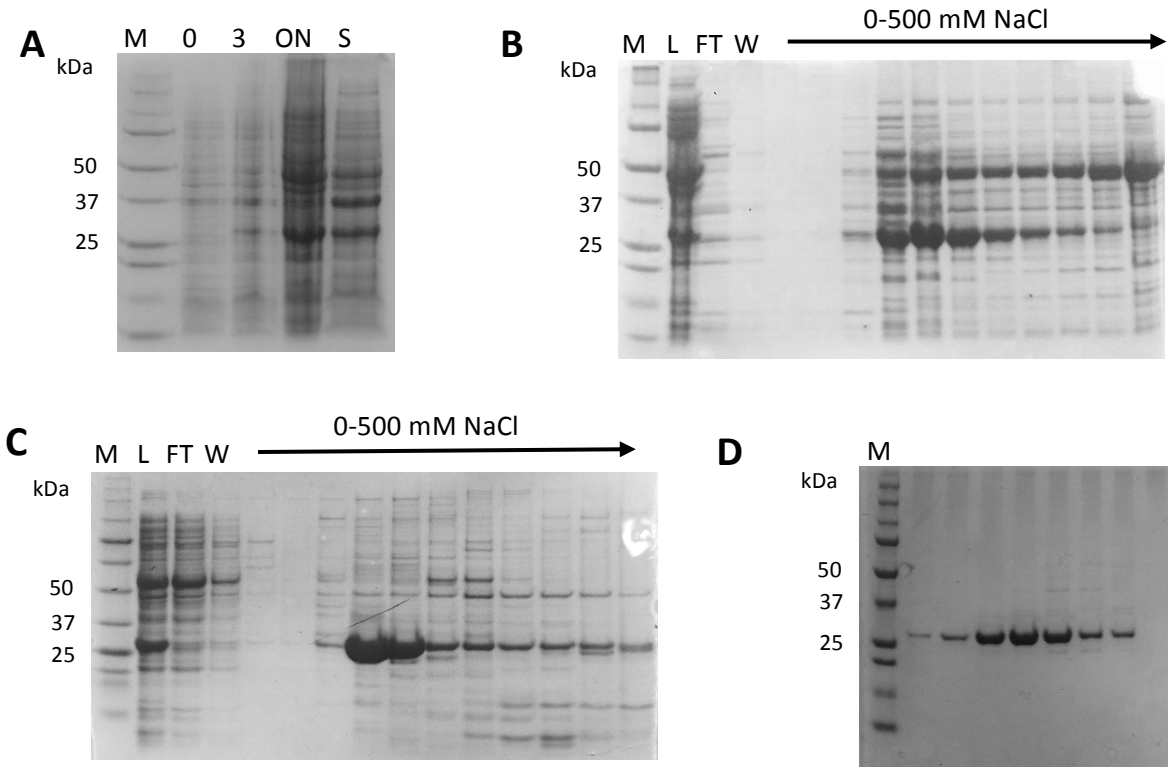

Figure 4.5 Large-scale expression and purification of Gly1ORF2
ORF2 was overexpressed in *E. coli* M72, panel **A)** shows the cell pellet before induction (0) after 3 hours at 42°C (3) and after overnight growth at 30°C (ON) and ORF2 protein is visible in the ON sample and in the soluble fraction after cell lysis (S). **B)** ORF2 was purified by anion exchange using a Q Hi-Trap column at pH 7.5 followed by **C)** cation exchange on an SP Hi-Trap column at pH 6.5, proteins were eluted from both columns over a 0-500 mM NaCl gradient. **D)** Size exclusion chromatography using a Superdex-200 column was used as a final purification step

4.2.4 Gly1ORF2 Pre-crystallisation test

A pre-crystallisation test (PCT) was carried out to find the optimum concentration for crystallisation trials as described in Materials and Methods section 2.6.9 (Watson and O'Callaghan, 2005). This test can also indicate issues with sample purity or homogeneity that could prevent successful crystallisation.

Gly1ORF2 was tested at 3 mg/ml and 10 mg/ml and heavy precipitate was present in the A1, A2 and B2 conditions. This indicated that there were issues with sample purity or homogeneity that could cause problems during crystallisation. Very small crystals grew in the B1 condition with 10 mg/ml protein after 24 hours of incubation. These were collected and sent for data collection but did not diffract. They are most likely to be ammonium sulphate crystals as this is present at 1.0 M concentration in this buffer.

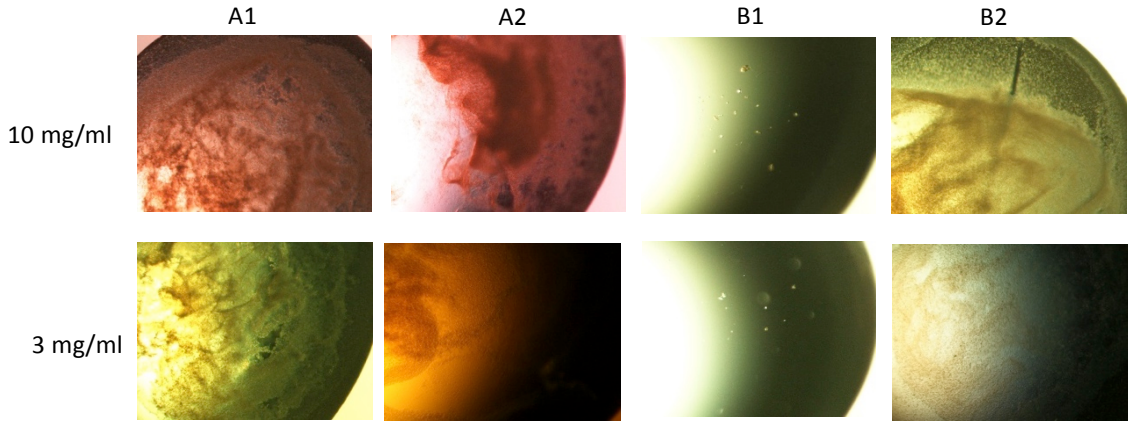

Figure 4.6 Pre-crystallisation test Gly1ORF2
Gly1ORF2 was used at 3 mg/ml and 10 mg/ml in the pre-crystallisation test. Heavy precipitate was observed in all of the buffers except B1. Heavy precipitate indicates that there are problems with sample purity or homogeny that could inhibit successful crystal formation. Small non-diffracting crystals formed in the B1 condition.

4.2.5 Gly1ORF2 crystallisation trials

Despite the unfavourable results of the pre-crystallisation test the purified Gly1ORF2 was used for crystallisation screens using the sitting drop method. Screens were carried out in 96 well format and protein was mixed with buffer condition in a 1:1 ratio. Molecular dimensions screens JCSG+, PACT and Morpheus screens were carried out at 5 mg/ml and 12 mg/ml and incubated at 17°C and 7°C. No single protein crystals were obtained despite incubation for several months and most conditions contained light or heavy precipitate, with very few clear drops. Several conditions containing light crystalline precipitate were selected for optimisation using microseeding. This method attempts to decrease the number of nucleation events occurring and allow large single crystals to grow but this optimization was also unsuccessful in that it failed to yield diffracting crystals.

4.2.6 Gly1ORF2 circular dichroism spectroscopy

Circular dichroism (CD) spectroscopy was used to identify secondary structure features of Gly1ORF2 and determine whether the purified protein was folded. Data was collected at a protein concentration of 5 µM over a wavelength range of 190-250 nm as described in Materials and Methods section 2.6.11. Estimations of the secondary structure of proteins can be achieved by comparison with previously observed

proteins, as the structural features each give rise to a characteristic CD spectra. Proteins with a large proportion of anti-parallel β-sheet structure have a negative peak at 218 nm and a positive peak at 195 nm, and predominantly α-helical proteins have double negative peaks at 222 nm and 208 nm, and a positive peak at 193 nm. Disordered proteins have negative peaks around 195 nm and very little absorbance above 210 nm (Greenfield, 2006). The spectra of UroS shown in Figure 4.7 indicated that the protein is not disordered and contains regular secondary structure elements, as there is a positive peak at 197 nm and a negative peak at 217 nm. The JASCO secondary structure prediction program was used to estimate the percentage of secondary structures in the protein using the reference spectra CD-Yang.jwr (Yang et al., 1986). This program predicted roughly a third each of α-helical structure, β structure, turns and 10% unstructured.

The protein sequence was also analysed by secondary structure prediction software Phyre2 and SABLE (Adamczak et al., 2005; Kelley et al., 2015). A representation of the SABLE prediction is shown in Figure 4.7. These both predicted a higher proportion of α-helices (46% and 45% respectively) and a lower proportion of β structures (22% and 20%).

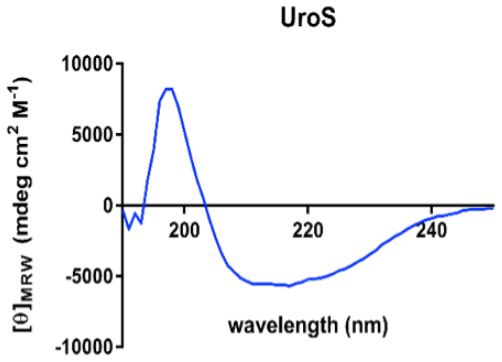

Structural element	JASCO
α-helix	31.7%
β-strand	30.1%
Turn/coil	27.3%
Unstructured	10.9%

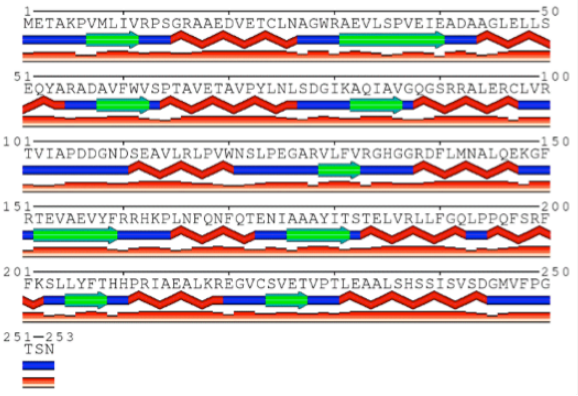

Structural element	SABLE	Phyre2
α-helix	45%	46%
β-strand	21%	22%
Turn/coil	34%	25%
Unstructured	N/A	7%

Figure 4.7 CD spectrum and secondary structure prediction UroS (Gly1ORF2)
The CD spectrum of Gly1ORF2 (UroS) shows that it is folded and contains secondary structure. It has a positive peak at 197 nm and a negative peak at 217 nm. JASCO and DichroWeb estimations of secondary structure content are shown in the top table. The SABLE and Phyre2 secondary structure predictions are shown in the bottom table and the SABLE prediction is represented here with the protein sequence. Green arrows signify β-strands, red zigzags denote α-helices and blue lines are turns or coils. The red lines below indicate confidence in the prediction, higher the red bars indicate more confidence.

4.2.7 Cloning, expression and purification of hydroxymethylbilane synthase (HmbS)

In order to carry out the biochemical assay for uroporphyrinogen-III-synthase activity on the *gly1ORF2* gene product, the preceding enzyme in the porphyrin biosynthesis pathway, hydroxymethylbilane synthase (HmbS), is required in a relatively pure form (Peng et al., 2011; Roessner et al., 2002). HmbS catalyses the formation of the linear tetrapyrrole hydroxymethylbilane from porphobilinogen. HmbS is encoded by the *hemC* gene, which has been annotated in the *N. meningitidis* MC58 genome. BLAST searches do not identify any DNA sequence similarity to other *hemC* homologues outside of *Neisseria* and *Kingella* genera, but the protein sequence has 54% identity with *E. coli* HmbS (96% coverage, Expect value = 1e-110.)

4.2.8 Cloning and expression of 6His tag HmbS

The *hemC* gene was amplified from *N. meningitidis* MC58 genomic DNA using the primers NM_ HemC_CSHIS and NM_HemC_F (details in table 2.2 Materials and Methods), producing a 1003 bp DNA fragment that contained the sequence for a 6xhistidine tag to be added to the C-terminus of the protein. After digestion with restriction enzymes this was ligated into the pJONEX4 vector with complimentary sticky ends and the construct was transformed into chemically competent *E. coli* M72 cells. A band corresponding to 6His-HmbS was not readily detectable in SDS-PAGE analysis of small-scale expression cultures but using Ni-NTA beads in a pull-down experiment showed that the protein of predicted size 34.45 kDa was expressed and present in the soluble fraction (see Figure 4.4 B).

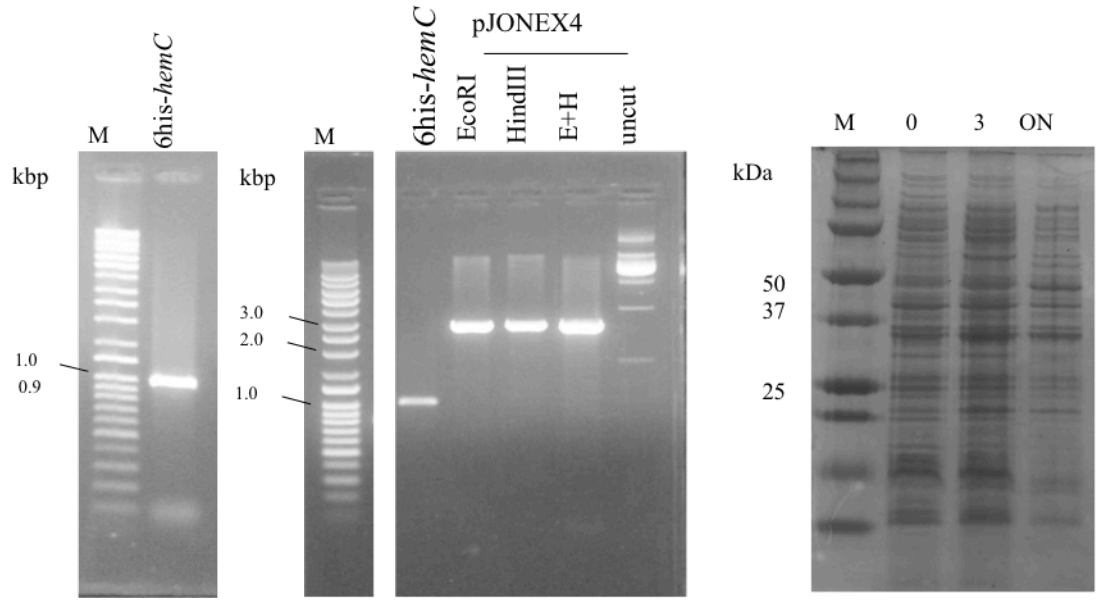

Figure 4.8 Cloning and expression of 6His-HmbS
A) PCR amplification of the hemC gene from MC58 genomic DNA generated a 1003 bp product with a 6his tag at the C terminus 6his-*hemC*. **B)** PCR product and pJONEX4 plasmid were digested with EcoRI and HindIII then ligated and transformed into M72 *E. coli* cells**. C)** Large scale expression of 6xHis-HmbS, cell lysates before induction (0) after 3 hours at 42°C (3) and after overnight growth at 30°C (ON) HmbS expression is not readily detectable in whole cell lysate but was present in soluble fraction after large scale cell lysis.

4.2.9 Large scale expression and purification of 6His-HmbS

Large-scale production of 6His-HmbS was carried out in fermenter culture, the cells were lysed and proteins precipitated from the soluble fraction using 3 M ammonium sulphate then dialysed into IMAC buffer pH 7.5 containing 20 mM imidazole. The 6His-HmbS was purified using affinity chromatography with nickel ions (Hi-Trap chelating column, GE). Elution was first carried out in two steps, 100 mM and 500 mM imidazole. Most of the HmbS was eluted in the 100 mM fraction and there were several contaminating bands. The 100 mM fraction was dialysed into low imidazole buffer and reapplied to the column and elution was carried using and imidazole gradient 20-500 mM to try and remove some contaminating proteins (Figure 4.9 A). Fractions containing 6His-HmbS were pooled and dialysed into Q buffer pH 8 and applied to an anion exchange chromatography column (Q Hi-Trap, GE. Figure 4.9 B). In both chromatography stages there were two elution peaks of proteins that seemed to have the same molecular weight as determined by SDS-PAGE analysis, one at a low

NaCl/imidazole concentration and another at the higher end of the gradient (Figure 4.9). Mass spectrometry analysis of fractions from the two peaks after anion exchange chromatography showed that both contained proteins of exactly the same molecular weight, indicating that they are both HmbS. Purified protein was concentrated and buffer exchanged into 20 mM Tris, 100 mM NaCl pH 8.2 then stored at -80°C or in 50% glycerol at -20°C.

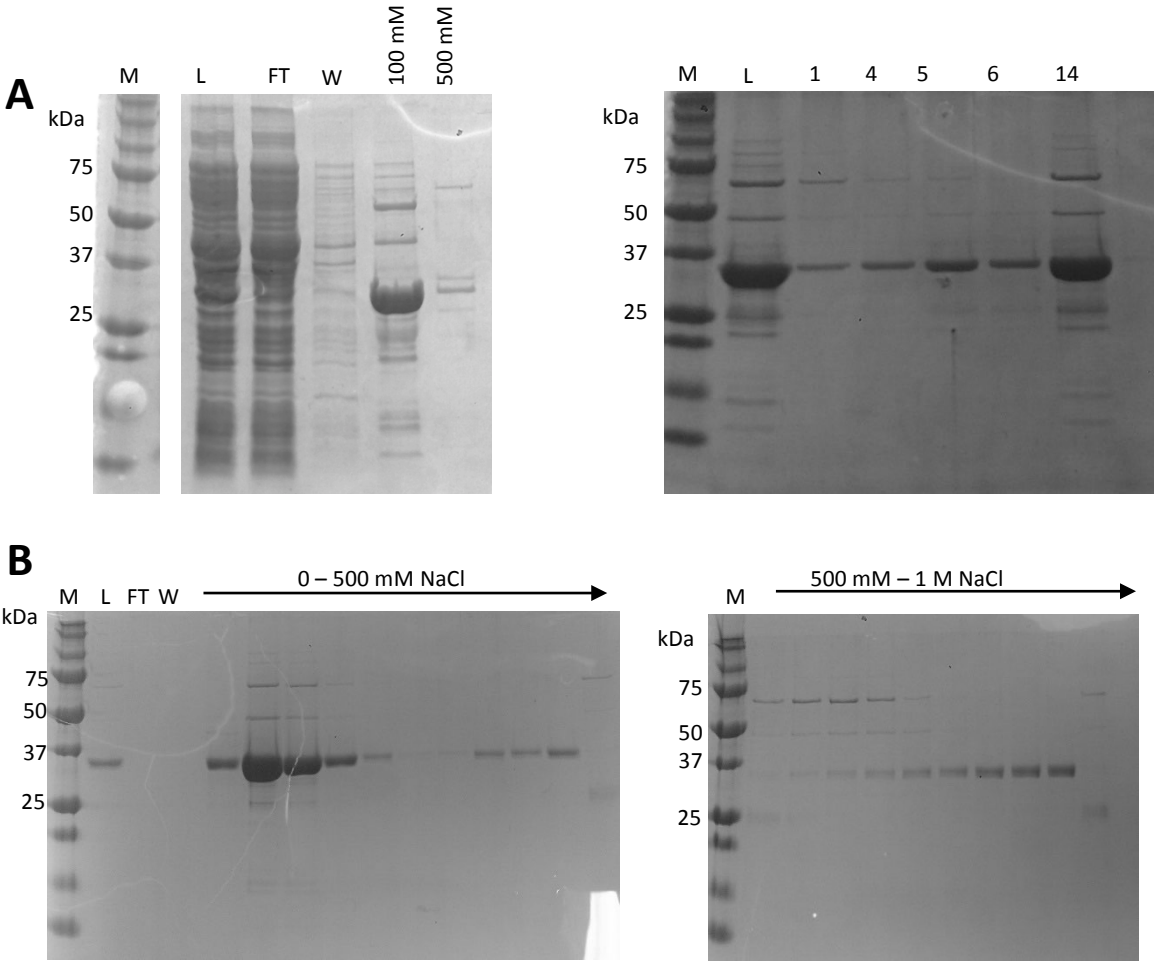

Figure 4.9 Purification of 6His-HmbS
A) 6xHis-HmbS was purified using a nickel ion IMAC column. L indicates protein loaded onto the column, FT is flowthrough, and W is low imidazole wash. Most HmbS protein was eluted at 100 mM imidazole. The 100 mM imidazole fraction was diluted to reduce imidazole concentration then reapplied to the column. Protein was eluted over a 20-500 mM gradient of imidazole and HmbS was eluted over several fractions that are numbered. **B)** Anion exchange purification using a Q column, proteins were eluted by gradient between 0-500 mM NaCl. Two species with the same apparent molecular weight are eluted at different points in the gradient.

4.2.10 Cloning and small-scale expression of non-tagged HmbS

To produce a non-tagged version of HmbS, the *hemC* gene was amplified from *N. meningitidis* MC58 genomic DNA using the primers NM_HemC_F and NM_HemC_R (details in table 2.2 Materials and Methods) generating a 972 bp PCR product containing EcoRI and HindIII restriction sites. This was purified by gel extraction, digested with the restriction enzymes and ligated into the pJONEX4 vector with complimentary sticky ends. This construct was transformed into chemically competent *E. coli* M72 cells for small scale expression studies. In SDS-PAGE analysis of the small-scale expression tests it was difficult to discern a band corresponding to HmbS (data not shown). However, upon cell lysis a more readily visible band could be seen so it was decided to attempt a large-scale production.

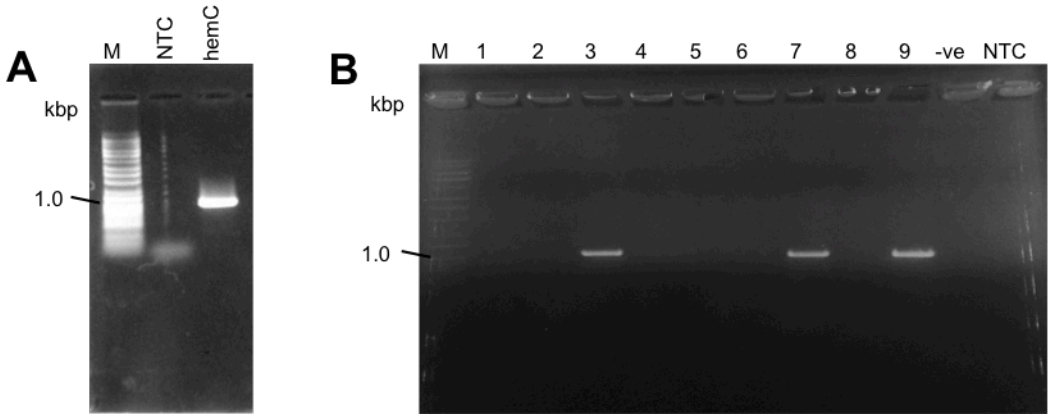

Figure 4.10 Cloning non-tagged *hemC* (HmbS) into pJONEX4
A) PCR amplification of *hemC* from MC58 genomic DNA. NTC indicates no template negative control. **B)** Candidate colony diagnostic PCR from individual *E. coli* transformants. Correct clones (3, 7 and 9) were identified by PCR screening with M13 forward and reverse primers.

4.2.11 Large-scale expression of HmbS and purification by ion exchange purification

Overexpression of HmbS was carried out by heat-shock induction in M72 *E. coli* cells in a 4 L fermenter culture and the 33.48 kDa protein was visible on Coomassie-stained SDS-PAGE analysis in the soluble fraction after cell lysis (Figure 4.11 A). Proteins were precipitated from the lysate using 3 M ammonium sulphate and dialysed against Q buffer pH 8. HmbS was purified using anion exchange chromatography (Q Hi-Trap, GE) at pH 8. The fractions containing the highest concentrations of HmbS were pooled and

dialysed into 50 mM sodium acetate buffer pH 5.4 (see materials and methods section 2.6.4 for recipe) and then purified using a cation exchange column (SP Hi-Trap GE). This was followed by size exclusion chromatography on a Superdex-200 column to produce a sample of over 95% purity (as determined by SDS-PAGE and densitometry analysis using ImageJ software.) The pure protein was buffer exchanged into 20 mM Tris HCl, 100 mM NaCl pH 8.2 concentrator then stored at -80°C or in 50% glycerol at -20°C.

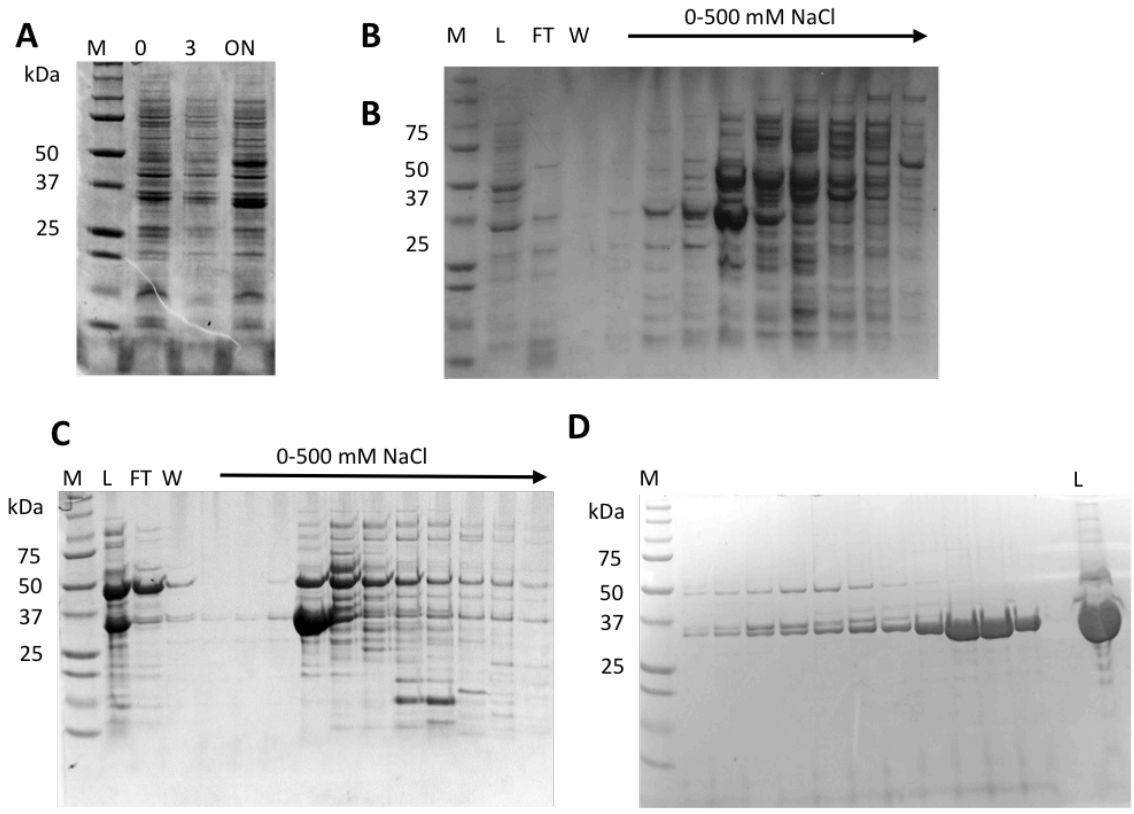

Figure 4.11 Expression and purification of non-tagged *N. meningitidis* HmbS
A) Expression of HmbS from M72 cells in 5 L fermenter culture. Lanes show cells before induction (0), after 3 hours at 42°C (3) and after overnight growth at 28°C (ON). A darker band just below the 37 kDa marker indicates expression in the overnight culture. **B)** HmbS was purified by anion exchange using a Q Hi-trap column at pH 7.5 eluted over a 0-500 mM NaCl gradient, followed by; **C)** cation exchange at pH 5.4 using an SP Hi-trap column with a 0-500 mM NaCl gradient elution. **D)** The final purification step was size exclusion chromatography carried out on a Superdex200 column at pH 7.5. For all purification gels L=Load, FT=flow through, W= low salt wash.

4.2.12 HmbS dimerization

At times during purification of 6His-HmbS the protein eluted from the column in two distinct peaks (Q and IMAC, Figure 4.9). Denaturing SDS-PAGE (Figure 4.12 right hand panel) showed that the proteins migrated at the same rate indicating similar size, and

they were confirmed to have the same molecular weight by mass spectrometry analysis of fractions from the two peaks.

On one occasion that the native HmbS was purified there were two peaks in the elution from the size exclusion chromatography column, but SDS-PAGE analysis showed single bands running at the same level on the gel suggesting a similar molecular weight. By extrapolation from a previous separation of BSA and lysozyme the first peak was shown to be around double the size of the second peak, suggesting that this was forming a dimer in solution.

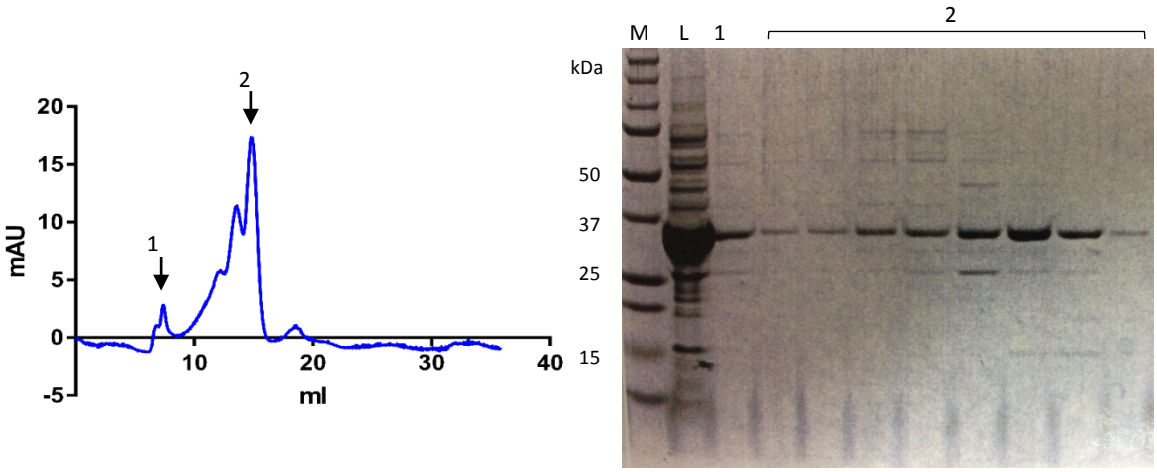

Figure 4.12 HmbS dimers detected by size exclusion chromatography.
The purification plot shows two separate peaks in UV absorbance at approximately 7 ml (1) and 15 ml (2) SDS-PAGE analysis of fractions collected from the two peaks show that both contain protein that migrates to the same level, corresponding to the expected size of HmbS around 34 kDa. Lane M is the molecular weight marker and L is the load onto the SEC column.

The ability of purified HmbS to form dimers *in vitro* was investigated using glutaraldehyde crosslinking (Materials and Methods 2.7.2). Non-tagged HmbS at a concentration of 0.15 mg/ml in PBS was incubated alone or in the presence of 0.02% glutaraldehyde and the results analysed by SDS-PAGE. In the presence of 0.02% glutaraldehyde the band corresponding to HmbS appeared weaker and an extra protein band appeared that migrated slightly faster than HmbS alone. This is most likely caused by intermolecular crosslinks within the protein that produce a more compact version of the protein. No slower migrating bands were present that would have indicated formation of multimers.

HmbS dimer formation was also studied using biolayer interferometry on the BLItz machine (ForteBio). This method analyses the interference pattern of white light reflected from a biosensor tip. The target protein is immobilised onto the tip of the sensor and any changes in the thickness of this layer caused by ligand binding causes a shift in wavelength in comparison to an internal reference layer. Interactions can be quantitatively measured in real time in solution. The 6xHis-HmbS was loaded onto the Ni-NTA probe and non-tagged HmbS was tested for association at 1.5 mg/ml. No interaction could be detected by this method between the tagged and non-tagged protein.

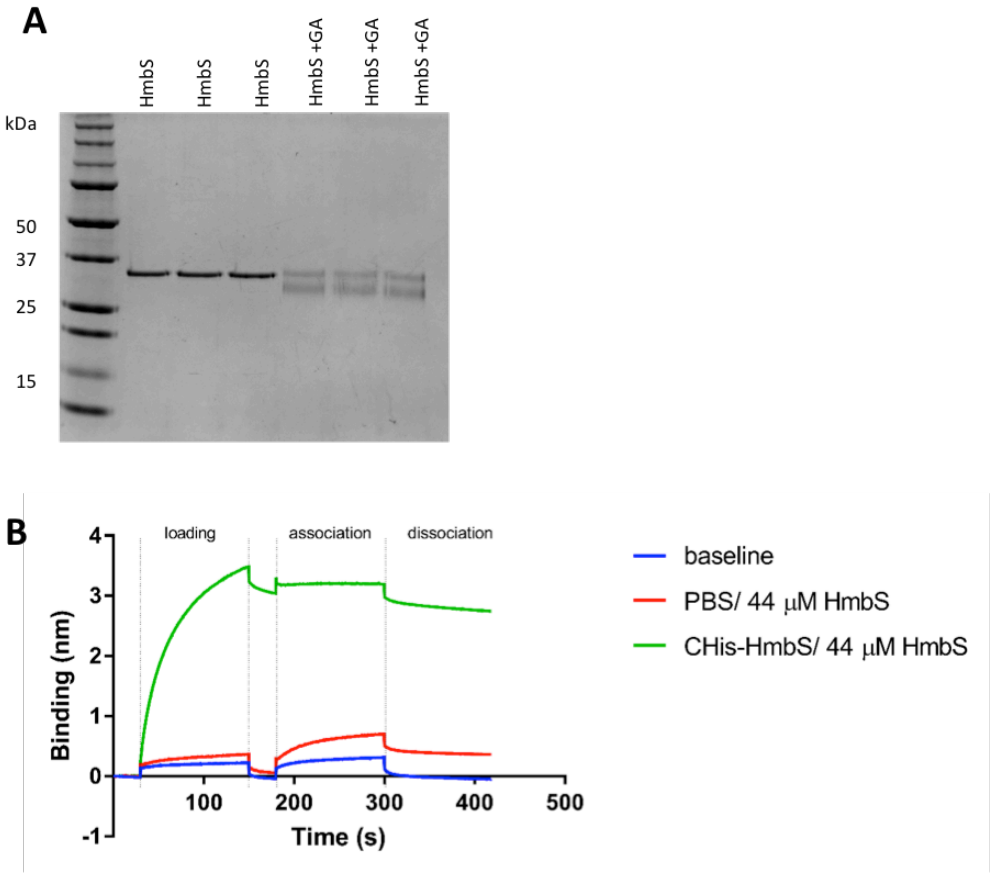

Figure 4.13 Ability of purified HmbS to form dimers.
A) Non-tagged HmbS was incubated alone in PBS or in the presence of 0.02% glutaraldehyde (GA). Glutaraldehyde treatment caused the formation of a faster migrating protein band probably caused by intermolecular crosslinks between domains. **B)** Dimer formation of HmbS studied by Blitz biolayer interferometry. 6xHis-HmbS was loaded onto Ni-NTA probe and non-tagged HmbS was used for association/dissociation. No binding was detected.

4.2.13 Crystallisation trials of HmbS

The purified non-tagged HmbS enzyme was concentrated to 8 mg/ml in 20 mM Tris 100 mM NaCl pH 8.2 using a Vivaspin 10,000 MWCO concentrator. Screens were carried out in 96 well format using the sitting drop method with a 1:1 ratio protein to buffer condition. Molecular dimensions screens JCSG+, PACT and Morpheus were used for the initial screens and plates were incubated at 17°C. Small crystals and spherulites formed in 4 conditions and needle shapes in another (see Figure 4.14 for conditions).

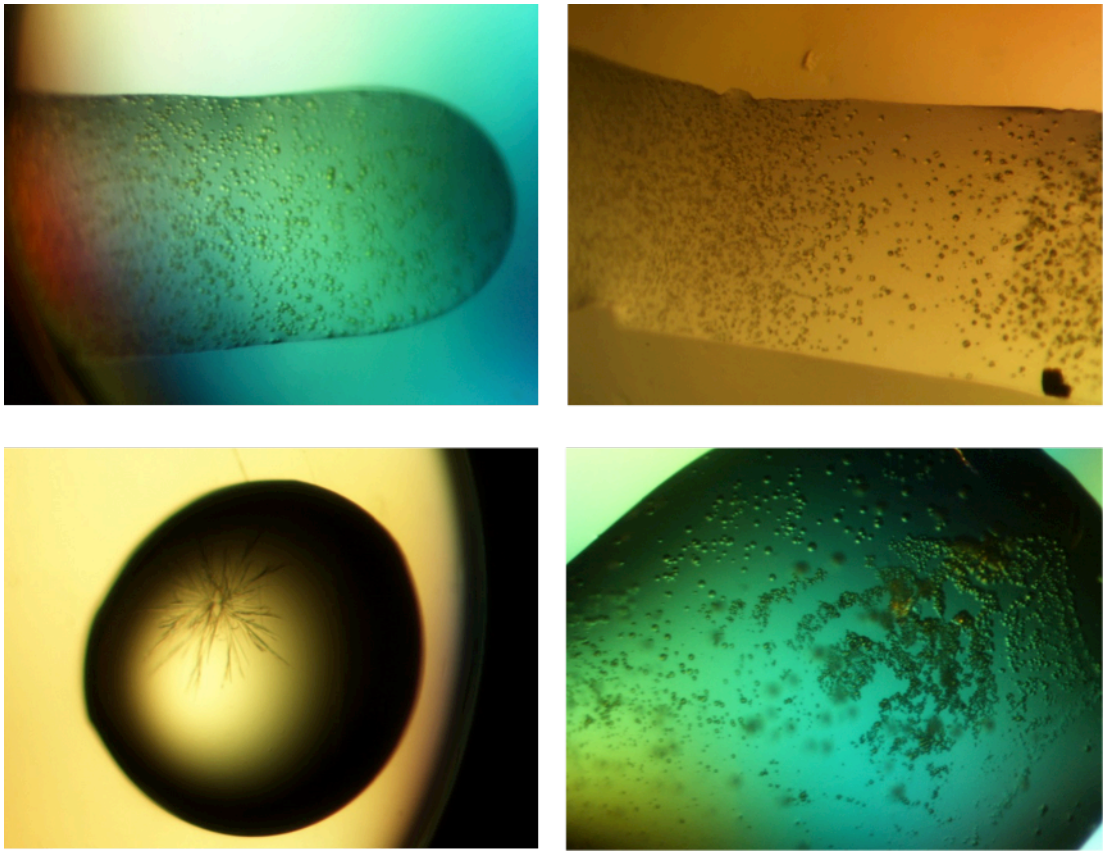

Figure 4.14 Crystallisation trials using non-tagged HmbS
Initial crystallisation trials did not produce single three-dimensional crystals suitable for x-ray data collection. Some drops contained very small crystals or spherulites, and one contained needle-like structures. Clock wise from top left: PACT A7 (0.2M sodium chloride 0.1M sodium acetate pH 5 20% w/v PEG 6000), PACT C11 (0.2M calcium chloride 0.1M HEPES pH 7 20% w/v PEG 6000), PACT C12 (0.2M zinc chloride 0.1M HEPES pH 7 20% w/v PEG 6000), JCSG+ C7 (0.2M Zinc acetate 0.1M sodium acetate pH4.5 10% w/v PEG 3000).

Optimization experiments were carried out based on the PACT C11 and C12 conditions to attempt to produce three-dimensional diffracting crystals. The pH and precipitant concentrations were varied in a grid pattern around the original conditions using the

hanging drop method. The pH was varied from 6 to 7.5 in 0.5 steps and the precipitant (PEG 6000) varied from 16 to 24 % in 2% increments. Larger crystals were formed in several conditions (see Figure 4.15), some single crystals and others clusters of plate shaped crystals. Crystals from the conditions shown in Figure 4.15 were collected and sent for data collection at Diamond Light Source by Jason Wilson (University of Sheffield), however they did not produce diffraction patterns.

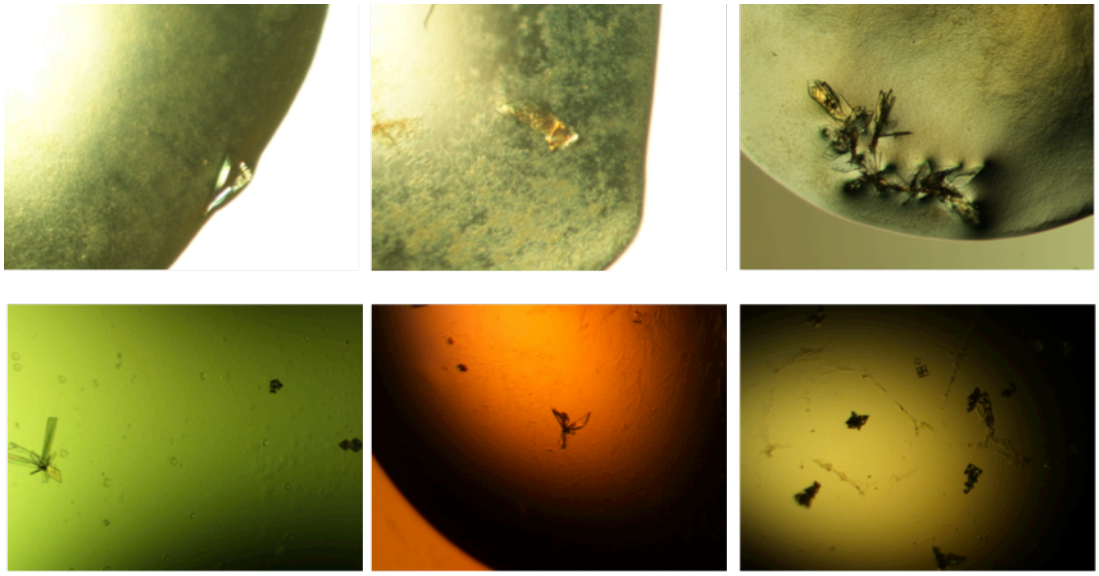

Figure 4.15 Optimization of HmbS crystallization crystals by varying pH and precipitant concentration.
Crystals from optimization trials sent for data collection. Top row conditions PACT C11 (0.2M calcium chloride 0.1M HEPES) pH 6.5, 20% PEG 6000, pH 6 22% PEG 6000, pH 7 20% PEG 6000. Bottom row conditions PACT C12 (0.2M zinc chloride 0.1M HEPES) pH 6 16% PEG 6000, pH7 16% PEG 6000, pH7 20% PEG 6000.

4.2.14 HmbS Circular dichroism spectroscopy

Non-tagged HmbS was analysed by Circular dichroism (CD) spectroscopy to determine whether the protein was folded and estimate the secondary structure elements present. The HmbS spectrum contains a positive peak at 197 nm and a negative at 209 nm. The spectrum also has a slight second negative peak around 222 nm. A double negative peak at 208 nm and 222 nm is characteristic of α-helices (Greenfield, 2006) but the positive peak at 197 nm also suggests β structures. Analysis using the JASCO secondary structure program with the reference spectra CD-Yang.jwr (Yang et al., 1986) predicts 22.4% α-helices, 33.9% β elements, 19.1% turns and 24.6% unstructured. These results contrast with the SABLE server secondary structure prediction, which suggested 40% α-helices and 20% β-strands and Phyre2 prediction of 37% α-helices and 27% β-strands. The proportion of unstructured peptide identified in the CD spectra is higher than expected, 24% compared to 4% predicted by Phyre2, and could indicate that the protein is unstable or not properly folded throughout the whole of the polypeptide chain and might account for difficulties in producing protein crystals.

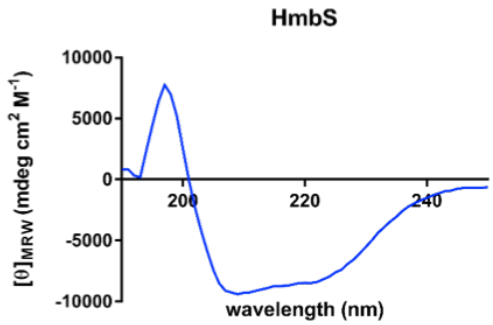

Structural element	JASCO
α-helix	22.4%
β-strand	33.9%
Turn/coil	19.1%
Unstructured	24.6%

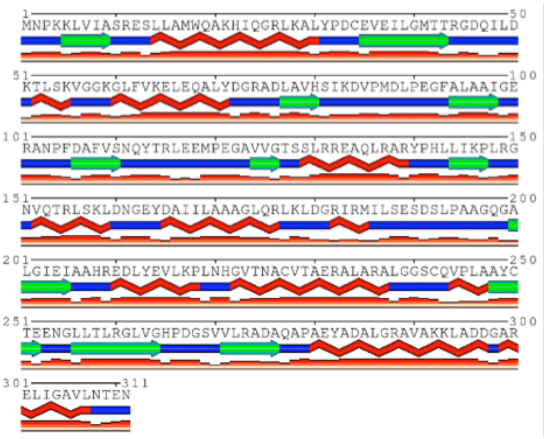

Structural element	SABLE	Phyre2
α-helix	40%	37%
β-strand	20%	27%
Turn/coil	40%	32%
Unstructured	N/A	4%

Figure 4.16 CD spectrum and secondary structure prediction HmbS
The CD spectra of HmbS shows that it is folded and contains secondary structure. It has a positive peak at 197 nm and a negative at 209 nm with an additional negative peak around 222 nm. JASCO estimations of secondary structure content are shown in the top table. The SABLE and Phyre2 secondary structure predictions are shown in the bottom table and the SABLE prediction is represented here with the protein sequence. Green arrows signify β-strands, red zigzags denote α-helices and blue lines are turns or coils. The red lines below indicate confidence in the prediction, higher the red bars indicate more confidence

4.2.15 HmbS enzyme assay for determination of specific activity

Purified fractions were assayed for HmbS activity as described in Materials and Methods section 2.8.4, using the method developed by Anderson and Desnick (1980). The specific activity of the purified protein was 42 µmol/mg/hour, which is very similar to the specific activity of the *E. coli* HmbS enzyme of 43 µmol/mg/hour (Jordan et al., 1988).

The enzyme assay was also carried out over a pH range of 6 to 10 to find the optimum activity. The assay was performed as previously described but in three different buffers suited to the pH ranges, with overlaps. Experiments at pH 6 to 8 were carried out in 20 mM sodium phosphate, 20 mM Tris was used between pH 7 and 9 and 20mM CHES was used between pH 8 and 10. Peak activity in this assay was between pH 7.5 and 8.5 as can be seen in Figure 4.15. The enzyme activity is negligible at pH 6 and below, but there is still some activity even at pH 10. The peak specific activity calculated here was between 13 and 15 µmol/mg/hour. This is much lower than the specific activity calculated from the freshly purified protein above but these experiments were carried out with protein stored at 4°C and this can result in loss of activity (see section 4.3.3 for discussion).

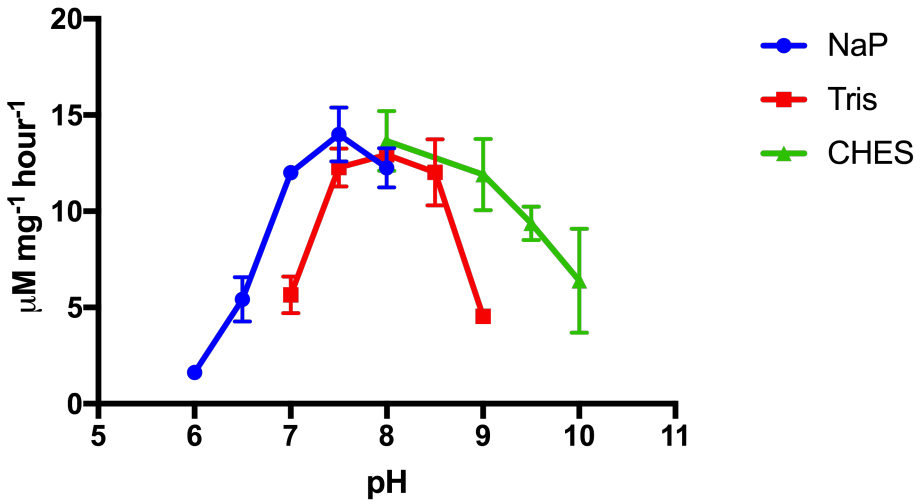

Figure 4.17 Effect of pH on specific activity of HmbS
Activity assays performed over a pH range of 6 -10 in 20mM sodium phosphate (blue circles), Tris (red squares) and CHES (green triangles) buffers. Peak activity was detected between pH 7.5 and 8.5 of 13-15 µmol/mg/hour

4.2.16 Protein-protein Interactions

Interactions between purified HmbS and UroS were investigated using biolayer interferometry using the BLItz machine. 6xHis-HmbS was loaded onto the Ni-NTA probe and UroS at 5 µM was tested for association. As can be seen in Figure 4.17 no binding was detected confirming that there is no interaction of these proteins *in vitro.*

Glutaraldehyde treatment was also used to attempt to fix any transient interactions between HmbS and UroS. Non-tagged versions of both of the proteins were incubated alone and together in the presence or absence of 0.02% glutaraldehyde and the results analysed by SDS-PAGE. Both proteins are present as single bands in the absence of glutaraldehyde. Upon glutaraldehyde treatment HmbS formed two protein bands, one migrating slightly faster than the other due to intermolecular crosslinks as discussed in section 4.2.12. In the UroS glutaraldehyde treated condition a protein band appeared that had an apparent molecular weight just over 50 kDa and the band corresponding to the monomeric protein appeared weaker. When HmbS and UroS were incubated together in the presence of glutaraldehyde the previous two patterns are visible, but no extra band that could correspond to a complex of the two proteins (expected MW ~62 kDa) is visible. The slower migrating band visible after glutaraldehyde treatment of UroS could correspond to a dimer of this protein, which would have an expected molecular weight of around 56 kDa. There was no indication during purification that UroS behaved as a dimer, as it appeared to elute from the size exclusion column in a single peak with apparent molecular weight corresponding to a monomer, suggesting that it was monomeric in solution.

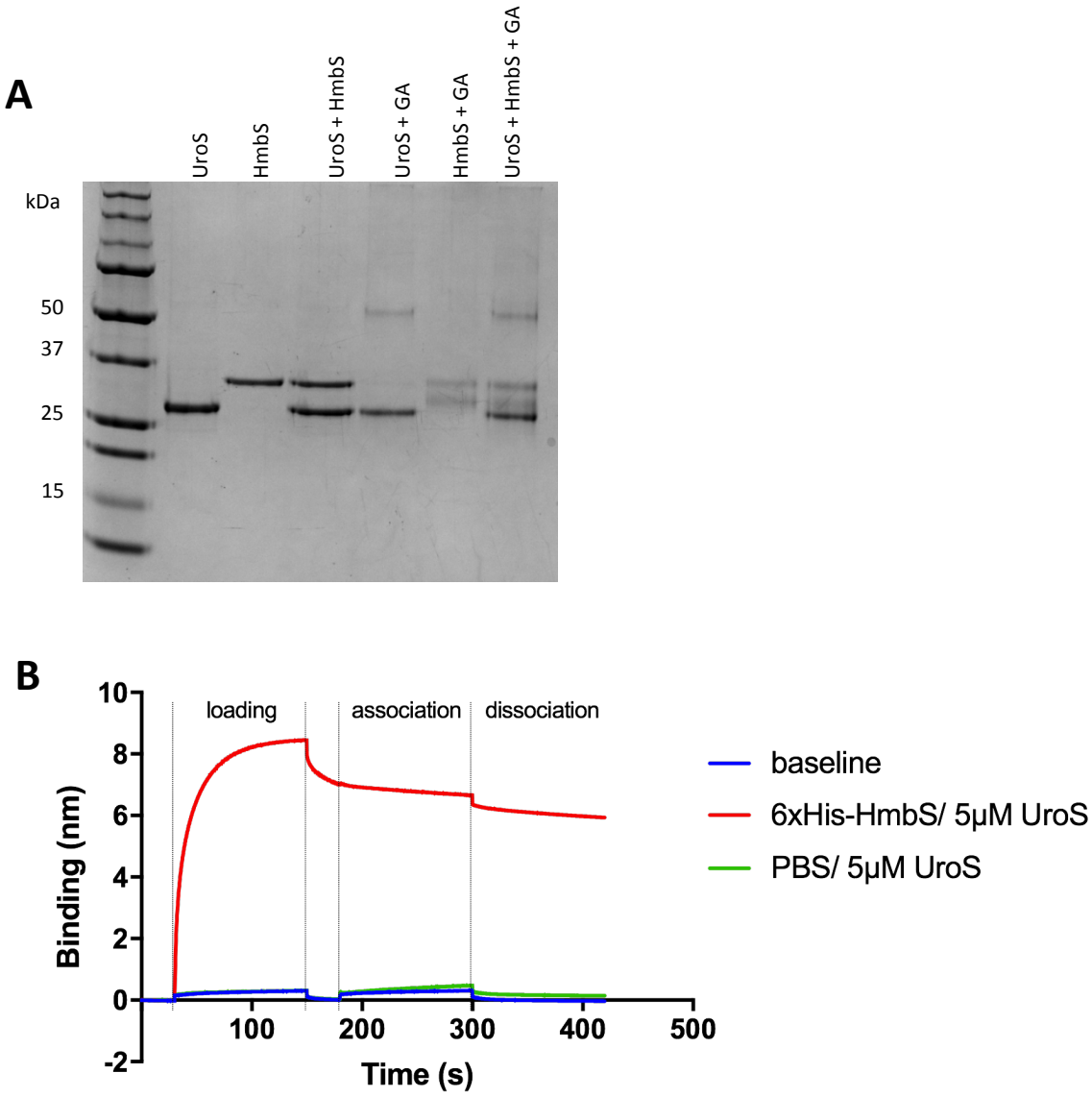

Figure 4.18 Interactions of HmbS and UroS.
A) Proteins were incubated alone (UroS, HmbS) and together (Uros + HmbS) in the absence and presence of 0.02% Glutaraldehyde (GA). A slower migrating band above 50 kDa was present with UroS alone and in combination with HmbS. HmbS alone formed a second band slightly faster migrating. **B)** Interactions were studied using Blitz biolayer interferometry using Ni-NTA probes. 6xHis-HmbS was loaded onto the probe and UroS was used at 5 µM concentration for association/dissociation. Baseline (blue) shows PBS only signal during all stages, and UroS was tested for binding to the empty probe against PBS control (green). No binding of UroS to HmbS was observed.

4.2.17 Genetic complementation of *E. coli* UroS deficient mutants with *gly1ORF2*

Genetic complementation assays were carried out to test whether the *N. meningitidis* MC58 *gly1ORF2* gene product had uroporphyrinogen III synthase activity. An *E. coli* mutant deficient in UroS activity, SASZ31 (CGSC# 7153) was obtained from the Coli Genetic Stock Centre at Yale (Chartrand et al., 1979). This strain has been used in several studies to identify *HemD* homologues (Fujino et al., 1995; Hansson et al., 1991; Wu et al., 2009).

4.2.17.1 Cloning *gly1ORF2* into pUC18

N. meningitidis gly1ORF2 was sub-cloned from pJONEX4 into pUC18 using complementary restriction enzymes to make the plasmid pORF2. The plasmid pUC18 was chosen for its relatively low levels of expression of the recombinant protein. To test whether *gly1ORF1* had any effect on the growth rate a separate construct was created by subcloning *gly1ORF1* and *ORF2* together into pUC18 to make the plasmid pORF1+2. The pUC18 constructs were transformed into chemically competent SASZ31, plated onto BHI agar supplemented with yeast extract, glucose and ampicillin and grown at 37°C.

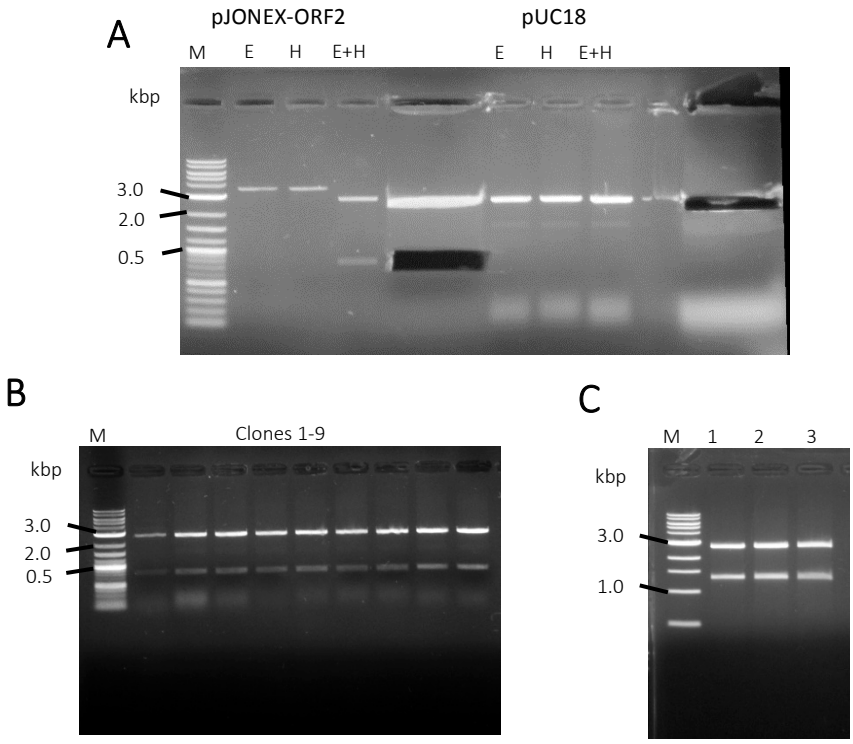

Figure 4.19 Assembling puc18 expression constructs for SASZ31 complementation
A) pJONEX-ORF2 and pUC18 digested using EcoRI (E) and HindIII (H) and the *gly1ORF2* gene insert and pUC18 plasmid purified by gel extraction. **B)** The presence of the *ORF2* insert in pUC18 was confirmed by restriction digestion. **C)** *gly1ORF1* and *ORF2* were also subcloned together into pUC18, and presence of this 1330 bp insert was confirmed by restriction digestion.

Table 4.1 Plasmids used in *E. coli* complementation experiments

Plasmid name	**Description**
pUC18	pUC18 plasmid, no insert
pORF2	pUC18 with *gly1ORF2* insert
pORF1+2	pUC18 with *gly1ORF1* and *ORF2* insert
pX1+ORF2	Modified pORF1+2, start codon deleted from *ORF1* using Q5 SDM

4.2.18 SASZ31 complementation on solid media

The presence of *ORF2* alone appeared to slightly increase the rate of growth. Small colonies (0.5 mm average diameter, n=13) were visible on the plates after 24 hours

with SASZ31 transformed with pORF2, whereas there were no colonies visible in the empty pUC18 control. After 36 hours larger colonies (average 1.1 mm diameter, n=13) had grown on the pORF2, plates, and small (average 0.5 mm diameter, n=13) colonies were visible on the empty pUC18 control plate. The presence of pORF1+2 greatly improved SASZ31 growth on agar plates compared to pORF2 and appeared to completely rescue the mutant phenotype. Colonies 1.0 mm in diameter were visible after 17 hours. To test whether this effect was due to the expression of *gly1ORF1*, the start codon of this gene was removed by Q5 site directed mutagenesis (Materials and Methods 2.3.4) to make plasmid pX1+ORF2. SASZ31 cells transformed with this construct showed a similar growth phenotype to the intact pORF1+2 construct. Western blotting confirmed that Gly1ORF1 was not expressed from the construct with the deleted start codon, indicating that the rescue of the phenotype was not facilitated by the Gly1ORF1 protein.

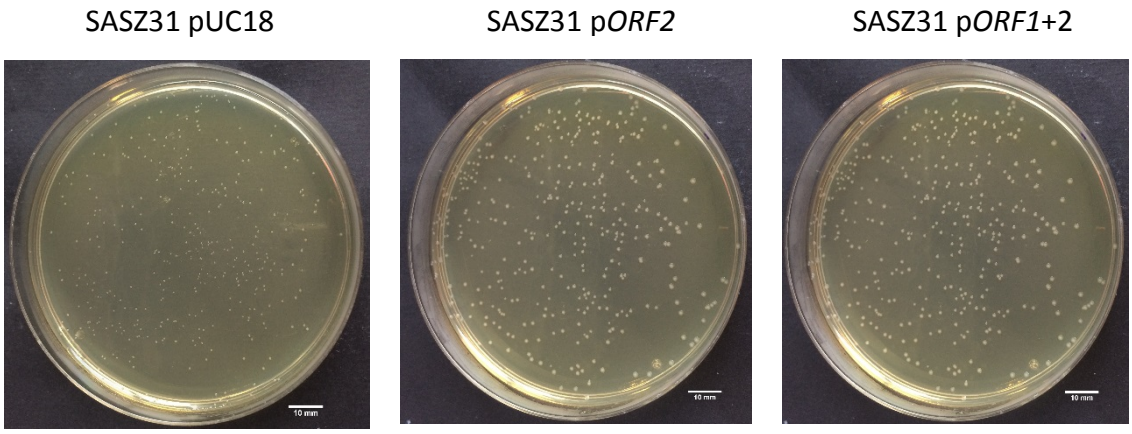

Figure 4.20 *Gly1ORF2* complements growth deficiency in *hemD* mutant *E. coli* strain SASZ31
Colonies with average 0.5 mm diameter were visible for SASZ31 transformed with empty puc18 vector only after 36 hours incubation. SASZ31 transformed with pUC18*ORF2* appeared after 24 hours, and grew to an average diameter of 1.1 mm after 36 hours. Colonies with an average diameter of 1.0 mm appeared on plates containing SASZ31 transformed with pUC19*ORF1+ORF2* after 17 hours. All agar plated contained BHI media, 0.5% yeast extract, 0.2% glucose, 100 µg/ml carbenicillin and were incubated at 37°C. White scale bar represents 10 mm. Colony diameters were measured using ImageJ. Experiments were repeated 3 times and representative plates are shown here.

4.2.19 SASZ31 complementation in liquid media

Growth curve experiments were carried out using BHI liquid media (with supplements as before) by measuring the absorbance of cultures at A_{600} over a 24-hour period. The presence of pORF2 did allow growth to a higher density than the empty pUC18 plasmid, reaching an average peak A_{600} measurement at 7 hours of 1.47, compared to a peak of A_{600} = 0.8 at 9 hours for the empty plasmid control. However, the increase in specific growth rate (μ) of the cells containing pORF2 (0.63 h^{-1} ± 0.06) when compared to empty plasmid control puc18 (0.54 h^{-1} ± 0.22) was not statistically significant. The presence of pORF1+2 increased the maximum absorbance to A_{600} = 3.17 at 8 hours, and a similar density was achieved with pX1+ORF2 where the *gly1ORF1* start codon was deleted. The specific growth rate of cells containing pX1+ORF2 was 1.21 h^{-1} (± 0.13), significantly increased compared to pORF2 and the empty plasmid puc18. Cells containing pORF1+2 had a specific growth rate 0.95 h^{-1} (± 0.27), this was not significantly different to the other plasmids due to variation in the replicates. The cultures containing pORF1+2 had a much longer lag phase than those containing pX1+ORF2 only beginning to grow after around 5 hours of incubation.

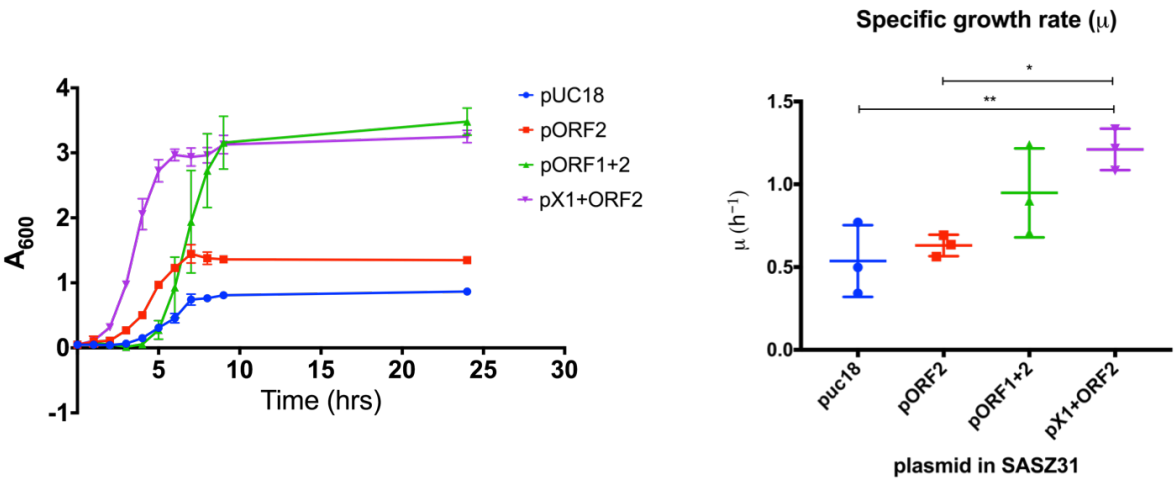

Figure 4.21 Gly1ORF2 *hemD* complementation in liquid media
A) pORF2 improved SASZ31 growth compared to pUC18, allowing growth to optical density of A_{600} = 1.47 at 7 hours. pORF1+2 and pX1+ORF2 both allowed for increased growth to a maximum optical density to around A_{600} = 3.2. **B)** The specific growth rates (μ) of SASZ31 cells containing the complementation plasmids calculated from log phase growth showing the mean and standard deviation. Analysis by ordinary one-way ANOVA (Tukey's multiple comparisons test) *p ≤ 0.05, **p ≤ 0.01.

4.3 Discussion

The aim of this chapter was to identify whether the product of the *gly1ORF2* gene is a neisserial uroporphyrinogen-III-synthase (UroS). UroS catalyses the conversion of hydroxymethylbilane (HMB) into uroporphyrinogen-III (uro'gen III) the first cyclic intermediate in the porphyrin pathway. HMB is an unstable, short lived linear tetrapyrrole that readily cyclises non-enzymatically to form the metabolically inactive uroporphyrinogen-I (uro'gen I) isomer. Due to the instability of the substrate of UroS, an assay was developed that includes the preceding enzyme in the pathway HmbS, encoded by the gene *hemC* (Jordan et al., 1980). Here the Gly1ORF2 protein has been expressed and purified and the *N. meningitidis hemC* gene was also cloned and the protein product purified in order to carry out this assay on the purified Gly1ORF2 protein.

4.3.1 Purification and crystallography

The *gly1ORF2* gene product was successfully purified by ion exchange chromatography after overexpression in *E. coli.* Despite numerous attempts and optimizations, no protein crystals were produced that were suitable for structure solution from x-ray diffraction. (864 conditions – three 96 well screens all at 5 mg/ml and 12mg/ml. Plus three screens 12 mg/ml at 7 degrees.) Previously solved UroS structures from several organisms share very similar overall structure, consisting of two asymmetrical domains connected by a two stranded anti-parallel β-sheet linker (Mathews et al., 2001; Moynie et al., 2013; Peng et al., 2011; Schubert et al., 2008). Each domain contains a central β-sheet surrounded by α-helices, the number of which varies between organisms. Comparison of UroS structures from several organisms indicates that there is a high degree of flexibility between the two domains, and that in some cases the linker does not form β-sheet secondary structure. This facilitates rotations of up to 90° of the domains relative to each other (Schubert et al., 2008).

During this project crystallisation trials for Gly1ORF2 were carried out at 7°C to try and limit domain movement. Previously solved structure of UroS homologues have been generated from crystals grown between 4 and 8°C (Mathews et al., 2001; Moynie et al., 2013; Peng et al., 2011; Schubert et al., 2008). A common solution for crystallising flexible multi-domain proteins is to create a truncated protein or to clone and express

each domain separately. This is not possible for UroS as the N and C terminus are in the same domain and each domain is not encoded by consecutive DNA sequence.

Co-crystallising the enzyme with substrate or product can increase stability of proteins and enhance crystal formation. The *T. thermophilus* enzyme does adopt a more condensed structure in the enzyme-product complex, but this co-crystallisation was very hard to achieve (Schubert et al., 2008). The substrate HMB is short lived and unstable as it rapidly converted either non-enzymatically to uro'gen I or enzymatically to uro'gen III, so it would be unlikely to co-crystallise. In the future synthetic substrate or product analogues such as the spirolactam inhibitor that mimics the proposed transition state intermediate could be utilized in crystallography as they may be more stable and would give insight into the catalytic mechanism and any conformational changes that occur (Pichon et al., 1994).

The *N. meningitidis* HmbS (*hemC*) homologue was also cloned, expressed in *E. coli* and purified to homogeneity. Crystallisation trials in this project produced crystals that were sent for x-ray analysis but unfortunately did not produce diffraction patterns that could be used for structure solution. Further experiments such as Coomassie staining should be carried out to determine whether the crystals are formed from protein or salt from the buffer solution. The structures of the human, *Bacillus megaterium, Arabidopsis thaliana* and *E. coli* HmbS homologues have been determined and consist of three domains with the active site containing the covalently attached dipyrromethane co-factor between domains 1 and 2. The protein is predicted to undergo significant conformational changes during the synthesis of HMB to accommodate the elongation of the pyrrole chain (Bung et al., 2014; Roberts et al., 2013). If further crystallisation optimization on the full-length protein are unsuccessful it may be possible to generate a truncated version of the protein and crystallise each domain independently, as they are encoded in a consecutive manner.

4.3.2 Structure prediction & CD spectra

Although attempts to solve the tertiary structure of nmUroS (*gly1ORF2*) by x-ray crystallography were unsuccessful in this project, useful information can be gained from analysis of the secondary structure and bioinformatics predictions. Analysis of the CD spectra of nmUroS using JASCO predicted that the overall secondary structure

contained 31.7% α-helices and 30% β-strand structures. This differed from the structure composition predicted by the Phyre2 and SABLE servers, which predict structure from primary amino acid sequence (45-46% α-helices, 21-22% β-strand). All of these analyses are predictions the accuracy of which depend on the input and, in the case of the case of CD spectra analysis, the reference protein set used. SABLE has been evaluated as having around 78% accuracy, whereas Phyre2 is quoted to reach between 75-80% accuracy. It has been observed that CD spectra peptide data sets can often overestimate β-strand content and underestimate α-helices (Greenfield, 2006).

The Phyre2 server was used to predict the tertiary structure of nmUroS and the model generated is shown in Figure 4.20. The model is based on the *Pseudomonas syringae* homologue (PDB identifier: 3RE1), which has 22% protein sequence identity to nmUroS. This predicted structure is typical of UroS homologues, with two domains consisting of a central β-sheet surrounded by α-helices. The N- and C- termini are located in the same domain and there is a two-stranded linker connecting the domains.

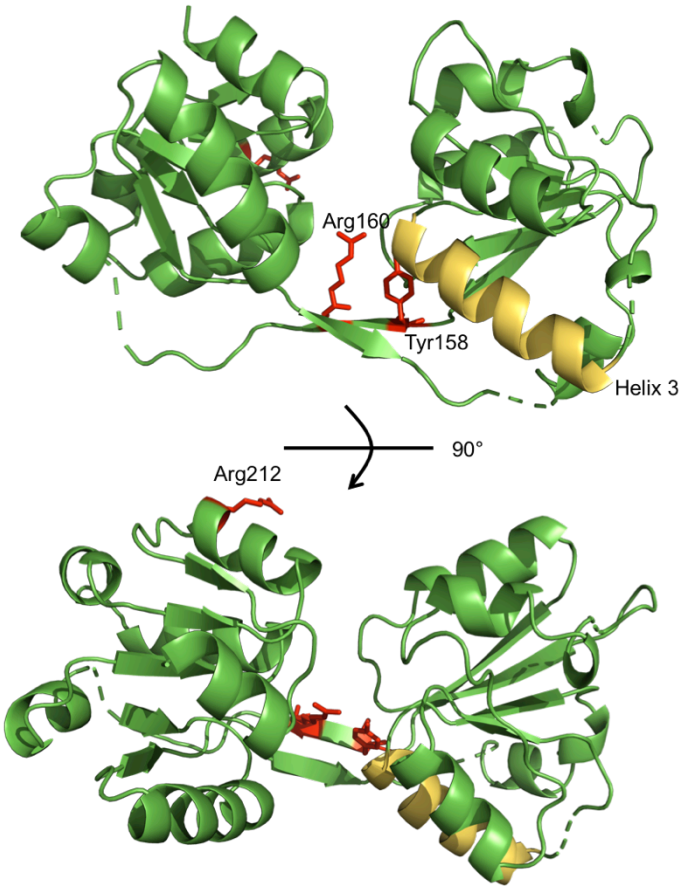

Figure 4.22 Predicted tertiary structure of nmUroS
Cartoon representation of the predicted structure of nmUros. The protein shares the highly conserved bi-lobed fold and anti-parallel β-strand linker that is characteristic of the protein family. The three residues that have altered enzyme activity in mutagenesis studies Tyr158, Arg160 and Arg212 are shown as red sticks. The helix containing disease causing mutations in the human homologue "helix 3" is shown in yellow. Model was predicted using Phyre2 server (Kelley et al., 2015) based on the crystal structure of *P. syringae* UroS (PDB: 3RE1). Figure created in Pymol.

Site-directed mutagenesis studies aimed at identifying important residues for UroS enzymatic activity have produced conflicting results. One invariant tyrosine residue (Tyr158 in *N. meningitidis*) is the most likely involved in catalysis. Mutation of the corresponding residue Tyr166 to phenylalanine resulted in inactivation of the *S. elongatus* enzyme and a 50% decrease in activity of the human enzyme (Mathews et al., 2001; Roessner et al., 2002). This residue is positioned on or near to the β-strand linker facing into the active site in all the solved structures and on the *N. meningitidis* predicted structure (highlighted in red Figure 4.20). Other mutations that reduce enzyme activity include the partially conserved Arg164 in *S. elongatus* (30% reduction

in activity when substituted for Ala) and Arg219Ala in *Pseudomonas syringae* (25% decrease in activity) (Peng et al., 2011; Roessner et al., 2002) .

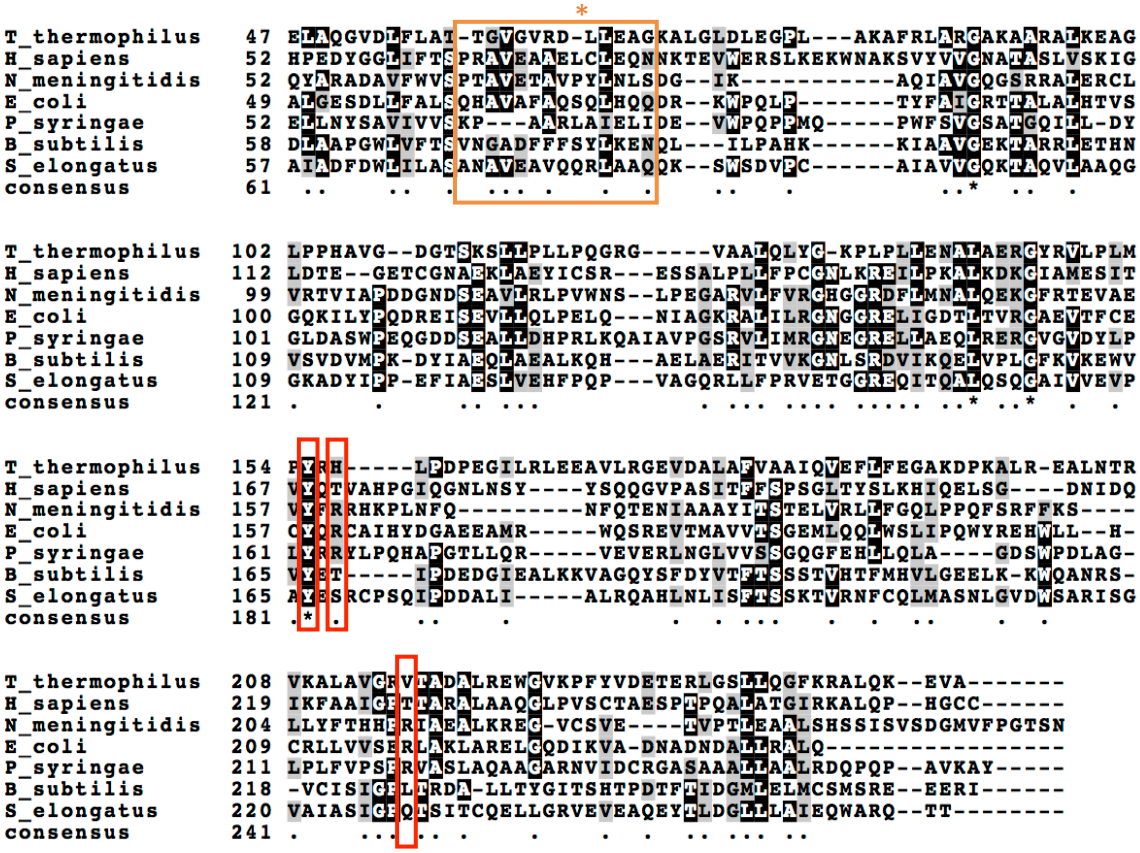

Figure 4.23 Multiple sequence alignment of UroS homologues
Sequence alignment of UroS homologues chosen because they have either been biochemically studied or their crystal structure has been solved. Tyr166 (*S. elongatus*), Arg164 (*P. syringae*) and Arg219 (*P. syringae*) shown in red boxes reduced enzyme activity in mutation studies. The important structural α helix containing Cys73 (*H. sapiens*) is contained in an orange box and the cysteine marked with orange asterisk. Ascension numbers: *T. thermophilus* AAS80660.1, *H. sapiens* AAG36795.1, *N. meningitidis* AJC62688.1, *E. coli* EIG92184.1, *P. syringae* NP_789988.1, *B. subtilis* AEP87662.1, *S. elongatus* CAA50303.1. Residues conserved at a position in over 50% of the sequences are shaded black. Residues completely conserved are also marked with a black asterisk (*). Black dots and shading indicate that the majority of sequences share similar amino acids (e.g. polar/ non-polar). Figure created using Clustal Omega and BoxShade.

The only structure solved so far showing the conformation of the enzyme during catalysis is that of *Thermus thermophilus* UroS with the product (uro'gen III) bound (Schubert et al., 2008). This structure does not greatly enhance our understanding of essential catalytic residues in the enzyme as most hydrogen bonding of the tetrapyrrole is with main chain NH groups (Schubert et al., 2008). Three active site

residue side chains form hydrogen bonds with the A ring of the substrate (Lys141, His165, and Gln194) but none are totally conserved within the UroS family.

Because the substrate, HMB, can cyclize non-enzymatically to form Uro'gen I, UroS functions to provide the optimal spatial environment to allow formation of Uro'gen III isomer through D ring inversion. This could explain the low sequence conservation and why there are no specific residues that are essential in the active site, as the overall structure and interaction between the substrate and protein backbone is most essential for enzyme activity. Schubert *et al.* (2008) suggest a mechanism where the A and B ring of the substrate are held rigidly in place by hydrogen bonds between their own acetate, propionate and carboxylate groups and the enzyme main chain and side chains. This leaves the C and D rings with more flexibility to allow for the conformational changes during inversion of D ring. In this model, the conserved tyrosine residue (Tyr158 shown in red in fig 4.19) could play a catalytic role by contributing to loss of hydroxyl group from HMB C20 and initiating the reaction.

Mutations in the human homologue (UROS) cause the autosomal recessive disease congenital erythropoietic porphyria. A wide variety of mutations are found in patients, but C73R accounts for around 40% of cases and is a so-called "hotspot mutation" as it has occurred multiple times independently (Frank et al., 1998). Structural and biochemical characterisation of all the known human mutations has been carried out and although some mutations reduce the enzyme activity *in vitro,* many (including C73R) do not (Fortian et al., 2009). The helix that contains C73 (shown as orange helix 3 on nmUroS model and marked in orange box on MSA) has been shown to be vital for the stability of the protein *in vivo*, as proteins with mutations in this area are targeted for degradation by the proteasome (Fortian et al., 2011). These studies show that stability of the overall structure is the most important factor for human UROS function *in vivo*, and due to the high level of structural homology to bacterial enzymes it is reasonable to assume that this is also the case for them. Still, very little is understood about the UroS catalytic mechanism. The protein has inherent flexibility and a change in conformation is seen when product bound but it is not known whether further changes are necessary during catalysis, nor how the substrate binds initially. Structures

of substrate or intermediate bound complexes in combination with computer modelling will be required to answer these questions.

4.3.3 Activity assays

Activity assay measurements indicate that *N. meningitidis* HmbS protein has a specific activity of 42 µmol/mg/hour, which is comparable to the *E. coli* homologue (43 µmol/mg/hour) (Jordan et al., 1988). This assay was carried out on freshly purified protein after the purification protocol had been performed in the shortest timeframe possible. Specific activity measurements recorded during the pH optimization assay were around 3-fold lower at their peak (12-13 µmol/mg/hour). The pH optimization assay was carried out using protein that had been stored at 4°C for at least a week before use. Gradual loss of enzyme activity over several weeks has been reported in the literature for other HmbS homologues, and is hypothesized to be caused by oxidation of the dipyrromethane co-factor to dypyrromethenone (Azim et al., 2014). After overexpression of both the tagged and non-tagged HmbS the *E. coli* lysates had a pink colouration and the concentrated purified proteins had a pink hue during and directly after purification which faded to a yellow colour after storage at 4°C. This has been observed previously, and there is structural evidence that the oxidised co-factor adopts a different conformation, which could account for the changes in colour and loss of enzyme activity (Azim et al., 2014). This could have been avoided by ensuring that there was a fresh reducing agent such as DTT present in the storage buffers and by carrying out assays with freshly purified protein.

After confirming that the HmbS protein was functional, the co-activity assay was attempted using previously described methods (Mathews et al., 2001; Peng et al., 2011; Roessner et al., 2002). This assay is similar to the HmbS assay but uses much shorter reaction times. UroS has a very high turnover rate and can convert HMB to uro'gen III faster than uro'gen I is formed, so short reaction times take advantage of this meaning the majority of the product measured is uro'gen III. No increase in formation of uroporphyrinogen product was detected with the addition of the Gly1ORF2 when compared to HmbS alone, indicating that Gly1ORF2 did not perform UroS function. Unfortunately, as there was no positive control available for this assay, the results are not presented here. The results of the genetic complementation

experiments (discussed in section 4.3.6) show that the *gly1ORF2* gene can rescue *hemD* mutant phenotype in *E. coli,* indicating that it can produce a functional UroS enzyme. The purified protein was confirmed to be the correct expected molecular weight for UroS by mass spectrometry.

The failure to biochemically confirm the activity of the protein could have been caused by enzyme inactivation or modification during the overexpression or purification protocol. Human UroS is temperature sensitive and can be irreversibly inactivated at temperatures around 50°C (Tsai et al., 1987). In this project recombinant *N. meningitidis* UroS was expressed in a heat inducible system where cultures were grown at 42°C for 3 hours and this could have contributed to denaturation or inactivation of the final purified enzyme. Expression using an alternative system that allows growth at lower temperatures such as the T7 lactose inducible system could be attempted in the future to improve protein stability.

It has been reported that the presence of thiol reducing agents such as DTT greatly enhances UroS activity and that its activity may depend on reduced cysteine residues (Tsai et al., 1987). This compound was not present in the storage or reaction buffers in this study and this could account in part for the lack of enzyme activity observed in this study. An alternative direct UroS assay using chemically synthesised HMB as a substrate instead of a coupled assay does exist and can be used to gather more detailed kinetic data but synthesis of the substrate is a labour intensive procedure (Kohashi et al., 1984).

4.3.4 HmbS dimerization

Several HmbS homologues have been purified and characterised biochemically, and their crystal structures have been solved and in all of these studies the protein has been identified as monomeric (Azim et al., 2014; Louie et al., 1996; Roberts et al., 2012). A recent study where a FLAG-tagged version of the human HmbS was expressed in murine cell lines found that the human enzyme co-purified with the murine homologue in a 1:1 ratio as determined by mass spectrometry measurements, suggesting that the proteins were forming dimers (Medlock et al., 2015). The human enzyme also crystallised as a dimer in the asymmetric unit, and bioinformatics analysis predicted a weak dimer interface (Gill et al., 2009).

During this project the *N. meningitidis* HmbS protein was purified several times and on occasion seemed to be present as a dimer or as two distinct species. The 6xHis tagged protein eluted from both the IMAC and anion exchange column (Q Hi-Trap) in two peaks during the elution gradients, one at low imidazole concentration or ionic strength and one at the higher end of the gradient. Analysis by ESI mass spectrometry showed that the proteins contained in both peaks had the same molecular weight. This could suggest interaction between HmbS monomers, as weaker protein-protein interactions would be disrupted at lower ionic strength or imidazole concentration but protein-purification resin interactions would be stronger and only disrupted at the top end of the elution gradients. On one occasion during size exclusion purification of the non-tagged HmbS protein two peaks of protein were observed, the first with an estimated apparent molecular weight double that of the second peak. When fractions from the two peaks were analysed by SDS-PAGE they both contained a protein band corresponding to the size of the HmbS monomer around 34 kDa. This also suggests that the protein can behave as a dimer in solution.

The ability of the purified protein to form dimers was investigated using biolayer interferometry using the BLItz machine. No binding was observed between the 6xHis tagged protein loaded on to the probe and the non-tagged protein in solution, indicating that they could not form dimers. In addition, attempts to fix interactions in solution with glutaraldehyde treatment were unsuccessful, although the protein concentration may have been too low to visualise any dimers using SDS-PAGE. The development of antibodies against these proteins would facilitate more sensitive assays in this area. The inability of the proteins to dimerize in the BLItz experiment could have been caused by the orientation of the tagged protein when it was loaded onto the probe blocking the dimer interface, or differences in folding between the tagged and non-tagged protein.

The above experiments were both carried with purified protein from the main band of correct apparent molecular weight or from purifications where there was only one band on gel filtration. It is possible that there is more than one form of the protein, one more likely to form dimers than the other. Enzyme heterogeneity was observed during the purification of *E. coli* HmbS, where several bands were visible during native-

PAGE and high resolution anion-exchange chromatography (Jordan et al., 1988). All the species had the same apparent molecular weight in SDS-PAGE analysis, had exactly the same specific activity and were not different enzyme product complexes. They were hypothesised to be slightly different structural forms of the enzyme (Jordan et al., 1988). If nmHmbS is purified again in the future the behaviour of proteins purified from the two peaks could be compared to determine whether there is any difference in their ability to form dimers.

4.3.5 Interactions between HmbS and UroS

Little is known about whether there are any physical interactions between enzymes in the prokaryotic haem biosynthesis pathway. Evidence for a eukaryotic haem "metabolon" in mitochondria has recently been observed using affinity purification and mass spectrometry (Medlock et al., 2015). This study did not detect any direct interactions between the cytosolic human enzymes PbgS, HmbS, UroD and UroS. However, this method would not be suitable for detecting very weak or transient interactions. Some early studies suggested a physical interaction between HmbS and UroS (Higuchi and Bogorad, 1975; Tsai et al., 1987) and this is illustrated by the fact that the UroS was originally named Uroporphyrinogen III co-synthase because it often co-purified with HmbS and the two were thought to function in a complex (Dailey et al., 2017; Jordan et al., 1980).

No evidence of an interaction between *N. meningitidis* UroS and HmbS was detected via biolayer interferometry or glutaraldehyde crosslinking in this project. These results confirm previous observations that HmbS and UroS do not appear to form a stable complex *in vitro* (Cunha et al., 2008; Medlock et al., 2015), and that hydroxymethylbilane is released as an enzyme free intermediate (Burton et al., 1979). It has been suggested that metabolic enzymes sometimes "cluster" to facilitate faster channelling of intermediates (Castellana et al., 2014). This might be expected for HmbS and UroS because of the risk of the metabolically inactive uro'gen-I isomer that is formed by non-enzymatic closure of the pyrrole ring in the absence of UroS. Any interaction could be transient and only facilitated by presence of the substrates, which were not present in the experiments in this project. Alternatively, they could require

the presence of other enzymes or small molecules from the porphyrin pathway or be dependent on specific conditions such as the pH or salt concentration.

Interestingly, upon glutaraldehyde treatment of UroS alone an additional band appeared on the SDS-PAGE gel that migrated to just above the 50 kDa marker. A dimer of this protein has a predicted MW of 56 kDa. The band could be caused by contaminating proteins. However, the band corresponding to the monomeric protein does seem to be weaker after glutaraldehyde treatment suggesting that this form depleted in the sample. NmUroS behaved as a monomeric protein during purification, eluting from the size exclusion column in a single peak. UroS homologues from other species have also behaved monomers during purification (Hartt and Battersby, 1985; Peng et al., 2011; Tsai et al., 1987). If an antibody against nmUroS was produced in the future it could be used to confirm whether this larger species contains UroS protein and therefore determine whether this protein can form dimers.

4.3.6 HemD complementation

The results of the *E. coli* complementation experiment further support the hypothesis that *gly1ORF2* is a *hemD* homologue, despite low DNA and protein sequence homology with other species. When the *hemD* deficient *E. coli* strain SASZ31 was transformed with the pORF2 plasmid, colonies appeared at earlier time points and grew to larger diameters than with the empty pUC18 plasmid. In liquid culture the presence of the pORF2 plasmid allowed growth to a higher cell density than the empty plasmid but did not increase the specific growth rate. Growth to higher cell densities was observed when *gly1ORF1* and *ORF2* were present, even when Gly1ORF1 protein was not expressed because the start codon was deleted in plasmid pX1+ORF2. The expression of ORF1 may actually have been detrimental to growth, as there was a longer lag phase (up to 5 hours) observed with pORF1+2 compared to pX1+ORF2. The specific growth rate of cells containing pX1+ORF2 was significantly increased compared to those containing puC18 or pORF2, whereas pORF1+2 did not significantly increase the specific growth rate. This indicates that rescue of the phenotype was due to expression of ORF2 only, and that the increase in growth observed when both genes were present when compared to *ORF2* alone was simply due to the presence of the *ORF1* DNA/RNA and not the expressed ORF1 protein. This could possibly be because

ORF2 messenger RNA stability was improved by the presence of the upstream gene and therefore the amount of ORF2 protein was increased. Alternatively, there could have been a mutation elsewhere in the pORF2 plasmid that decreased protein expression efficiency. However, several of the original transformation clones were tested all giving the same results so this is unlikely. Considering their proximity in the genome and the fact that there is no obvious promoter sequence for *ORF2* in between these genes, it has been suggested that ORF1 and ORF2 are co-transcribed (Arvidson et al., 1999). The results of this experiment could support this idea, as the mRNA stability may be improved by the presence of both open reading frames. The observations in chapter 3 of improved native Gly1ORF1 expression when ORF2 was present also support this hypothesis. This could be investigated further using reverse transcription PCR in Neisseria to find the mRNA sequence produced from this locus.

These results raise a more general point about interpreting genetic complementation experiments where the genes are introduced on a plasmid. It is important to consider the efficiency of protein expression from the plasmid as this can vary greatly between different genes and can be affected by mRNA stability, which is difficult to predict. Inefficient expression of the gene and subsequent failure to complement the mutant strain could lead to uncertainty about the gene function.

Chapter 5: The *gly1* locus *in vivo*

5.1 Introduction

The role of the *gly1* locus *in vivo* has been investigated in both *N. gonorrhoeae* and *N. meningitidis* in several studies but its exact function is still unclear. The locus was first identified in an *E. coli* library screen for *N. gonorrhoeae* toxins, as colonies expressing the fragment had a haemolytic phenotype on blood agar plates (Arvidson et al., 1999).

No growth defect or phenotype was detected in *N. gonorrhoeae* MS11 mutants where the entire locus was deleted by insertion of an antibiotic cassette (Arvidson et al., 1999). The Gly1ORF1 protein was detected associated with the outer membrane and secreted into the culture supernatant, and consequently it was investigated as a potential adhesin. However, the ability of the *gly1* locus deletion mutant to adhere to or invade human epithelial cells was unaffected (Arvidson et al., 1999). An interesting finding from this early study was that the *Δgly1* mutant caused increased damage to human fallopian tubes in culture. The cultures infected with *Δgly1* bacteria show more severe changes in morphology and pronounced loss of ciliated cells when compared to infection with wild-type MS11. Deletion of *Δgly1* did not increase the abundance of bacteria, as colony forming units recovered from the samples did not differ from wild type (Arvidson et al., 1999). This seemed to indicate that deletion of the *gly1* locus increased the toxicity of the bacteria, but no mechanism was identified for this.

Further studies investigated *gly1ORF1* as a potential adhesin in *N. meningitidis* and identified contact-regulated promoter elements (CREN a.k.a. Rep2) upstream of the gene (Deghmane et al., 2003; Morelle et al., 2003). CREN elements are found throughout pathogenic neisserial genomes and are thought to be involved in gene regulation upon contact with epithelial cells (Deghmane et al., 2002). Expression of *N. meningitidis gly1ORF1* was upregulated between 2.6 fold and 3.9 fold (P <0.05) upon contact with epithelial cells at all time points in these experiments (Deghmane et al., 2003; Morelle et al., 2003). However, a *gly1ORF1* deletion mutant created in *N. meningitidis* serogroup A strain Z5463 had similar adhesion abilities to wild type (Morelle et al., 2003). These findings indicate that *gly1ORF1* is upregulated in response to epithelial cell contact, but do not support a direct role in adhesion. DNA microarray

experiments have shown that almost 350 genes are differentially regulated in response to epithelial cell contact, including known nutrient transporters and many cell membrane structural proteins (Grifantini et al., 2002).

The role of *gly1ORF1* in *N. meningitidis* was studied in our group using a deletion mutant in serogroup B strain MC58 (Sathyamurthy, 2011). Adhesion and invasion assays replicated previous findings that Gly1ORF1 is not directly involved in these processes in *N. meningitidis*. This mutant was used to investigate the hypothesis that Gly1ORF1 is involved in haem uptake and utilization as an iron source through a series of growth experiments in chemically defined media. The Gly1ORF1 MC58 mutant was not able to grow when haemin or human haemoglobin were the only iron source. This phenotype could be partially rescued by the addition of purified recombinant Gly1ORF1 to the media, suggesting that the protein was involved in utilization of haem as an iron source.

As shown in the *E. coli* complementation experiments in in Chapter 4, *gly1ORF2* encodes a functional *hemD* homologue with uroporphyrinogen III synthase activity. Arvidson and coworkers deleted *gly1ORF1 and gly1ORF2* in *N. gonorrhoeae* MS11 and this mutant did not possess any discernable growth defect or mutant phenotype in rich media (Arvidson et al., 1999). The role of *gly1ORF2* alone *in vivo* has not been studied, and similarly there is very little evidence regarding any neisserial haem biosynthesis genes *in vivo.* One study found that *N. gonorrhoeae* Δ*hemA* and Δ*hemH* (the first and final enzymes in the pathway, respectively) were unable to grow in liquid culture without additional haem or haemoglobin, and had reduced intracellular survival (Turner et al., 1998).

The aim of this chapter was to investigate the function of the *gly1* locus *in vivo* in *N. gonorrhoeae.* Deletion mutants were created in both of the open reading frames of the *gly1* locus in *N. gonorrhoeae* MS11 and used to:

- Ascertain whether *gly1ORF1* plays a role in haem acquisition as hypothesised for *N. meningitidis* using growth experiments in the presence of different iron sources

- Test whether *gly1ORF2* deletion causes growth defects due to haem biosynthesis deficiency
- Observe any other phenotypes affected by deletion within the locus, and examine potential alternative functions

5.2 Results

5.2.1. Creation of *Neisseria gonorrhoeae* mutant strains

Neisseria gonorrhoeae MS11 mutant strains were created in order to investigate the roles of Gly1ORF1 and ORF2 *in vitro*. Linear PCR products were created containing a kanamycin resistance cassette flanked by regions homologous to the target genes in the genome. These were used to create deletion mutants via double cross over events. The genes were knocked out separately in two mutants and then together in a third double mutant. Figure 5.1 below shows the general method used to create the mutants. Throughout this chapter the mutants will be referred to as follows: Δ*ORF1* (deletion of *gly1ORF1*), Δ*ORF2* (deletion of *gly1ORF2*), and Δdouble (deletion of ORF1 and ORF2 together).

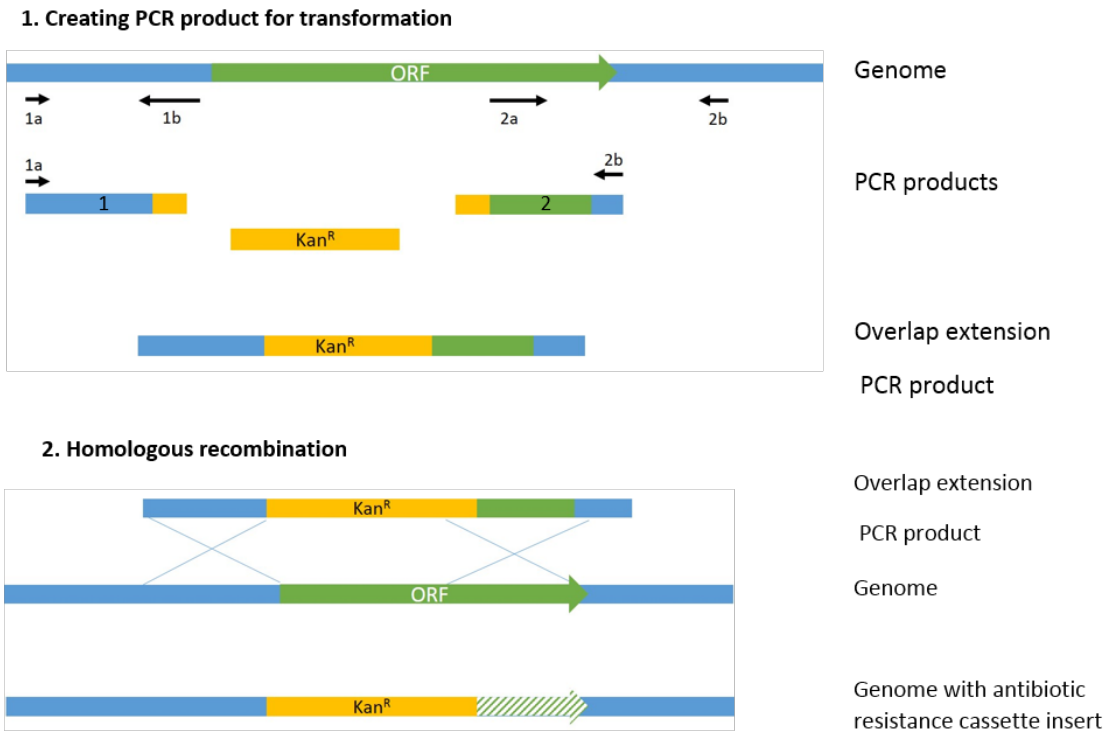

Figure 5.1 Overview of method for creating *N. gonorrhoeae* mutants
1) Two sections of genomic DNA around 500 bp long and flanking or overlapping the open reading frame to be knocked out were amplified using primer pairs 1a, 1b and 2a,2b. The reverse primer 1b and forward primer 2a contained regions of homology to the kanamycin resistance cassette. PCR products 1 and 2 were produced which encode sequence homologous to the genomic DNA and some sequence homologous to the kanamycin cassette. A second "overlap extension" PCR reaction was then carried out which contained fragments 1 and 2, the kanamycin resistance cassette and primers 1a and 2b. **2)** This created the PCR product to be transformed into *N. gonorrhoeae,* which recombined with the genome and replaced part of the open reading frame with the antibiotic resistance cassette, preventing expression of the open reading frame and allowing for selection on antibiotic media.

Genomic DNA from *N. gonorrhoeae* MS11 was isolated as described in Materials & Methods. The four DNA fragments G1, G2, H1 and H2 (corresponding to fragments 1 and 2 in Figure 5.1 above) were amplified from genomic DNA with the primers detailed in table 2.2 (Materials & Methods). Fragments G1 and G2 contain sequence homologous to and surrounding *gly1ORF1* and H1 and H2 regions homologous to and surrounding *gly1ORF2*. The 1361 bp kanamycin cassette was amplified from a storage plasmid using primers KanF and KanR and all of the PCR products were purified using gel extraction kits and confirmed as correct by DNA sequencing. Figure 5.2 A shows the purified fragments and the Kan^R cassette. The three linear constructs were then created by overlap extension PCR as described in Materials & Methods and

represented in Figure 5.1. The construct to delete *gly1ORF1* was created from fragments G1, G2 and the Kan^R cassette. The *gly1ORF2* deletion construct was created from H1, H2 and the Kan^R cassette and the double knock out construct from G1, H2 and the Kan^R cassette. The three constructs are shown in Figure 5.2 B after purification by gel extraction.

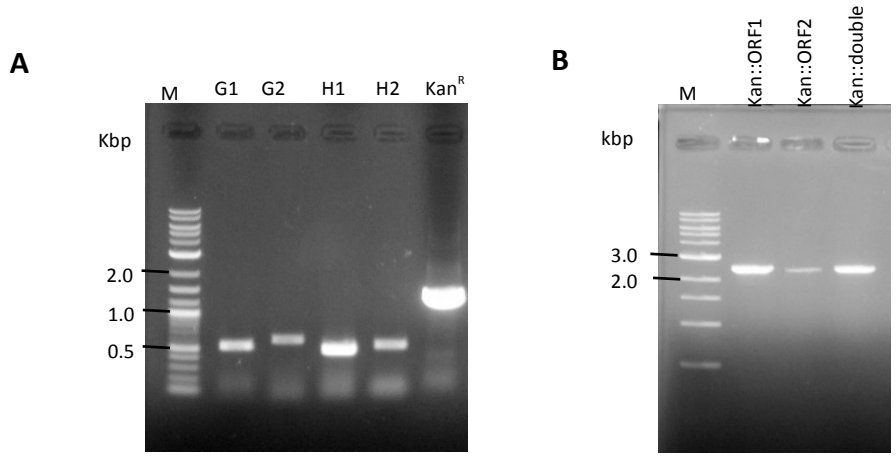

Figure 5.2 Creating antibiotic resistant cassette constructs for insertion knockouts in *N. gonorrhoeae*
A) Genomic fragments >500bp surrounding the open reading frames to be knocked out were amplified from *N. gonorrhoeae* MS11 genomic DNA. G1 and G2 surround *gly1ORF1* and H1, H2 surround *gly1ORF*2. The kanamycin resistance cassette Kan^R was amplified from storage plasmid. **B)** The purified products of overlap extension PCR reactions Kan::ORF1 is a fusion of G1, G2 and Kan^R, Kan::ORF2 is made from H1, H2 and Kan^R and Kan:: double from G1, H2 and Kan^R.

The linear PCR products were used to transform *N. gonorrhoeae* as described in Materials and Methods. In this method, after incubation with the DNA, the bacteria are plated onto GC agar supplemented with 1% Vitox and 80 µg/ml kanamycin. The *ΔORF1* mutant produced transformation colonies on GC agar but initial attempts to create the Δ*ORF2* and Δdouble mutant were unsuccessful. In some instances colonies grew on the transformation plates but upon PCR screening they were shown to be wild type. A subsequent effort where the transformation mix was plated onto chocolate

agar plates containing 80 µg/ml kanamycin did yield successful Δ*ORF2* and Δdouble mutant clones. These mutants were able to grow when re-streaked on chocolate agar plates in the presence of kanamycin. However, when they were streaked onto GC agar either with or without kanamycin they failed to produce detectable colonies, indicating that this media cannot fulfil the nutritional requirements of the Δ*ORF2* and Δdouble mutants.

Colonies were picked from the transformation plates and screened by PCR using the primers NGGly1Fwd, NGGly1Rvs, NGHemDFwd, NGHemDRvs, these primers anneal outside of the area that was replaced by homologous recombination and are denoted by primers 3a and 3b in Figure 5.1. Figure 5.3 shows the increased size of the PCR products in the mutant compared the wild type indicating that the Kan^R cassette has been inserted into the genome between the two priming sites as expected. The PCR products were purified and sequenced using the same primers and the internal primers NGGlyInt and NGHemInt to achieve full coverage of the sequence and confirm that the cassette was correctly inserted, knocking out the genes of interest. The entire *gly1* locus in the wild type strain was also sequenced to ensure it was intact. Correct clones were re-streaked onto Chocolate agar plates containing kanamycin then suspended in GCBL media and frozen at -80°C with cryogenic beads.

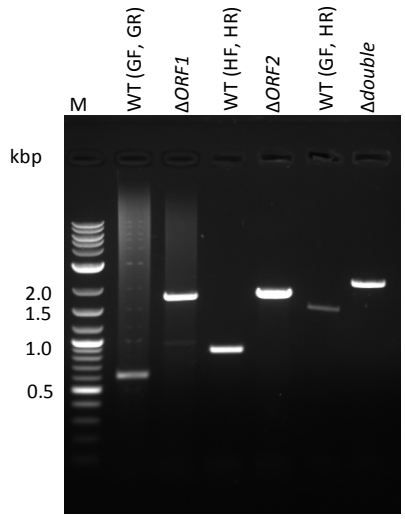

Figure 5.3 PCR confirmation of mutations in *N. gonorrhoeae* MS11
Wild type (WT) and mutants were screened using PCR with primers in brackets: GF – NGGly1Fwd, GR- NGGly1Rvs, HF – NGHemDFwd, HR- NGHemDRvs. Increased size of the PCR products confirms insertion of the 1361 bp kanamycin resistance cassette. Products analysed by electrophoresis on a 1% agarose gel.

5.2.2 Growth phenotypes of *N. gonorrhoeae* WT and mutant strains

Growth in rich media

Growth curve experiments in liquid media were carried out to assess whether any of the mutants showed a change in growth phenotype. A rich media consisting of brain heart infusion (BHI) broth supplemented with 0.5% yeast extract (YE) was chosen, as this has been shown to support good growth of *N. gonorrhoeae* strains (Annear and Grubb, 1982). Colonies produced from freezer stocks streaked onto chocolate agar were scraped from plates, washed three times in PBS and re-suspended in pre-warmed media. The optical density of the cell suspensions was determined by measuring absorbance at 540nm and then used to inoculate 2 ml of warmed media to an absorbance of A_{540}=0.1. Growth was then measured using A_{540} over a 24 hour period.

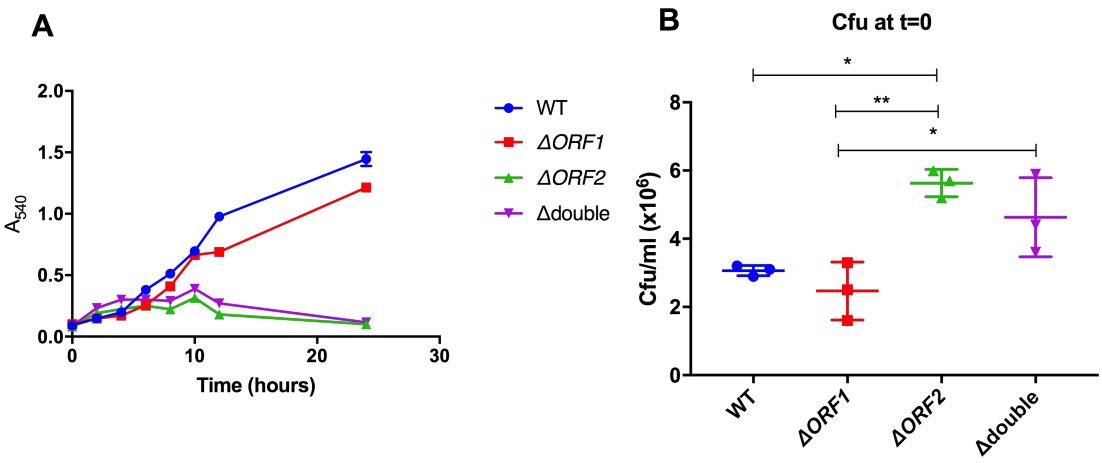

Figure 5.4 Growth of mutants in brain heart infusion media, 0.5% yeast extract (BHI) **A)** Growth monitored by absorbance at 540 nm in brain BHI media + 0.5% yeast extract. WT and Δ*ORF1* cultures grew similarly at a steady rate. The Δ*ORF2* and Δdouble cultures had an initial period of growth followed by decline in the optical density indicating cell death. **B)** Counts of colony forming units in the initial inocula show that failure of Δ*ORF2* and Δdouble to grow was not due to insufficient starting cell density, n=3. CFU analysed by ordinary one way ANOVA (Tukey's multiple comparisons test) *p ≤ 0.05, **p ≤ 0.01.

There is no significant difference between the growth of the WT and *ΔORF1* strains, both grew steadily, reaching an absorbance of A_{540}= 1.2-1.4 at 24 hours. The *ΔORF2* and Δdouble strains grew to a maximum absorbance of between A_{540}= 0.3 and 0.4, and the absorbance began to decline after 10 hours, indicating that the cultures were dying.

N. gonorrhoeae is often difficult to culture in liquid broth, and cultures can die if they are not inoculated to a sufficient starting cell density (Dillard, 2011). To test whether the initial inocula contained similar amounts of live bacteria 100 µl was removed from each of the cultures at t=0 and used to perform a count of colony forming units (cfu). The Δ*ORF2* cultures had a significantly higher cfu/ml count than the WT and *ΔORF1* cultures, and Δdouble had a higher cfu/ml than Δ*ORF1.* This indicates that the failure of the Δ*ORF2* and Δdouble cultures to grow in liquid culture was not due to insufficient inoculate.

5.2.3 Growth in rich media supplemented with human haemoglobin

Human haemoglobin was supplemented into the BHI 0.5% YE media at a final concentration of 5 µM, to test whether this could rescue the growth defect observed

in the Δ*ORF2* and Δdouble mutants. All of the strains, including Δ*ORF2* and Δdouble showed improved growth in the presence of haemoglobin. The WT and all the mutants reached a similar maximum absorbance and there was no significant difference between their specific growth rates (all had mean rates between 0.47 and 0.52 h^{-1}). This supports the idea that the Δ*ORF2* and Δdouble mutant growth defect was caused by a haem deficiency, as *N. gonorrhoeae* can import intact haem from haemoglobin to compensate for lack of a functional haem biosynthesis pathway (Turner et al., 1998). All strains grew at a significantly faster rate and to a higher cell density in the media with the addition of haemoglobin compared to BHI 0.5% YE media without haemoglobin as shown in Figure 5.5. This suggests that BHI 0.5% YE is not optimal for growth of MS11 and that haemoglobin is important as either a haem or an iron source to support growth in this media for wild type strains. The WT and Δ*ORF1* strains have a slightly longer lag periods than the Δ*ORF2* and Δdouble mutants here, possibly due to the inoculum containing a smaller proportion of live cells as discussed above.

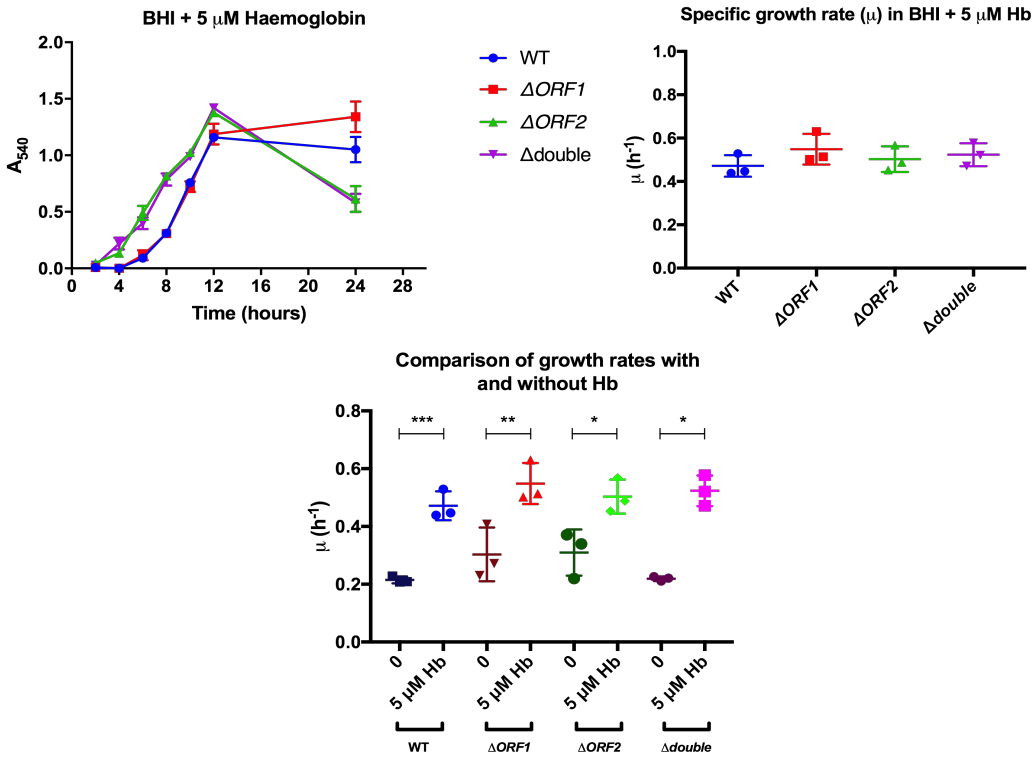

Figure 5.5 Growth of mutants in BHI media with human haemoglobin

A) The growth of wild type (WT) and mutant cultures in BHI + 0.5% yeast extract with the addition of 5 μM human haemoglobin. All reached absorbance (A_{540}) of between 1.0 and 1.5 at the 12 hour time point **B)** There was no statistically significant difference in the specific growth rate of any of the mutants and WT – analysed by ordinary one-way ANOVA, Tukey's multiple comparisons test. **C)** The addition of 5 μM haemoglobin (Hb) significantly increased the specific growth rates of all strains compared to BHI media with no haemoglobin (0). Analysed by unpaired t-test, *** p≤0.001 **p≤0.01 *p≤0.05. n=3.

5.2.4 Growth in gonococcal chemically defined media (GCCDM)

In order to determine the ability of the mutants to utilize iron from different sources, a chemically defined media (GCCDM) devised for *N. gonorrhoeae* was used (Materials & Methods section 2.1.2). The normal iron source in this media is in the form of an iron(III) nitrate solution at a final concentration of 4 µg/ml, which can be omitted or replaced to change the iron availability.

Both WT and Δ*ORF1* cultures grew well in GCCDM using iron(III) nitrate as an iron source, reaching a maximum absorbance of A_{540} 1.95 and 2.29 respectively. When the ferric nitrate solution was omitted from GCCDM, WT and Δ*ORF1* MS11 grew to an absorbance of around 0.7. This growth was probably enabled by intracellular iron carried over from growth on the chocolate agar plates, but low levels of iron contamination from the media or culture vessels used could have contributed to this. The Δ*ORF2* and Δdouble mutants did not grow at all in GCCDM in the presence or absence of ferric nitrate.

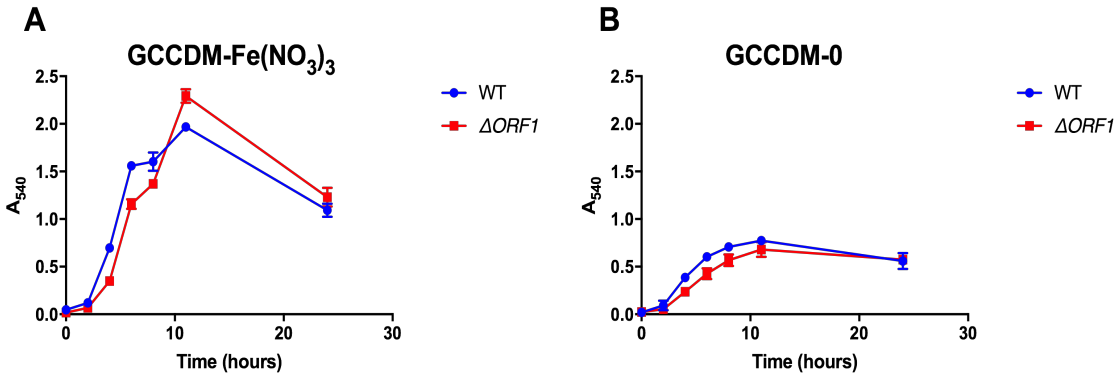

Figure 5.6 Growth of wild type and Δ*ORF1* strains in chemically defined media with and without iron(III) nitrate

A) Wild type (WT) and Δ*ORF1* cultures grown in GCCDM with 4 µg/ml iron(III) nitrate. **B)** Wild type (WT) and Δ*ORF1* cultures grown in GCCDM with iron(III) nitrate solution omitted, there should be no external iron source in these cultures. The Δ*ORF2* and Δdouble cultures did not exhibit any growth in this media so are omitted from the Figures, n=3.

5.2.5 Growth in GCCDM using haemoglobin as an iron source

The ability of the mutants to use haemoglobin as an iron source was tested by replacing the ferric nitrate solution in GCCDM with a human haemoglobin solution to a final concentration of 5 µM. WT and Δ*ORF1* cultures grew at similar rates and reached

a maximum absorbance of between A_{540}= 1.6 and 1.7 at 8 hours, before starting to die off. The Δ*ORF2* culture grew slowly and reached a maximum absorbance of A_{540}= 0.43 at 12 hours. The Δdouble culture showed little evidence of growth, with a very slight increase in absorbance over the 24 hour period, from A_{540}= 0.057 to 0.153. Control experiments carried out simultaneously again show that WT and Δ*ORF1* had limited growth in the absence of an additional iron source, and that Δ*ORF2* and Δdouble did not grow in GCCDM.

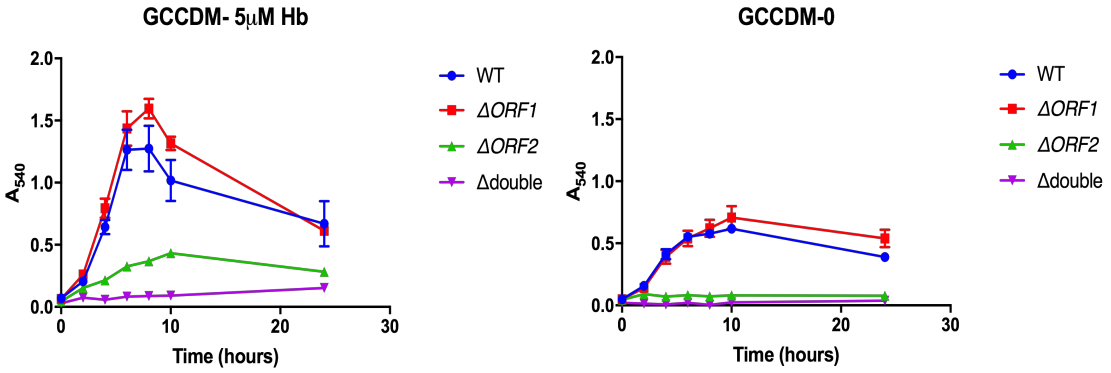

Figure 5.7 Growth of mutants in GCCDM with and without human haemoglobin
A) Wild type (WT) and mutant strains growth in GCCDM with 5 μM human haemoglobin monitored by absorbance at 540 nm over 24 hours. WT and Δ*ORF1* grew at similar rates, Δ*ORF2* grew slowly up to a maximum absorbance of 0.43 and Δdouble did not grow. **B)** WT and mutants growth with no haemoglobin. WT and Δ*ORF1* showed limited growth and Δ*ORF2* and Δdouble did not grow in this media, n=3.

5.2.6 Growth in the presence of iron chelator DTPA

To eliminate the possibility that the growth observed with haemoglobin as a sole iron source was due to contaminating free iron and not the direct uptake and utilization of haem, growth experiments were carried out in the presence of an iron chelator. Diethylenetriaminepentaacetic acid (DTPA) has a very high affinity for iron(III), and the stability constant (log K) of the resulting metal complex is 27.3, making it a very effective iron chelator (Zhou et al., 2010). DTPA is a polar compound and cannot penetrate the bacterial cell membrane, so depletes only the extracellular pool of iron.

The growth of WT and Δ*ORF1* strains in GCCDM with 1 μM DTPA was measured using either no additional iron source, 2.5 μM human holo-transferrin, 7 μM haemin or 5 μM human haemoglobin. The addition of 1 μM DTPA did not abolish growth with any of the additional iron sources confirming that the observed growth was due to their

direct utilisation as iron sources and not due to the presence of contaminating free iron. There was no significant difference between the ability of WT and Δ*ORF1* strains to grow with any of the iron sources tested.

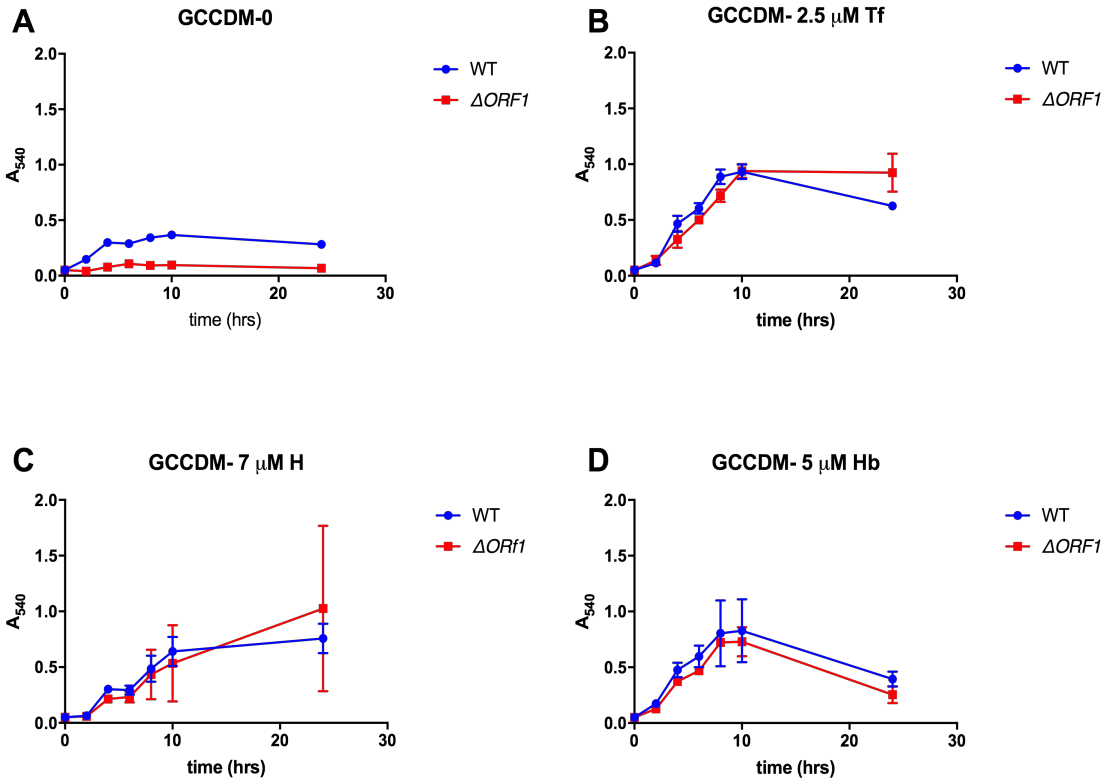

Figure 5.8 Growth of wild type and Δ*ORF1* strains in GCCDM and different iron sources in the presence of DTPA iron chelator

A) Wild type (WT) and Δ*ORF1* cultures grown in GCCDM with no additional iron source and 1 µM DTPA. **B)** Cultures grown in GCCDM and 2.5 µM human holo transferrin (Tf) and 1 µM DTPA. **C)** Cultures grown in GCCDM with 7 µM haemin and 1 µM DTPA. **D)** Cultures grown in GCCDM with 5 µM human haemoglobin and 1 µM DTPA. For all experiments n=3.

5.2.7 Ability of mutants to survive with different iron sources – iron disk assay

The ability of the WT and Δ*ORF1* MS11 to grow using haemin and haemoglobin as iron sources was also examined on solid media. The bacteria were plated onto GC agar that had been depleted of iron by the addition of 50 μM deferoxamine mesylate. Sterile filter paper disks that had been soaked in either 10 mg/ml human haemoglobin or 2.5 mg/ml haemin were placed on top of the plates to act as an iron source. Disks soaked in 1 x PBS were used as a negative control, and no growth was detected surrounding these disks.

The presence of haemin on the disks supported a ring of confluent growth of both wild type and Δ*ORF1* MS11. This growth surrounded a zone of inhibition, where the haemin concentration reached levels toxic to the bacterial cells. Measurement of the zone of inhibition showed that there was no significant difference in sensitivity to the toxic effects of haemin between the two strains (mean radius ± SEM: WT= 6.5 ± 0.4509 mm, Δ*ORF1* = 5.793 ± 0.1556 mm). Measurements from the centre of the disks to the outer edges of the area of growth were also not significantly different between the wild type and mutant strain (mean radius ± SEM: WT= 11.03 ± 0.5783 mm, Δ*ORF1* = 9.443 ± 0.1841 mm).

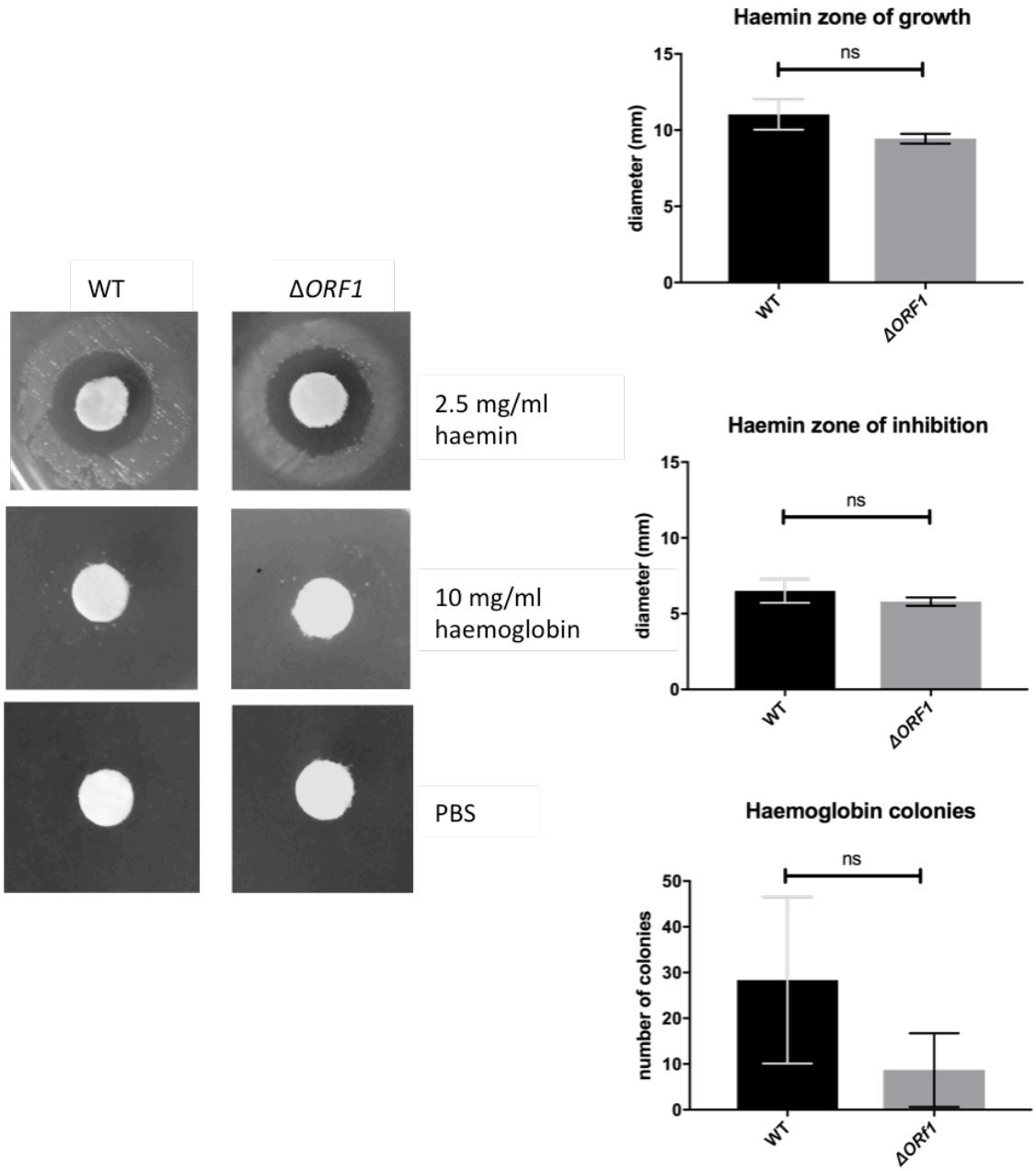

Figure 5.9 Iron disk assay - growth of WT and *ΔORF1* MS11 using haemin and haemoglobin iron sources

Growth of WT and *ΔORF1* strains on GCB/Vitox plates supplemented with 50 µM deferoxamine mesylate using haemin (2.5 mg/ml) or haemoglobin (10 mg/ml) as sole iron source. A zone of inhibition surrounded by a zone of confluent growth is seen around the haemin disk for both strains. There is no significant difference in the size of these zones on the WT and *ΔORF1* plates. Discreet colonies surround the haemoglobin disk for both WT and mutant. There was a wide variation in number of colonies for both. Images representative of 3 repeats. Plates were photographed and growth/inhibition zones measured using ImageJ.

Both WT and Δ*ORF1* MS11 grew in discrete colonies surrounding the haemoglobin-soaked disk rather than a bacterial lawn as observed with haemin. Although the wild-type strain had a higher mean number of colonies surrounding the disk, the variation between experiments was very high, and there was no statistically significant difference between the number of colonies supported by haemoglobin.

5.2.8 Investigation of potential alternative Gly1ORF1 functions - Lysozyme sensitivity of wild type and Δ*ORF1* MS11 *in vivo*

The results presented above indicate that unlike in *N. meningitidis* MC58, Gly1ORF1 may not be essential for utilising haem or haemoglobin as an iron source in *N. gonorrhoeae* strain MS11. Therefore, other potential roles for the protein were investigated. *Neisseria meningitidis* adhesin complex protein (NmACP) NMB2095 was identified by Magda Wierzbicka as a potential Gly1ORF1 paralogue through PSI-BLAST searches to identify distantly related proteins that could be part of the same family (Wierzbicka, 2014). A structure of NmACP has recently been published, along with evidence that it could function as a lysozyme inhibitor (Humbert *et al.* 2017).

Methods modified from the study on NmACP were used to investigate whether *N. gonorrhoeae gly1ORF1* provides protection from lysozyme *in vitro.* The wild type and Δ*gly1* mutant were grown in liquid media in the presence (N) and absence (N_0) of human lysozyme, and the fold change in colony forming units after 7 hours was calculated using N_0/N. A higher fold change value indicates a greater decrease in colony forming units following incubation with lysozyme. The mean fold change in the growth of Δ*ORF1* in the presence of human lysozyme was higher than for the wild type (WT= 1.342 ± 0.3823, Δ*ORF1* = 2.409 ± 0.601) but this was not statistically significant when analysed using an unpaired t-test (p value = 0.185).

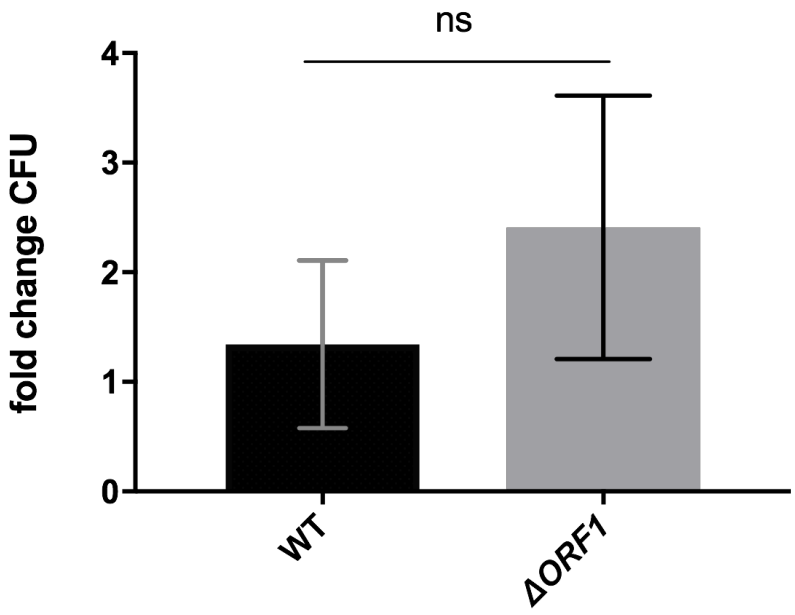

Figure 5.10 Sensitivity of live *N. gonorrhoeae* to human lysozyme
Fold change in colony forming units for wild type (WT) and Δ*ORF1* mutant after exposure to 10 µg/ml human lysozyme for 7 hours. Calculated by dividing CFU after incubating without lysozyme by CFU with lysozyme, n=4

5.2.9 Interactions of purified CHis-Gly1ORF1 with human lysozyme

Due to problems with reproducibility the ability of Gly1ORF1 to function as a lysozyme inhibitor *in vivo* could not be determined. Therefore, the ability of purified CHis-Gly1ORF1 to bind to human lysozyme was investigated, as this could indicate whether the protein possesses lysozyme inhibitory functions. Initially Gly1ORF1 and human lysozyme were incubated in the presence of the chemical crosslinker glutaraldehyde, in an attempt to fix any complexes for analysis by SDS-PAGE. Human lysozyme and Gly1ORF1 both formed a small amount of dimers when incubated with glutaraldehyde. Gly1ORF1 also formed a smaller molecular weight band with glutaraldehyde, which is likely to be from intermolecular crosslinks forming a more compact protein structure and faster migrating band. A higher molecular weight band is visible when the two proteins are incubated together, which may be between the bands corresponding to the Gly1ORF1 and lysozyme homodimers and could be a complex of the two proteins. However, a complex would have an expected weight of around 29 kDa, which would

be indistinguishable from a Gly1ORF1 dimer at just over 30 kDa, so it is not possible to conclude whether there is an interaction using this method.

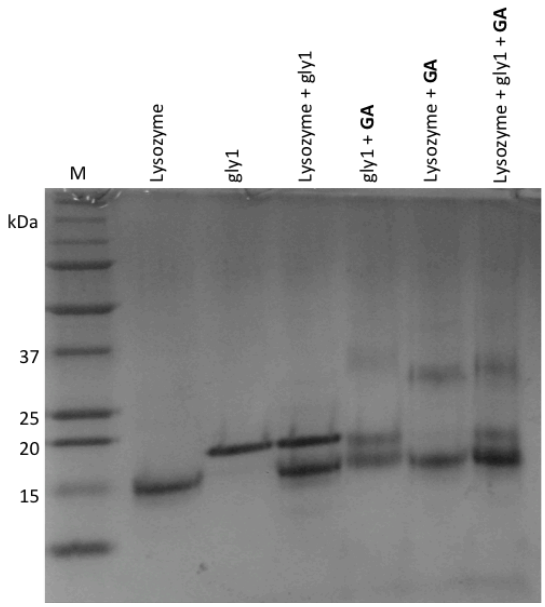

Figure 5.11 Crosslinking interactions between Gly1ORF1 and human lysozyme with glutaraldehyde
Gly1ORF1 (gly1) incubated with human lysozyme in the presence of 0.02% glutaraldehyde (**GA**) in an attempt to crosslink any heterodimers formed. The proteins were incubated separately and together with and without GA, then analysed by SDS-PAGE using a 15% agarose gel. Both Gly1ORF1 and lysozyme formed small amounts of dimers alone in the presence of GA, making it unclear whether the higher molecular weight species formed when they were incubated together was a complex of the two proteins.

5.2.10 Interactions of human lysozyme and Gly1ORF1 studied using biolayer interferometry

Biolayer interferometry analysis of potential Gly1ORF1-lysozyme interactions was carried out using the BLItz system (ForteBio). C-His Gly1ORF1 was immobilised onto a nickel chelate coated probe (Ni-NTA) and this loading was confirmed by the association of anti-Gly1ORF1 antibody (shown in purple in Figure 5.12). Human lysozyme could not be used for this experiment as control experiments where no Gly1ORF1 was loaded onto the probe showed that the human lysozyme bound very strongly to the probe itself. Hen egg white lysozyme (HEWLysozyme) was used as a substitute, this shares

61% sequence identity with human lysozyme (98% coverage E value = 1e-58) and did not show such strong binding to the probe alone. The green line in Figure 5.12 represents the Gly1ORF1-lysozyme interaction and although there is a small association/dissociation curve, the dissociation constant calculated by the BLItz software for this line is lower than that of the control sample of lysozyme interaction with the Ni-NTA probe itself (red line). Therefore there is no significant interaction between Gly1ORF1 and HEWLysozyme.

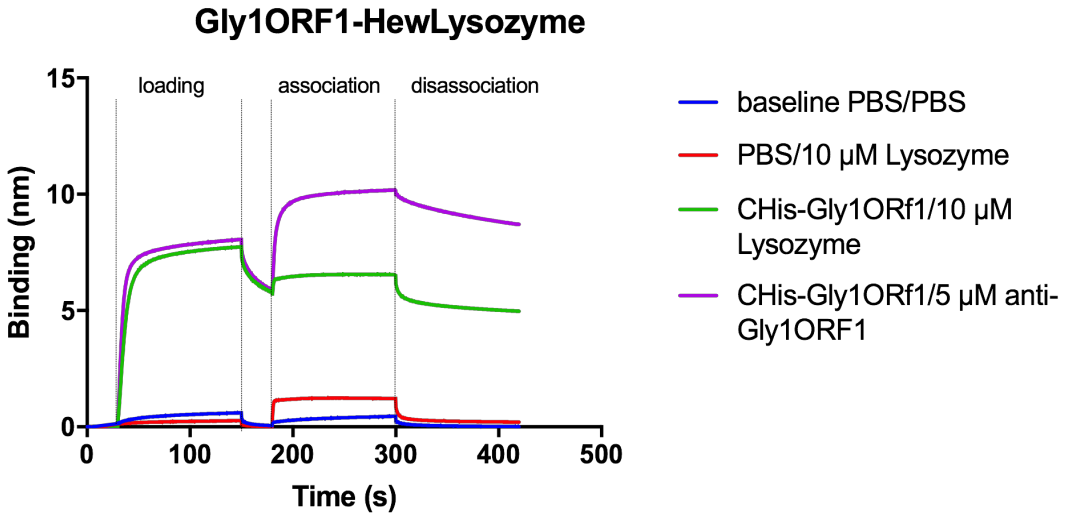

Figure 5.12 Gly1ORF1 interactions with hen egg white lysozyme analysed using biolayer interferometry
C-His Gly1ORF1 at 0.75 mg/ml was loaded onto the Ni-NTA probe, the binding curve is shown during the loading stage as an increase in nm. Lysozyme (green line) was added to assess binding (association) and washed (dissociation). No binding was observed between lysozyme and C-His Gly1ORF1. Polyclonal anti-Gly1ORF1 antibody at 5 µM was used as a positive control to confirm Gly1ORF1 loading onto the probe. The K_d of Gly1ORF1 interaction with anti-Gly1ORF1 antibodies was estimated to be 9.66 x 10^{-8} M.

5.2.11 Microscale thermophoresis (MST) of Gly1ORF1-human lysozyme interactions

Microscale thermophoresis (MST) was used to detect any interaction between Gly1ORF1 and human lysozyme. Gly1ORF1 was fluorescently labelled using the Monolith NT^{TM} His-Tag Labelling Kit RED-tris-NTA, which specifically labels the 6xhis tag of the protein according to the manufacturer's instructions. Control experiments

confirmed that the labelling of Gly1ORF1 was efficient, with a K_d 143 nM that is within the expected range. An additional control experiment using a control peptide labelled with the RED-tris-NTA dye showed that lysozyme did not interact with the his-tag label.

In the Gly1ORF1-lysozme binding experiment, fluorescently labelled Gly1ORF1 concentration was constant at 100 nm and was incubated with serial dilutions of human lysozyme ranging from 10 µM to 0.3 nM at 37°C. The samples were loaded into standard treated glass capillaries, which had been determined as optimal for these measurements. MST generates a temperature gradient across the capillary and can detect the movement (thermophoresis) of fluorescently labelled proteins across this. Any changes in the size or charge of the protein that could be caused by protein-protein interactions will alter the thermophoresis of the fluorescently labelled protein. There was no lysozyme concentration dependent change in the thermophoresis of Gly1ORF1 in this experiment. The dose responses plot shows a high signal to noise ratio. This indicates that there was no interaction between Gly1ORF1 and Lysozyme in this context.

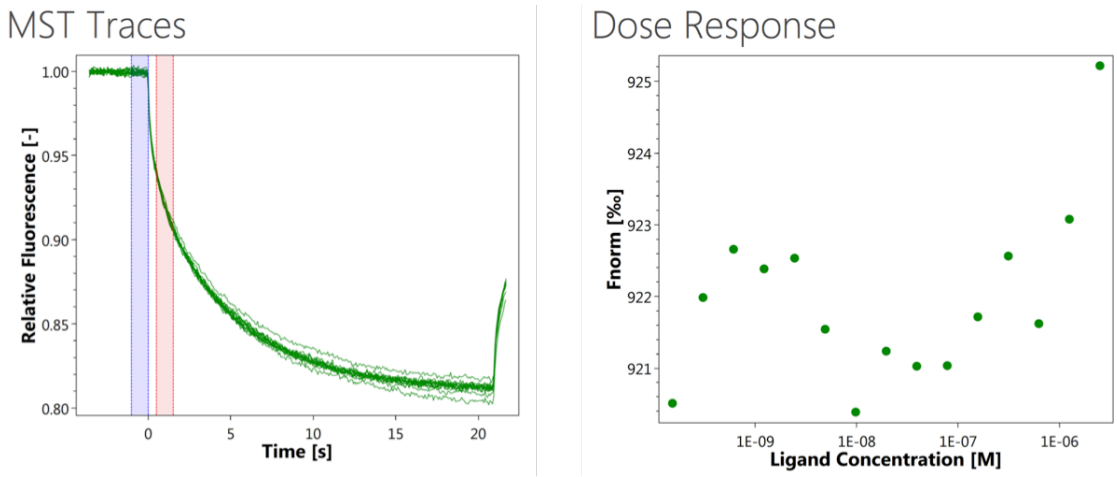

Figure 5.13 Microscale thermophoresis analysis of Gly1ORF1 and human lysozyme binding
MST traces (left) and dose response plot (right) for Gly1ORF1-human lysozyme interactions across a series of lysozyme concentrations (Ligand Concentration M). The dose response plot shows that there is no concentration dependent change in the thermophoresis of fluorescently labelled Gly1ORF1, indicating that the two proteins are not interacting. Fnorm=normalised fluorescence.

5.2.12 Sensitivity of *ΔORF1* mutant to hydrophobic agents

The sensitivity of the Δ*ORF1* mutant to a variety of hydrophobic agents was compared to that of the wild type using an agar plate assay. Sensitivity to hydrophobic agents can be an indicator that membrane or cell wall integrity is compromised in Gram-negative bacteria (Rasmussen et al., 2005). When the *gly1* locus was initially identified it was observed that MS11 mutants lacking the locus were more toxic to human fallopian tube explants (Arvidson et al., 1999). Possible explanations for this could be that *gly1* is involved in peptidoglycan or LPS synthesis, or play a role in membrane stability or production of OMVs, and that deletion of this locus could result in deregulation of these processes and increased release of toxic components.

Filter paper disks soaked in Triton X-100 (1% v/v), haemin (7 µM), erythromycin (1.25 µg per disk) or PBS were placed on top of agar plates spread with 100 µl of cell suspension. As can be seen in Figure 5.15 (top left disk) the presence of 7 µM haemin produced a zone of inhibition in the growth of both WT and Δ*ORF1* MS11. The diameter of the zone of inhibition caused by haemin did not vary significantly between the WT and mutant strains (WT = 12.55 mm, Δ*ORF1*= 13.44 mm. n=3). Both WT and Δ*ORF1* MS11 demonstrated similar sensitivity to erythromycin, which caused zones of inhibition 12.94 mm diameter in WT growth and 13.54 mm in Δ*ORF1.* Neither strain was sensitive to Triton x-100 or PBS.

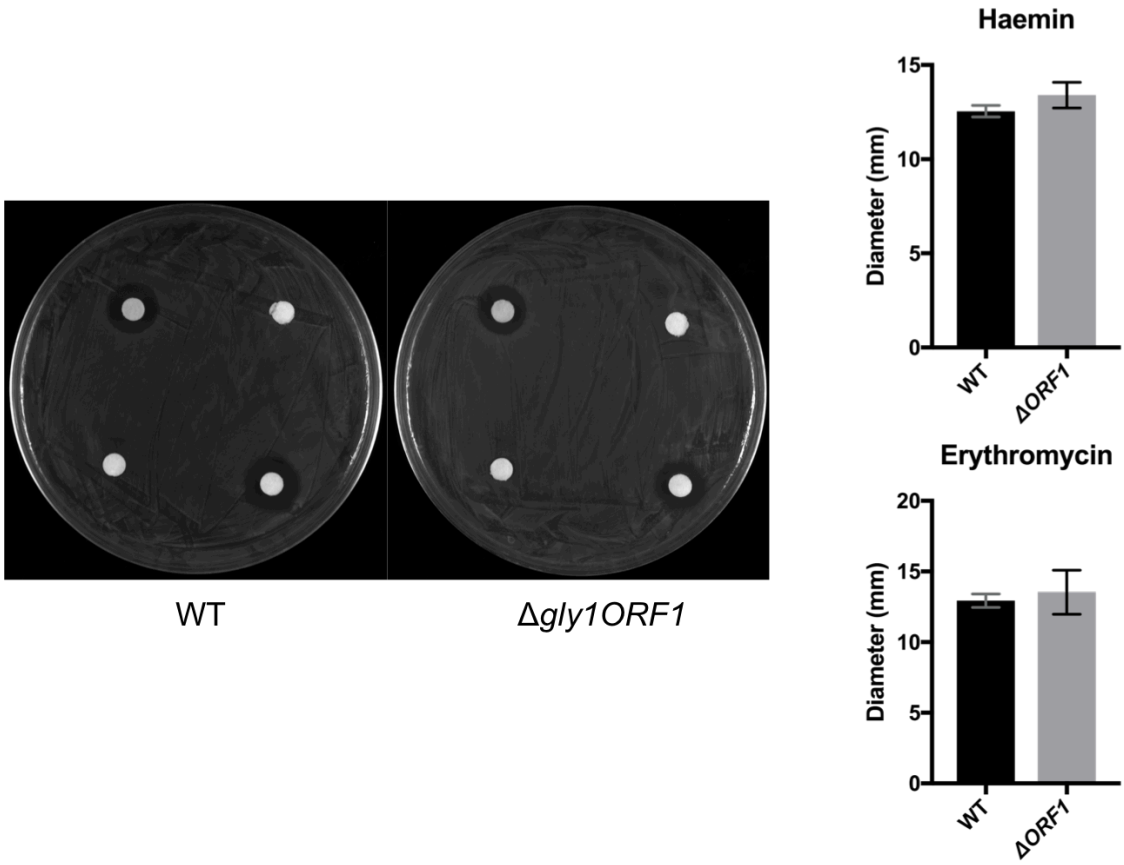

Figure 5.14 Plate assay of sensitivity of WT and *ΔORF1* MS11 to hydrophobic agents
Growth of wild type (WT) and *ΔORF1* MS11 on GCB/Vitox plates in the presence of filter paper disks soaked in hydrophobic agents haemin (7 µM, top left), Triton X-100 (1%, bottom left), erythromycin (1.25 µg, bottom right) and control disks soaked in PBS (top right). Zones of inhibition are observed surrounding both haemin and erythromycin disks but their diameter does not differ significantly between the WT and *ΔORF1* strains. Images representative of 3 plates. Zone of inhibition measurements carried out using ImageJ software

5.3 Discussion

In this chapter deletion mutants in the *gly1* locus have been created in *N. gonorrhoeae* strain MS11 by insertion of an antibiotic cassette, and used to study the potential roles of the genes *in vivo.* Creation of the Δ*ORF1* mutant lacking *gly1ORF1* was straightforward, with mutant transformants growing on GCB/ kanamycin plates. The creation of Δ*ORF2* and Δdouble mutants was more difficult, and mutant colonies could only be achieved by plating onto chocolate agar plates containing kanamycin after transformation. This indicates that the Δ*ORF2* and Δdouble mutants are auxotrophic due to the absence of *ORF2* and their nutritional requirements can only be met in the enriched chocolate agar media. The ability of Δ*ORF1* to grow in the less complex media suggests that there are no polar effects in this mutant and that the *ORF2* gene is intact, which has also been confirmed by sequencing of the mutants.

In rich media (BHI 0.5% yeast extract) in liquid culture Δ*gly1* showed no growth defect in comparison to WT but both the Δ*ORF2* and Δdouble mutants failed to grow. CFU counts at the beginning of the experiment confirmed that this was not due to deficiencies in the starting inoculum. This observation contrasts with the previously published study by Arvidson *et al.,* which found no difference in growth rate between the WT MS11 and the mutant lacking the entire *ORF1* locus in BHI media (Arvidson et al., 1999). Upon addition of human haemoglobin to the BHI media, all the mutants in this study grew at a comparable rate to WT. This indicates that haemoglobin can fulfil the nutritional requirements of Δ*ORF2* and Δdouble and that the deletion of *gly1ORF1* in Δdouble does not prevent exogenous haem utilization. These findings support the hypothesis that *gly1ORF2* is the *hemD* homologue in *Neisseria,* and is essential for haem biosynthesis.

5.3.1 Utilization of different iron sources

To test the ability of the mutants to use iron from different sources, a chemically defined media was used. This media usually contains iron(III) nitrate as an iron source, but this solution can be omitted or replaced with an alternative source. WT and Δ*ORF1* grew very effectively in this media with iron(III) nitrate. Both the WT and Δ*ORF1* strains also grew, although at a much slower rate, without any additional iron source

(GCCDM-0), possibly supported by intracellular iron reserves or trace amounts of iron in the media. The Δ*ORF2* and Δdouble mutants could not grow at all in GCCDM-0 with or without the addition of iron(III) nitrate.

WT and Δ*ORF1* strains could both use human haemoglobin as an iron source in GCCDM but Δ*ORF2* and Δdouble could not grow at all in this media. The 5 µM concentration used in this experiment may not have been sufficient to fulfil both the iron and haem requirements of the mutants lacking the *ORF2* gene. Experiments to determine whether higher concentrations of haemoglobin could support Δ*ORF2* and Δdouble could be carried out. However, the full nutritional requirements of these mutants are not known. Uroporphyrinogen III synthase (*hemD*) is part of the core tetrapyrrole biosynthesis pathway that also makes essential cofactors such as sirohaem, which is involved in sulphate reduction. These could be missing from the chemically defined media, explaining why the addition of haemoglobin did not rescue the mutant phenotype (Frankenberg et al., 2003; Mendum et al., 2011).

To address the concern that the growth observed in this study could have been due to contaminating free iron in the haemoglobin or haemin stock solutions and not direct use of haem as an iron source, the iron chelator DTPA was added to the media. DTPA has been used previously to deplete iron in microbial growth experiments and has a very strong affinity for iron (logK 27.3) so can be used at low concentrations (O'May et al., 2009; Qiu et al., 2011; Zhou et al., 2010). In these experiments the ability of the strains to grow using human holo-transferrin was used as a positive control to demonstrate that the chelator is not toxic to the cells. In the presence of DTPA WT and Δ*ORF1* MS11 could grow using haemin, haemoglobin or human holo-transferrin at similar rates (Figure 5.8). This shows that *gly1ORF1* is not essential for the use of haem as an iron source in MS11, or for the use of iron extracted from human transferrin.

The Δ*ORF1* mutant could also use haemin and haemoglobin as an iron source on solid media in the presence of the chelator deferoxamine mesylate. Both WT and Δ*ORF1* MS11 strains grew in a confluent zone around the haemin disk, but only in discrete colonies around the haemoglobin disk. The reason for the presence of discrete colonies is unclear, it is possible that the diffusion of haemoglobin through the agar could have been inefficient or that the mechanisms of haemin and haemoglobin

uptake could vary. MS11 possess the HpuAB haemoglobin receptor genes, which are controlled at the translational level through phase variation and the majority of cells in a population under laboratory conditions are phase-OFF and unable to utilize Hb (Chen et al., 1998). The presence of haemoglobin could be selecting for only those bacterial cells that are "phase-ON" for this receptor. Alternatively, the conditions could be selecting for compensating mutations that allow entry of haem through other routes. The observation of different growth phenotypes with haem and haemoglobin would suggest that free haemin is able to enter the cell in a different manner to haemoglobin, which could be TonB independent or through as yet uncharacterised TonB dependent receptors. It is also worth noting the difference between iron chelators used in the liquid and solid media assays. DTPA cannot enter the cells so can only chelate extracellular iron. There is evidence that deferoxamine mesylate may be able to enter cells and chelate intracellular iron (Bridges and Cudkowicz, 1984). This could affect intracellular processes involving iron causing additional growth defects that could account for the different growth phenotypes in liquid and solid media.

The ability of *N. gonorrhoeae* Δ*ORF1* to use haem and haemoglobin as an iron source contradicts previous findings in *N. meningitidis* MC58, where it was concluded that Gly1ORF1 was essential for haem utilization (Sathyamurthy, 2011). This disparity could be explained by the different haem/haemoglobin receptor systems expressed by *N. meningitidis* and *N. gonorrhoeae. N. meningitidis* MC58 encodes both HmbR and HpuAB, whereas in *N. gonorrhoeae* the *hmbR* gene is not functional due to the presence of a premature stop codon (Stojiljkovic et al., 1996). It was previously hypothesised that Gly1ORF1 could function as part of a bipartite receptor or haemophore system with HmbR, and preliminary experiments suggested an interaction (Wierzbicka, 2014). However, attempts to replicate these findings in this study were unsuccessful (data not shown). *N. gonorrhoeae* also encodes the putative haem receptor TdfG, which is absent in meningococcal genomes that could possibly be supporting growth using haem or haemoglobin in these experiments (Turner et al., 2001). Future work should aim to repeat the iron source growth experiments in strains with known haemoglobin receptor backgrounds. This could be achieved by sequencing to determine the phase variation status of receptors or using strains with haemoglobin

receptor deletions. The effect of *gly1* deletion on the expression of other proteins could also be investigated using transcriptomic or proteomic techniques and could provide crucial insight into its function. A recent study showed that deletion of an uncharacterised periplasmic located protein (NMB0419) in *N. meningitidis* resulted in down regulation of haemoglobin receptors and the TonB complex (Li et al., 2017). Although evidence presented in Chapter 3 suggests that Gly1ORF1 does bind to haem, it may not be directly involved in haem uptake, and could function as part of a sensing or regulatory system.

5.3.2 Alternative functions of Gly1ORF1 - Lysozyme inhibitor

The neisserial adhesin complex protein (ACP) was identified as a potential Gly1ORF1 paralogue due to similarities in size, periplasmic location, predicted structure and limited sequence conservation (McMellon, 2016; Wierzbicka, 2014). ACP functions as an adhesin, *N. meningitidis* null mutants show reduced adhesion to epithelial and endothelial cells and the purified protein has been observed directly binding to the human cell surface (Hung et al., 2013). Recently published evidence suggests that ACP may also function as a lysozyme inhibitor, as its expression protects *Neisseria* from lysozyme induced lysis and the purified protein binds to human lysozyme *in vitro* (Humbert et al., 2017). Lysozyme is an important component of the innate immune system, both for its ability to kill bacteria through degradation of the cell wall and because this action generates peptidoglycan fragments that stimulate other immune responses (Davis et al., 2011; Sorbara and Philpott, 2011). Lysozyme is abundant at mucous membranes and is present in neutrophil granules, both sites key to neisserial colonisation and pathogenesis.

Several classes of bacterial lysozyme inhibitor exist and are classified based on their subcellular location and lysozyme specificity. These include *E.coli* Ivy type, MliC/PliC (membrane/periplasmic c-type), PliG and PliI (periplasmic g-type and i-type) (Callewaert et al., 2008; Liu et al., 2015; Monchois et al., 2001). A putative MliC homologue (NGO_1063) has been annotated in the *N. gonorrhoeae* FA1090 genome (GenBank no. AE004969) but no further evidence of lysozyme inhibitors in *Neisseria* has been reported. All of the characterised lysozyme inhibitors act by binding strongly

to lysozyme and preventing binding and cleavage of glycosidic bonds in the sugar backbone of peptidoglycan (Callewaert et al., 2012).

Gly1ORF1 was investigated as a potential lysozyme inhibitor to ascertain if this could be a shared function of the Gly1 family. There was no significant difference in the sensitivity of Δ*ORF1* and WT MS11 to human lysozyme. The variation between the experiments was very high, especially for the Δ*ORF1* mutant strain. This could have been affected by slight differences in the experimental conditions between repeats. *N. gonorrhoeae* growth phenotypes are particularly sensitive to environmental variations such as the amount of time grown on agar plates, the speed of shaking and temperature fluctuations (Annear and Grubb, 1982; Kraus, 1979). This experiment could be repeated with tighter controls for other growth conditions to ascertain whether there is any real effect. *In vitro* experiments failed to detect any interaction between Gly1ORF1 and human or chicken egg white lysozyme. A high molecular weight protein species was detected after glutaraldehyde crosslinking, but it was impossible to distinguish whether this was a complex of the two proteins or a homodimer of one of them. To improve on this assay, the proteins and complexes could be transferred to nitrocellulose membrane after separation and probed using anti-Gly1ORF1 and anti-lysozyme antibodies for dual colour Western blotting.

Although Gly1ORF1 and ACP do not share any significant sequence identity, comparison of their crystal structures reveals some structural similarities (see Figure 5.16). Both proteins have a core consisting of two antiparallel 4 stranded β-sheets, with a disulphide bond that connects the first and last β-strand (shown in yellow and orange sticks in Figure 5.15). Through *in silico* docking and NMR chemical shift mapping “loop 4” containing residues 76-82 (shown as red sticks in Figure 5.15) was predicted to be the most likely binding site between ACP and lysozyme (Humbert et al., 2017). There is no corresponding site in the Gly1ORF1 structure, the β-sheet of Gly1ORF1 is more structured than ACP and is formed of extended β-strands that are present in the area of loop 4 in the structural alignment. These structural differences along with the failure to detect any binding between purified Gly1ORF1 and lysozyme *in vitro* establish that Gly1ORF1 does not act as a lysozyme inhibitor in a traditional sense like the MliC/PliC or Ivy family proteins. A major factor in lysozyme resistance of

Gram-negative bacteria is the presence of the outer membrane, which prevents easy access to the peptidoglycan cell wall. Disruption of outer membrane stability increases the lysozyme sensitivity of Gram-negative bacteria (Ellison and Giehl, 1991; Ragland et al., 2016). *N. gonorrhoeae* lacking two lytic transglycosylases involved in peptidoglycan turnover are more sensitive to lysozyme due to increased membrane permeability (Ragland et al., 2016). Gly1ORF1 may contribute to lysozyme resistance if it plays a role in regulating or maintaining cell surface structures.

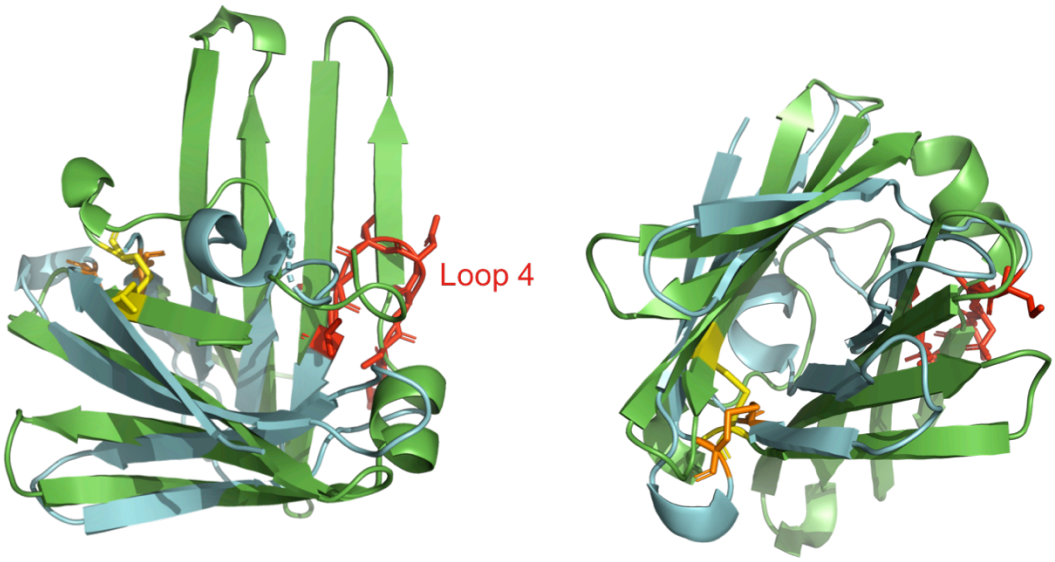

Figure 5.15 Structural alignment of Gly1ORF1 and ACP structures
Cartoon representation of the side (left) and bottom (right) view of aligned Gly1ORF1 (green) and ACP structures (blue). Both proteins have a disulphide bond shown as sticks (yellow Gly1ORF1, orange ACP). Loop 4 (residues 76-82) of ACP is the predicted lysozyme binding site. Structural alignment carried out using the CE algorithm in Pymol that detects structural similarities in proteins with little or no sequence homology.

5.3.3 Sensitivity to hydrophobic agents

It has been hypothesised that the increased toxicity of Δ*ORF1* mutants towards human fallopian tube tissue could be due to defects in membrane integrity or peptidoglycan and LPS synthesis (Arvidson et al., 1999). Detailed studies of *N. gonorrhoeae* tissue damage in fallopian tube culture showed that it is caused by the presence of LPS and release of peptidoglycan monomers, which stimulate upregulation of the pro-

inflammatory cytokine TNF-α (Gregg et al., 1981; McGee et al., 1999; Melly et al., 1981, 1984). The Δ*ORF1* mutant was tested to determine whether there was any defect in membrane integrity, indicated by increased sensitivity to hydrophobic agents, which could result in increased release of toxic cell membrane or cell wall components. This assay was also used to determine whether Δ*ORF1* had decreased membrane integrity that would make it more sensitive to haem toxicity. Increased sensitivity to haem toxicity could be an alternative explanation for the observations in *N. meningitidis* where the Δ*ORF1* mutant could not grow with haem or haemoglobin (Sathyamurthy, 2011). Proteins that are involved in cell surface assembly have previously been identified in transposon mutant library screens for putative haem uptake proteins, as their deletion can make mutants more sensitive to haem toxicity and they therefore fail to grow at concentrations of haem or haemoglobin that are intended to support growth as a sole iron source (Putker et al., 2014; Rasmussen et al., 2005).

The results of the hydrophobic plate assay show that the membrane integrity of Δ*ORF1* was not compromised, as there was no significant difference in the diameter of the zones of inhibition caused by haemin and erythromycin when compared to wild type. Mutations that cause defects in membrane or cell wall integrity can also cause growth defects in rich media but no such defects were observed for Δ*ORF1* (Putker et al., 2014). The hydrophobic compounds in this assay were only used at one concentration, based upon those used in previous studies with *N. meningitidis* and different *N. gonorrhoeae* strains (Chen et al., 2004; Rasmussen et al., 2005). Minimum inhibitory concentrations of these compounds could be determined to improve this assay. *N. gonorrhoeae* strain MS11 has a higher level of resistance than other laboratory strains to some antibiotics and detergents, mainly conferred by overexpression of the Mtr efflux pump (Dillard, 2011; Ohneck et al., 2011; Warner et al., 2008). The sensitivity of clinical isolates to hydrophobic agents is unknown, and any potential membrane stability effects of Gly1ORF1 could be studied in these isolates to gain a more accurate idea of its importance in disease.

6. Conclusion

Pathogenic *Neisseriaceae* continue to present significant challenges to human health. *N. meningitidis* is one of the most common causes of bacterial meningitis and septicaemia worldwide (Brouwer et al., 2010). Great advances in countering meningococcal pathogenesis have been made, particularly with the development of the elusive serogroup B vaccines. Preliminary evidence indicates the introduction of serogroup B vaccines to the infant immunization programme in the UK has decreased incidence of invasive disease caused by this serogroup by 42% (Feavers and Maiden, 2017). There has also been success with serogroup A conjugate vaccines, which have reduced rates of invasive disease to their lowest ever levels in the sub-Saharan African "meningitis belt" (Mohammed et al., 2017). However, there are still drivers for further research including the high mortality rate and potentially life changing disabilities faced by survivors, concerns over vaccine cost-effectiveness, and the evolving antigenic profile of invasive strains (Christensen et al., 2014; Harrison et al., 2006; Lucidarme et al., 2011). The increasing spread of antibiotic resistance in *N. gonorrhoeae* and the lack of any preventative vaccine has led to the World Health Organisation classifying it as a high priority organism for the development of new treatments and preventative measures (World Health Organization, 2017). It is now critical that we work to understand the main aspects of neisserial pathogenesis and explore all potential avenues to novel treatments.

The focus of this study was the *gly1* locus consisting of two open reading frames, first identified in *N. gonorrhoeae* as encoding potential cytotoxins (Arvidson et al., 1999). Previous studies in our group have investigated the function of Gly1ORF1, finding that it is outer membrane located or secreted, possesses haem-binding function, and possibly interacts with erythrocytes (McMellon, 2016; Meadows, 2005; Sathyamurthy, 2011; Wierzbicka, 2014). These studies have shown that Gly1ORF1 is not a neisserial cytotoxin, as the purified protein does not cause rupture of erythrocytes, human epithelial cell lines or mouse fibroblast cell lines (Meadows, 2005; Sathyamurthy, 2011). The haemolytic phenotype first observed by Arvidson and colleagues was most likely caused by the overexpression of Gly1ORF1 in *E. coli* cells causing rupture of the outer membranes or even entire cells and release of toxic *E. coli* proteins. The

presence of many *E. coli* proteins in the culture medium after Gly1ORF1 overexpression has been observed often in our group, for example in Chapter 3, Figure 3.4 in this thesis. No work to characterise ORF2 had been carried out, but due to sequence homology it is predicted to be the neisserial porphyrin biosynthesis enzyme UroS. The overall aims of this project were to further investigate the biological functions of the proteins expressed from the *gly1* locus and whether they are significant for neisserial pathogenesis. The hypothesis was that the proteins played a role in resisting haem/iron based nutritional immunity imposed by the human host. This could be achieved through scavenging and uptake of haem in the case of Gly1ORF1, and haem biosynthesis in the case of Gly1ORF2.

6.1 Haem binding/ interactions of Gly1ORF1

One of the aims of this study was to investigate the haem binding ability of Gly1ORF1 and determine whether this interaction has any significance for the survival or pathogenesis of *Neisseria in vivo.* Previous studies in our group showed that Gly1ORF1 interacts with haemin. However, many issues with protein or haemin precipitation in these experiments, along with the potential interference of 6xHis tag prevented collection of any biophysical data on this interaction.

To address these questions I aimed to develop an efficient protocol to express and purify soluble non-tagged Gly1ORF1. The heat inducible expression vector containing both ORF1 and ORF2 seemed to produce high levels of soluble Gly1ORF1 in *E. coli* supernatants, producing readily visible protein bands on SDS-PAGE analysis which made up approximately 11% of total protein estimated from densitometry analysis. Unfortunately, despite numerous optimization attempts, only a small amount of soluble non-tagged Gly1ORF1 could be purified. This enabled haemin agarose pull-down assays that showed native Gly1ORF1 does have intrinsic haem binding ability and was supported by the observation of the increased haemin binding capacity of *E. coli* cells expressing native Gly1ORF1 (Chapter 3 sections 3.2.4-5).

Further haemin binding assays were carried out with C-His Gly1ORF1 in attempt to quantify the binding affinities and shed more light on the specifics of the interaction. The results of the UV-visible absorbance spectra experiments (Chapter 3 section 3.2.7) suggested that binding might be iron dependent, as the haemin analogues that do not

contain iron did not show any Gly1ORF1 concentration-dependent changes in their visible spectra. Microscale thermophoresis analysis of the interaction with haemin (Chapter 3 section 3.2.8) produced a dissociation constant (K_d) of 5.55 μM, but issues with protein aggregation prevented successful replication of these experiments. This value is higher than the K_d previously determined for several Gly1ORF1 mutants, showing that the mutations increased the affinity of the protein for haemin (Wierzbicka, 2014). These affinities are still much weaker than those reported for well-characterised bacterial haem uptake proteins, which range between 10-500 nM (Izadi et al., 1997; Rohde and Dyer, 2004; Wójtowicz et al., 2013). This suggests that the function of Gly1ORF1 is not to directly bind and scavenge haem from the human host, as it would be unable to outcompete human plasma proteins such as albumin (K_d ~10 nM) and haemopexin (K_d ~1 nM) for free haem (Ascenzi et al., 2005). Gly1ORF1 could bind haem for another purpose, such as sensing or storage and distribution. For example the *H. influenzae* adhesin protein E (PE) may serve as a storage pool for haem. The dimer binds haemin with a K_d in micromolar range and can distribute it to *H. influenzae* that are haemin starved (Al Jubair et al., 2014). It is possible that the haem binding serves as a regulatory mechanism for another function of Gly1ORF1 through oligomerisation of the protein. Haem-induced oligomerisation as a regulatory mechanism has been observed for several microbial and human proteins, including RNA binding proteins, tRNA synthetases and proteins regulating cell wall composition (Edgar et al., 2016; Faller et al., 2007; Yang et al., 2010).

It has not been possible to determine whether the observed haemin-Gly1ORF1 interaction is specific and serves a biological purpose from knock out experiments conducted on *N. gonorrhoeae* reported in Chapter 5. Gly1ORF1 is not essential for *N. gonorrhoeae* MS11 growth using haem or haemoglobin as the sole iron source. This is in contrast to *N. meningitidis* MC58, where Gly1ORF1 was found to be essential for this function (Sathyamurthy, 2011). These contradictory results do not rule out a role for Gly1ORF1 in haem acquisition, as there may be more redundancy in these systems in *N. gonorrhoeae* than *N. meningitidis. In silico* genome comparisons of *N. meningitidis* and *N. gonorrhoeae* show that genes tend to be either highly conserved in both species, or present in one species and absent in the other. Over 75% of *N*. *meningitidis*

Z2491 genes had homologues in *N. gonorrhoeae* FA1090 that were over 80% amino acid similarity, but 12% of had no significant homology to any gonococcal genes (Perrin et al., 2002). These differences are mainly due to the presence of genomic "islands" such as the gonococcal genetic island (GGI) that encodes the type IV secretion system that has been implicated in iron uptake as discussed in Chapter 1 section 1.3.8. It would be beneficial to repeat these experiments in a more controlled strain background, possibly through deletion of known and putative haem uptake systems such as HpuAB and TdfG or determination of their phase variation states.

6.2. Structural characterisation of proteins expressed from the *gly1* locus

A second aim of this study was to structurally characterise the two proteins produced from the *gly1* locus. It was hoped that further knowledge of these protein structures could help identify their functions, as some functionally related proteins share high structural homology even though they have low primary sequence homology.

Crystal trials on the wild type *N. meningitidis* Gly1ORF1 protein were successful and produced many crystals that diffracted to between 2.2 and 2.5 Å. Crystal structures have previously been solved for GlyORF1 homologues from *N. gonorrhoeae* and *M. haemolytica,* along with a *N. meningitidis* Gly1ORF1 K12A mutant (Arvidson et al., 2003; McMellon, 2016; Wierzbicka, 2014). The *N. meningitidis* wild-type structure presented here is the most complete yet, with peptide backbone built along entire the length of the protein. This improved structure has allowed further analysis of potential dimer interfaces in Gly1ORF1, which readily forms dimers in solution (McMellon, 2016; Sathyamurthy, 2011; Wierzbicka, 2014). PISA analysis identified a potential dimer interface but it was not certain whether the assembly would be stable in solution. Experimental confirmation *in vitro* will be required to verify if this is a biological dimer found in solution and not an artefact of crystal packing. No diffracting crystals were produced in the Gly1ORF1 co-crystallisation trials with haemin. Significant optimizations would be required to produce a Gly1ORF1-haemin structure and it may not be possible due to the binding affinities described above and the high concentrations of haemin required. It could be that the haem(Fe(II)) ligand form is required for binding rather than the Fe(III) form that is present in haemin. This could be achieved using reducing conditions under nitrogen with the presence of sodium

dithionite, however this was not possible within the timescales of this project. If the dimer assembly predicted in this study can be experimentally confirmed, the structure could be used for *in silico* docking with haemin to identify binding sites, overcoming the limitations of co-crystallisation.

There are still no proteins with significant structural homology to Gly1ORF1 in the protein data bank (PDB). Searches using servers such as Dali (Holm and Rosenström, 2010), which searches for conserved structural motifs regardless of primary sequence, do not return any significant matches. This highlights the fact that the Gly1ORF1 family share a novel protein fold, the function(s) of which is as yet unknown. Therefore, other experimental methods will have to be employed to ascertain their functions.

Crystallisation trials for the product of *gly1ORF2* were not successful. Despite many attempts (approximately 864 conditions) no diffracting crystals were produced. Structure prediction software used to model the tertiary structure of Gly1ORF2 showed very likely structural homology with UroS *(hemD*) family proteins despite low levels of primary sequence conservation (less than 25%). These proteins are particularly temperature sensitive and also contain a flexible linker section between the two domains, which may cause an issue with stability during crystallisation. Optimization of the protein purification protocol and crystallisation, using similar conditions as previously crystallised homologues such as low temperatures, should be carried out in the future. The same is true for the preceding enzyme in the porphyrin pathway, HmbS (*hemC*), also purified and characterised in this project. HmbS also contains multiple domains connected by flexible linkers. It may be possible to engineer truncated versions enabling expression of distinct domains of HmbS that may crystallise more easily, for example isolating one domain at a time. However, this would not be possible for UroS, as the N and C termini of the protein are located in the same domain.

6.3 Alternative potential Gly1ORF1 functions

Some preliminary work to investigate potential alternative functions of Gly1ORF1 was undertaken in this project. Although there are no proteins that share significant primary sequence homology with Gly1ORF1 outside of the *Neisseriaceae* family, a large number of potential Gly1ORF1 homologues have been identified through

structural homology and PSI-BLAST techniques that identify distantly related protein sequences (McMellon, 2016; Sathyamurthy, 2011; Wierzbicka, 2014). They are mostly uncharacterised but some studies in our group and elsewhere have suggested they may perform varied functions including haem binding, adhesion, protection from host antimicrobial enzymes, or cell wall maintenance (Arvidson et al., 1999; Deghmane et al., 2003; Humbert et al., 2017; Hung et al., 2013; McMellon, 2016; Morelle et al., 2003; Sathyamurthy, 2011; Wierzbicka, 2014).

The potential for Gly1ORF1 to act as a lysozyme inhibitor was investigated, following recent evidence that showed the potential paralogue ACP (NMB2095) possessed this function (Humbert et al., 2017). In the present study, purified Gly1ORF1 did not demonstrate lysozyme binding ability, and the Δ*ORF1* MS11 strain did not have a significantly increased sensitivity to human lysozyme in culture. These results agree with previous findings for *M. haemolytica* Gly1ORF1 paralogue and do not support a role for Gly1ORF1 in lysozyme inhibition (McMellon, 2016). Structural comparison of the wild type *N. meningitidis* Gly1ORF1 structure and the ACP protein (chapter 5 Figure 5.16) shows that Gly1ORF1 does not posses a 7 residue loop (loop 4) that was identified as the interaction site between ACP and lysozyme (Humbert et al., 2017) .

Another suggested function for Gly1ORF1 is that of an adhesin, due to its partial cell-surface location and contact-regulated expression profile. Several studies using cell culture models to investigate this hypothesis have shown that Gly1ORF1 is not essential for adhesion or invasion of bacteria to epithelial cells (Arvidson et al., 1999; Deghmane et al., 2003; Morelle et al., 2003; Sathyamurthy, 2011). However, fluorescence microscopy experiments showed that purified *M. haemolytica* Gly1ORF1 paralogue exhibited specific binding to epithelial cells in the porcine upper respiratory tract (McMellon, 2016). Similar experiments could be carried out for neisserial Gly1ORF1 but would require the use of human tissue samples such as fallopian tube explants, which have often been used to study *N. gonorrhoeae* interactions with ciliated mucosa (Draper et al., 1980; Gorby et al., 1994; Juica et al., 2017; Velasquez et al., 2012).

The increased toxicity of Δ*ORF1 N. gonorrhoeae* to human fallopian tubes observed by Arvidson *et al.* could point to a role for Gly1ORF1 in cell wall or cell surface assembly

and maintenance. *N. gonorrhoeae* toxicity in fallopian tube cultures is known to be caused by LOS and peptidoglycan monomer release and correlates with the induction of TNF-α to cause apoptosis and loss of ciliated cells (Gregg et al., 1981; McGee et al., 1999; Melly et al., 1981, 1984). A phenotype diagnostic for compromised outer membrane stability due to defects in LOS and peptidoglycan metabolism is the sensitivity to hydrophobic compounds like haemin (Putker et al., 2014). In this study, the sensitivity of Δ*ORF1 N. gonorrhoeae* to hydrophobic agents was not significantly increased compared to wild-type cells. The sensitivity of the plate assay used is unknown and could be improved by optimization to determine minimum inhibitory concentrations of the hydrophobic agents. This would be useful to compare with *N. meningitidis* MC58. It may be possible previous results showing the inability of *N. meningitidis* to grow where haemin was the only iron source could have been due to the toxicity of haemin to MC58 Δ*ORF1* mutant at that concentration. Addition of purified Gly1ORF1 in these experiments partially rescued the phenotype of the MC58 Δ*ORF1* (Sathyamurthy, 2011). This could have been due to the purified protein contributing to haemin uptake, but it might also be explained by the tendency of Gly1ORF1 to precipitate with haemin. The concentration of free haemin in the media may have been lowered as it bound to and precipitated with Gly1ORF1, allowing the bacteria to survive. Other techniques such as monitoring the turnover of radiolabelled PG or quantification of LOS in culture supernatants could be employed to further study whether increased toxicity of Δ*ORF1 N. gonorrhoeae* is due to deregulation of processes maintaining the outer membrane or cell wall (Cloud and Dillard, 2002; Lee and Tsai, 1999).

The increased toxicity levels could also be interpreted as support for the hypothesis that the locus is involved in iron uptake. Iron starvation can induce dramatic changes in gene expression profile and some studies have shown that iron-induced changes resulted in increased virulence in mice (Brener et al., 1981; Holbein et al., 1979). The creation of both the novel single *gly1ORF1* and *gly1ORF2* (*hemD*) *N. gonorrhoeae* mutants in addition to the double mutant in this study provides scope for further investigation of the increased toxicity phenotype, including pinpointing the effect to a single gene in the locus. They could also be used for transcriptome analysis to

determine whether Gly1ORF1 is involved in signalling or regulation of other proteins. These types of experiments may be essential for finally determining Gly1ORF1 function.

6.4 Characterising *gly1ORF2*

Another aim of this study was to carry out the first characterisation of *gly1ORF2*, the putative neisserial *hemD* homologue. The protein product of this gene was not studied when the locus was originally identified because the researchers were unable to express it to a sufficient level in *E. coli* to allow for purification.

In this study an expression vector with optimised ribosome binding site and stop codon was created that allowed expression and purification of high yields of soluble Gly1ORF2 protein (up to approximately 20% of total protein). The *N. meningitidis hemC* gene was also cloned here, and the protein product (HmbS) was purified with the aim of carrying out the coupled UroS activity assay (Mathews et al., 2001; Peng et al., 2011; Roessner et al., 2002). The assay for HmbS activity showed that *N. meningitidis hemC* encodes a functional HmbS homologue with a specific activity of 42 µmol/mg/hour at optimum pH when freshly purified, which is comparable to the *E. coli* enzyme activity reported in the literature (43 µmol/mg/hour).

Gly1ORF2 did not exhibit UroS activity in the coupled assay. However, *E. coli* genetic complementation studies in chapter 4 section 4.2.17 showed that *gly1ORF2* could rescue the *hemD* deficient phenotype of SASZ31. Further support for the hypothesis that Gly1ORF2 is a functional UroS homologue was provided by the observation that the *N. gonorrhoeae* deletion mutant required exogenous source of haem for growth on solid or liquid media, indicating a defect in haem biosynthesis. The inability to confirm Gly1ORF2 UroS activity using the biochemical assay could have been due to denaturation of this temperature-sensitive enzyme during heat-induced expression, or the absence of appropriate additives and reducing agents in the storage and reaction buffers. Further work should include the development of a protocol for *E. coli* expression of this protein at low temperatures, such as using the autoinduction method (Studier, 2005) rather than the heat-shock system used here. Structural and functional characterisation of UroS is an important goal. UroS is a core enzyme shared

by all organisms that carry out haem biosynthesis and mutations in the human enzyme are responsible for the autosomal disease congenital erythropoietic porphyria. UroS enzymatic mechanism is not well understood and is complicated by the low sequence conservation between homologues. Any insights gained through study of the neisserial homologue will not only advance knowledge of neisserial biochemistry but could also translate to understanding of the human metabolic disorder.

This study represents the first time any haem biosynthesis proteins from *Neisseria* have been purified and characterised. The significance of haem biosynthesis for neisserial pathogenesis has not yet been studied in any depth. *Neisseria* encode several well-characterised systems that capture and import intact host haem, but it is unknown whether they incorporate host haem into their haemoproteins or rely solely on haem biosynthesis for this function during pathogenesis. A functioning haem biosynthesis pathway is not essential *in vitro* when exogenous haem is supplied but it is unlikely that availability of free haem is high enough in most niches in the human body to fulfil this requirement due to tight regulation (Dyer et al., 1987). Only one example of a study creating neisserial haem biosynthetic mutants has been reported in the literature, which suggested that biosynthesis was important for survival inside epithelial cells (Turner et al., 1998). This shows that there is scope for further investigation of the significance on haem biosynthesis during different stages of colonization and pathogenesis, which may be facilitated by the creation of the Δ*ORF2* MS11 mutant in this project. This, along with a more detailed understanding of the enzymatic mechanism will determine whether UroS has potential as a target for antimicrobial therapies.

6.5 Summary

In this project further insight has been gained into the structure and function of the proteins expressed by the *gly1* locus in *N. meningitidis* and *N. gonorrhoeae.* The *gly1ORF2* gene has been studied for the first time and has been identified as the neisserial *hemD* gene through genetic complementation. Protocols were developed for expressing and purifying Gly1ORF2 (UroS) and the preceding enzyme in the porphyrin synthesis pathway HmbS. The preliminary biochemical experiments and optimization of crystallography conditions should pave the way for future in depth study of these

enzymes and of neisserial haem biosynthesis in general. Gly1ORF1 has been confirmed to have innate haem-binding ability and some biophysical data on the interaction has been collected. The solution of the wild-type crystal structure and analysis of a potential biological dimer presented here will inform future studies of this protein, for example using site-directed mutagenesis to identify haem-binding sites or dimer interfaces. The observation that Gly1ORF1 is not essential for *N. gonorrhoeae* survival with haem as the only iron source was surprising considering its apparent importance for *N. meningitidis* survival (Sathyamurthy, 2011). This result highlights that there may be different or redundant nutrient acquisition systems in these two species and findings in one species may not easily be translated to the other despite their close phylogenetic relationship. Several other possible functions of Gly1ORF1 have been explored in this study but the function *in vivo* and significance for pathogenesis is still ultimately unknown. This question does merit further study, particularly due to the presence of homologues in many Gram-negative pathogens and their potential as vaccine candidates.

7. Appendices

7.1 Mass Spectrometry analysis of native Gly1ORF1

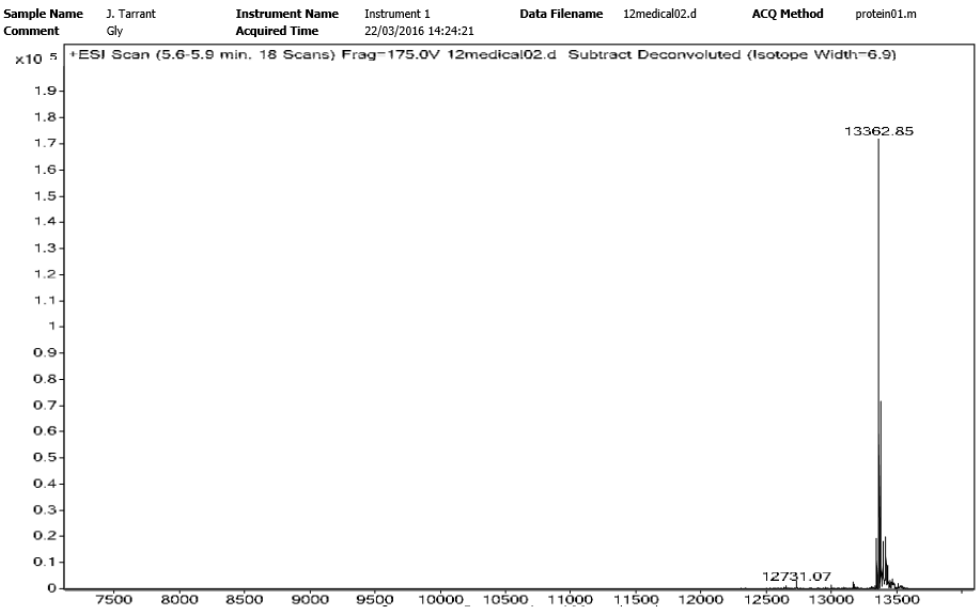

ESI mass spectrometry analysis of purified native Gly1ORF1 (from Chapter 3). The main species present in the sample is a protein with molecular weight of 13.36 kDa, which is the predicted molecular weight of Gly1ORF1 with the N-terminal signal sequence processed and removed.

Bibliography

Adamczak, R., Porollo, A., and Meller, J. (2005). Combining prediction of secondary structure and solvent accessibility in proteins. Proteins Struct. Funct. Genet. *59*, 467–475.

Agarwal, S., King, C.A., Klein, E.K., Soper, D.E., Rice, P.A., Wetzler, L.M., and Genco, C.A. (2005). The gonococcal Fur-regulated tbpA and tbpB genes are expressed during natural mucosal gonococcal infection. Infect. Immun. *73*, 4281–4287.

Agarwal, S., Vasudhev, S., DeOliveira, R.B., and Ram, S. (2014). Inhibition of the Classical Pathway of Complement by Meningococcal Capsular Polysaccharides. J. Immunol. *193*, 1855–1863.

de Amorim, G.C., Prochnicka-Chalufour, A., Delepelaire, P., Lefèvre, J., Simenel, C., Wandersman, C., Delepierre, M., and Izadi-Pruneyre, N. (2013). The Structure of HasB Reveals a New Class of TonB Protein Fold. PLoS One *8*, e58964.

Anderson, P.M., and Desnick, R.J. (1980). Purification and Properties of Uropophyrinogen I Synthase from Human Erythrocytes. J. Biol. Chem. *245*, 1993–1999.

Anderson, J.E., Sparling, P.F., and Cornelissen, C.N. (1994). Gonococcal transferrin-binding protein 2 facilitates but is not essential for transferrin utilization. J. Bacteriol. *176*, 3162–3170.

Andreini, C., Bertini, I., Cavallaro, G., Holliday, G.L., and Thornton, J.M. (2008). Metal ions in biological catalysis: From enzyme databases to general principles. J. Biol. Inorg. Chem. *13*, 1205–1218.

Annear, D., and Grubb, W. (1982). Growth of *Neisseria gonorrhoeae* in brain heart infusion. J. Clin. Pathol. *35*, 118–119.

Arnoux, P., Haser, R., Izadi, N., Lecroisey, A., Delepierre, M., Wandersman, C., and Czjzek, M. (1999). The crystal structure of HasA, a hemophore secreted by *Serratia marcescens*. Nat. Struct. Biol. *6*, 516–520.

Arvidson, C.G., Kirkpatrick, R., Witkamp, M.T., Larson, J.A., Schipper, C.A., Waldbeser, L.S., O'Gaora, P., Cooper, M., and So, M. (1999). Neisseria gonorrhoeae mutants altered in toxicity to human fallopian tubes and molecular characterization of the genetic locus involved. Infect. Immun. *67*, 643–652.

Arvidson, D.N., Pearson, R.F., and Arvidson, C.G. (2003). Purification, characterization and preliminary X-ray crystallographic studies on *Neisseria gonorrhoeae* Gly1ORF1. Acta Crystallogr. D. Biol. Crystallogr. *59*, 747–748.

Ascenzi, P., Bocedi, A., Visca, P., Altruda, F., Tolosano, E., Beringhelli, T., and Fasano, M. (2005). Hemoglobin and heme scavenging. IUBMB Life *57*, 749–759.

Azim, N., Deery, E., Warren, M.J., Wolfenden, B.A.A., Erskine, P., Cooper, J.B., Coker, A., Wood, S.P., and Akhtar, M. (2014). Structural evidence for the partially oxidized dipyrromethene and dipyrromethanone forms of the cofactor of porphobilinogen deaminase: Structures of the *Bacillus megaterium* enzyme at near-atomic resolution. Acta Crystallogr. Sect. D Biol. Crystallogr. *70*, 744–751.

Bali, S., Lawrence, A.D., Lobo, S.A., Saraiva, L.M., Golding, B.T., Palmer, D.J., Howard, M.J., Ferguson, S.J., and Warren, M.J. (2011). Molecular hijacking of siroheme for the synthesis of heme and d1 heme. Proc. Natl. Acad. Sci. *108*, 18260–18265.

Banerjee, S., Parker Siburt, C.J., Mistry, S., Noto, J.M., DeArmond, P., Fitzgerald, M.C., Lambert, L.A., Cornelissen, C.N., and Crumbliss, A.L. (2012). Evidence of Fe3+ interaction with the plug domain of the outer membrane transferrin receptor protein of *Neisseria gonorrhoeae*: implications for Fe transport. Metallomics *4*, 361.

Barber, M.F., and Elde, N.C. (2015). Buried Treasure: Evolutionary Perspectives on Microbial Iron Piracy. Trends Genet. *31*, 627–636.

Basler, M., Linhartová, I., Halada, P., Novotná, J., Bezoušková, S., Osička, R., Weiser, J., Vohradský, J., and Šebo, P. (2006). The iron-regulated transcriptome and proteome of *Neisseria meningitidis* serogroup C. Proteomics *6*, 6194–6206.

Bautista, C.T., Wurapa, E.K., Sateren, W.B., Morris, S.M., Hollingsworth, B.P., and Sanchez, J.L. (2017). Repeat infection with *Neisseria gonorrhoeae* among active duty U.S. Army personnel: a population-based case-series study. Int. J. STD AIDS *28*, 962–968.

Beck, S.C., and Meyer, T.F. (2000). IgA1 protease from *Neisseria gonorrhoeae* inhibits TNFα-mediated apoptosis of human monocytic cells. FEBS Lett. *472*, 287–292.

Bernard, S.C., Simpson, N., Join-Lambert, O., Federici, C., Laran-Chich, M.-P., Maïssa, N., Bouzinba-Ségard, H., Morand, P.C., Chretien, F., Taouji, S., et al. (2014). Pathogenic *Neisseria meningitidis* utilizes CD147 for vascular colonization. Nat. Med. *20*, 725–731.

Bhat, K.S., Gibbs, C.P., Barrera, O., Morrison, S.G., Jähnig, F., Stern, A., Kupsch, E. -M, Meyer, T.F., and Swanson, J. (1991). The opacity proteins of *Neisseria gonorrhoeae* strain MS11 are encoded by a family of 11 complete genes. Mol. Microbiol. *5*, 1889–1901.

Bidmos, F.A., Chan, H., Praekelt, U., Tauseef, I., Ali, Y.M., Kaczmarski, E.B., Feavers, I., and Bayliss, C.D. (2015). Investigation into the antigenic properties and contributions to growth in blood of the meningococcal haemoglobin receptors, HpuAB and HmbR. PLoS One *10*, 1–22.

Biegel Carson, S.D.B., Klebba, P.E., Newton, S.M.C., and Sparling, P.F. (1999). Ferric enterobactin binding and utilization by *Neisseria gonorrhoeae*. J. Bacteriol. *181*, 2895–2901.

Bilek, N., Ison, C.A., and Spratt, B.G. (2009). Relative contributions of recombination and mutation to the diversification of the opa gene repertoire of *Neisseria gonorrhoeae*. J. Bacteriol. *191*, 1878–1890.

Boukhalfa, H., and Crumbliss, A.L. (2002). Chemical aspects of siderophore mediated iron transport. BioMetals *15*, 325–339.

Bracken, C.S., Baer, M.T., Abdur-Rashid, A., Helms, W., and Stojiljkovic, I. (1999). Use of heme-protein complexes by the *Yersinia enterocolitica* HemR receptor: Histidine residues are essential for receptor function. J. Bacteriol. *181*, 6063–6072.

Brener, D., DeVoe, I.W., and Holbein, B.E. (1981). Increased virulence of *Neisseria meningitidis* after in vitro iron-limited growth at low pH. Infect. Immun. *33*, 59–66.

Bridges, K.R., and Cudkowicz, A. (1984). Effect of iron chelators on the transferrin receptor in K562 cells. J. Biol. Chem. *259*, 12970–12977.

Brinkmann, V., Reichard, U., Goosmann, C., Fauler, B., Uhlemann, Y., Weiss, D.S., Weinrauch, Y., and Zychlinsky, A. (2004). Neutrophil Extracellular Traps Kill Bacteria. Science (80-.). *303*, 1532–1535.

Brissac, T., Mikaty, G., Duménil, G., Coureuil, M., and Nassif, X. (2012). The meningococcal minor pilin PilX is responsible for type IV pilus conformational changes associated with signaling to endothelial cells. Infect. Immun. *80*, 3297–3306.

Brooks, C.L., Arutyunova, E., and Lemieux, M.J. (2014). The structure of lactoferrin-binding protein B from *Neisseria meningitidis* suggests roles in iron acquisition and neutralization of host defences. Acta Crystallogr. Sect. FStructural Biol. Commun. *70*, 1312–1317.

Brouwer, M.C., Tunkel, A.R., and Van De Beek, D. (2010). Epidemiology, diagnosis, and antimicrobial treatment of acute bacterial meningitis. Clin. Microbiol. Rev. *23*, 467–492.

Bung, N., Pradhan, M., Srinivasan, H., and Bulusu, G. (2014). Structural Insights into E. coli Porphobilinogen Deaminase during Synthesis and Exit of 1-Hydroxymethylbilane. PLoS Comput. Biol. *10*.

Burg, N.D., and Pillinger, M.H. (2001). The neutrophil: function and regulation in innate and humoral immunity. Clin. Immunol. *99*, 7–17.

Burton, G., Fagerness, P.E., Hosozawa, S., Jordan, P.M., and Scott, A.I. (1979). 13C n.m.r. evidence for a new intermediate, pre-uroporphyrinogen, in the enzymic transformation of porphobilinogen into uroporphyrinogens I and III. J. Chem. Soc. Chem. Commun. 202–204.

Callewaert, L., Aertsen, A., Deckers, D., Vanoirbeek, K.G.A., Vanderkelen, L., Van Herreweghe, J.M., Masschalck, B., Nakimbugwe, D., Robben, J., and Michiels, C.W. (2008). A new family of lysozyme inhibitors contributing to lysozyme tolerance in gram-negative bacteria. PLoS Pathog. *4*.

Callewaert, L., Van Herreweghe, J.M., Vanderkelen, L., Leysen, S., Voet, A., and Michiels, C.W. (2012). Guards of the great wall: bacterial lysozyme inhibitors. Trends Microbiol. *20*, 501–510.

Calmettes, C., Alcantara, J., Yu, R.-H., Schryvers, A.B., and Moraes, T.F. (2012). The structural basis of transferrin sequestration by transferrin-binding protein B. Nat. Struct. Mol. Biol. *19*, 358–360.

Calmettes, C., Ing, C., Buckwalter, C.M., El Bakkouri, M., Chieh-Lin Lai, C., Pogoutse, A., Gray-Owen, S.D., Pomès, R., and Moraes, T.F. (2015). The molecular mechanism of Zinc acquisition by the neisserial outer-membrane transporter ZnuD. Nat. Commun. *6*, 7996.

Carson, S.D., Klebba, P.E., Newton, S.M., and Sparling, P.F. (1999). Ferric enterobactin binding and utilization by *Neisseria gonorrhoeae*. J. Bacteriol. *181*, 2895–2901.

Carson, S.D.B., Stone, B., Beucher, M., Fu, J., and Sparling, P.F. (2000). Phase variation of the gonococcal siderophore receptor FetA. Mol. Microbiol. *36*, 585–593.

Castellana, M., Wilson, M.Z., Xu, Y., Joshi, P., Cristea, I.M., Rabinowitz, J.D., Gitai, Z., and Wingreen, N.S. (2014). Enzyme clustering accelerates processing of intermediates through metabolic channeling. Nat. Biotechnol. *32*, 1011–1018.

Celia, H., Noinaj, N., Zakharov, S.D., Bordignon, E., Botos, I., Santamaria, M., Barnard, T.J., Cramer, W.A., Lloubes, R., and Buchanan, S.K. (2016). Structural insight into the role of the Ton complex in energy transduction. Nature *538*, 60–65.

Chartrand, P., Tardif, D., and Sasarman, A. (1979). Uroporphyrin- and Coproporphyrin I-accumulating Mutant of *Escherichia coli* K 1 2. Virology 61–66.

Chen, C. -Y, Berish, S.A., Morse, S.A., and Mietzner, T.A. (1993). The ferric iron-binding protein of pathogenic *Neisseria* spp. functions as a periplasmic transport protein in iron acquisition from human transferrin. Mol. Microbiol. *10*, 311–318.

Chen, C.J., Elkins, C., and Sparling, P.F. (1998). Phase variation of hemoglobin utilization in *Neisseria gonorrhoeae*. Infect. Immun. *66*, 987–993.

Chen, C.J., Tobiason, D.M., Thomas, C.E., Shafer, W.M., Seifert, H.S., and Sparling, P.F. (2004). A Mutant Form of the *Neisseria gonorrhoeae* Pilus Secretin Protein PilQ Allows Increased Entry of Heme and Antimicrobial Compounds. J. Bacteriol. *186*, 730–739.

Chen, T., Belland, R.J., Wilson, J., and Swanson, J. (1995). Adherence of pilus- Opa+ gonococci to epithelial cells in vitro involves heparan sulfate. J. Exp. Med. *182*, 511–517.

Chen, V.B., Arendall, W.B., Headd, J.J., Keedy, D.A., Immormino, R.M., Kapral, G.J., Murray, L.W., Richardson, J.S., Richardson, D.C., and Richardson, D.C. (2010). MolProbity: all-atom structure validation for macromolecular crystallography. Acta Crystallogr. D. Biol. Crystallogr. *66*, 12–21.

Chen, W., Wright, L., Lee, S., Cosloy, S.D., and Russell, C.S. (1996). Expression of glutamyl-tRNA reductase in *Escherichia coli.* Biochim. Biophys. Acta - Gene Struct. Expr. *1309*, 109–121.

Chimento, D.P., Kadner, R.J., and Wiener, M.C. (2005). Comparative structural analysis of TonB-dependent outer membrane transporters: Implications for the transport cycle. Proteins *59*, 240–251.

Christensen, H., May, M., Bowen, L., Hickman, M., and Trotter, C.L. (2010). Meningococcal carriage by age: A systematic review and meta-analysis. Lancet Infect. Dis. *10*, 853–861.

Christensen, H., Trotter, C.L., Hickman, M., and Edmunds, W.J. (2014). Re-evaluating cost effectiveness of universal meningitis vaccination (Bexsero) in England: Modelling study. BMJ *349*.

Chruszcz, M., Potrzebowski, W., Zimmerman, M.D., Grabowski, M., Zheng, H., Lasota,

P., and Minor, W. (2008). Analysis of solvent content and oligomeric states in protein crystals--does symmetry matter? Protein Sci. *17*, 623–632.

Cloud, K.A., and Dillard, J.P. (2002). A lytic transglycosylase of *Neisseria gonorrhoeae* is involved in peptidoglycan-derived cytotoxin production. Infect. Immun. *70*, 2752–2757.

Cobessi, D., Meksem, A., and Brillet, K. (2010). Structure of the heme/hemoglobin outer membrane receptor ShuA from *Shigella dysenteriae*: heme binding by an induced fit mechanism. Proteins Struct. Funct. Bioinforma. *78*, 286–294.

Collins, R.F., Davidsen, L., Derrick, J.P., Ford, R.C., and Tønjum, T. (2001). Analysis of the PilQ secretin from *Neisseria meningitidis* by transmission electron microscopy reveals a dodecameric quaternary structure. J. Bacteriol. *183*, 3825–3832.

Cooper, M.D., McGee, Z.A., Mulks, M.H., Koomey, J.M., and Hindman, T.L. (1984). Attachment to and invasion of human fallopian tube mucosa by an IgA1 protease-deficient mutant of *Neisseria gonorrhoeae* and its wild-type parent. J. Infect. Dis. *150*, 737–744.

Cope, L., Thomas, S., Latimer, J., Slaughter, C., U, M.-E., and Hansen, E. (1994). The 100 kDa haem:haemopexin-binding protein of *Haemophilus influenzae*: structure and localization. Mol. Microbiol. *13*, 863–873.

Cope, L.D., Yogev, R., Muller-Eberhard, U., and Hansen, E.J. (1995). A gene cluster involved in the utilization of both free heme and heme:hemopexin by *Haemophilus influenzae* type b. J. Bacteriol. *177*, 2644–2653.

Cope, L.D., Thomas, S.E., Hrkal, Z., and Hansen, E.J. (1998). Binding of heme-hemopexin complexes by soluble HxuA protein allows utilization of this complexed heme by *Haemophilus influenzae.* Infect. Immun. *66*, 4511–4516.

Cornelissen, C.N. (2003). Transferrin-iron uptake by Gram-negative bacteria. Front Biosci *8*, d836-47.

Cornelissen, C.N., and Hollander, A. (2011). TonB-dependent transporters expressed by *Neisseria gonorrhoeae.* Front. Microbiol. *2*, 117.

Cornelissen, C.N., Biswas, G.D., Tsai, J., Paruchuri, D.K., Thompson, S.A., and Sparling, P.F. (1992). Gonococcal transferrin-binding protein 1 is required for transferrin utilization and is homologous to tonB-dependent outer membrane receptors. J. Bacteriol. *174*, 5788–5797.

Coureuil, M., Mikaty, G., Miller, F., Lécuyer, H., Bernard, C., Bourdoulous, S., Duménil, G., Mège, R.M., Weksler, B.B., Romero, I.A., et al. (2009). Meningococcal type IV pili recruit the polarity complex to cross the brain endothelium. Science (80-.). *325*, 83–87.

Coureuil, M., Lécuyer, H., Scott, M.G.H., Boularan, C., Enslen, H., Soyer, M., Mikaty, G., Bourdoulous, S., Nassif, X., and Marullo, S. (2010). Meningococcus hijacks a β2-adrenoceptor/β-arrestin pathway to cross brain microvasculature endothelium. Cell *143*, 1149–1160.

Coureuil, M., Bourdoulous, S., Marullo, S., and Nassif, X. (2014). Invasive meningococcal disease: A disease of the endothelial cells. Trends Mol. Med. *20*, 571–578.

Criss, A.K., and Seifert, H.S. (2012). A bacterial siren song: intimate interactions between *Neisseria* and neutrophils. Nat. Rev. Microbiol. *10*, 178–190.

Criss, A.K., Katz, B.Z., and Seifert, H.S. (2009). Resistance of *Neisseria gonorrhoeae* to non-oxidative killing by adherent human polymorphonuclear leucocytes. Cell. Microbiol. *11*, 1074–1087.

Cunha, L., Kuti, M., Bishop, D.F., Mezei, M., Zeng, L., Zhou, M.M., and Desnick, R.J. (2008). Human uroporphyrinogen III synthase: NMR-based mapping of the active site. Proteins Struct. Funct. Genet. *71*, 855–873.

Czjzek, M., Létoffé, S., Wandersman, C., Delepierre, M., Lecroisey, A., and Izadi-Pruneyre, N. (2007). The Crystal Structure of the Secreted Dimeric Form of the Hemophore HasA Reveals a Domain Swapping with an Exchanged Heme Ligand. J. Mol. Biol. *365*, 1176–1186.

Dailey, H.A., Dailey, T.A., Gerdes, S., Jahn, D., Jahn, M., O'Brian, M.R., and Warren, M.J. (2017). Prokaryotic Heme Biosynthesis: Multiple Pathways to a Common Essential Product. Microbiol. Mol. Biol. Rev. *81*, e00048-16.

Davis, K.M., Nakamura, S., and Weiser, J.N. (2011). Nod2 sensing of lysozyme-digested peptidoglycan promotes macrophage recruitment and clearance of S. pneumoniae colonization in mice. J. Clin. Invest. *121*, 3666–3676.

Deasy, A.M., Guccione, E., Dale, A.P., Andrews, N., Evans, C.M., Bennett, J.S., Bratcher, H.B., Maiden, M.C.J., Gorringe, A.R., and Read, R.C. (2015). Nasal inoculation of the commensal *Neisseria lactamica* inhibits carriage of neisseria meningitidis by young adults: A controlled human infection study. Clin. Infect. Dis. *60*, 1512–1520.

Deghmane, A.E., Giorgini, D., Larribe, M., Alonso, J.M., and Taha, M.K. (2002). Down-regulation of pili and capsule of *Neisseria meningitidis* upon contact with epithelial cells is mediated by CrgA regulatory protein. Mol. Microbiol. *43*, 1555–1564.

Deghmane, A.E., Larribe, M., Giorgini, D., Sabino, D., and Taha, M.K. (2003). Differential expression of genes that harbor a common regulatory element in *Neisseria meningitidis* upon contact with target cells. Infect. Immun. *71*, 2897–2901.

Deniau, C., Gilli, R., Izadi-Pruneyre, N., Létoffé, S., Delepierre, M., Wandersman, C., Briand, C., and Lecroisey, A. (2003). Thermodynamics of heme binding to the HasASM hemophore: Effect of mutations at three key residues for heme uptake. Biochemistry *42*, 10627–10633.

Desai, P.J., Garges, E., and Genco, C.A. (2000). Pathogenic neisseriae can use hemoglobin, transferrin, and lactoferrin independently of the tonB locus. J. Bacteriol. *182*, 5586–5591.

Dillard, J.P. (2011). Genetic manipulation of *Neisseria gonorrhoeae*. Curr. Protoc. Microbiol. *Chapter 4*, Unit4A.2.

Dillard, J.P., and Hackett, K.T. (2005). Mutations affecting peptidoglycan acetylation in *Neisseria gonorrhoeae* and *Neisseria meningitidis.* Infect. Immun. *73*, 5697–5705.

Drake, S.L., and Koomey, M. (1995). The product of the pilQ gene is essential for the biogenesis of type IV pili in *Neisseria gonorrhoeae*. Mol. Microbiol *18*, 975–986.

Draper, D.L., Donegan, E.A., James, J.F., Sweet, R.L., and Brooks, G.F. (1980). Scanning electron microscopy of attachment of *Neisseria gonorrhoeae* colony phenotypes to surfaces of human genital epithelia. Am. J. Obstet. Gynecol. *138*, 818–826.

Ducey, T.F., Carson, M.B., Orvis, J., Stintzi, P., Dyer, D.W., and Stintzi, A.P. (2005). Identification of the Iron-Responsive Genes of *Neisseria gonorrhoeae* by Microarray Analysis in Defined Medium. J. Bacteriol. *187*, 4865–4874.

Dyer, D.W., West, E.P., and Sparling, P.F. (1987). Effects of serum carrier proteins on the growth of pathogenic neisseriae with heme-bound iron. Infect. Immun. *55*, 2171–2175.

Edgar, R.J., Chen, J., Kant, S., Rechkina, E., Rush, J.S., Forsberg, L.S., Jaehrig, B., Azadi, P., Tchesnokova, V., Sokurenko, E. V, et al. (2016). SpyB, a Small Heme-Binding Protein, Affects the Composition of the Cell Wall in *Streptococcus pyogenes.* Front. Cell. Infect. Microbiol. *6*, 126.

Edwards, J.L., and Apicella, M.A. (2004). The molecular mechanisms used by *Neisseria gonorrhoeae* to initiate infection differ between men and women. Clin. Microbiol. Rev. *17*, 965–81, table of contents.

Edwards, J.L., and Apicella, M.A. (2005). I-domain-containing integrins serve as pilus receptors for *Neisseria gonorrhoeae* adherence to human epithelial cells. Cell. Microbiol. *7*, 1197–1211.

Edwards, J.L., and Butler, E.K. (2011). The pathobiology of *Neisseria gonorrhoeae* lower female genital tract infection. Front. Microbiol. *2*, 102.

Edwards, J.L., Shao, J.Q., Ault, K.A., and Apicella, M.A. (2000). *Neisseria gonorrhoeae* elicits membrane ruffling and cytoskeletal rearrangements upon infection of primary human endocervical and ectocervical cells. Infect. Immun. *68*, 5354–5363.

Edwards, J.L., Brown, E.J., Ault, K. a, and Apicella, M. a (2001). The role of complement receptor 3 (CR3) in *Neisseria gonorrhoeae* infection of human cervical epithelia. Cell. Microbiol. *3*, 611–622.

Edwards, J.L., Brown, E.J., Uk-Nham, S., Cannon, J.G., Blake, M.S., and Apicella, M.A. (2002). A co-operative interaction between *Neisseria gonorrhoeae* and complement receptor 3 mediates infection of primary cervical epithelial cells. Cell. Microbiol. *4*, 571–584.

Edwards, J.L., Jennings, M.P., Apicella, M.A., and Seib, K.L. (2016). Is gonococcal disease preventable? The importance of understanding immunity and pathogenesis in vaccine development. Crit. Rev. Microbiol. *7828*, 1–14.

Von Eiff, C., Heilmann, C., Proctor, R.A., Woltz, C., Peters, G., and Götz, F. (1997). A site-directed *Staphylococcus aureus* hemB mutant is a small-colony variant which

persists intracellularly. J. Bacteriol. *179*, 4706–4712.

Elkins, C., Carbonetti, N.H., Varela, V.A., Stirewalt, D., Klapper, D.G., and Sparling, P.F. (1992). Antibodies to N-terminal peptides of gonococcal porin are bactericidal when gonococcal lipopolysaccharide is not sialylated. Mol. Microbiol. *6*, 2617–2628.

Ellison, R.T., and Giehl, T.J. (1991). Killing of gram-negative bacteria by lactoferrin and lysozyme. J. Clin. Invest. *88*, 1080–1091.

Emsley, P., Lohkamp, B., Scott, W.G., and Cowtan, K. (2010). Features and development of Coot. Acta Crystallogr. Sect. D Biol. Crystallogr. *66*, 486–501.

Evans, C.M., Pratt, C.B., Matheson, M., Vaughan, T.E., Findlow, J., Borrow, R., Gorringe, A.R., and Read, R.C. (2011). Nasopharyngeal colonization by *Neisseria lactamica* and induction of protective immunity against *Neisseria meningitidis*. Clin. Infect. Dis. *52*, 70–77.

Evans, N.J., Harrison, O.B., Clow, K., Derrick, J., Feavers, I., and Maiden, M. (2010). Variation and molecular evolution of {HmbR,} the *Neisseria meningitidis* haemoglobin receptor. Microb. Pathog. *156*, 1384–1393.

Everts, R.J., Speers, D., George, S.T., Ansell, B.J., Karunajeewa, H., and Ramos, R.D. (2010). *Neisseria lactamica* arthritis and septicemia complicating myeloma. J. Clin. Microbiol. *48*, 2318.

Faller, M., Matsunaga, M., Yin, S., Loo, J.A., and Guo, F. (2007). Heme is involved in microRNA processing. Nat. Struct. Mol. Biol. *14*, 23–29.

Feavers, I.M., and Maiden, M.C.J. (2017). Recent Progress in the Prevention of Serogroup B Meningococcal Disease. Clin. Vaccine Immunol. *24*, e00566-16.

Figueroa, J.E., and Densen, P. (1991). Infectious diseases associated with complement deficiencies. Clin. Microbiol. Rev. *4*, 359–395.

Fortian, A., Castaño, D., Ortega, G., Laín, A., Pons, M., and Millet, O. (2009). Uroporphyrinogen III synthase mutations related to congenital erythropoietic porphyria identify a key helix for protein stability. Biochemistry *48*, 454–461.

Fortian, A., González, E., Castaño, D., Falcon-Perez, J.M., and Millet, O. (2011). Intracellular rescue of the uroporphyrinogen III synthase activity in enzymes carrying the hotspot mutation C73R. J. Biol. Chem. *286*, 13127–13133.

Fox, D.A., Larsson, P., Lo, R.H., Kroncke, B.M., Kasson, P.M., and Columbus, L. (2014). Structure of the neisserial outer membrane protein Opa60: Loop flexibility essential to receptor recognition and bacterial engulfment. J. Am. Chem. Soc. *136*, 9938–9946.

Frank, J., Wang, X., Lam, H.M., Aita, V.M., Jugert, F.K., Goerz, G., Merk, H.F., Poh-Fitzpatrick, M.B., and Christiano, A.M. (1998). C73R is a hotspot mutation in the uroporphyrinogen III synthase gene in congenital erythropoietic porphyria. Ann Hum Genet *62*, 225–230.

Frankenberg, N., Moser, J., and Jahn, D. (2003). Bacterial heme biosynthesis and its biotechnological application. Appl. Microbiol. Biotechnol. *63*, 115–127.

Fujino, E., Fujino, T., Karita, S., Sakka, K., and Ohmiya, K. (1995). Cloning and sequencing of some genes responsible for porphyrin biosynthesis from the anaerobic bacterium *Clostridium josui*. J. Bacteriol. *177*, 5169–5175.

Fusco, D., and Charbonneau, P. (2014). Competition between monomeric and dimeric crystals in schematic models for globular proteins. J. Phys. Chem. B *118*, 8034–8041.

Gandhi, A., and Balmer, P. (2016). Characteristics of a new meningococcal serogroup B vaccine, bivalent rLP2086 (MenB-FHbp; Trumenba®). Postgrad. Med. *128*, 548–556.

Gangaiah, D., Raterman, E., Wu, H., Fortney, K.R., Gao, H., Liu, Y., Jerse, A.E., and Spinola, S.M. (2017). Both MisR (CpxR) and MisS (CpxA) are Required for *Neisseria gonorrhoeae* Infection in a Murine Model of Lower Genital Tract Infection. Infect. Immun. *85*, IAI.00307-17.

Ganz, T., and Nemeth, E. (2015). Iron homeostasis in host defence and inflammation. Nat. Rev. Immunol. *15*, 500–510.

Gao, J.L., Nguyen, K.A., and Hunter, N. (2010). Characterization of a hemophore-like protein from *Porphyromonas gingivalis*. J. Biol. Chem. *285*, 40028–40038.

Gasparini, R., and Panatto, D. (2011). Meningococcal glycoconjugate vaccines. Hum. Vaccin. *7*, 170–182.

Gasteiger, E., Hoogland, C., Gattiker, A., Duvaud, S., Wilkins, M.R., Appel, R.D., and Bairoch, A. (2005). Protein Identification and Analysis Tools on the ExPASy Server. Proteomics Protoc. Handb. 571–607.

Ge, H., Lv, X., Fan, J., Gao, Y., Teng, M., and Niu, L. (2010). Crystal structure of Glutamate1-semialdehyde aminotransferase from *Bacillus subtilis* with bound pyridoxamine-5'-phosphate. Biochem. Biophys. Res. Commun. *402*, 356–360.

Gelin, M., Delfosse, V., Allemand, F., Hoh, F., Sallaz-Damaz, Y., Pirocchi, M., Bourguet, W., Ferrer, J.L., Labesse, G., and Guichou, J.F. (2015). Combining "dry" co-crystallization and in situ diffraction to facilitate ligand screening by X-ray crystallography. Acta Crystallogr. Sect. D Biol. Crystallogr. *71*, 1777–1787.

Geoffroy, M.C., Floquet, S., Métais, A., Nassif, X., and Pelicic, V. (2003). Large-scale analysis of the meningococcus genome by gene distruption: Resistance to complement-mediated lysis. Genome Res. *13*, 391–398.

Ghigo, J., Létoffé, S., and Wandersman, C. (1997). A new type of hemophore-dependent heme acquisition system of *Serratia marcescens* reconstituted in *Escherichia coli.* J. Bacteriol. *179*, 3572–3579.

Ghosh, J., and Postle, K. (2005). Disulphide trapping of an in vivo energy-dependent conformation of *Escherichia coli* TonB protein. Mol. Microbiol. *55*, 276–288.

Gill, R., Kolstoe, S.E., Mohammed, F., Al D-Bass, A., Mosely, J.E., Sarwar, M., Cooper, J.B., Wood, S.P., and Shoolingin-Jordan, P.M. (2009). Structure of human porphobilinogen deaminase at 2.8 A: the molecular basis of acute intermittent porphyria. Biochem. J. *420*, 17–25.

Gilles-Gonzalez, M.A., and Gonzalez, G. (2005). Heme-based sensors: Defining

characteristics, recent developments, and regulatory hypotheses. J. Inorg. Biochem. *99*, 1–22.

Goodman, S.D., and Scocca, J.J. (1988). Identification and arrangement of the DNA sequence recognized in specific transformation of *Neisseria gonorrhoeae*. Proc. Natl. Acad. Sci. U. S. A. *85*, 6982–6986.

Gorby, G., Simon, D., and Rest, R.F. (1994). Escherichia coli That Express *Neisseria gonorrhoeae* Opacity-Associated Proteins Attach to and Invade Human Fallopian Tube Epithelium. Ann. N. Y. Acad. Sci. *730*, 286–289.

Gordon, D.L. (1989). Meningococcal disease and complement. Med. J. Aust. *150*, 286.

Gorringe, A.R., and Pajon, R. (2012). Bexsero: A multicomponent vaccine for prevention of meningococcal disease. Hum. Vaccines Immunother. *8*, 174–183.

Greenfield, N.J. (2006). Using circular dichroism spectra to estimate protein secondary structure. Nat. Protoc. *1*, 2876–2890.

Gregg, C.R., Melly, M.A., Hellerqvist, C.G., Coniglio, J.G., and Mc Gee, Z.A. (1981). Toxic Activity of Purified Lipopolysaccharide of *Neisseria gonorrhoeae* for Human Fallopian Tube Mucosa. J. Infect. Dis. *143*, 432–439.

Grifantini, R., Bartolini, E., Muzzi, a, Draghi, M., Frigimelica, E., Berger, J., Ratti, G., Petracca, R., Galli, G., Agnusdei, M., et al. (2002). Previously unrecognized vaccine candidates against group B meningococcus identified by DNA microarrays. Nat Biotechnol *20*, 914–921.

Grifantini, R., Sebastian, S., Frigimelica, E., Draghi, M., Bartolini, E., Muzzi, A., Rappuoli, R., Grandi, G., and Genco, C.A. (2003). Identification of iron-activated and -repressed Fur-dependent genes by transcriptome analysis of *Neisseria meningitidis* group B. Proc. Natl. Acad. Sci. U. S. A. *100*, 9542–9547.

Grifantini, R., Frigimelica, E., Delany, I., Bartolini, E., Giovinazzi, S., Balloni, S., Agarwal, S., Galli, G., Genco, C., and Grandi, G. (2004). Characterization of a novel *Neisseria meningitidis* Fur and iron-regulated operon required for protection from oxidative stress: Utility of DNA microarray in the assignment of the biological role of hypothetical genes. Mol. Microbiol. *54*, 962–979.

Griffiths, N.J., Hill, D.J., Borodina, E., Sessions, R.B., Devos, N.I., Feron, C.M., Poolman, J.T., and Virji, M. (2011). Meningococcal surface fibril (Msf) binds to activated vitronectin and inhibits the terminal complement pathway to increase serum resistance. Mol. Microbiol. *82*, 1129–1149.

Gumbart, J., Wiener, M.C., and Tajkhorshid, E. (2007). Mechanics of Force Propagation in TonB-Dependent Outer Membrane Transport. Biophys. J. *93*, 496–504.

Gunderson, C.W., and Seifert, H.S. (2015). *Neisseria gonorrhoeae* elicits extracellular traps in primary neutrophil culture while suppressing the oxidative burst. MBio *6*, e02452-14.

Hagblom, P., Segal, E., Billyard, E., and So, M. (1985). Intragenic recombination leads to pilus antigenic variation in *Neisseria gonorrhoeae.* Nature *315*, 156–158.

Hagen, T.A., and Cornelissen, C.N. (2006). *Neisseria gonorrhoeae* requires expression of TonB and the putative transporter TdfF to replicate within cervical epithelial cells. Mol. Microbiol. *62*, 1144–1157.

Hamilton, H.L., Domínguez, N.M., Schwartz, K.J., Hackett, K.T., and Dillard, J.P. (2005). *Neisseria gonorrhoeae* secretes chromosomal DNA via a novel type IV secretion system. Mol. Microbiol. *55*, 1704–1721.

Hammer, N.D., Reniere, M.L., Cassat, J.E., Zhang, Y., Hirsch, A.O., Hood, M.I., and Skaar, E.P. (2013). Two heme-dependent terminal oxidases power *Staphylococcus aureus* organ-specific colonization of the vertebrate host. MBio *4*.

Hamza, I., Chauhan, S., Hassett, R., and O'Brian, M.R. (1998). The bacterial irr protein is required for coordination of heme biosynthesis with iron availability. J. Biol. Chem. *273*, 21669–21674.

Hansson, M., Rutberg, L., Schroder, I., and Hederstedt, L. (1991). The Bacillus subtilis hemAXCDBL gene cluster, which encodes enzymes of the biosynthetic pathway from glutamate to uroporphyrinogen III. J. Bacteriol. *173*, 2590–2599.

Harrison, L.H., Jolley, K. a, Shutt, K. a, Marsh, J.W., O'Leary, M., Sanza, L.T., and Maiden, M.C.J. (2006). Antigenic shift and increased incidence of meningococcal disease. J. Infect. Dis. *193*, 1266–1274.

Harrison, O., Evans, N., Blair, J., Grimes, H., Tinsley, C., Nassif, X., Kriz, P., Ure, R., Gray, S., Derrick, J., et al. (2009). Epidemiological evidence for the role of the hemoglobin receptor, (*hmbR*) in meningococcal virulence. J. Infect. Dis. *200*, 94–98.

Harrison, O.B., Bennett, J.S., Derrick, J.P., Maiden, M.C.J., and Bayliss, C.D. (2013). Distribution and diversity of the haemoglobin-haptoglobin iron-acquisition systems in pathogenic and non-pathogenic *Neisseria*. Microbiol. (United Kingdom) *159*, 1920–1930.

Hartt, G.J., and Battersby, A.R. (1985). Purification and properties of uroporphyrinogen III synthase (co-synthetase) from *Euglena gracilis*. Biochem. J *232*, 151–160.

Harvey, H.A., Jennings, M.P., Campbell, C.A., Williams, R., and Apicella, M.A. (2001). Receptor-mediated endocytosis of *Neisseria gonorrhoeae* into primary human urethral epithelial cells: The role of the asialoglycoprotein receptor. Mol. Microbiol. *42*, 659–672.

Hauck, C.R., and Meyer, T.F. (1997). The lysosomal/phagosomal membrane protein h-lamp-1 is a target of the IgA1 protease of *Neisseria gonorrhoeae*. FEBS Lett. *405*, 86–90.

Hélaine, S., Carbonnelle, E., Prouvensier, L., Beretti, J.L., Nassif, X., and Pelicic, V. (2005). PilX, a pilus-associated protein essential for bacterial aggregation, is a key to pilus-facilitated attachment of *Neisseria meningitidis* to human cells. Mol. Microbiol. *55*, 65–77.

Heras, B., and Martin, J.L. (2005). Post-crystallization treatments for improving diffraction quality of protein crystals. Acta Crystallogr. Sect. D Biol. Crystallogr. *61*, 1173–1180.

Heras, B., Edeling, M.A., Byriel, K.A., Jones, A., Raina, S., and Martin, J.L. (2003). Dehydration converts DsbG crystal diffraction from low to high resolution. Structure *11*, 139–145.

Higgs, P.I., Larsen, R.A., and Postle, K. (2002). Quantification of known components of the Escherichia coli TonB energy transduction system: TonB, ExbB, ExbD and FepA. Mol. Microbiol. *44*, 271–281.

Higuchi, M., and Bogorad, L. (1975). The purification and properties of Uroporphyrinogen I Synthases and Uroporphyrinogen III Cosynthase. Interactions between the enzymes. Ann. N. Y. Acad. Sci. 244, 401–418.

Hill, L.D., Sun, L., Leuschen, M.P., and Zach, T.L. (1993). C3 synthesis by A549 alveolar epithelial cells is increased by interferon-gamma and dexamethasone. Immunology *79*, 236–240.

Ho, W.W., Li, H., Eakanunkul, S., Tong, Y., Wilks, A., Guo, M., and Poulos, T.L. (2007). Holo- and apo-bound structures of bacterial periplasmic heme-binding proteins. J. Biol. Chem. *282*, 35796–35802.

Hoeppner, A., Schmitt, L., and Smits, S.H.J. (2013). Proteins and Their Ligands : Their Importance and How to Crystallize Them. Adv. Top. Cryst. Growth 3–42.

Holbein, B.E., Jericho, K.W.F., and Likes, G.C. (1979). *Neisseria meningitidis* infection in mice: influence of iron, variations in virulence among strains, and pathology. Infect. Immun. *24*, 545–551.

Hollander, A., Mercante, A.D., Shafer, W.M., and Cornelissen, C.N. (2011). The iron-repressed, AraC-like regulator MpeR activates expression of fetA in *Neisseria gonorrhoeae.* Infect. Immun. *79*, 4764–4776.

Holm, L., and Rosenström, P. (2010). Dali server: conservation mapping in 3D. Nucleic Acids Res. *38*, W545-9.

Hood, M.I., and Skaar, E.P. (2012). Nutritional immunity: transition metals at the pathogen-host interface. Nat. Rev. Microbiol. *10*, 525–537.

Hopper, S., Vasquez, B., Merz, A., Clary, S., Wilbur, J.S., and So, M. (2000). Effects of the immunoglobulin A1 protease on Neisseria gonorrhoeae trafficking across polarized T84 epithelial monolayers. Infect. Immun. *68*, 906–911.

Hosenfeld, C.B., Workowski, K.A., Berman, S., Zaidi, A., Dyson, J., Mosure, D., Bolan, G., and Bauer, H.M. (2009). Repeat infection with Chlamydia and gonorrhea among females: a systematic review of the literature. Sex. Transm. Dis. *36*, 478–489.

Huang, Q., and Szebenyi, D.M.E. (2016). Improving diffraction resolution using a new dehydration method. Acta Crystallogr. Sect. F, Struct. Biol. Commun. *72*, 152–159.

Hughes, G., and Field, N. (2015). The epidemiology of sexually transmitted infections in the UK: impact of behavior, services and interventions. Future Microbiol. *10*, 35–51.

Humbert, M.V., Awanye, A.M., Lian, L.-Y., Derrick, J.P., Christodoulides, M., and Llinas, M. (2017). Structure of the Neisseria Adhesin Complex Protein (ACP) and its role as a

novel lysozyme inhibitor.

Hung, M.C., Heckels, J.E., and Christodoulides, M. (2013). The adhesin complex protein (ACP) of *Neisseria meningitidis i*s a new adhesin with vaccine potential. MBio *4*, 1–10.

Imhaus, A.-F., and Duménil, G. (2014). The number of *Neisseria meningitidis* type IV pili determines host cell interaction. EMBO J. *33*, 1767–1783.

Islam, E. a., Shaik-Dasthagirisaheb, Y., Kaushic, C., Wetzler, L.M., and Gray-Owen, S.D. (2015). The reproductive cycle is a pathogenic determinant during gonococcal pelvic inflammatory disease in mice. Mucosal Immunol. *9*, 1–14.

Izadi, N., Henry, Y., Haladjian, J., Goldberg, M.E., Wandersman, C., Delepierre, M., and Lecroisey, A. (1997). Purification and characterization of an extracellular heme-binding protein, HasA, involved in heme iron acquisition. Biochemistry *36*, 7050–7057.

Jackson, L.A., Ducey, T.F., Day, M.W., Zaitshik, J.B., Orvis, J., and Dyer, D.W. (2010). Transcriptional and functional analysis of the *Neisseria gonorrhoeae* fur regulon. J. Bacteriol. *192*, 77–85.

Jackson, L.A., Day, M., Allen, J., Scott, E., and Dyer, D.W. (2017). Iron-regulated small RNA expression as *Neisseria gonorrhoeae* FA 1090 transitions into stationary phase growth. BMC Genomics *18*, 317.

Jaffe, E.K. (2000). The porphobilinogen synthase family of metalloenzymes. Acta Crystallogr. Sect. D Biol. Crystallogr. *56*, 115–128.

Jahn, D., Verkamp, E., and Soll, D. (1992). Glutamyl-transfer TNA: a precursor of heme and chlorophyll biosynthesis. Trends Biochem. Sci. *17*, 215–218.

Jain, R., Sonkar, S.C., Chaudhry, U., Bala, M., and Saluja, D. (2016). In-silico Hierarchical Approach for the Identification of Potential Universal Vaccine Candidates (PUVCs) from *Neisseria gonorrhoeae.* J. Theor. Biol. *410*, 36–43.

Javor, G.T., and Febre, E.F. (1992). Enzymatic basis of thiol-stimulated secretion of porphyrins by Escherichia coli. J. Bacteriol. *174*, 1072–1075.

Jean, S., Juneau, R.A., Criss, A.K., and Cornelissen, C.N. (2016). *Neisseria gonorrhoeae* evades calprotectin-mediated nutritional immunity and survives neutrophil extracellular traps by production of TdfH. Infect. Immun. *84*, 2982–2994.

Jennings, M.P., Srikhanta, Y.N., Moxon, E.R., Kramer, M., Poolman, J.T., Kuipers, B., and Van Der Ley, P. (1999). The genetic basis of the phase variation repertoire of lipopolysaccharide immunotypes in *Neisseria meningitidis.* Microbiology *145*, 3013–3021.

Jerse, A.E., Crow, E.T., Bordner, A.N., Rahman, I., Cornelissen, C.N., Moench, T.R., and Mehrazar, K. (2002). Growth of *Neisseria gonorrhoeae* in the female mouse genital tract does not require the gonococcal transferrin or hemoglobin receptors and may be enhanced by commensal lactobacilli. Infect. Immun. *70*, 2549–2558.

Johannsen, D.B., Johnston, D.M., Koymen, H.O., Cohen, M.S., and Cannon, J.G. (1999). A *Neisseria gonorrhoeae* immunoglobulin A1 protease mutant is infectious in the human challenge model of urethral infection. Infect. Immun. *67*, 3009–3013.

Johnson, S.R., Steiner, B.M., Cruce, D.D., Perkins, G.H., and Arko, R.J. (1993). Characterization of a catalase-deficient strain of *Neisseria gonorrhoeae*: Evidence for the significance of catalase in the biology of *N. gonorrhoeae*. Infect. Immun. *61*, 1232–1238.

Jongerius, I., Lavender, H., Tan, L., Ruivo, N., Exley, R.M., Caesar, J.J.E., Lea, S.M., Johnson, S., and Tang, C.M. (2013). Distinct Binding and Immunogenic Properties of the Gonococcal Homologue of Meningococcal Factor H Binding Protein. PLoS Pathog. *9*, e1003528.

Jordan, P.M. (1991). Chapter 1 The biosynthesis of 5-aminolaevulinic acid and its transformation into uroporphyrinogen III. New Compr. Biochem. *19*, 1–66.

Jordan, P.M., and Warren, M.J. (1987). Evidence for a dipyrromethane cofactor at the catalytic site of *E. coli* porphobilinogen deaminase. FEBS Lett. *225*, 87–92.

Jordan, P.M., Nordwv, H., Burton, G., and Scott, A.I. (1980). A rapid direct assay for uroporphyrinogen III cosynthetase. FEBS Lett. *115*, 269–272.

Jordan, P.M., Thomas, S.D., and Warren, M.J. (1988). Purification, crystallization and properties of porphobilinogen deaminase from a recombinant strain of *Escherichia coli* K12. Biochem. J. *254*, 427–435.

Jordan, P.W., Snyder, L.A., and Saunders, N.J. (2005). Strain-specific differences in *Neisseria gonorrhoeae* associated with the phase variable gene repertoire. BMC Microbiol. *5*, 21.

Al Jubair, T., Singh, B., Fleury, C., Blom, A.M., Mörgelin, M., Thunnissen, M.M., and Riesbeck, K. (2014). *Haemophilus influenzae* stores and distributes hemin by using Protein E. Int. J. Med. Microbiol. *304*, 662–668.

Juica, N.E., Rodas, P.I., Solar, P., Borda, P., Vargas, R., Muñoz, C., Paredes, R., Christodoulides, M., and Velasquez, L.A. (2017). *Neisseria gonorrhoeae* Challenge Increases Matrix Metalloproteinase-8 Expression in Fallopian Tube Explants. Front. Cell. Infect. Microbiol. *7*, 399.

Källström, H., Liszewski, M.K., Atkinson, J.P., and Jonsson, a B. (1997). Membrane cofactor protein (MCP or CD46) is a cellular pilus receptor for pathogenic *Neisseria*. Mol. Microbiol. *25*, 639–647.

Kandler, J.L., Acevedo, R.V., Dickinson, M.K., Cash, D.R., Shafer, W.M., and Cornelissen, C.N. (2016). The genes that encode the gonococcal transferrin binding proteins, TbpB and TbpA, are differentially regulated by MisR under iron-replete and iron-depleted conditions. Mol. Microbiol. *102*, 137–151.

Kantardjieff, K.A., and Rupp, B. (2003). Matthews coefficient probabilities: Improved estimates for unit cell contents of proteins, DNA, and protein-nucleic acid complex crystals. Protein Sci. *12*, 1865–1871.

Karnaukhova, E., Rutardottir, S., Rajabi M., M., Rosenlöf, L.W., Alayash, A.I., and Åkerström, B. (2014). Characterization of heme binding to recombinant α1-microglobulin. Front. Physiol. *5*, 1–11.

Kelley, L.A., Mezulis, S., Yates, C.M., Wass, M.N., and Sternberg, M.J.E. (2015). The Phyre2 web portal for protein modeling, prediction and analysis. Nat. Protoc. *10*, 845–858.

Khun, H.H., Kirby, S.D., and Lee, B.C. (1998). A *Neisseria meningitidis fbpABC* mutant is incapable of using nonheme iron for growth. Infect. Immun. *66*, 2330–2336.

Kirchner, M., and Meyer, T.F. (2005). The PilC adhesin of the *Neisseria* type IV pilus - binding specificities and new insights into the nature of the host cell receptor. Mol. Microbiol. *56*, 945–957.

Kirchner, M., Heuer, D., and Meyer, T.F. (2005). CD46-independent binding of neisserial type IV pili and the major pilus adhesin, PilC, to human epithelial cells. Infect. Immun. *73*, 3072–3082.

Kohashi, M., Clement, R.P., Tse, J., and Pipert, W.N. (1984). Rat hepatic uroporphyrinogen III co-synthase Purification and evidence for a bound folate coenzyme participating in the biosynthesis of uroporphyrinogen III. Biochem. J *220*, 755–765.

Kolappan, S., Coureuil, M., Yu, X., Nassif, X., Egelman, E.H., and Craig, L. (2016). Structure of the *Neisseria meningitidis* Type IV Pilus. Nat. Commun. *7*, 1–12.

Kraus, S.J. (1979). Culture Methods for *Neisseria Gonorrhoea*. Arch. Androl. *3*, 343–349.

Krauss, I.R., Sica, F., Mattia, C.A., and Merlino, A. (2012). Increasing the X-ray diffraction power of protein crystals by dehydration: The case of bovine serum albumin and a survey of literature data. Int. J. Mol. Sci. *13*, 3782–3800.

Krieg, S., Huché, F., Diederichs, K., Izadi-Pruneyre, N., Lecroisey, A., Wandersman, C., Delepelaire, P., and Welte, W. (2009). Heme uptake across the outer membrane as revealed by crystal structures of the receptor-hemophore complex. Proc. Natl. Acad. Sci. U. S. A. *106*, 1045–1050.

Kristiansen, M., Graversen, J.H., Jacobsen, C., Sonne, O., Hoffman, H.J., Law, S.K., and Moestrup, S.K. (2001). Identification of the haemoglobin scavenger receptor. Nature *409*, 198–201.

Kriz, P., Bobak, M., and Kriz, B. (2000). Parental smoking, socioeconomic factors, and risk of invasive meningococcal disease in children: a population based case-control study. Arch. Dis. Child. *83*, 117–121.

Kühner, M., Haufschildt, K., Neumann, A., Storbeck, S., Streif, J., and Layer, G. (2014). The alternative route to heme in the methanogenic archaeon methanosarcina barkeri. Archaea *2014*.

Kumar, P., Sannigrahi, S., and Tzeng, Y.L. (2012). The Neisseria meningitidis ZnuD Zinc Receptor Contributes to Interactions with Epithelial Cells and Supports Heme Utilization when Expressed in *Escherichia coli.* Infect. Immun. *80*, 657–667.

Kuo, A., Bowler, M.W., Zimmer, J., Antcliff, J.F., and Doyle, D.A. (2003). Increasing the diffraction limit and internal order of a membrane protein crystal by dehydration. J.

Struct. Biol. *141*, 97–102.

Lansky, I.B., Lukat-Rodgers, G.S., Block, D., Rodgers, K.R., Ratliff, M., and Wilks, A. (2006). The cytoplasmic heme-binding protein (PhuS) from the heme uptake system of *Pseudomonas aeruginosa* is an intracellular heme-trafficking protein to the δ-regioselective heme oxygenase. J. Biol. Chem. *281*, 13652–13662.

Lappann, M., Danhof, S., Guenther, F., Olivares-Florez, S., Mordhorst, I.L., and Vogel, U. (2013). In vitro resistance mechanisms of *Neisseria meningitidis* against neutrophil extracellular traps. Mol. Microbiol. *89*, 433–449.

Lappann, M., Otto, A., Brauer, M., Becher, D., Vogel, U., and Johswich, K. (2016). Impact of Moderate Temperature Changes on *Neisseria meningitidis* Adhesion Phenotypes and Proteome. Infect. Immun. *84*, 3484–3495.

Lee, C.H., and Tsai, C.M. (1999). Quantification of bacterial lipopolysaccharides by the purpald assay: measuring formaldehyde generated from 2-keto-3-deoxyoctonate and heptose at the inner core by periodate oxidation. Anal Biochem *267*, 161–168.

Lefèvre, J., Delepelaire, P., Delepierre, M., and Izadi-Pruneyre, N. (2008). Modulation by Substrates of the Interaction between the HasR Outer Membrane Receptor and Its Specific TonB-like Protein, HasB. J. Mol. Biol. *378*, 838–849.

Letoffe, S., Ghigo, J.M., and Wandersman, C. (1994). Iron acquisition from heme and hemoglobin by a *Serratia marcescens e*xtracellular protein. Proc. Natl. Acad. Sci. *91*, 9876–9880.

Létoffé, S., Deniau, C., Wolff, N., Dassa, E., Delepelaire, P., Lecroisey, A., and Wandersman, C. (2001). Haemophore-mediated bacterial haem transport: Evidence for a common or overlapping site for haem-free and haem-loaded haemophore on its specific outer membrane receptor. Mol. Microbiol. *41*, 439–450.

Létoffé, S., Wecker, K., Delepierre, M., Delepelaire, P., and Wandersman, C. (2005). Activities of the *Serratia marcescens* heme receptor HasR and isolated plug and β-barrel domains: The β-barrel forms a heme-specific channel. J. Bacteriol. *187*, 4637–4645.

Lewis, L.A., Sung, M.H., Gipson, M., Hartman, K., and Dyer, D.W. (1998). Transport of intact porphyrin by HpuAB, the hemoglobin-haptoglobin utilization system of *Neisseria meningitidis*. J. Bacteriol. *180*, 6043–6047.

Lewis, L.A., Gipson, M., Hartman, K., Ownbey, T., Vaughn, J., and Dyer, D.W. (1999). Phase variation of HpuAB and HmbR, two distinct haemoglobin receptors of *Neisseria meningitidis* DNM2. Mol. Microbiol. *32*, 977–989.

Lewis, L.A., Choudhury, B., Balthazar, J.T., Martin, L.E., Ram, S., Rice, P.A., Stephens, D.S., Carlson, R., and Shafer, W.M. (2009). Phosphoethanolamine substitution of lipid A and resistance of *Neisseria gonorrhoeae* to cationic antimicrobial peptides and complement-mediated killing by normal human serum. Infect. Immun. *77*, 1112–1120.

Lewis, L.A., Ngampasutadol, J., Wallace, R., Reid, J.E.A., Vogel, U., and Ram, S. (2010). The meningococcal vaccine candidate neisserial surface protein a (NspA) binds to factor H and enhances meningococcal resistance to complement. PLoS Pathog. *6*, 1–

20.

Li, J., Egelman, E.H., and Craig, L. (2012). Structure of the Vibrio cholerae Type IVb pilus and stability comparison with the *Neisseria gonorrhoeae* Type IVa pilus. J. Mol. Biol. *418*, 47–64.

Li, M.-S., Langford, P.R., and Kroll, J.S. (2017). Inactivation of *NMB0419* encoding a Sel1-like repeat (SLR) protein in *Neisseria meningitidis* is associated with differential expression of genes belonging to the Fur regulon and reduced intra-epithelial replication. Infect. Immun. IAI.00574-16.

Lin, L., Ayala, P., Larson, J., Mulks, M., Fukuda, M., Carlsson, S.R., Enns, C., and So, M. (1997). The Neisseria type 2 IgA1 protease cleaves LAMP1 and promotes survival of bacteria within epithelial cells. Mol. Microbiol. *24*, 1083–1094.

Liu, Y., Feinen, B., and Russell, M.W. (2011). New concepts in immunity to *Neisseria gonorrhoeae*: Innate responses and suppression of adaptive immunity favor the pathogen, not the host. Front. Microbiol. *2*, 1–8.

Liu, Z., García-Díaz, B., Catacchio, B., Chiancone, E., and Vogel, H.J. (2015). Protecting Gram-negative bacterial cell envelopes from human lysozyme: Interactions with Ivy inhibitor proteins from *Escherichia coli* and *Pseudomonas aeruginosa.* Biochim. Biophys. Acta - Biomembr. *1848*, 3032–3046.

Lo, H., Tang, C.M., and Exley, R.M. (2009). Mechanisms of avoidance of host immunity by *Neisseria meningitidis* and its effect on vaccine development. Lancet Infect. Dis. *9*, 418–427.

Lobo, S.A.L., Scott, A., Videira, M.A.M., Winpenny, D., Gardner, M., Palmer, M.J., Schroeder, S., Lawrence, A.D., Parkinson, T., Warren, M.J., et al. (2015). *Staphylococcus aureus* haem biosynthesis: Characterisation of the enzymes involved in final steps of the pathway. Mol. Microbiol. *97*, 472–487.

Loh, E., Kugelberg, E., Tracy, A., Zhang, Q., Gollan, B., Ewles, H., Chalmers, R., Pelicic, V., and Tang, C.M. (2013). Temperature triggers immune evasion by *Neisseria meningitidis.* Nature *502*, 237–240.

Louie, G. V, Brownlie, P.D., Lambert, R., Cooper, J.B., Blundell, T.L., Wood, S.P., Malashkevich, V.N., Hädener, A., Warren, M.J., and Shoolingin-Jordan, P.M. (1996). The three-dimensional structure of *Escherichia coli* porphobilinogen deaminase at 1.76-Å resolution. Proteins *25*, 48–78.

Louie GV, Brownlie PD, Lambert R, Cooper JB, Blundell TL, Wood SP, Warren MJ, Woodcock SC, J.P. (1992). Structure of porphobilinogen deaminase reveals a flexible multidomain polymerase with a single catalytic site. Nature *355*, 242–244.

Luan, B., Caffrey, M., and Aksimentiev, A. (2007). Structure refinement of the OpcA adhesin using molecular dynamics. Biophys. J. *93*, 3058–3069.

Lucas, S. (2013). Unprotected Nation; The Financial and Economic Impacts of Restricted Contraceptive and Sexual Health Services. 1–74.

Lucidarme, J., Tan, L., Exley, R.M., Findlow, J., Borrow, R., and Tang, C.M. (2011).

Characterization of *Neisseria meningitidis* isolates that do not express the virulence factor and vaccine antigen factor H binding protein. Clin. Vaccine Immunol. *18*, 1002–1014.

Lüer, C., Schauer, S., Möbius, K., Schulze, J., Schubert, W.D., Heinz, D.W., Jahn, D., and Moser, J. (2005). Complex formation between glutamyl-tRNA reductase and glutamate-1- semialdehyde 2,1-aminomutase in *Escherichia coli* during the initial reactions of porphyrin biosynthesis. J. Biol. Chem. *280*, 18568–18572.

Mackinnon, F.G., Borrow, R., Gorringe, A.R., Fox, A.J., Jones, D.M., and Robinson, A. (1993). Demonstration of lipooligosaccharide immunotype and capsule as virulence factors for *Neisseria meningitidis* using an infant mouse intranasal infection model. Microb. Pathog. *15*, 359–366.

Madico, G., Welsch, J.A., Lewis, L.A., McNaughton, A., Perlman, D.H., Costello, C.E., Ngampasutadol, J., Vogel, U., Granoff, D.M., and Ram, S. (2006). The Meningococcal Vaccine Candidate GNA1870 Binds the Complement Regulatory Protein Factor H and Enhances Serum Resistance. J. Immunol. *177*, 501–510.

Madico, G., Ngampasutadol, J., Gulati, S., Vogel, U., Rice, P. a, and Ram, S. (2007). Factor H binding and function in sialylated pathogenic neisseriae is influenced by gonococcal, but not meningococcal, porin. J. Immunol. *178*, 4489–4497.

Maiden, M.C.J., Bygraves, J.A., Feil, E., Morelli, G., Russell, J.E., Urwin, R., Zhang, Q., Zhou, J., Zurth, K., Caugant, D.A., et al. (1998). Multilocus sequence typing: A portable approach to the identification of clones within populations of pathogenic microorganisms. Proc. Natl. Acad. Sci. *95*, 3140–3145.

Mansa, B., and Kilian, M. (1986). Retained antigen-binding activity of Fab(α) fragments of human monoclonal immunoglobulin A1 (IgA1) cleaved by IgA1 protease. Infect. Immun. *52*, 171–174.

Martin, J.N., Ball, L.M., Solomon, T.L., Dewald, A.H., Criss, A.K., and Columbus, L. (2016). Neisserial Opa Protein-CEACAM Interactions: Competition for Receptors as a Means of Bacterial Invasion and Pathogenesis. Biochemistry *55*, 4286–4294.

Mathews, M.A.A., Schubert, H.L., Whitby, F.G., Alexander, K.J., Schadick, K., Bergonia, H.A., Phillips, J.D., and Hill, C.P. (2001). Crystal structure of human uroporphyrinogen III synthase. EMBO J. *20*, 5832–5839.

Matthews, B.W. (1968). Solvent content of protein crystals. J. Mol. Biol. *33*, 491–497.

Mattle, D., Zeltina, A., Woo, J.S., Goetz, B.A., and Locher, K.P. (2010). Two Stacked Heme Molecules in the Binding Pocket of the Periplasmic Heme-Binding Protein HmuT from Yersinia pestis. J. Mol. Biol. *404*, 220–231.

McClure, R., Nudel, K., Massari, P., Tjaden, B., Su, X., Rice, P.A., and Genco, C.A. (2015). The gonococcal transcriptome during infection of the lower genital tract in women. PLoS One *10*, 1–19.

McCoy, A.J., Grosse-Kunstleve, R.W., Adams, P.D., Winn, M.D., Storoni, L.C., and Read, R.J. (2007). Phaser crystallographic software. J. Appl. Crystallogr. *40*, 658–674.

McGee, Z., Jensen, R.L., Clemens, C.M., Taylor-Robinson, D., Johnson, A.P., and Gregg, C.R. (1999). Gonococcal infection of human fallopian tube mucosa in organ culture: Relationship of mucosal tissue TNF-α concentration to sloughing of ciliated cells. Sex. Transm. Dis. *26*, 160–165.

McKenna, W.R., Mickelsen, P.A., Sparling, P.F., and Dyer, D.W. (1988). Iron uptake from lactoferrin and transferrin by *Neisseria gonorrhoeae*. Infect. Immun. *56*, 785–791.

McMellon, H. (2016). Structure-Function Studies on Putative Gly1 Homologues in Gram-negative Bacteria. Univerisity of Sheffield.

Meadows, C. (2005). Characterisation of the Emi protein and the alpha peptides of *Neisseria meningitidis.* University of Sheffield.

Medlock, A.E., Shiferaw, M.T., Marcero, J.R., Vashisht, A.A., Wohlschlegel, J.A., Phillips, J.D., and Dailey, H.A. (2015). Identification of the mitochondrial heme metabolism complex. PLoS One *10*, e0135896.

Melly, M., Gregg, C.R., and Mc Gee, Z.A. (1981). Studies of toxicity of *Neisseria gonorrhoeae* for human fallopian tube mucosa. J. Infect. Dis. *143*, 423–431.

Melly, M.A., McGee, Z.A., and Rosenthal, R.S. (1984). Ability of monomeric peptidoglycan fragments from *Neisseria gonorrhoeae* to damage human fallopian-tube mucosa. J. Infect. Dis. *149*, 378–386.

Mendum, T.A., Newcombe, J., Mannan, A.A., Kierzek, A.M., and McFadden, J. (2011). Interrogation of global mutagenesis data with a genome scale model of *Neisseria meningitidis* to assess gene fitness in vitro and in sera. Genome Biol. *12*, R127.

Mey, A.R., and Payne, S.M. (2001). Haem utilization in *Vibrio cholerae i*nvolves multiple tonB-dependent haem receptors. Mol. Microbiol. *42*, 835–849.

Mikaty, G., Soyer, M., Mairey, E., Henry, N., Dyer, D., Forest, K.T., Morand, P., Guadagnini, S., Prévost, M.C., Nassif, X., et al. (2009). Extracellular bacterial pathogen induces host cell surface reorganization to resist shear stress. PLoS Pathog. *5*.

Mills, A., Le, H.T., Coulton, J.W., and Duong, F. (2014). FhuA interactions in a detergent-free nanodisc environment. Biochim. Biophys. Acta - Biomembr. *1838*, 364–371.

Minor, S.Y., Banerjee, A., and Gotschlich, E.C. (2000). Effect of α-oligosaccharide phenotype of *Neisseria gonorrhoeae* strain MS11 on invasion of Chang conjunctival, HEC-1-B endometrial, and ME-180 cervical cells. Infect. Immun. *68*, 6526–6534.

Mohammed, I., Iliyasu, G., and Habib, A.G. (2017). Emergence and control of epidemic meningococcal meningitis in sub-Saharan Africa. Pathog. Glob. Health *111*, 1–6.

Mokry, D.Z., Nadia-Albete, A., Johnson, M.K., Lukat-Rodgers, G.S., Rodgers, K.R., and Lanzilotta, W.N. (2014). Spectroscopic evidence for a 5-coordinate oxygenic ligated high spin ferric heme moiety in the *Neisseria meningitidis* hemoglobin binding receptor. Biochim. Biophys. Acta - Gen. Subj. *1840*, 3058–3066.

Monchois, V., Abergel, C., Sturgis, J., Jeudy, S., and Claverie, J.M. (2001). *Escherichia coli* ykfE ORFan Gene Encodes a Potent Inhibitor of C-type Lysozyme. J. Biol. Chem.

276, 18437–18441.

Morelle, S., Carbonnelle, E., and Nassif, X. (2003). The {REP2} repeats of the genome of *Neisseria meningitidis* are associated with genes coordinately regulated during bacterial cell interaction. J. Bacteriol. *185*, 2618–2627.

Morgenthau, A., Livingstone, M., Adamiak, P., and Schryvers, A.B. (2012). The role of lactoferrin binding protein B in mediating protection against human lactoferricin. Biochem. Cell Biol. *90*, 417–423.

Morton, D.J., Seale, T.W., Madore, L.L., VanWagoner, T.M., Whitby, P.W., and Stull, T.L. (2007). The haem-haemopexin utilization gene cluster (hxuCBA) as a virulence factor of *Haemophilus influenzae.* Microbiology *153*, 215–224.

Moser, J., Schubert, W.D., Beier, V., Bringemeier, I., Jahn, D., and Heinz, D.W. (2001). V-shaped structure of glutamyl-tRNA reductase, the first enzyme of tRNA-dependent tetrapyrrole biosynthesis. EMBO J. *20*, 6583–6590.

Mosleh, I.M., Huber, L.A., Steinlein, P., Pasquali, C., Günther, D., and Meyer, T.F. (1998). *Neisseria gonorrhoeae* porin modulates phagosome maturation. J. Biol. Chem. *273*, 35332–35338.

Moynie, L., Schnell, R., McMahon, S.A., Sandalova, T., Boulkerou, W.A., Schmidberger, J.W., Alphey, M., Cukier, C., Duthie, F., Kopec, J., et al. (2013). The AEROPATH project targeting *Pseudomonas aeruginosa*: Crystallographic studies for assessment of potential targets in early-stage drug discovery. Acta Crystallogr. Sect. F Struct. Biol. Cryst. Commun. *69*, 25–34.

Muenzner, P., Dehio, C., Fujiwara, T., Achtman, M., Meyer, T.F., and Gray-Owen, S.D. (2000). Carcinoembryonic antigen family receptor specificity of *Neisseria meningitidis* Opa variants influences adherence to and invasion of proinflammatory cytokine-activated endothelial cells. Infect. Immun. *68*, 3601–3607.

Muenzner, P., Naumann, M., Meyer, T.F., and Gray-Owen, S.D. (2001). Pathogenic *Neisseria* Trigger Expression of Their Carcinoembryonic Antigen-related Cellular Adhesion Molecule 1 (CEACAM1; Previously CD66a) Receptor on Primary Endothelial Cells by Activating the Immediate Early Response Transcription Factor, Nuclear Facto. J. Biol. Chem. *276*, 24331–24340.

Müller, I. (2017). Guidelines for the successful generation of protein-ligand complex crystals. Acta Crystallogr. Sect. D Struct. Biol. *73*, 79–92.

Murphy, K. (2011). Janeway's Immunobiology (New York: Garland Science, Taylor and Francis Group).

Murshudov, G.N., Skubák, P., Lebedev, A.A., Pannu, N.S., Steiner, R.A., Nicholls, R.A., Winn, M.D., Long, F., and Vagin, A.A. (2011). REFMAC5 for the refinement of macromolecular crystal structures. Acta Crystallogr. Sect. D Biol. Crystallogr. *67*, 355–367.

Naoe, Y., Nakamura, N., Rahman, M.M., Tosha, T., Nagatoishi, S., Tsumoto, K., Shiro, Y., and Sugimoto, H. (2017). Structural Basis for Binding and Transfer of Heme in Bacterial Heme-Acquisition Systems. Proteins Struct. Funct. Bioinforma.

Newcombe, J., Jeynes, J.C., Mendoza, E., Hinds, J., Marsden, G.L., Stabler, R.A., Marti, M., and McFadden, J.J. (2005). Phenotypic and transcriptional characterization of the meningococcal PhoPQ system, a magnesium-sensing two-component regulatory system that controls genes involved in remodeling the meningococcal cell surface. J. Bacteriol. *187*, 4967–4975.

Nogaj, L.A., and Beale, S.I. (2005). Physical and kinetic interactions between glutamyl-tRNA reductase and glutamate-1-semialdehyde aminotransferase of *Chlamydomonas reinhardtii.* J. Biol. Chem. *280*, 24301–24307.

Noinaj, N., Guillier, M., Barnard, T.J., and Buchanan, S.K. (2010). TonB-dependent transporters: regulation, structure, and function. Annu. Rev. Microbiol. *64*, 43–60.

Noinaj, N., Easley, N.C., Oke, M., Mizuno, N., Gumbart, J., Boura, E., Steere, A.N., Zak, O., Aisen, P., Tajkhorshid, E., et al. (2012). Structural basis for iron piracy by pathogenic *Neisseria*. Nature *483*, 53–58.

Noinaj, N., Cornelissen, C.N., and Buchanan, S.K. (2013). Structural insight into the lactoferrin receptors from pathogenic *Neisseria.* J. Struct. Biol. *184*, 83–92.

Norrander, J., Kempe, T., and Messing, J. (1983). Construction of improved M13 vectors using oligodeoxynucleotide-directed mutagenesis. Gene *26*, 101–106.

Noto, J.M., and Cornelissen, C.N. (2008). Identification of TbpA residues required for transferrin-iron utilization by *Neisseria gonorrhoeae*. Infect. Immun. *76*, 1960–1969.

O'Connor, C.D., and Timmis, K.N. (1987). Highly repressible expression system for cloning genes that specify potentially toxic proteins. J. Bacteriol. *169*, 4457–4462.

O'May, C.Y., Sanderson, K., Roddam, L.F., Kirov, S.M., and Reid, D.W. (2009). Iron-binding compounds impair *Pseudomonas aeruginosa* biofilm formation, especially under anaerobic conditions. J. Med. Microbiol. *58*, 765–773.

Ochsner, U.A., Johnson, Z., and Vasil, M.L. (2000). Genetics and regulation of two distinct haem-uptake systems, phu and has, in *Pseudomonas aeruginosa.* Microbiology *146*, 185–198.

Ohneck, E.A., Zalucki, Y.M., Johnson, P.J.T., Dhulipala, V., Golparian, D., Unemo, M., Jerse, A.E., and Shafer, W.M. (2011). A novel mechanism of high-level, broad-spectrum antibiotic resistance caused by a single base pair change in *Neisseria gonorrhoeae*. MBio *2*.

Ollis, A.A., Kumar, A., and Postle, K. (2012). The ExbD periplasmic domain contains distinct functional regions for two stages in TonB energization. J. Bacteriol. *194*, 3069–3077.

Ostan, N.K.H., Yu, R.-H., Ng, D., Lai, C.C.-L., Pogoutse, A.K., Sarpe, V., Hepburn, M., Sheff, J., Raval, S., Schriemer, D.C., et al. (2017). Lactoferrin binding protein B – a bi-functional bacterial receptor protein. PLOS Pathog. *13*, e1006244.

Otto, B.R., Verweij-van Vught, a M., and MacLaren, D.M. (1992). Transferrins and heme-compounds as iron sources for pathogenic bacteria. Crit. Rev. Microbiol. *18*, 217–233.

Pace, D., and Pollard, A.J. (2012). Meningococcal disease: Clinical presentation and sequelae. Vaccine *30*, 3–9.

Palace, S.G., Proulx, M.K., Lu, S., Baker, R.E., and Goguen, J.D. (2014). Genome-wide mutant fitness profiling identifies nutritional requirements for optimal growth of *Yersinia pestis* in deep tissue. MBio *5*.

Panek, H., and O'Brian, M.R. (2002). A whole genome view of prokaryotic haem biosynthesis. Microbiology *148*, 2273–2282.

Paquelin, A., Ghigo, J.M., Bertin, S., and Wandersman, C. (2001). Characterization of HasB, a *Serratia marcescens* TonB-like protein specifically involved in the haemophore-dependent haem acquisition system. Mol. Microbiol. *42*, 995–1005.

Parikh, S.R., Andrews, N.J., Beebeejaun, K., Campbell, H., Ribeiro, S., Ward, C., White, J.M., Borrow, R., Ramsay, M.E., and Ladhani, S.N. (2016). Effectiveness and impact of a reduced infant schedule of 4CMenB vaccine against group B meningococcal disease in England: a national observational cohort study. Lancet *388*, 2775–2782.

Parsons, H.K., Vitovski, S., and Sayers, J.R. (2004). Immunoglobulin A1 proteases: a structure-function update. Biochem. Soc. Trans. *32*, 1130–1132.

Pawelek, P.D., Croteau, N., Ng-Thow-Hing, C., Khursigara, C.M., Moiseeva, N., Allaire, M., and Coulton, J.W. (2006). Structure of TonB in Complex with FhuA, E. coli Outer Membrane Receptor. Science (80-.). *312*, 1399–1402.

Peak, I.R., Chen, A., Jen, F.E.C., Jennings, C., Schulz, B.L., Saunders, N.J., Khan, A., Seifert, H.S., and Jennings, M.P. (2016). *Neisseria meningitidis* lacking the major porins PorA and PorB is viable and modulates apoptosis and the oxidative burst of neutrophils. J. Proteome Res. *15*, 2356–2365.

Peng, S., Zhang, H., Gao, Y., Pan, X., Cao, P., Li, M., and Chang, W. (2011). Crystal structure of uroporphyrinogen III synthase from *Pseudomonas syringae* pv. tomato DC3000. Biochem. Biophys. Res. Commun. *408*, 576–581.

Perkins-Balding, D., Baer, M.T., and Stojiljkovic, I. (2003). Identification of functionally important regions of a haemoglobin receptor from *Neisseria meningitidis*. Microbiology *149*, 3423–3435.

Perrin, A., Bonacorsi, S., Carbonnelle, E., Talibi, D., Dessen, P., Nassif, X., and Tinsley, C. (2002). Comparative genomics identifies the genetic islands that distinguish *Neisseria meningitidis,* the agent of cerebrospinal meningitis, from other Neisseria species. Infect. Immun. *70*, 7063–7072.

Perry, A.C., Hart, C.A., Nicolson, I.J., Heckels, J.E., and Saunders, J.R. (1987). Inter-strain homology of pilin gene sequences in *Neisseria meningitidis* isolates that express markedly different antigenic pilus types. J.Gen.Microbiol. *133 (Pt 6*, 1409–1418.

Petrovieh, R.M., Litwin, S., and Jaffe, E.K. (1996). *Bradyrhizobium japonicum* porphobilinogen synthase uses two Mg(II) and monovalent cations. J. Biol. Chem. *271*, 8692–8699.

Pichon, C., Atshaves, B.P., Stolowich, N.J., and Scott, A.I. (1994). Evidence for an

intermediate in the enzymatic formation of Uroporphyrinogen III. Bioorganic Med. Chem. *2*, 153–168.

Plaut, A.G., Gilbert, J. V, Artenstein, M.S., and Capra, J.D. (1975). *Neisseria gonorrhoeae* and *Neisseria meningitidis:* extracellular enzyme cleaves human immunoglobulin A. Science *190*, 1103–1105.

Pogoutse, A.K., and Moraes, T.F. (2017). Iron acquisition through the bacterial transferrin receptor. Crit. Rev. Biochem. Mol. Biol. *0*, 000.

Prince, S.M., Achtman, M., and Derrick, J.P. (2002). Crystal structure of the OpcA integral membrane adhesin from *Neisseria meningitidis*. Proc. Natl. Acad. Sci. U. S. A. *99*, 3417–3421.

Public Health England (2016). Outbreak of high level azithromycin resistant gonorrhoea in England. Heal. Prot. Wkly. Rep. *10*, 3–4.

Public Health England (2017). Invasive meningococcal disease in England : annual laboratory confirmed reports for epidemiological year 2016 to Invasive meningococcal disease in England : annual laboratory confirmed reports for epidemiological year 2016 to 2017.

Pujol, C., Eugène, E., Marceau, M., and Nassif, X. (1999). The meningococcal PilT protein is required for induction of intimate attachment to epithelial cells following pilus-mediated adhesion. Proc. Natl. Acad. Sci. U. S. A. *96*, 4017–4022.

Putker, F., Grutsch, A., Tommassen, J., and Bos, M.P. (2014). Ght protein of *Neisseria meningitidis* is involved in the regulation of lipopolysaccharide biosynthesis. J. Bacteriol. *196*, 780–789.

Qi, Z., Hamza, I., and O'Brian, M.R. (1999). Heme is an effector molecule for iron-dependent degradation of the bacterial iron response regulator (Irr) protein. Proc. Natl. Acad. Sci. U. S. A. *96*, 13056–13061.

Qiu, D.-H., Huang, Z.-L., Zhou, T., Shen, C., and Hider, R.C. (2011). In vitro inhibition of bacterial growth by iron chelators. FEMS Microbiol. Lett. *314*, 107–111.

Quillin, S.J., and Seifert, H.S. (2018). *Neisseria gonorrhoeae* host adaptation and pathogenesis. Nat. Rev. Microbiol. *16*, 226–240.

Ragland, S.A., Schaub, R.E., Hackett, K.T., Dillard, J.P., and Criss, A.K. (2016). Two lytic transglycosylases in *Neisseria gonorrhoeae* impart resistance to killing by lysozyme and human neutrophils. Cell. Microbiol.

Ram, S., Sharma, A.K., Simpson, S.D., Gulati, S., McQuillen, D.P., Pangburn, M.K., and Rice, P.A. (1998a). A novel sialic acid binding site on factor H mediates serum resistance of sialylated *Neisseria gonorrhoeae*. J Exp Med *187*, 743–752.

Ram, S., McQuillen, D.P., Gulati, S., Elkins, C., Pangburn, M.K., and Rice, P.A. (1998b). Binding of complement factor H to loop 5 of porin protein 1A: a molecular mechanism of serum resistance of nonsialylated *Neisseria gonorrhoeae.* J. Exp. Med. *188*, 671–680.

Ram, S., Mackinnon, F.G., Gulati, S., McQuillen, D.P., Vogel, U., Frosch, M., Elkins, C., Guttormsen, H.K., Wetzler, L.M., Oppermann, M., et al. (1999). The contrasting

mechanisms of serum resistance of *Neisseria gonorrhoeae* and group B Neisseria meningitidis. Mol. Immunol. *36*, 915–928.

Ram, S., Lewis, L.A., and Agarwal, S. (2011). Meningococcal group W-135 and Y capsular polysaccharides paradoxically enhance activation of the alternative pathway of complement. J. Biol. Chem. *286*, 8297–8307.

Ramsey, M.E., Woodhams, K.L., and Dillard, J.P. (2011). The gonococcal genetic island and type IV secretion in the pathogenic *Neisseria*. Front. Microbiol. *2*, 61.

Rasmussen, A.W., Alexander, H.L., Perkins-Balding, D., Shafer, W.M., and Stojiljkovic, I. (2005). Resistance of Neisseria meningitidis to the toxic effects of heme iron and other hydrophobic agents requires expression of ght. J. Bacteriol. *187*, 5214–5223.

Retzer, M.D., Yu, R., Zhang, Y., Gonzalez, G.C., and Schryvers, A.B. (1998). Discrimination between apo and iron-loaded forms of transferrin by transferrin binding protein B and its N-terminal subfragment. Microb. Pathog. *25*, 175–180.

Rice, P.A., and Kasper, D.L. (1982). Characterization of serum resistance of Neisseria gonorrhoeae that disseminate. Roles of blocking antibody and gonococcal outer membrane proteins. J. Clin. Invest. *70*, 157–167.

Rice, P., Vayo, H., Tam, M., and Blake, M. (1986). Immunoglobulin G antibodies directed against protein III block killing of serum-resistant *Neisseria gonorrhoeae* by immune serum. J. Exp. Med. *164*, 1735–1748.

Roberts, A., Gill, R., Hussey, R.J., Mikolajek, H., Erskine, P.T., Cooper, J.B., Wood, S.P., Chrystal, E.J.T., and Shoolingin-Jordan, P.M. (2012). Crystallization and preliminary X-ray characterization of the tetrapyrrole-biosynthetic enzyme porphobilinogen deaminase from *Arabidopsis thaliana.* Acta Crystallogr. Sect. F Struct. Biol. Cryst. Commun. *68*, 1491–1493.

Roberts, A., Gill, R., Hussey, R.J., Mikolajek, H., Erskine, P.T., Cooper, J.B., Wood, S.P., Chrystal, E.J.T., and Shoolingin-Jordan, P.M. (2013). Insights into the mechanism of pyrrole polymerization catalysed by porphobilinogen deaminase: High-resolution X-ray studies of the *Arabidopsis thaliana e*nzyme. Acta Crystallogr. Sect. D Biol. Crystallogr. *69*, 471–485.

Roessner, C.A., Ponnamperuma, K., and Scott, A.I. (2002). Mutagenesis identifies a conserved tyrosine residue important for the activity of uroporphyrinogen III synthase from *Anacystis nidulans*. FEBS Lett. *525*, 25–28.

Rohde, K.H., and Dyer, D.W. (2004). Analysis of Haptoglobin and Hemoglobin-Haptoglobin Interactions with the *Neisseria meningitidis* TonB-Dependent Receptor HpuAB by Flow Cytometry. Infect. Immun. *72*, 2494–2506.

Rossi, M.S., Fetherston, J.D., Létoffé, S., Carniel, E., Perry, R.D., and Ghigo, J.M. (2001). Identification and characterization of the hemophore-dependent heme acquisition system of Yersinia pestis. Infect. Immun. *69*, 6707–6717.

Roussel-Jazédé, V., Jongerius, I., Bos, M.P., Tommassen, J., and Van Ulsen, P. (2010). NalP-mediated proteolytic release of lactoferrin-binding protein B from the meningococcal cell surface. Infect. Immun. *78*, 3083–3089.

Rudel, T., Scheurerpflug, I., and Meyer, T.F. (1995). *Neisseria* PilC protein identified as type-4 pilus tip-located adhesin. Nature *373*, 357–359.

Sachla, A.J., Le Breton, Y., Akhter, F., McIver, K.S., and Eichenbaum, Z. (2014). The crimson conundrum: heme toxicity and tolerance in GAS. Front. Cell. Infect. Microbiol. *4*, 159.

Sathyamurthy, S. (2011). The role of Gly1, a secreted neisserial protein in meningococcal pathogenesis. University of Sheffield.

Sayers, J.R., and Eckstein, F. (1991). A single-strand specific endonuclease activity copurifies with overexpressed T5 D15 exonuclease. Nucleic Acids Res. *19*, 4127–4132.

Schifman, R.B., and Ryan, K.J. (1983). *Neisseria lactamica* septicemia in an immunocompromised patient. J. Clin. Microbiol. *17*, 934–935.

Schiött, T., Throne-Holst, M., and Hederstedt, L. (1997). *Bacillus subtilis* CcdA-defective mutants are blocked in a late step of cytochrome C biogenesis. J. Bacteriol. *179*, 4523–4529.

Schryvers, A.B., and Gonzalez, G.C. (1989). Comparison of the abilities of different protein sources of iron to enhance *Neisseria meningitidis* infection in mice. Infect. Immun. *57*, 2425–2429.

Schryvers, a B., and Gonzalez, G.C. (1990). Receptors for transferrin in pathogenic bacteria are specific for the host's protein. Can. J. Microbiol. *36*, 145–147.

Schubert, H.L., Phillips, J.D., Heroux, A., and Hill, C.P. (2008). Structure and mechanistic implications of a uroporphyrinogen III synthase-product complex. Biochemistry *47*, 8648–8655.

Schuller, D.J., Zhu, W., Stojiljkovic, I., Wilks, A., and Poulos, T.L. (2001). Crystal structure of heme oxygenase from the gram-negative pathogen *Neisseria meningitidis* and a comparison with mammalian heme oxygenase-1. Biochemistry *40*, 11552–11558.

Semchenko, E.A., Day, C.J., and Seib, K.L. (2016). MetQ of *Neisseria gonorrhoea*e is a surface expressed antigen that elicits bactericidal and functional blocking antibodies. Infect. Immun. *85*, IAI.00898-16.

Shoolingin-Jordan, P.M., Warren, M.J., and Awan, S.J. (1996). Discovery that the assembly of the dipyrromethane cofactor of porphobilinogen deaminase holoenzyme proceeds initially by the reaction of preuroporphyrinogen with the apoenzyme. Biochem. J. *376*, 373–376.

Siburt, C.J.P., Roulhac, P.L., Weaver, K.D., Noto, J.M., Mietzner, T.A., Cornelissen, C.N., Fitzgerald, M.C., and Crumbliss, A.L. (2009). Hijacking transferrin bound iron: protein-receptor interactions involved in iron transport in *N. gonorrhoeae.* Metallomics *1*, 249–255.

Skaar, E.P., Humayun, M., Bae, T., DeBord, K.L., and Schneewind, O. (2004). Iron-source preference of *Staphylococcus aureus* infections. Science *305*, 1626–1628.

Skurnik, D., Roux, D., Aschard, H., Cattoir, V., Yoder-Himes, D., Lory, S., and Pier, G.B.

(2013). A Comprehensive Analysis of In Vitro and In Vivo Genetic Fitness of *Pseudomonas aeruginosa* Using High-Throughput Sequencing of Transposon Libraries. PLoS Pathog. *9*, e1003582.

Smith, A.D., Modi, A.R., Sun, S., Dawson, J.H., and Wilks, A. (2015). Spectroscopic determination of distinct heme ligands in outer-membrane receptors PhuR and HasR of *Pseudomonas aeruginosa.* Biochemistry *54*, 2601–2612.

Söderholm, N., Vielfort, K., Hultenby, K., and Aro, H. (2011). Pathogenic neisseria hitchhike on the uropod of human neutrophils. PLoS One *6*, 1–12.

Soler-García, A., and Jerse, A.E. (2004). A *Neisseria gonorrhoeae* catalase mutant is more sensitive to hydrogen peroxide and paraquat, an inducer of toxic oxygen radicals. Microb. Pathog. *37*, 55–63.

Song, G., Li, Y., Cheng, C., Zhao, Y., Gao, A., Zhang, R., Joachimiak, A., Shaw, N., and Liu, Z.-J. (2009). Structural insight into acute intermittent porphyria. FASEB J. *23*, 396–404.

Sorbara, M.T., and Philpott, D.J. (2011). Peptidoglycan: A critical activator of the mammalian immune system during infection and homeostasis. Immunol. Rev. *243*, 40–60.

Spolaore, B., De Filippis, V., and Fontana, A. (2005). Heme binding by the N-terminal fragment 1-44 of human growth hormone. Biochemistry *44*, 16079–16089.

Stamford, N.P.J., Capretta, A., and Battersby, A.R. (1995). Expression, Purification and Characterisation of the Product from the *Bacillus Subtilis* hemD gene, Uroporphyrinogen III Synthase. Eur. J. Biochem. *231*, 236–241.

Stanwell-Smith, R.E., Stuart, J.M., Hughes, A.O., Robinson, P., Griffin, M.B., Cartwright, K., and Stanwell, R.E. (1994). Smoking, the environment and meningococcal disease: a case control study. Epidemiol. Infect. *112*, 315–328.

Stephens, D.S. (2009). Biology and pathogenesis of the evolutionarily successful, obligate human bacterium *Neisseria meningitidis.* Vaccine *27*, 71–77.

Stern, A., Brown, M., Nickel, P., and Meyer, T.F. (1986). Opacity genes in *Neisseria gonorrhoeae*: Control of phase and antigenic variation. Cell *47*, 61–71.

Stojiljkovic, I., and Srinivasan, N. (1997). *Neisseria meningitidis* tonB, exbB, and exbD genes: Ton-dependent utilization of protein-bound iron in Neisseriae. J. Bacteriol. *179*, 805–812.

Stojiljkovic, I., Hwa, V., De Saint Martin, L., O'Gaora, P., Nassif, X., Heffron, F., and So, M. (1995). The *Neisseria meningitidis* haemoglobin receptor: Its role in iron utilization and virulence. Mol. Microbiol. *15*, 531–541.

Stojiljkovic, I., Larson, J., Hwa, V., Anic, S., and Magdalene, S.O. (1996). HmbR outer membrane receptors of pathogenic *Neisseria* spp.: Iron- regulated, hemoglobin-binding proteins with a high level of primary structure conservation. J. Bacteriol. *178*, 4670–4678.

Strange, H.R., Zola, T.A., and Cornelissen, C.N. (2011). The *fbpABC* operon is required for ton-independent utilization of xenosiderophores by *Neisseria gonorrhoeae* strain

FA19. Infect. Immun. *79*, 267–278.

Studier, F.W. (2005). Protein production by auto-induction in high-density shaking cultures. Protein Expr. Purif. *41*, 207–234.

Subramanian, S., and Ross, P.D. (1984). Dye-ligand affinity chromatography: The interaction of cibacron blue f3GA® with proteins and enzyme. Crit. Rev. Biochem. Mol. Biol. *16*, 169–205.

Swanson, K. V., Jarvis, G.A., Brooks, G.F., Barham, B.J., Cooper, M.D., and McLeod Griffiss, J. (2001). CEACAM is not necessary for *Neisseria gonorrhoeae* to adhere to and invade female genital epithelial cells. Cell. Microbiol. *3*, 681–691.

Swartley, J.S., Marfin, a a, Edupuganti, S., Liu, L.J., Cieslak, P., Perkins, B., Wenger, J.D., and Stephens, D.S. (1997). Capsule switching of *Neisseria meningitidis.* Proc. Natl. Acad. Sci. U. S. A. *94*, 271–276.

Talà, A., Monaco, C., Nagorska, K., Exley, R.M., Corbett, A., Zychlinsky, A., Alifano, P., and Tang, C.M. (2011). Glutamate utilization promotes meningococcal survival in vivo through avoidance of the neutrophil oxidative burst. Mol. Microbiol. *81*, 1330–1342.

Trotter, C., Findlow, J., Balmer, P., Holland, A., Barchha, R., Hamer, N., Andrews, N., Miller, E., and Borrow, R. (2007). Seroprevalence of bactericidal and anti-outer membrane vesicle antibodies to *Neisseria meningitidis* group B in England. Clin. Vaccine Immunol. *14*, 863–868.

Trotter, C.L., Findlow, H., and Borrow, R. (2012). Seroprevalence of serum bactericidal antibodies against group W135 and Y meningococci in England in 2009. Clin. Vaccine Immunol. *19*, 219–222.

Troxell, B., and Hassan, H.M. (2013). Transcriptional regulation by Ferric Uptake Regulator (Fur) in pathogenic bacteria. Front. Cell. Infect. Microbiol. *3*, 59.

Tsai, S.-F., Bishop, D.F., and Desnick, R.J. (1987). Purification and Properties of Uroporphyrinogen III Synthase from Human Erythrocytes. J. Biol. Chem. *262*, 126–1273.

Tsang, R. (2007). Capsule switching and capsule replacement in vaccine-preventable bacterial diseases. Lancet Infect. Dis. *7*, 569–570.

Turner, P.C., Thomas, C.E., Elkins, C., Clary, S., and Sparling, P.F. (1998). *Neisseria gonorrhoeae* heme biosynthetic mutants utilize heme and hemoglobin as a heme source but fail to grow within epithelial cells. Infect. Immun. *66*, 5215–5223.

Turner, P.C., Thomas, C.E., Stojiljkovic, I., Elkins, C., Kizel, G., Ala'Aldeen, D.A.A., and Sparling, P.F. (2001). Neisserial TonB-dependent outer-membrane proteins: Detection, regulation and distribution of three putative candidates identified from the genome sequences. Microbiology *147*, 1277–1290.

Tzeng, Y.-L., Thomas, J., and Stephens, D.S. (2016). Regulation of capsule in *Neisseria meningitidis*. Crit. Rev. Microbiol. *42*, 759–772.

Tzeng, Y.L., Kahler, C.M., Zhang, X., and Stephens, D.S. (2008). MisR/MisS two-component regulon in *Neisseria meningitidis*. Infect. Immun. *76*, 704–716.

Unemo, M. (2015). Current and future antimicrobial treatment of gonorrhoea – the rapidly evolving *Neisseria gonorrhoeae* continues to challenge. BMC Infect. Dis. *15*, 364.

Uria, M.J., Zhang, Q., Li, Y., Chan, A., Exley, R.M., Gollan, B., Chan, H., Feavers, I., Yarwood, A., Abad, R., et al. (2008). A generic mechanism in *Neisseria meningitidis* for enhanced resistance against bactericidal antibodies. J. Exp. Med. *205*, 1423–1434.

Vannini, V., Rodríguez, A., Vera, J.L., de Valdéz, G.F., Taranto, M.P., and Sesma, F. (2011). Cloning and heterologous expression of *Lactobacillus reuteri* uroporphyrinogen III synthase/methyltransferase gene (cobA/hemD): Preliminary characterization. Biotechnol. Lett. *33*, 1625–1632.

Velasquez, L., García, K., Morales, F., Heckels, J.E., Orihuela, P., Rodas, P.I., Christodoulides, M., and Cardenas, H. (2012). *Neisseria gonorrhoeae* pilus attenuates cytokine response of human fallopian tube explants. J. Biomed. Biotechnol. *2012*, 491298.

Virji, M., Saunders, J.R., Sims, G., Makepeace, K., Maskell, D., and Ferguson, D.J.P. (1993). Pilus-facilitated adherence of *Neisseria meningitidis* to human epithelial and endothelial cells: modulation of adherence phenotype occurs concurrently with changes in primary amino acid sequence and the glycosylation status of pilin. Mol. Microbiol. *10*, 1013–1028.

Virji, M., Makepeace, K., Peak, I.R.A., Ferguson, D.J.P., Jennings, M.P., and Moxon, E.R. (1995). Opc- and pilus-dependent interactions of meningococci with human endothelial cells: molecular mechanisms and modulation by surface polysaccharides. Mol. Microbiol. *18*, 741–754.

Vitovski, S., and Sayers, J.R. (2007). Relaxed cleavage specificity of an immunoglobulin A1 protease from *Neisseria meningitidis*. Infect. Immun. *75*, 2875–2885.

Vu, D.M., Shaughnessy, J., Lewis, L.A., Ram, S., Rice, P.A., and Granoff, D.M. (2012). Enhanced bacteremia in human factor H transgenic rats infected by neisseria meningitidis. Infect. Immun. *80*, 643–650.

Wally, J., and Buchanan, S.K. (2007). A structural comparison of human serum transferrin and human lactoferrin. Biometals *20*, 249–262.

Wang, L., Elliott, M., and Elliott, T. (1999). Conditional stability of the HemA protein (Glutamyl-tRNA reductase) regulates heme biosynthesis in *Salmonella typhimurium.* J. Bacteriol. *181*, 1211–1219.

Wang, N., Ozer, E.A., Mandel, M.J., and Hauser, A.R. (2014). Genome-wide identification of *Acinetobacter baumannii* genes necessary for persistence in the lung. MBio *5*.

Warner, D.M., Shafer, W.M., and Jerse, A.E. (2008). Clinically relevant mutations that cause derepression of the *Neisseria gonorrhoeae* MtrC-MtrD-MtrE Efflux pump system confer different levels of antimicrobial resistance and in vivo fitness. Mol. Microbiol. *70*, 462–478.

Watson, A.A., and O'Callaghan, C.A. (2005). Crystallization and X-ray diffraction

analysis of human CLEC-2. Acta Crystallogr. Sect. F Struct. Biol. Cryst. Commun. *61*, 1094–1096.

Wierzbicka, M. (2014). Studies on Structure, Function and Immunogenicity of Neisserial Secreted Protein Gly1ORF1. Univerisity of Sheffield.

Wilks, A., and Burkhard, K.A. (2007). Heme and virulence: how bacterial pathogens regulate, transport and utilize heme. Nat. Prod. Rep. *24*, 511.

Wilks, K.E., Dunn, K.L.R., Farrant, J.L., Reddin, K.M., Gorringe, A.R., Langford, P.R., and Simon Kroll, J. (1998). Periplasmic superoxide dismutase in meningococcal pathogenicity. Infect. Immun. *66*, 213–217.

Wójtowicz, H., Bielecki, M., Wojaczyński, J., Olczak, M., Smalley, J.W., and Olczak, T. (2013). The *Porphyromonas gingivalis* HmuY haemophore binds gallium(iii), zinc(ii), cobalt(iii), manganese(iii), nickel(ii), and copper(ii) protoporphyrin IX but in a manner different to iron(iii) protoporphyrin IX. Metallomics *5*, 343.

Wolff, N. (2002). Histidine pKa shifts and changes of tautomeric states induced by the binding of gallium-protoporphyrin IX in the hemophore HasASM. Protein Sci. *11*, 757–765.

Wolfgang, M., Park, H.S., Hayes, S.F., van Putten, J.P., and Koomey, M. (1998a). Suppression of an absolute defect in type IV pilus biogenesis by loss-of-function mutations in *pilT,* a twitching motility gene in Neisseria gonorrhoeae. Proc. Natl Acad. Sci. USA *95*, 14973–14978.

Wolfgang, M., Lauer, P., Park, H.S., Brossay, L., Hébert, J., and Koomey, M. (1998b). PilT mutations lead to simultaneous defects in competence for natural transformation and twitching motility in piliated *Neisseria gonorrhoeae.* Mol. Microbiol. *29*, 321–330.

Wong, C.T., Xu, Y., Gupta, A., Garnett, J.A., Matthews, S.J., and Hare, S.A. (2015). Structural analysis of haemoglobin binding by HpuA from the *Neisseriaceae* family. Nat. Commun. *6*, 10172.

Woof, J.M., and Kerr, M.A. (2006). The function of immunoglobulin A in immunity. J. Pathol. *208*, 270–282.

World Health Organization (2017). WHO | Global priority list of antibiotic-resistant bacteria to guide research, discovery, and development of new antibiotics. WHO.

Wu, H., and Jerse, A.E. (2006). Alpha-2,3-sialyltransferase enhances *Neisseria gonorrhoeae* survival during experimental murine genital tract infection. Infect. Immun. *74*, 4094–4103.

Wu, B., Novelli, J., Foster, J., Vaisvila, R., Conway, L., Ingram, J., Ganatra, M., Rao, A.U., Hamza, I., and Slatko, B. (2009). The heme biosynthetic pathway of the obligate Wolbachia endosymbiont of *Brugia malayias* a potential anti-filarial drug target. PLoS Negl. Trop. Dis. *3*, e475.

Wyckoff, E.E., Lopreato, G.F., Tipton, K.A., and Payne, S.M. (2005). Shigella dysenteriae ShuS promotes utilization of heme as an iron source and protects against heme toxicity. J. Bacteriol. *187*, 5658–5664.

Yang, F., Xia, X., Lei, H.Y., and Wang, E.D. (2010). Hemin binds to human cytoplasmic arginyl-tRNA synthetase and inhibits its catalytic activity. J. Biol. Chem. *285*, 39437–39446.

Yang, J.T., Wu, C.S.C., and Martinez, H.M. (1986). Calculation of Protein Conformation from Circular Dichroism. Methods Enzymol. *130*, 208–269.

Yang, X., Yu, R.H., Calmettes, C., Moraes, T.F., and Schryvers, A.B. (2011). Anchor peptide of transferrin-binding protein B is required for interaction with transferrin-binding protein A. J. Biol. Chem. *286*, 45165–45173.

Yu, C., and Genco, C.A. (2012). Fur-mediated global regulatory circuits in pathogenic *Neisseria* species. J. Bacteriol. *194*, 6372–6381.

Yu, C., McClure, R., Nudel, K., Daou, N., and Genco, C.A. (2016). Characterization of the Neisseria gonorrhoeae Iron and Fur Regulatory Network. J. Bacteriol. *198*, JB.00166-16.

Yue, W.W., Grizot, S., and Buchanan, S.K. (2003). Structural evidence for iron-free citrate and ferric citrate binding to the TonB-dependent outer membrane transporter FecA. J. Mol. Biol. *332*, 353–368.

Zarantonelli, M.-L., Szatanik, M., Giorgini, D., Hong, E., Huerre, M., Guillou, F., Alonso, J.-M., and Taha, M.-K. (2007). Transgenic mice expressing human transferrin as a model for meningococcal infection. Infect. Immun. *75*, 5609–5614.

Zavascki, A.P., Fritscher, L., Superti, S., Dias, C., Kroth, L., Traesel, M.A., Antonello, I.C.F., and Saitovitch, D. (2006). First case report of *Neisseria lactamica* causing cavitary lung disease in an adult organ transplant recipient. J. Clin. Microbiol. *44*, 2666–2668.

Zhao, A., Fang, Y., Chen, X., Zhao, S., Dong, W., Lin, Y., Gong, W., and Liu, L. (2014). Crystal structure of *Arabidopsis* glutamyl-tRNA reductase in complex with its stimulator protein. Proc. Natl. Acad. Sci. *111*, 6630–6635.

Zhao, S., Montanez, G.E., Kumar, P., Sannigrahi, S., and Tzeng, Y.L. (2010). Regulatory role of the MisR/S two-component system in hemoglobin utilization in *Neisseria meningitidis*. Infect. Immun. *78*, 1109–1122.

Zhou, S., Zhang, B., Sturm, E., Teagarden, D.L., Schöneich, C., Kolhe, P., Lewis, L.M., Muralidhara, B.K., and Singh, S.K. (2010). Comparative evaluation of disodium edetate and diethylenetriaminepentaacetic acid as iron chelators to prevent metal-catalyzed destabilization of a therapeutic monoclonal antibody. J. Pharm. Sci. *99*, 4239–4250.

Zhu, P., Morelli, G., and Achtman, M. (1999). The opcA and ψopcB regions in *Neisseria*: Genes, pseudogenes, deletions, insertion elements and DNA islands. Mol. Microbiol. *33*, 635–650.

Zhu, W., Hunt, D.J., Richardson, A.R., and Stojiljkovic, I. (2000a). Use of Heme Compounds as Iron Sources by Pathogenic *Neisseriae* Requires the Product of the hemO Gene. J. Bacteriol. *182*, 439–447.

Zhu, W., Wilks, A., and Stojiljkovic, I. (2000b). Degradation of heme in gram-negative bacteria: The product of the hemO gene of *Neisseriae* is a heme oxygenase. J. Bacteriol. *182*, 6783–6790.

Zola, T.A., Strange, H.R., Dominguez, N.M., Dillard, J.P., and Cornelissen, C.N. (2010). Type IV secretion machinery promotes ton-independent intracellular survival of *Neisseria gonorrhoeae* within cervical epithelial cells. Infect. Immun. *78*, 2429–2437.

Zughaier, S.M., Kandler, J.L., and Shafer, W.M. (2014). *Neisseria gonorrhoeae* modulates iron-limiting innate immune defenses in macrophages. PLoS One *9*, e87688.